Snow-stubble-atmosphere interactions during snowmelt on the Canadian Prairies

A Thesis Submitted to the College of

Graduate and Postdoctoral Studies

In Partial Fulfillment of the Requirements

For the Degree of Doctor of Philosophy

In the Department of Geography and Planning

(Centre for Hydrology)

University of Saskatchewan

Saskatoon

By

Phillip Stephen Harder

Permission to Use

In presenting this thesis in partial fulfilment of the requirements for a Postgraduate degree from the University of Saskatchewan, I agree that the Libraries of this University may make it freely available for inspection. I further agree that permission for copying of this thesis in any manner, in whole or in part, for scholarly purposes may be granted by the professor or professors who supervised my thesis work or, in their absence, by the Head of the Department or the Dean of the College in which my thesis work was done. It is understood that any copying or publication or use of this thesis or parts thereof for financial gain shall not be allowed without my written permission. It is also understood that due recognition shall be given to me and to the University of Saskatchewan in any scholarly use which may be made of any material in my thesis.

Disclaimer

Reference in this thesis/dissertation to any specific commercial products, process, or service by trade name, trademark, manufacturer, or otherwise, does not constitute or imply its endorsement, recommendation, or favouring by the University of Saskatchewan. The views and opinions of the author expressed herein do not state or reflect those of the University of Saskatchewan, and shall not be used for advertising or product endorsement purposes.

Requests for permission to copy or to make other uses of materials in this thesis/dissertation in whole or part should be addressed to:

Head of the Department of Geography and Planning

117 Science Place
University of Saskatchewan
Saskatoon, Saskatchewan S7N 1J9
Canada

OR

Dean
College of Graduate and Postdoctoral Studies
University of Saskatchewan
116 Thorvaldson Building, 110 Science Place
Saskatoon, Saskatchewan S7N 5C9
Canada

Abstract

Snowmelt is a critical component of the Canadian Prairie hydrological cycle and has significant hydrological and agronomic implications. Within this region, snowmelt can also be a very complicated phenomenon to accurately observe and model due to the occurrence of shallow snowpacks, the unknown energy balance implications of emerging crop stubble during melt on cultivated fields, and the effects of spatiotemporal heterogeneity of snowcover on local-scale advection. The objective of this research was to improve the physical understanding of these complex and interacting processes with deployment of novel observation systems and development and application of new physics-based process models. Intensive field campaigns for the 2015 and 2016 snowmelt season were conducted near Rosthern, Saskatchewan and provided the observations necessary to conduct this research. Application of novel observation systems demonstrated: 1) the ability to remotely-sense maximum prairie snow depth with imagery collected from an unmanned aerial vehicle and processed with Structure from Motion techniques, and 2) the first identification and quantification of latent heat advection from ponded meltwater to snow with development and deployment of a water vapor, air temperature, and wind speed profiling system. Model development resolved: 1) the small scale and dynamic energy balance interactions between the stubble, snow, and atmosphere in a physically based, uncalibrated energy balance model, 2) local-scale sensible and latent heat advection contributions to snowmelt in a modelling framework that facilitates easy coupling to existing one-dimensional snowmelt models, and 3) the influence of stubble upon meltwater partitioning in a coupled model that accounts for snow accumulation, melt and infiltration processes. This study demonstrates that: 1) compensatory interactions with emerging stubble result in negligible differences in the net snow surface energy balance, 2) the inclusion of advection into snow models improves their physical realism and snowmelt predictions, and 3) that the compensatory interactions of stubble on accumulation and melt processes are secondary to the frozen soil infiltration process which is the dominant control on meltwater partitioning. The advances in observational and modelling capacity shown here improve the understanding and predictive capacity of the complex interactions governing the melt processes of prairie snowpacks.

Acknowledgments

I feel that the proverb, “it takes a village to raise a child” is a metaphor that also applies to the journey of completing a PhD. So with the completion of this dissertation I want to acknowledge my village for getting me across the PhD finish line. The financial support that I was able to access via the University of Saskatchewan (Dean’s Scholarship), NSERC (Postgraduate Scholarship, Research Tools and Instruments and Discovery grants and Changing Cold Regions Network), the Global Institute for Water Security and the Canada Research Chairs programme allowed me to do fascinating research and still live a “normal” life at the same time. My supervisors, Dr. John Pomeroy and Dr. Warren Helgason, provided the opportunity, mentorship, freedom, and the resources to propose and execute, in hindsight, a ridiculously large research program despite my limited field experience at the start. I appreciate the staff and students at the Centre for Hydrology for assistance in the field and the mental trenches (you know who you are). I am especially grateful for the camaraderie and support of my fellow students (in no particular order) Chris Marsh, Holly Annand, Dan Karran, Nicolas Leroux, Seba Krogh and Evan Siemens. This work would not have been possible without the cooperation of Nathan Janzen and Robert Regehr, the farmers who tolerated my field campaigns and stubble height requests.

And my family. My parents for raising me to, apparently, be curious about the world around me. Kristen for being supportive of this path through all the highs and lows, reading my work when you’d rather be reading anything else, and giving me the reasons and motivation to always do my best. Everett and Annaliese for reminding me that life happens in the moment and making my laugh no matter the situation.

Thank you village.

This work is dedicated to my dear Everett and Annaliese.

You have brains in your head. You have feet in your shoes. You can steer yourself any direction you choose.

Dr. Seuss, Oh, The Places You'll Go!

Table of Contents

List of Figures

List of Tables

List of Acronyms

Acronym	Definition
Canola16	2016 canola stubble treatment
CI	Confidence Interval
CRHM	Cold Region Hydrological Modelling platform
CV	Coefficient of Variation
DSM	Digital Surface Model
EBSM	Energy Balance Snowmelt Model
EC	Eddy Covariance
GCP	Ground Control Points
GM2002	Granger et al. (2001) boundary layer integration advection model
GNSS	Global Navigation Satellite System
GPS	Global-Positioning System
HAWTS	Heat and Water Transport in frozen Soils Model
IMU	Inertial Momentum Units
LiDAR	Light Detection And Ranging
MB	Model Bias
PAR	Photosynthetically-Active Radiation
PBSM	Prairie Blowing Snow Model
RGB	Red-Green-Blue
RMSE	Root Mean Square Error
RTK	Real Time Kinematic
SCA	Snowcovered Area
SD	Standard Deviation
SfM	Structure from Motion
SGM	Semi-Global Matching
SHAW	Simultaneous Heat and Water Model
Short 15	2015 short wheat stubble treatment
SLHAM	Sensible and Latent Heat Advection Model
SNR	Signal-to-Noise Ratio
SSAM	Stubble-Snow-Atmosphere Model
SWE	Snow Water Equivalent
Tall15	2015 tall wheat stubble treatment
UAV	Unmanned Aerial Vehicle
Wheat 16	2016 wheat stubble treatment

List of Symbols

Symbol	Units/Value	Definition
A	m^2	Stubble stalk surface area
a	-	Advection coefficient
A_{max}	m^2	Maximum expected patch size
a_{min}	-	Minimum snow albedo
A_p	m^2	Patch area
a_{snow}	-	Snow albedo
a_{stub}	-	Stubble albedo
b	-	Advection coefficient
c	-	Scalar
C	-	Prairie soil infiltration coefficient
c_1	1 m^2	Snow patch scaling threshold coefficient
c_2	1	Patch length scaling coefficient
c_{air}	1005 J kg^{-1} K^{-1}	Specific heat capacity of air
c_{fd}	0.5	Drag coefficient of stubble element
C_h	-	Surface exchange coefficient
c_{ice}	2010 kJ kg^{-1} K^{-1}	Specific heat capacity of ice
c_{stub}	1630 J kg^{-1} K^{-1}	Specific heat capacity of the stubble
c_{water}	4184 kJ kg^{-1} K^{-1}	Specific heat capacity of water
d	$1.458x10^{-6}$kg $m^{-1}s^{-1}K^{-1/2}$	Viscosity coefficient
D'	-	Patch length scaling dimension
d_0	m	Displacement height
D_h	$20.2x10^{-6}$ m^2 s^{-1}	Molecular diffusivity for heat in air
D_k	-	Fractal dimension of snow patch area scaling
dt	s	Interval duration
E	kg m^{-2}	Snowpack sublimation or deposition
e_{sc}	kPa	Snowcover surface vapor pressure
e_{sf}	kPa	Snow-free surface vapor pressure
e_{soil}	kPa	Soil surface water vapor
e_{wat}	kPa	Water surface water vapor
$F(A_p)$	-	Fraction of snow patches greater than a given area
$f(A_p)$	-	Normalized areal fraction of the unit area represented by patch
f_a	0.05	Shortwave absorption factor
f_d	-	Diffuse fraction of incoming shortwave radiation
f_s	-	Advection source
F_{water}	-	Surface fraction of ponded water
g	9.81 m s^{-2}	Acceleration due to gravity
Gr	-	Grashof number
H	W m^{-2}	Areal average sensible heat flux

H_A	W m^{-2}	Local-scale sensible heat advection
h_{forced}	-	Forced convection coefficient between stubble stalk and air
h_{free}	-	Free convection coefficient between stubble stalk and air
h_s	m	Snow depth
H_{snow}	W m^{-2}	Snow surface sensible heat flux
H_{stalk}	W	Sensible heat flux from stubble stalk to air
H_{stub}	W m^{-2}	Areal average sensible heat flux from stubble to atmosphere
h_v	m	Height of vegetation/exposed stubble height
i	-	Interval
INF	mm	Infiltration
j	-	Number of samples
k	-	Extinction coefficient
k_b	-	Direct beam extinction coefficient
k_b'	-	Direct beam extinction coefficient with forward scattering
k_d	-	Diffuse extinction coefficient
K_h	-	Eddy diffusion coefficient
L	m	Patch length
LAI	m^2 m^{-2}	Leaf area index
LE	W m^{-2}	Areal average latent heat flux
LE_A	W m^{-2}	Local-scale sensible heat advection
LE_{snow}	W m^{-2}	Snow surface latent heat flux
L_f	334 kJ kg^{-1}	Latent heat of fusion
L_s	2835 kJ kg^{-1}	Latent heat of sublimation
LW_{atm}	W m^{-2}	Longwave radiation above canopy
LWC	mm or kg m^{-2}	Snowpack liquid water content
LWC_{max}	mm or kg m^{-2}	Snowpack maximum liquid water content
LW_{snow}	W m^{-2}	Snow surface longwave radiation
LW_{stalk}	W	Stubble stalk longwave radiation
M	mm or kg m^{-2}	Snowpack meltwater discharge
M_{excess}	mm or kg m^{-2}	Excess meltwater
n	-	Exponential wind decay coefficient
N_{forced}	-	Forced convection Nusselt number
N_{free}	-	Free convection Nusselt number
PAI	m^2 m^{-2}	Plant area index
$p(A_p)$	-	Patch area probability
$p(L)$	-	Patch length probability
Ppt	mm or kg m^{-2}	Precipitation
q	kg kg^{-1}	Specific humidity
Q_A	W m^{-2}	Advected energy flux
$\overline{Q_A}$	W	Areal average advection to snow surface

Q_g	W m^{-2}	Ground heat flux
Q_m	W m^{-2}	Snowmelt energy
Q_{net}	W m^{-2}	One-dimensional net snow surface energy
Q_p	W m^{-2}	Advected energy from precipitation
q_s	mm or kg m^{-2}	Blowing snow sublimation
q_{sat}	kg kg^{-1}	Saturated specific humidity
q_{sc}	kg kg^{-1}	Snow surface specific humidity
q_{sf}	kg kg^{-1}	Snow-free surface specific humidity
Q_{snow}	W m^{-2}	Snowpack energy
r	m	Stubble stalk radius
r_a	s m^{-1}	Aerodynamic resistance between snow and atmosphere
$Rain$	mm or kg m^{-2}	Rainfall
Re	mm or kg m^{-2}	Reynolds number
RH	%	Relative humidity
R_{net}	W m^{-2}	Net snow surface radiation
row	m	Stubble row spacing
r_s	s m^{-1}	Sensible heat resistance between stubble stalk and atmosphere
S	-	Scalar source/sink rate
s	110.4 K	Viscosity coefficient
S_0	-	Soil surface saturation
SAI	m^2 m^{-2}	Silhouette area index
S_i	-	Antecedent soil saturation
S_{max}	mm or kg m^{-2}	Maximum detention storage
$Snow$	mm or kg m^{-2}	Snowfall
S_{ret}	-	Ratio of filled detention storage
SW_{atm}	W m^{-2}	Above canopy shortwave radiation
SW_{snow}	W m^{-2}	Snow surface shortwave radiation
SW_{stalk}	W	Stubble stalk shortwave radiation
t	s	Time
t_0	hr	Infiltration opportunity time
T_a	°C or K	Air temperature
T_i	K	Precipitation temperature
T_m	273.15 K	Melting temperature of water
T_{min}	K	Minimum snowpack temperature
T_{rad}	K	Radiometric snow surface temperature
T_{sc}	°C	Snowcover surface temperature
T_{sf}	°C	Snow-free surface temperature
T_{si}	K	Initial soil temperature
T_{snow}	K	Snowpack temperature
T_{soil}	°C	Soil surface temperature
T_{stub}	K	Stubble temperature

T_{wat}	°C	Ponded water surface temperature
u	m s^{-1}	Horizontal wind speed
u^*	m s^{-1}	Friction velocity
u_h	m s^{-1}	Wind speed at the top of the stubble canopy
U_{snow}	J	Snowpack internal energy
$U_{snow-min}$	J	Minimum snowpack internal energy
U_{stalk}	J	Stubble stalk internal energy
v	-	Albedo decay coefficient
V	m^3	Stubble stalk volume
vf_{sky}	-	Sky view factor from the perspective of the snow
vf_{stub}	-	Stubble view factor from perspective of a single stalk
w	m s^{-1}	Vertical wind speed
W	-	Weisman stability parameter
x	m	Horizontal distance
z_0	m	Aerodynamic surface roughness
z_{0s}	0.005 m	Snow-surface roughness
z_m	m	Measurement height
z_p	m	Profile depth of interest
β	J K^{-1}	Stubble stalk heat capacity
ε_{snow}	-	Snow emissivity
ε_{stub}	-	Stubble emissivity
θ_{elev}	rad	Solar elevation angle
θ_{lw}	-	Liquid water capacity of snow
κ	0.4	von karman constant
μ	kg m^{-1} s^{-1}	Viscosity of air
ξ	mm or kg m^{-2}	Blowing snow erosion or deposition
ρ_{air}	kg m^{-3}	Density of air
ρ_{A-stub}	number of stalks m^{-2}	Areal density of stubble stalks
ρ_{ice}	917 kg m^{-3}	Density of ice
ρ_s	121 kg m^{-3}	Volumetric mass density of stubble
ρ_{snow}	kg m^{-3}	Snow density
ρ_{water}	1000 kg m^{-3}	Density of water
σ	$5.6x10^{-8}$ W m K^{-4}	Stefan-Boltzmann constant
σ_0	mm or kg m^{-2}	Standard deviation of pre-melt SWE
τ	-	Transmittance
τ_b	-	Direct beam transmittance
τ_{bulk}	-	Bulk direct and diffuse transmittance
τ_d	-	Diffuse transmittance
ϕ_{snow}	-	Snow porosity
χ	-	F_{water} coefficient
ω	-	Scattering coefficient
γ	kPa K^{-1}	Psychrometric constant

Superscripts

$*$	-	Net
$\downarrow$	-	Incoming
$\uparrow$	-	Outgoing

Chapter 1: Introduction

1.1 Introduction

A defining feature of Canadian Prairie hydrology is the development of a seasonal snowpack. The resulting springtime snowmelt is typically the largest annual water source for runoff, 80% annually (Gray and Landine, 1988), and can lead to significant infiltration (Granger et al., 1984). A dominant factor in shaping the surface characteristics and consequently the hydrological processes of the Canadian prairie surface is agriculture. Crop production systems in Alberta, Saskatchewan and Manitoba cover over 25 million hectares (~50% of the prairie ecozone) and, with a large-scale shift to zero tillage since the early 1990's, lead to large scale dynamic exposure of standing stubble over the snowmelt season. The physical relationships between the stubble remaining after harvest and the role it has in modifying snow-atmosphere interactions have implications for a large area of the Canadian prairies and other areas with similar climates and crops including the Great Plains of the United States and the Eurasian steppes.

Patterns of snow accumulation and ablation (spatial variability of melt rates, timing and quantity) have direct impact upon the partitioning of infiltration and runoff (Gray et al., 2001). The runoff and infiltration generated from snowmelt have significant hydrologic, agronomic and land-atmosphere interactions implications that vary interannually. In this context the role of stubble left behind by agricultural management practices, and how it modifies the partitioning of surface-atmosphere energy exchanges over the snow surface needs to be understood as these exchanges influence snow accumulation and ablation processes, which in turn controls snowmelt runoff, infiltration and evaporation/sublimation. A concurrent and poorly constrained snowmelt process in this region is the local-scale advection of energy from snow-free surfaces to the snowpack as snowcover disaggregates over melt. The combination of dynamic energy contributions from emerging stubble and advection from the expanding snow-free areas over melt complicate the understanding and prediction of snowmelt in the Canadian Prairies.

Snowcover in this semi-arid cold region is typically shallow and has high variability during accumulation and ablation leading to significant unresolved challenges in quantifying the

snow surface energy balance in the presence of exposed stubble. The drought of 2001-2002 (Hanesiak et al., 2011) and flooding events since of 2009 (Dumanski et al., 2015) have renewed interest in agricultural water management. Snowmelt water has broad implications for agricultural production (Gray et al., 1990), is a water source for rural populations and economies (Corkal et al., 2004) and can cause intermittent localized flooding (Dumanski et al., 2015). Despite the significant socioeconomic implications of snowmelt on the Canadian Prairies, understanding and prediction of this shallow snowpack and its melt, is limited. Advancing snowmelt understanding on the Canadian Prairies will only become more critical to ensure agriculture and socioeconomic resilience as the climate changes (Pomeroy et al., 2009b).

1.2. Literature Review

The literature review provides an overview of pertinent features of prairie hydrology and summarizes work pertinent to the process understanding of snow-soil-stubble-atmosphere interactions, local-scale advection, and meltwater partitioning on the Canadian prairies during snowmelt.

1.2.1. Prairie Hydrology

The hydrology of the Canadian Prairies is defined by its high latitude continental interior locations leading to large variations in seasonal temperatures and limited precipitation, annual precipitation average 300-400 mm (Pomeroy et al., 2007) of which about a third occurs as snowfall (Gray and Landine, 1987a). This leads to two distinct but interrelated hydrological periods for winter and summer. Winter processes are characterised by snow accumulation and wind redistribution with mid-winter melt events frequent in south-western and infrequent in the north-eastern regions (Fang et al., 2007). Infiltrability of soils is limited seasonally as the soils freeze (Gray et al., 2001). Spring time is the interface of the two seasons and is characterised by high runoff rates as a result of frozen soils with limited infiltration coincident with the often rapid snowmelt water release from snowpacks (Gray et al., 1985). After spring melt and soil thaw the warm season (summer) processes are defined by rainfall events that are frontal in spring and early summer and convective in late summer (Gray, 1970). The summer rainfall inputs are typically balanced by evapotranspiration (Gray, 1970) and high unfrozen infiltration rates and soil water–holding capacities leading to limited warm season runoff (Elliot and Efetha, 1999).

Recent observations show a shift to more rainfall events being generated by frontal systems (Shook and Pomeroy, 2012) and an increase in mid-summer runoff (Pomeroy et al., 2014). Due to limited topographic relief and geologically recent glaciation the drainage network of the Canadian Prairies is poorly developed resulting in large non-contributing areas (Pomeroy et al., 2005). Subsurface lateral movements are limited and recharge is depression focused due to the low hydraulic conductivity of the underlying unconsolidated glacial tills (Hayashi et al., 2003). The resulting surface water features, in the absence of agricultural drainage, are generally ephemeral wetland complexes which in high runoff years connect and disconnect through fill and spill mechanisms (Phillips et al., 2011). The spring snowmelt event is typically the largest consistent flux of water across the region that has implications for water resources throughout the year due to its role in recharging the hydrological system.

1.2.2. Snow Accumulation

Snowmelt is a function of the pre-melt snowpack and a large body of work has been aimed at characterizing snowcover in relation to topography, land cover and climate. In open environments the dominant process affecting the accumulation and spatial variability of a snowpack is blowing snow (Clark et al., 2011; Pomeroy et al., 1993). The blowing snow process is a function of snow availability, fetch, wind speed, surface roughness and temperature (Pomeroy et al., 1993) and on the Canadian Prairies can be responsible for the sublimation, transport and redistribution of up to 75% of the annual snowfall (Pomeroy and Gray, 1995). Physically, blowing snow is comprised of three fluxes including saltation, suspension and sublimation and these were first fully described by Pomeroy et al. (1993) in the Prairie Blowing Snow Model (PBSM). Spatial distribution of PBSM has been accomplished with its coupling to a windflow model (Walmsley et al., 1986) to develop the Distributed Blowing Snow Model (Essery et al., 1999).

Exposed vegetation determines the surface roughness that in turn controls the various blowing snow processes leading to snow erosion or deposition. In areas of little surface roughness, minimal stubble or bare soil, blowing snow is initiated sooner leading to greater sublimation losses and transport (Pomeroy et al., 1991). Areas of greater surface roughness, such as standing stubble, will have greater deposition though snow erosion can be still initiated when wind velocities produce a shear stress that exceeds the sum of that exerted on the stubble and the

threshold shear stress for snow erosion (Pomeroy et al., 1993). Exposure of vegetation greatly diminishes the shear stress exerted by the wind on the snow and typically limits snow erosion until the snow depth is near the height of the vegetation (Pomeroy and Brun, 2001). Differences in exposed vegetation become less relevant as snow accumulates to the vegetation height; filled stubble will behave as a bare field (Pomeroy and Gray, 1994). The feasibility to manage end of winter snow water equivalent (SWE) distributions for agricultural purposes has been well studied (Pomeroy et al., 1990) with results summarized in Table 1. Modelling has estimated that the saltation and suspension fluxes are doubled and sublimation increases by 7% for bare fields with respect to stubble fields (Gray et al. 1989).

Table 1.1: Agricultural Snow Management Practices on the Canadian Prairies

Snow Management Practice	SWE increase*
Tall Stubble: crop swathed/combined to leave stubble of uniform height	2.7mm/cm stubble**
Alternate Height Stubble: height of the stubble is alternated between low and high for each swather/combine pass	32%
Trap Strips-Clipper: strip of crop with grain heads clipped left each swather/combine pass	104%
Trap Strip- Deflector: strip of crop with grain heads intact left each swather/combine pass	22%
Leave Strip: 30cm strip of crop unharvested every 1, 2 or 3 swather/combine widths	91%
Competitive barrier: tall grass barriers planted in rows spaced 9 m to 15 m apart	120%

*SWE increase with respect to normal uniform height (~25cm) stubble, **Tall stubble SWE increase as a function of snow density. Values summarised from Nicholaichuk et al. (1985)

1.2.3. Snowmelt

Snow ablation on the Canadian Prairies is driven by the surface energy balance and its interactions with the properties of the end of season snow accumulation. The snow surface energy balance is given by Gray and Male (1981) as:

$$Q_m = SW^*_{snow} + LW^*_{snow} + H_{snow} + LE_{snow} + Q_p + Q_g + \frac{dU_{snow}}{dt} \quad (1.1)$$

where Q_m is the net energy available for snowmelt, SW^*_{snow} and LW^*_{snow} are the net short and long wave radiation respectively, H_{snow} and LE_{snow} are the turbulent sensible and latent heat fluxes respectively, Q_p is the energy advected by precipitation (often ignored on the

Prairies), Q_g is the ground het flux and dU_{snow}/dt is the net change in snowpack internal energy. In open high latitude environments with shallow snow, such as the Canadian Prairies, the variable response of snowmelt to variable meteorology and land surface characteristics is complicated with the challenges in implementing an energy balance approach to these unique snowpacks. The source of energy for early or mid-winter melt is typically longwave radiation (Granger et al., 1978). As day lengths and sun angles increase shortwave radiation becomes the dominant forcing relative to longwave radiation (Gray and Landine, 1987b). Turbulent fluxes are much more dynamic and dependent upon meteorology as they are related to wind speeds and temperature gradients (Granger and Male, 1978). Latent heat flux, sublimation during daytime and condensation during nighttime has been observed to have a minimal net contribution while sensible heat can have a large impact on the cumulative net energy balance (Granger and Male, 1978). The sensible heat flux contributions increase over the course of melt as the snow surface transitions from continuous snowcover into a heterogeneous surface of bare soil and snow patches (Granger and Male, 1978). In addition, differences in energetics across snowcovered and snow-free areas leads to a heterogeneous distribution of surface temperatures that acts to increase near surface air temperatures and local scale advection of sensible heat to snow as air moves over surface transitions (Shook and Gray, 1997). An additional challenging dynamic of shallow snow is the relative importance of tracking cold content as it buffers melt processes (Granger and Male, 1978). Shallow snows have a small heat capacity to moderate energy fluxes relative to deeper snow and therefore exhibit diurnal patterns of melt water release and refreezing (Gray and Landine, 1987b). Land surface characteristics, primarily vegetation and topography, increase the spatial variability of the melt processes. Specific dynamics of each relevant term of the snow pack energy balance are discussed in detail hereafter.

1.2.3.1. Shortwave Radiation

Shortwave radiation typically dominates the end of winter snowmelt event of high latitude environments (Gray and Landine, 1986). Inter-annual differences in its relative magnitude to the overall energy balance depends upon the timing of melt as the incident solar radiation increases over the course of the season (Shook, 1995). The main driver of the incoming shortwave radiation spatial variability is the geometric relationship between incident radiation and the land surface and often accounted for by the methods of Garnier and Ohmura (1968). The absorption of the shortwave radiation by the surface is governed by the surface albedo, typically

between 80 and 90% for fresh snow (Gray and Landine, 1987a). Snow albedo decreases with time due to metamorphism changing radiation attenuation factors such as particle size, density, structure, wetness, foreign matter, snow depth and wavelength (Gray and Landine, 1987a; Kung et al., 1964).

Exposed vegetation modifies shortwave radiation by altering albedo decay and transmittance. The influence of vegetation exposure on albedo is predicated on approaching albedo as either an areal average or specific to snow. Vegetation has a lower albedo than snow thus the decay of areal average albedo over the course of snowmelt becomes a function of fractional vegetation exposure (Liston and Hiemstra, 2011). Upon the breakup of continuous snowcover Shook et al. (1993) showed a linear relationship between snowpack areal albedo and snowcovered area leading to a dramatic increase in the magnitude of net shortwave radiation over the course of melt (O'Neill and Gray, 1973). Vegetation can also influence the shortwave radiation flux by shading the snowpack, intercepting the radiation before it reaches the surface (Aase and Siddoway, 1980; Bewley et al., 2007). This is apparent in the observations of an inverse relationship between albedo and stubble height (Aase and Siddoway, 1980). Stubble and soil albedos also vary over the course of the winter as the decay of stubble and breakdown of soil clods lead to an increase and decrease in albedo respectively.

Most of the work on radiative transfer through canopies to underlying snowcover has focused on large vegetation (i.e. forest canopies). Approaches have included relating the interaction of solar angle and leaf area index (Pomeroy and Dion, 1996), sky view fraction (Musselman et al., 2012), ray tracing (Essery et al., 2008b), multi-stream models (Blyth et al., 1999) and taking into account shading in sparse canopies (Bewley et al., 2007). Radiative transfer through sparse canopies has also been studied from an agricultural perspective with approaches including dual stream models (Ross, 1981), clumped vegetation (Campbell and Norman, 1998; Kustas and Norman, 2000), and multi-layered canopies (Flerchinger, 2000; Zhao and Qualls, 2005). To date no literature has been found that quantifies the dynamic influence of short vegetation, specifically stubble, on the transmittance of incoming radiation to a snow surface of varying depth.

1.2.3.2. Longwave Radiation

Longwave radiation is dependent upon the temperature of its emission source according to the Stefan-Boltzmann equation, and the fluxes incident upon the surface come from either atmospheric or terrestrial origins (Sicart et al., 2006). The incoming atmospherically emitted longwave radiation is dependent upon the sky view fraction, cloud cover, air temperature and humidity which modifies the atmospheric emissivity (Sicart et al., 2006). The incoming longwave radiation from terrestrial sources in turn is dependent upon the residual of the sky view fraction and the effective surface temperature of the portion of terrain in view (Sicart et al., 2006). The emission of longwave radiation from the surface is simply a function of the surface temperature. The emissivities of the different sources vary and are generally higher for ground relative to sky sources (Sicart et al., 2006). Net longwave radiation can be similar or higher than shortwave radiation during cloudy periods due to increased atmospheric emissivity (Granger and Gray, 1990) and is important in the simulation of snowmelt in early spring due to the low solar energy and high fresh snow albedo (Sicart et al., 2006).

Like shortwave radiation the vegetation influence upon longwave radiation has been studied most extensively in forest environments (Essery et al., 2008a; Gelfan et al., 2004; Pomeroy et al., 2009a).The most striking case of this is with high trunk or branch temperatures as a result of a large net shortwave radiation flux upon the low albedo vegetation, which re-radiates this energy in the form of longwave radiation to the surrounding snow (Pomeroy et al., 2009). The case of longwave emissions from stubble and their magnitude with respect to the surface energy balance has not be explicitly measured but may be important as noted by Bewley et al., (2010) for the case of exposed shrubs.

Existing understandings of long and shortwave radiative transfer through short sparse canopies are sufficiently well developed to quantify radiative transfer through stubble. The challenge is in applying this understanding when the stubble structure, with respect to the depleting snow surface, is dynamic.

1.2.3.3. Turbulent Exchanges

Sensible and latent heat fluxes to the snow surface are a result of the turbulent transfer of heat and water vapor between the land surface and atmosphere. The relative contribution of these

fluxes to the annual snowmelt varies with respect to seasonal timing and location (Gray and Male, 1981; Morris, 1989). Studies have shown the turbulent transfer contributions to melt to be insignificant over continuous snowcover (Pomeroy et al., 1998), vary inter-annually (Granger and Male, 1978) and can make significant contributions to melt once snowcover becomes heterogeneous (Shook and Gray, 1997). Direct measurement of these fluxes over snow have utilized eddy covariance techniques (Andreas, 1987; Arck and Schertzer, 2002; Box and Steffen, 2001; Munro, 1989; Smeets et al., 1998) while estimation methods have relied upon bulk transfer (Kondo and Yamazawa, 1986; Moore, 1983), aerodynamic profiles (Denby and Snellen, 2002; Hood et al., 1999; Munro and Davies, 1978), or empirical correlation (Gray and Landine, 1986). Quantification methods often struggle with meeting the respective assumptions or required conditions (Helgason and Pomeroy, 2005; Helgason and Pomeroy, 2012).

As with radiative transfer, the studies of turbulent transfer through canopies have focused on forested environments. Validity of local gradient diffusion approaches, K-theory, has been questioned with dramatic failures associated with observations of counter-gradient fluxes in these environments. Improved methods have developed higher-order closure models (Wilson, 1989) as well as Lagrangian approaches (Raupach, 1989). In contrast K-theory is still considered valid in short and sparse canopies (growing season crops) due to low leaf area indices and uniform source density profiles (Wallace, 1991). In the absence of a contradictory analysis K-theory can be assumed to be valid for a melting exposed stubble surface. Thus K-theory predicts that as the exposure of short vegetation during melt increases the surface roughness, thereby increasing the ability of the surface to absorb momentum, the increased turbulence will increase turbulent transfer (Prueger and Kustas, 2005). Observations during the growing season have noted the suppression of latent heat transfer by the decoupling of the surface and atmosphere by the airflow displacement of the stubble (Brun et al., 1984; Burt et al., 2005; Cutforth and McConkey, 1997) and reduced wind speeds (Aase and Siddoway, 1980). Literature quantifying the influence of incremental stubble exposure on latent and sensible heat turbulent transfer during snowmelt has not been found to date.

1.2.3.4. Ground Heat Flux

The role of the ground heat flux varies over the course of the snowmelt on the Canadian Prairies but is typically negligible due to the small temperature gradient between the soil and

base of the snowpack (Granger and Male, 1978; Pomeroy et al., 1998; Zhao et al., 1997). Observations show that during early melt, ground heat flux contributions are negligible while during active melt it can remove up to 5.5% of the energy otherwise available for snow melt (Granger and Male, 1978). The ground heat flux is closely connected to the role of meltwater infiltrating the soil at the base of the snowpack which varies inter-annually and can be influenced by the commonly observed presence of basal ice layers which restrict infiltration (Zhao and Gray, 1999). The presence and type of crop residues has been shown to modify the soil heat fluxes with largest differences associated with flat stubble relative to standing stubble and bare soil respectively (Flerchinger et al., 2003). Observations are complicated by the need to estimate the thermal capacity of the soil matrix with its dynamic frozen and liquid water content, due to meltwater infiltration and soil thaw (Zhao et al., 1997). Numerical methods have been developed that solve coupled mass and energy equations that can account for heat and water inputs into a multiphase soil matrix (Flerchinger and Saxton, 1989; Zhao et al., 1996).

1.2.3.5. Snowpack Internal Energy

Fluctuations in the internal energy content of the snow can moderate the surface energy balance of the snowpack. Quantification is difficult due to the fact that snow is a multiphase porous structure with high permeability and heterogeneity that undergoes wind redistribution and metamorphism (Helgason and Pomeroy, 2012a). Physically based models (SNTHERM, Jordan (1991)) are available that account for many of these factors. The role of vegetation within and exposed above the snow complicates the internal energy dynamics, relative to pure snow that many models assume, by changing the snow density and adding additional energy pathways through the snow. There is increased conduction though stubble stalks and increased convection with a larger snow surface area through preferential melting of snow around exposed stalks.

1.2.3.6. Local-Scale Advection

Canadian Prairie snowcover is highly variable and shallow and during melt breaks up into a heterogeneous surface of bare and snow patches. The behaviour of the snowcover depletion phenomena can largely be described by the spatial variability of pre-melt SWE and the variability in the surface energy balance leading to spatially variable areal average melt rates. Statistically, assuming a log-normal SWE distribution, the depletion of snowcover can be estimated by a simple hyperbolic tangent function dependent upon the coefficient of variability

of the pre-melt SWE and melt amount (Essery and Pomeroy, 2004). On small scales, statistical description of the snow or bare ground patches area, perimeter, and length can be generated by taking advantage of applicable fractal scaling laws (Granger et al., 2006).

The differences in energetics across snowcovered and snow free areas leads to a heterogeneous distribution of surface temperatures that in the presence of air flow across the surface leads to local scale advection of sensible heat to snow. Sensible heat advection has been found to be responsible for providing the majority of the sensible heat flux, contributing up to 55% of the snowmelt energy balance (Granger and Male, 1978), resulting in areal melt rates being the greatest when snowcover is between 40% and 60% (Shook 1995; Marsh et al. 1997). The challenges in directly measuring advection across heterogeneous surfaces can be constrained in ideal experimental conditions, leading to reliable measurements (Kochendorfer and Paw U, 2011), but the dynamic nature of snowcover ablation has led to limited observations of the phenomena (Shook 1995; Granger et al. 2006; Mott et al. 2013). The flow of air over heterogeneous surfaces leads to the formation of internal boundary layers (Garratt, 1990). Measurements of these internal boundary layers across snow surface transitions reflect established power laws of boundary layer height (Shook 1995; Granger et al. 2006). Granger et al. (2002) used this behavior to calculate sensible heat advection through boundary layer integration. In contrast to these findings the formation of boundary layers has been attributed as a cause of atmospheric decoupling of the atmosphere from the snow surface leading to the suppression of sensible heat advection in the Alps (Mott et al., 2013). Due to the complexity of the process and difficulties in observation, modeling has been the focus of much more work on this topic. Early work by Weisman (1977) applied mixing length theory and subsequent approaches have employed the calculation of advection efficiency as a function of snowcovered area (Marsh et al., 1999), numerical modelling (Liston, 1995) and tile models taking into account the fractal nature of snowcover (Essery et al., 2006). Numerical models provide the most detailed description of the processes but are constrained to idealized boundary conditions and are not appropriate for application in hydrological models. In contrast the tractable tile based models that may be appropriate for implementation in hydrological models have insufficient representation of spatial energy redistribution across tile boundaries (Essery et al., 2006; Ménard et al., 2014). Most models also consider the snow free surface to be of constant temperature which differs from observations (Granger et al., 2006). Sensible heat advection is a difficult problem to

address with contrasting findings in the literature and latent heat advection from ponded meltwater has not had any consideration during snowmelt.

The characteristics of vegetation in open environments has been shown to influence the dynamics of surface heterogeneity. In terms of snowcover depletion, rougher surfaces lead to theoretically longer snowcover depletion periods (longer on stubble vs. fallow fields). More detailed observations considering stubble characteristics or type are not available to understand their role. Theoretical understandings (Garratt, 1990) and observations (Granger et al., 2006) of advection show that the greater the upwind surface roughness the quicker the establishment of and the greater the depth of the internal boundary layer resulting in greater energy advection. The theoretical influence of surface roughness on snowcover depletion and spatial variability of melt energy due to advection are contradictory and as a result, an understanding of how differences in stubble attributes may modify spatial heterogeneity during melt is currently unavailable.

1.2.4. Meltwater Partitioning

The snowmelt process governs the rate and spatial distribution of snowmelt water produced at the snow soil interface which, along with the spatial variability of frozen soil infiltrability, governs the runoff and infiltration processes; the most visible manifestation of the snowmelt process (Gray et al., 2001). The focus of studies relating agricultural practices and snowmelt to date has been the infiltration and runoff responses (Elliot and Efetha, 1999; Granger and Gray, 1984; Nicholaichuk and Gray, 1986; van der Kamp et al., 2003). How stubble changes the energetics of snowmelt processes has been a secondary consideration. These studies show that increases in pre-melt SWE led to increased infiltration though the relationship is not linear (Gray et al., 2001). Stubble does have the ability to influence these processes. Stubble can influence the amount of SWE (Nicholaichuk et al., 1985) and snowmelt rates (Willis et al., 1969), thus infiltration opportunity time and the associated tillage impacts the soil structure/macropore connectivity (Strudley et al., 2008), thus infiltration class (Pomeroy et al., 1990) and antecedent soil moisture (Gray and Maule, 1994). In small plot studies the presence of stubble has been noted to lead to earlier and faster melt of a snowcover leading to a greater amount of runoff (Willis et al., 1969). However, direct measurements of snowmelt runoff do not show clear land cover influences due to the large uncertainty in runoff gauging and delineation of contributing area (Hodder et al., 2013). The subtle influence of stubble on runoff and

infiltration has the potential to have regional hydrological implications, but the underlying process understandings are unresolved.

1.2.5. Summary

A large body of literature exists that describes the snow accumulation and ablation processes on the Canadian Prairies. In spite of this, there has been little work on understanding the role that the gradual exposure of vegetation over the course of snowmelt has on the energy balance and hydrological processes occurring at the time. This may be in part be due to two reasons. First, hydrological research has not maintained pace with the large changes observed in agricultural management practices in the last two decades. With the decline in soil and water conservation issues due to the widespread adoption of continuous cropping and zero-tillage, interest has shifted to other problems, without reconsidering the role new agricultural practices have on snowmelt processes in the region. Second, stubble influences and advection contributions on snowmelt processes are difficult to control for in experimental design and are often deemed to be negligible relative to other processes of interest.

1.3. Research Gaps

Substantial research describes the snow ablation processes on the Canadian Prairies. Four specific challenges are identified in this work that limit the understanding of prairie snow melt and its implications.

First, the ability to resolve snowmelt dynamics from directly observing snowmelt is hampered by the uncertainty inherent to observation of snowpack properties. Snow surveys are well established to be a generally reliable method to estimate SWE from sampling snow depth with a ruler and snow density with snow cores with the technique essentially unchanged for over a century (Mergen, 1992). Unfortunately, snow surveying has uncertainty associated with sampling strategies, number of samples and transect design to ensure SWE estimate is representative of domain in question (Steppuhn and Dyck, 1974; Pomeroy and Gray, 1995), as well as depth and density sampling errors (Berezovskaya and Kane, 2007; Goodison et al., 1987). It is also prone to observer bias as safe and accessible areas tend to be over sampled (DeBeer and Pomeroy, 2010), is a destructive sampling method (Kinar and Pomeroy, 2015), and is very labour intensive (Davis, 1973). Snow surveying is best suited to areas of deeper, rather

than shallow snow where errors are small relative to the snowpack (Goodison et al., 1987). The uncertainty associated with snow surveying may be inappropriate to observe the subtle and complex relationships associated with the melt forcings and their response to land cover on the Canadian Prairies. In addition, snowcover geometry is poorly constrained with snow survey observations or at sufficient spatiotemporal resolution in satellite remote sensing (Goodison et al., 1987; Shook and Gray, 1996). Alternative observation approaches to quantify snow water equivalent and snowcover at high spatial and temporal resolutions require investigation.

Second, the role that the gradual exposure of short vegetation over the course of snowmelt has on the snow surface energy balance and snowmelt process has not been fully addressed. Hydrological research has not maintained pace with the large changes observed in agricultural management practices in the last two decades. There has been widespread adoption of zero-tillage agriculture and continuous cropping across the Canadian Prairies (Awada, 2013). These practices are characterized by standing crop residues that remain erect throughout the snow accumulation and ablation periods in contrast to bare surfaces where crop stubbles are incorporated into the soil post-harvest. In 1990 zero-tillage was applied to 1.7 million hectares and this has increased to 17.3 million hectares in 2016, 65% of the total land area prepared for seeding (Figure 1.1: Statistics Canada, 2016). The literature available suggest that the presence of stubble will have an influence upon the surface energy balance. Notably; radiative flux through short sparse canopies may modify incident radiation at the surface (Kustas and Norman, 2000), partitioning of the radiative flux may enhance the long wave contribution (Ménard et al., 2014), turbulent transfer may be enhanced (Prueger and Kustas, 2005), with the potential for decoupling (suppression of turbulent transfer) in the presence of tall exposed stubble heights (Aase and Siddoway, 1980), and local scale sensible heat advection may be enhanced (Granger et al., 2006).

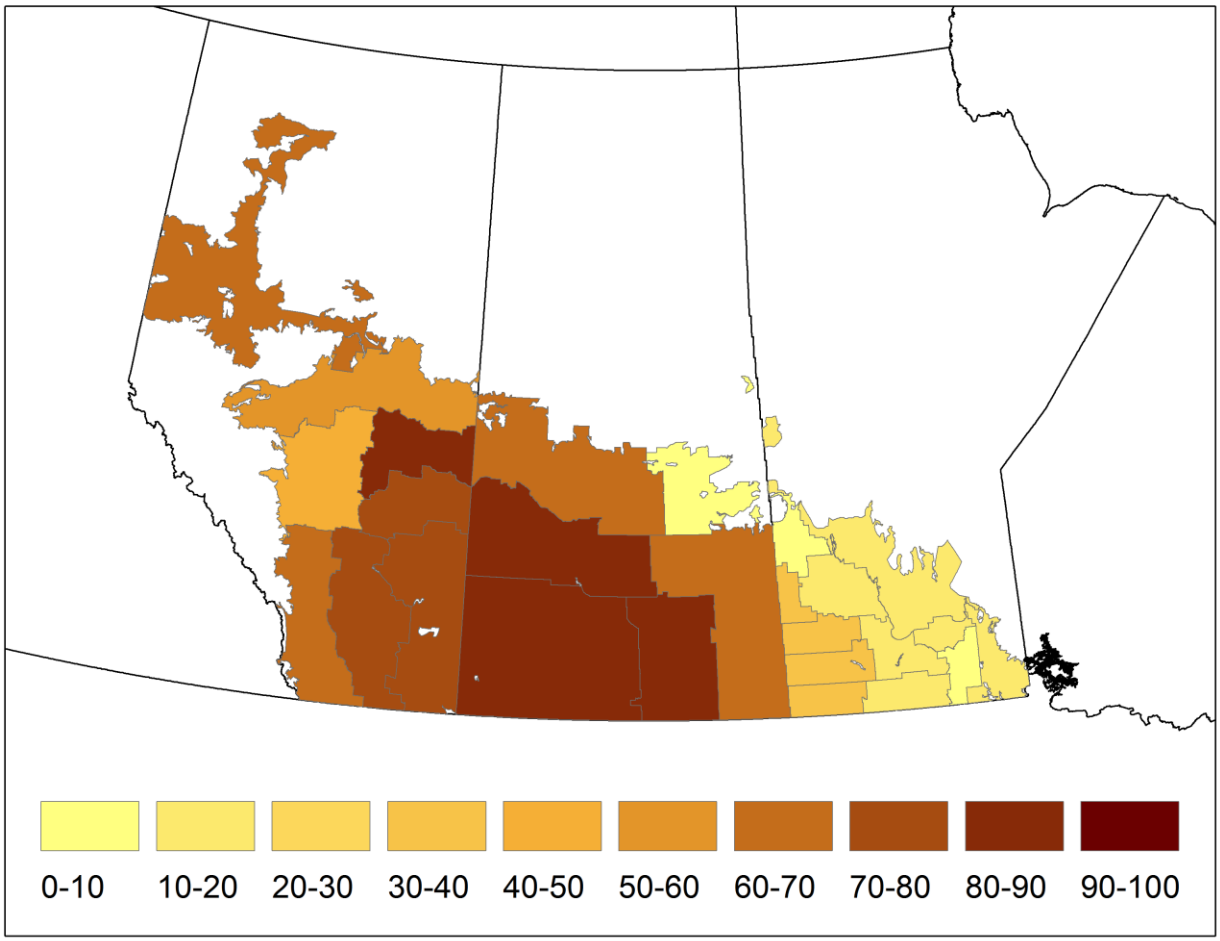

Figure 1.1: Percentage of prepared cropland managed with zero-tillage agricultural management practices. (Statistics Canada 2016)

Third, while local-scale advection has been conceptualized and indirectly observed, there have not been any rigorous attempts to directly measure advection fluxes for sensible or latent heat. From indirect observations, sensible heat advection has been found to be responsible for providing significant portions of the sensible heat flux that is greatest when snowcover is between 40% and 60% (Shook 1995; Marsh et al. 1997). The challenges in directly measuring advection across heterogeneous surfaces can be constrained in ideal experimental conditions, leading to reliable measurements (Kochendorfer and Paw U, 2011), but the dynamic nature of snowcover ablation has led to limited observations of the phenomena (Granger et al., 2006; Mott et al., 2016, 2013; Shook, 1995). The flow of air over heterogeneous surfaces leads to the formation of internal boundary layers (Garratt, 1990) and observations of their development across snow surface transitions reflect established power laws of boundary layer height (Shook 1995; Granger et al. 2006). Due to the complexity of the process and difficulties in observation,

modeling has been the focus of much more work on this topic (Essery et al., 2006; Granger et al., 2002; Liston, 1995; Mott et al., 2015, 2017; Weisman, 1977). Sensible heat advection is a difficult problem to address with contrasting significance in the literature (Essery et al., 2006; Mott et al., 2013) and latent heat advection from ponded meltwater has not had any consideration during snowmelt. The relative importance of sensible and latent heat with respect to the overall energy balance needs to be quantified. A model framework to address both sensible and latent heat advection is also needed to properly account for the energy fluxes driving snowmelt in predication models.

Fourth, there is no fully coupled process-based understanding of how stubble influences snow accumulation, snowmelt, and partitioning of meltwater into infiltration or runoff. Previous research has focused on stubble implications upon snow accumulation and how that modifies the amount of snow available to melt (Fang and Pomeroy, 2008; Gray and Granger, 1985; Gray and Maule, 1994; Maule and Gray, 1994; Pomeroy and Gray, 1995; Richards, 1986; Steppuhn and Erickson, 1978). Extensive research on stubble management influences on frozen soil infiltration and snow redistribution has developed an empirical understanding of the system dynamics (Pomeroy et al., 1990). A complete process representation of the stubble and meltwater partitioning relationship has been impossible to date without a physically based understanding of stubble-snowmelt interactions. Such a framework is needed to address, develop, and evaluate the ability to manage stubble for hydrologic or agronomic objectives now and when subjected to a different climate.

Significant research gaps limit the understanding and prediction of snowmelt on the Canadian Prairies and deserve investigation due to their potential socio-economic implications.

1.4. Objective and Research Questions

The overarching research objective of this work is:

To improve the understanding of the interactions between stubble, snow and the atmosphere of Canadian Prairie agricultural regions during snowmelt.

Four objectives have been defined to address the research gaps identified and are:

Objective 1: Assess unmanned aerial vehicle technology to observe properties and dynamics of shallow snowpacks.

Objective 2: Observe and model local-scale sensible and latent heat advection during snowmelt.

Objective 3: Quantify the relationship between stubble emergence and processes governing the snow surface energy balance.

Objective 4: Develop a process-based understanding of the influence of stubble management upon meltwater partitioning.

1.5. Thesis outline

The results are presented in the form of a manuscript style thesis. Specific objectives are associated with separate chapters.

Chapter 2 (Objective 1) determines if the quantification of prairie snow packs can be improved with an unmanned aerial vehicle (UAV) system, a novel observation technique. The spatial distribution of snow depth is a critical metric to quantify to understand the role of crop stubble on snowmelt processes. Ultimately SWE is the variable of interest but it has been shown that the bulk of the spatial variability of SWE in shallow situations is found in the spatial variability of snow depth (Jonas et al., 2009; Pomeroy and Gray, 1995). Imagery from UAVs combined with structure from motion (SfM) techniques are an emerging tool to generate high accuracy digital surface models in geosciences and have the potential to map snowcovered area and snow depth and are tested herein.

Chapter 3 (Observation portion of Objective 2) presents direct observations of local-scale advection and its influence upon the snowmelt energy balance. The development and deployment of a novel observation system that could directly measure the relative role of sensible and latent heat advection on the snowmelt energy balance is described. This work provides the empirical evidence necessary to more fully constrain the spatial heterogeneity of the snowmelt energy balance in future models. The results and implications of a novel observation campaign are presented that quantify the relative roles of sensible and latent heat advection in the context of the overall snow melt energy balance. The identification of latent heat advection

during snowmelt is an especially exciting observation as it has previously been an undocumented component of the snowmelt energy balance.

Chapter 4 (Objective 3) focuses on the implications of emerging crop stubble upon the snow surface energy balance. Much of the cropland on the Canadian Prairies is managed with zero-tillage agricultural practices. The resulting gradual emergence of stubble from the snowpack over snowmelt is a phenomenon unrealized in any snowmelt model. This chapter quantifies the influence of stubble emergence on the snow surface energy balance with the development and validation of a physics-based model. The model is used to describe the energy balance interactions between snow, stubble, and atmosphere and the overall compensation of the individual energy terms in the surface energy balance. The findings help to describe subtle differences in wheat and canola snowmelt patterns and improves the understanding and prediction of snowmelt on the Canadian Prairies.

Chapter 5 (Modelling portion of Objective 2) presents a simple local-scale sensible and latent heat advection model framework. The significant sensible and latent heat fluxes observed in Chapter 3 motivated the development of a model framework that can quantify this lateral energy flux in a manner that that can be easily coupled to existing one-dimensional snow surface energy balance models. Previous work on boundary layer integration of sensible heat advection (Granger et al., 2002) is adapted to also considered latent heat advection. Existing scaling relationships to describe snowcover geometry (Shook et al., 1993a) are validated with high resolution classified snowcovered area derived from UAV imagery, as described in Chapter 2. Theoretical snowcovered area depletion (Essery and Pomeroy, 2004) and a new conceptual relationship between ponded water and frozen soil infiltration is included to describe the land surface dynamics driving advection. The implications of coupling this advection framework to the one-dimensional snowmelt energy balance from Chapter 3 are explored. The developed energy balance model that accounts for stubble emergence and advection processes represents a major improvement in the modelling capability and understanding of snowmelt on the Canadian prairies and any other semi-arid agricultural cold region.

Chapter 6 (Objective 4) couples the snowmelt model developed in Chapters 4 and 5 to existing snow accumulation (Pomeroy et al., 1993) and frozen soil infiltration (Gray et al., 2001) models to synthesize a new physically based process understanding of the influence of stubble

management upon snow processes and meltwater partitioning. This coupled model is employed to explore the interaction of stubble management, antecedent soil moisture, interannual variability, and climatic differences upon snow accumulation, snow melt, and meltwater partitioning processes. This modelling framework provides a detailed process understanding of stubble-meltwater partitioning interactions that reconfirms findings based on extensive field observation-based research on stubble management and frozen soil infiltration. Recommendations on stubble management practices are presented.

Each chapter focuses on specific deficiencies in our understanding of the complex snowmelt dynamics in cold semi-arid agricultural regions. A final conclusions chapter summarizes the main findings and identifies areas of future research needs. Overall the research presented in this thesis advances the understanding of the unique snowmelt dynamics and processes on the Canadian Prairies.

1.6. References

Aase, J. K., Siddoway, F. H. (1980). Stubble height effects on seasonal microclimate, water balance, and plant development of no-till winter wheat. Agricultural Meteorology, 21, 1–20.

Andreas, E. L. (1987). Spectral Measurments in a disturbed boundary layer over snow. Journal of Atmopsheric Sciences, 44(15), 1912–1939.

Arck, M., Schertzer, D. (2002). Problems in the determination of sensible heat flux over snow. Geografiska Annaler: Series A, Physical Geography, 84(3–4), 157–169.

Awada, L. (2013). Factors Affecting the Adoption of Zero Tillage Innovation on the Canadian Prairies. PhD Thesis, University of Saskatchewan, Saskatoon, Saskatchewan.

Berezovskaya, S., Kane, D. L. (2007). Measuring snow water equivalent for hydrological applications: part 1, accuracy of observations. In 16th International Northern Research Basins Symposium and Workshop (pp. 29–35).

Bewley, D. S., Pomeroy, J. W., Essery, R. (2007). Solar Radiation Transfer Through a Subarctic Shrub Canopy. Arctic, Antarctic, and Alpine Research, 39(3), 365–374.

Bewley, D. S., Essery, R., Pomeroy, J. W., Ménard, C. (2010). Measurements and modelling of snowmelt and turbulent heat fluxes over shrub tundra. Hydrology and Earth System Sciences, 14(7), 1331–1340.

Blyth, E., Harding, R. J., Essery, R. (1999). A couple dual source GCM SVAT. Hydrology and Earth System Sciences, 31, 71–84.

Box, J. E., Steffen, K. (2001). Sublimation on the Greenland ice sheet from automated weather station observations. Journal of Geophysical Research, 106(D24), 33,965–33,981.

Brun, L. J., Enz, J. W., Larsen, J. K., Fanning, C. (1984). Springtime evaporation from bare and stubble-covered soil. Journal of Soil and Water Conservation, 41, 120–122.

Burt, C. M., Mutziger, A. J., Allen, R. G., Howell, T. A. (2005). Evaporation Research: Review and Interpretation. Journal of Irrigation and Drainage Engineering, 131, 37–58.

Campbell, G. S., Norman, J. M. (1998). An Introduction to Environmental Biophysics. New York, NY: Springer New York. https://doi.org/10.1007/978-1-4612-1626-1

Clark, M. P., Hendrikx, J., Slater, A. G., Kavetski, D., Anderson, B., Cullen, N. J., … Woods, R. (2011). Representing spatial variability of snow water equivalent in hydrologic and land-surface models: A review. Water Resources Research, 47(7). https://doi.org/10.1029/2011WR010745

Corkal, D., Schutzman, W. C., Hilliard, C. R. (2004). Rural water safety from the source to the on-farm tap. Journal of Toxicology and Environmental Health, 67, 1619–1642. https://doi.org/10.1080/15287390490491918

Cutforth, H. W., McConkey, B. G. (1997). Stubble height effects on microclimate , yield and water use efficiency of spring wheat grown in a semiarid climate on the Canadian prairies. Canadian Journal of Plant Science, 77, 359–366.

Davis, R. (1973). Operational snow sensors. In 30th Eastern SnowConference (pp. 57–70).

DeBeer, C. M., Pomeroy, J. W. (2010). Simulation of the snowmelt runoff contributing area in a small alpine basin. Hydrology and Earth System Sciences, 14(7), 1205–1219.

Denby, B., Snellen, H. (2002). A comparision of surface renewal theory with the observed roughness length for temperature on a melting glacier surface. Boundary-Layer Meteorology, 103, 459–468.

Dumanski, S., Pomeroy, J. W., Westbrook, C. J. (2015). Hydrological regime changes in a Canadian Prairie basin. Hydrological Processes, 29(18), 3893–3904.

Elliot, J. E., Efetha, A. A. (1999). Influence of tillage and cropping system on soil organic matter, structure and infiltration in a rolling landscape. Canadian Journal of Soil Science, 79, 457–463.

Elliot, J. E., Cessna, A. J., Hilliard, C. R. (2001). Influence of Tillage System on Water Quality and Quantity in Prairie Pothole Wetlands. Canadian Water Resources Journal, 26(2), 165–181. https://doi.org/10.4296/cwrj2602165

Ellis, C. R., Pomeroy, J. W., Brown, T., MacDonald, J. (2010). Simulation of snow accumulation and melt in needleleaf forest environments. Hydrology and Earth System Sciences, 14(6), 925–940. Retrieved from http://www.hydrol-earth-syst-sci.net/14/925/2010/

Essery, R., Pomeroy, J. W., Ellis, C. R., Link, T. E. (2008a). Modelling longwave radiation to snow beneath forest canopies using hemispherical photography or linear regression. Hydrological Processes, 22(15), 2788–2800.

Essery, R., Pomeroy, J. W. (2004). Implications of spatial distributions of snow mass and melt rate for snow-cover depletion: theoretical considerations. Annals of Glaciology, 38(1), 261–265. https://doi.org/10.3189/172756404781815275

Essery, R., Li, L., Pomeroy, J. W. (1999). A distributed model of blowing snow over complex terrain. Hydrological Processes, 13(14–15), 2423–2438. Retrieved from http://doi.wiley.com/10.1002/(SICI)1099-1085(199910)13:14/15%3C2423::AID-HYP853%3E3.0.CO;2-U

Essery, R., Granger, R. J., Pomeroy, J. W. (2006). Boundary-layer growth and advection of heat over snow and soil patches: modelling and parameterization. Hydrological Processes, 20(4), 953–967.

Essery, R., Bunting, P., Hardy, J., Link, T. E., Marks, D., Melloh, R., … Rutter, N. (2008b). Radiative Transfer Modeling of a Coniferous Canopy Characterized by Airborne Remote Sensing. Journal of Hydrometeorology, 9(2), 228–241. Retrieved from http://journals.ametsoc.org/doi/abs/10.1175/2007JHM870.1

Fang, X., Minke, A. G., Pomeroy, J. W., Brown, T., Westbrook, C. J., Guo, X., Guangul, S. (2007). A Review of Canadian Prairie Hydrology: Principles , Modelling and Response to Land Use and Drainage Change; Center for Hydrology Report No. 2. Saskatoon.

Fang, X., Pomeroy, J. W. (2008). Drought impacts on Canadian prairie wetland snow hydrology. Hydrological Processes, 22(15), 2858–2873.

Flerchinger, G. N. (2000). The Simultaneous Heat and Water (SHAW) Model: Technical Documentation. Boise, Idaho. https://doi.org/Technical Report NWRC 2000-09

Flerchinger, G. N., Sauer, T. J., Aiken, R. A. (2003). Effects of crop residue cover and architecture on heat and water transfer at the soil surface. Geoderma, 116(1–2), 217–233. https://doi.org/10.1016/S0016-7061(03)00102-2

Flerchinger, G. N., Saxton, K. E. (1989). Simulataneous Heat and Water Model of a Freezing Snow-Residue-Soil System I . Theory and Development. Trans. ASAE, 32(2), 565–567.

Garnier, B. J., Ohmura, A. (1968). A method of calculating the shortwave radiation income of slopes. Journal of Applied Meteorology, 7, 796–800.

Garratt, J. R. (1990). The Internal Boundary Layer - A Review. Boundary-Layer Meteorology, 50, 171–203.

Gelfan, A. N., Pomeroy, J. W., Kuchment, L. S. (2004). Modeling Forest Cover Influences on Snow Accumulation , Sublimation , and Melt. Journal of Hydrometeorology -Special Section, 5, 785–803.

Goodison, B. E., Glynn, J. E., Harvey, K. D., Slater, J. E. (1987). Snow Surveying in Canada: A Perspective. Canadian Water Resources Journal, 12(2), 27–42. https://doi.org/10.4296/cwrj1202027

Granger, R. J., Gray, D. M., Dyck, G. E. (1984). Snowmelt Infiltration to frozen Prairie Soils. Canadian Journal of Earth Sciences, 21(6), 669–677. https://doi.org/10.1016/0148-9062(85)92399-X

Granger, R. J., Gray, D. M. (1984). Snowmelt infiltration to frozen prairie soils. Canadian Journal of Earth Sciences, 21(6), 669–677.

Granger, R. J., Gray, D. M. (1990). Net Radiation Model for Calculating Daily Snowmelt in Open Environments. Nordic Hydrology, 21, 217–234.

Granger, R. J., Male, D. H., Gray, D. M. (1978). Prairie Snowmelt. In Symposium of the Water Studies Institute.

Granger, R. J., Male, D. H. (1978). Melting of a prairie snowpack. Journal of Applied Meteorology, 17, 1833–1842.

Granger, R. J., Pomeroy, J. W., Parviainen, J. (2002). Boundary-layer integration approach to advection of sensible heat to a patchy snow cover. Hydrological Processes, 16(18), 3559–3569.

Granger, R. J., Essery, R., Pomeroy, J. W. (2006). Boundary-layer growth over snow and soil patches: Field Observations. Hydrological Processes, 20(4), 943–951.

Gray, D. M. (1970). Handbook on the Principles of Hydrology. NY: Water Information Center.

Gray, D. M., Granger, R. J., Landine, P. G., Bayne, D. (1989). Snow Management and Meltwater Enhancement. Division of Hydrology, University of Saskatchewan, Saskatoon, Saskatchewan.

Gray, D. M., Granger, R. J. (1985). Snow Management Practices for Increasing Soil Water Reserves in Frozen Prairie Soils. Division of Hydrology, University of Saskatchewan, Saskatoon, Saskatchewan.

Gray, D. M., Landine, P. G., Granger, R. J. (1985). Simulating Infiltration into Frozen Prairie Soils in Streamflow Models. Canadian Journal of Earth Sciences, 22(3), 464–472.

Gray, D. M., Toth, B., Zhao, L., Pomeroy, J. W., Granger, R. J. (2001). Estimating areal snowmelt infiltration into frozen soils. Hydrological Processes, 15(16), 3095–3111. https://doi.org/10.1002/hyp.320

Gray, D. M., Landine, P. G. (1986). Energy Budget Snowmelt Model and Influence of Cloud Cover on Evapotranspiration Demand. Division of Hydrology, University of Saskatchewan, Saskatoon, Saskatchewan.

Gray, D. M., Landine, P. G. (1987a). Albedo Model for Shallow Prairie Snow Covers. Canadian Journal of Earth Sciences, 24(9), 1760–1768. https://doi.org/10.1139/e87-168

Gray, D. M., Landine, P. G. (1987b). Development and Performance Evaluation of an Energy Budget Snowmelt Model. Division of Hydrology, University of Saskatchewan, Saskatoon, Saskatchewan.

Gray, D. M., Landine, P. G. (1988). An Energy-Budget Snowmelt Model for the Canadian Prairies. Canadian Journal of Earth Sciences, 25(8), 1292–1303.

Gray, D. M., Male, D. H. (1981). Handbook of Snow: Principles, Processes, Management, and Use. Toronto, Canada: Pergamon Press.

Gray, D. M., Maule, C. P. (1994). Agricultural production and water conservation in semi-arid, cold environments. In Symposium on Global Environment and Friendly Energy Technology (p. 17).

Gray, D. M., Granger, R. J., Nicholaichuk, W. (1990). Snowmelt Infiltration into Completely-Frozen Subsoiled Soils. In Frozen Soil Symposium (p. 12). Spokane WS.

Hanesiak, J. M., Stewart, R. E., Bonsal, B. R., Harder, P., Lawford, R., Aider, R., … Zha, T. (2011). Characterization and Summary of the 1999–2005 Canadian Prairie Drought. Atmosphere-Ocean, 49(4), 421–452. https://doi.org/10.1080/07055900.2011.626757

Hayashi, M., van der Kamp, G., Schmidt, R. (2003). Focused infiltration of snowmelt water in partially frozen soil under small depressions. Journal of Hydrology, 270(3–4), 214–229. https://doi.org/10.1016/S0022-1694(02)00287-1

Helgason, W. D., Pomeroy, J. W. (2005). Uncertainties in Estimating Turbulent Fluxes to Melting Snow in a Mountain Clearing. In 62nd Eastern Snow Conference (pp. 129–142). Waterloo.

Helgason, W. D., Pomeroy, J. W. (2012). Problems Closing the Energy Balance over a Homogeneous Snow Cover during Midwinter. Journal of Hydrometeorology, 13, 557–572.

Hodder, K., Cade-Menun, B. J., Bell, G., Baker-Ismail, S., Mcmartin, D. W., Perez-Valdivia, C., Wu, K. (2013). Nutrient loss from Saskatchewan cropland and pasture in spring snowmelt runoff. Canadian Journal of Soil Science, 93, 445–458. https://doi.org/10.4141/CJSS2012-042

Hood, E., Williams, M., Cline, D. (1999). Sublimation from a seasonal snowpack at a continental, mid-latitude alpine site. Hydrological Processes, 13, 1781–1797.

Jonas, T., Marty, C., Magnusson, J. (2009). Estimating the snow water equivalent from snow depth measurements in the Swiss Alps. Journal of Hydrology, 378, 161–167. https://doi.org/10.1016/j.jhydrol.2009.09.021

Jordan, R. (1991). A One-Dimensional Temperature Model for a Snow Cover: Technical Documentation for SNTHERM.89. Hanover, N.H.

van der Kamp, G., Hayashi, M., Gallen, D. (2003). Comparing the hydrology of grassed and cultivated catchments in the semi-arid Canadian prairies. Hydrological Processes, 17(3), 559–575. https://doi.org/10.1002/hyp.1157

Kinar, N. J., Pomeroy, J. W. (2015). Measurement of the physical properties of the snowpack. Reviews of Geophysics, 53. https://doi.org/10.1002/2015RG000481

Kochendorfer, J., Paw U, K. T. (2011). Field estimates of scalar advection across a canopy edge. Agricultural and Forest Meteorology, 151(5), 585–594. https://doi.org/10.1016/j.agrformet.2011.01.003

Kondo, J., Yamazawa, H. (1986). Bulk transfer coefficient over a snow surface. Boundary-Layer Meteorology, 34(1973), 123–135.

Kung, E. C., Bryson, R. A., Lenschow, D. J. (1964). Study of a continental surface albedo on the basis of flight measurements and structure of the earth's surface cover over North America. Mon. Weather Rev., 92, 543–564.

Kustas, W. P., Norman, J. M. (2000). Observations for Sparse Canopy Covered Surfaces. Agronomy Journal, 92, 847–854.

Liston, G. E. (1995). Local advection of momentum, heat and moisture during the melt of patchy snow covers. Journal of Applied Meteorology, 34, 1705–1715.

Liston, G. E., Hiemstra, C. a. (2011). Representing Grass– and Shrub–Snow–Atmosphere Interactions in Climate System Models. Journal of Climate, 24(8), 2061–2079. https://doi.org/10.1175/2010JCLI4028.1

Marsh, P., Pomeroy, J. W., Neumann, N. (1997). Sensible heat flux and local advection over a heterogeneous landscape at an Arctic tundra site during snowtnelt. Annals of Glaciology, 25, 132–136.

Marsh, P., Essery, R., Neumann, N., Pomeroy, J. W. (1999). Model estimates of local advection of sensible heat over a patchy snow cover. In M. Tranter (Ed.), Interactions between the Cryosphere, Climate and Greenhouse Gases (pp. 103–110). IAHS Publ. No. 256.

Maule, C. P., Gray, D. M. (1994). Estimated Snowmelt Infiltration and Runoff for the Prairie Provinces. Canadian Water Resources Journal, 19(3), 253–265.

Ménard, C., Essery, R., Pomeroy, J. W. (2014). Modelled sensitivity of the snow regime to topography, shrub fraction and shrub height. Hydrology and Earth System Sciences, 11(6), 2375–2392. https://doi.org/10.5194/hessd-11-223-2014

Mergen, B. (1992). Seeking snow: James E. Church and the beginnings of the snow science. Nevada Historical Society, 35(2), 80.

Moore, R. D. (1983). On the use of bulk aerodynamic formulae over melting snow. Nordic Hydrology, 14(4), 193–206.

Morris, E. M. (1989). Turbulent transfer over snow and ice. Journal of Hydrology, 105, 205–223.

Mott, R., Lehning, M., Daniels, M. (2015). Atmospheric Flow Development and Associated Changes in Turbulent Sensible Heat Flux over a Patchy Mountain Snow Cover. Journal of Hydrometeorology, 16, 1315–1340. https://doi.org/10.1175/JHM-D-14-0036.1

Mott, R., Gromke, C., Grünewald, T., Lehning, M. (2013). Relative importance of advective heat transport and boundary layer decoupling in the melt dynamics of a patchy snow cover. Advances in Water Resources, 55, 88–97. https://doi.org/10.1016/j.advwatres.2012.03.001

Mott, R., Paterna, E., Horender, S., Crivelli, P., Lehning, M. (2016). Wind tunnel experiments: Cold-air pooling and atmospheric decoupling above a melting snow patch. The Cryosphere, 10(1), 445–458. https://doi.org/10.5194/tc-10-445-2016

Mott, R., Schlögl, S., Dirks, L., Lehning, M. (2017). Impact of Extreme Land Surface Heterogeneity on Micrometeorology over Spring Snow Cover. Journal of Hydrometeorology, 18(10), 2705–2722. https://doi.org/10.1175/JHM-D-17-0074.1

Munro, D. S. (1989). Surface roughness and bulk heat transfer on a glacier: Comparision with eddy correlation. Journal of Glaciology, 35(121), 343–348.

Munro, D. S., Davies, J. A. (1978). On fitting the log-linear model to wind speed and temperature profiles over a melting glacier. Boundary-Layer Meteorology, 15, 423–437.

Musselman, K. N., Molotch, N. P., Margulis, S., Kirchner, P. B., Bales, R. C. (2012). Influence of canopy structure and direct beam solar irradiance on snowmelt rates in a mixed conifer forest. Agricultural and Forest Meteorology, 161, 46–56. https://doi.org/10.1016/j.agrformet.2012.03.011

Nicholaichuk, W., Gray, D. M., Steppuhn, H., Dyck, G. E. (1985). Snow Management Practices for Trapping Snow in a Prairie Enviroment. Division of Hydrology, University of Saskatchewan, Saskatoon, Saskatchewan.

Nicholaichuk, W., Gray, D. M. (1986). Snow Trapping and Moisture Infiltration Enhancement. In Fifth Annual Western Provinces Conference.

O'Neill, A. D. ., Gray, D. M. (1973). Spatial and Temporal Variations of the Albedo of Prairie Snowpack. Unesco-WMO-IASH Symposia, 1, 176–186.

Phillips, R., Spence, C., Pomeroy, J. W. (2011). Connectivity and runoff dynamics in heterogeneous basins. Hydrological Processes, 25(May), 3061–3075. https://doi.org/10.1002/hyp.8123

Pomeroy, J. W., Shook, K., Fang, X., Dumanski, S., Westbrook, C. J., Brown, T. (2014). Improving and Testing the Prairie Hydrological Model at Smith Creek Research Basin, Centre for Hydrology Report #14. Saskatoon, SK.

Pomeroy, J. W., Brun, E. (2001). Physical Properties of Snow. In H. G. Jones, J. W. Pomeroy, D. A. Walker, and R. W. Hoham (Eds.), Snow Ecology: an Interdisciplinary Examination of Snow-covered Ecosystems (pp. 45–118). Cambridge University Press.

Pomeroy, J. W., Gray, D. M., Brown, T., Hedstrom, N. R., Quinton, W. L., Granger, R. J., Carey, S. K. (2007). The cold regions hydrological model : a platform for basing process representation and model structure on physical evidence. Hydrological Processes, 21(19), 2650–2667.

Pomeroy, J. W., Dion, K. (1996). Winter irradiance extinction and reflection in a boreal pine canopy: measurements and modelling. Hydrological Processes, 10(12), 1591–1608.

Pomeroy, J. W., Marks, D., Link, T. E., Ellis, C. R., Hardy, J., Rowlands, A., Granger, R. J. (2009a). The impact of coniferous forest temperature on incoming longwave radiation to melting snow. Hydrological Processes, 23(17), 2513–2525.

Pomeroy, J. W., Gray, D. M. (1994). Sensitivity of snow relocation and sublimation to climate and surface vegetation. In Snow and Ice Covers: Interactions with the Atmosphere and Ecosystems (pp. 213–225). IAHS Publ. No 223.

Pomeroy, J. W., Gray, D. M. (1995). Snow accumulation, relocation and management. Saskatoon, SK: Science Report No. 7, National Hydrology Research Institute, Environment Canada.

Pomeroy, J. W., Gray, D. M., Shook, K., Toth, B., Essery, R., Pietroniro, A., Hedstrom, N. R. (1998). An evaluation of snow accumulation and ablation processes for land surface modelling. Hydrological Processes, 12, 2339–2367.

Pomeroy, J. W., Gray, D. M., Landine, P. G. (1991). Modelling the Transport and Sublimation of Blowing Snow on the Prairies. In Eastern Snow Conference (pp. 175–188). Guelph, ON.

Pomeroy, J. W., Gray, D. M., Landine, P. G. (1993). The Prairie Blowing Snow Model: characteristics, validation, operation. Journal of Hydrology, 144(1–4), 165–192.

Pomeroy, J. W., Nicholaichuk, W., Gray, D. M., McConkey, B. G., Granger, R. J., Landine, P. G. (1990). Snow Management and Meltwater Enhancement: Final Report. NHRI Contribution No. CS-90021. Environment Canada, Saskatoon, SK.

Pomeroy, J. W., de Boer, D., Martz, L. W. (2005). Hydrology and Water Resources of Saskatchewan. Centre Report No. 1, Centre for Hydrology, University of Saskatchewan, Saskatoon, SK.

Pomeroy, J. W., Fang, X., Williams, B. (2009b). Impacts of Climate Change on Saskatchewan's Water Resources. Centre Report No. 6, Centre for Hydrology, University of Saskatchewan, Saskatoon, SK.

Prueger, J. H., Kustas, W. P. (2005). Aerodynamic Methods for Estimating Turbulent Fluxes. Agronomy, 47, 407–436.

Raupach, M. R. (1989). Applying lagrangian fluid mechanics to infer scalar source distributions from concentration profiles in plant canopies. Agricultural and Forest Meteorology, 47(47), 85–108.

Richards, D. R. (1986). Hydrologic Implications of Snow Management. In H. Steppuhn and W. Nicholaichuk (Eds.), Snow Management for Agriculture Symposium (pp. 580–590).

Ross, J. (1981). The Radiation Regime and Architecture of Plant Stands. New York: Springer.

Shook, K. (1995). Simulation of the Ablation of Prairie Snowcovers. University of Saskatchewan.

Shook, K., Gray, D. M. (1996). Small-Scale Spatial Structure of Shallow Snowcovers. Hydrological Processes, 10, 1283–1292.

Shook, K., Gray, D. M. (1997). Snowmelt Resulting from Advection. Hydrological Processes, 11, 1725–1736.

Shook, K., Pomeroy, J. W. (2012). Changes in the hydrological character of rainfall on the Canadian prairies. Hydrological Processes, 26, 1752–1766. https://doi.org/10.1002/hyp.9383

Shook, K., Gray, D. M., Pomeroy, J. W. (1993). Temporal Variation in Snowcover Area During Melt in Prairie and Alpine Environments. Nordic Hydrology, 24(2–3), 183–198.

Sicart, J. E., Pomeroy, J. W., Essery, R., Bewley, D. S. (2006). Incoming longwave radiation to melting snow: observations, sensitivity and estimation in northern environments. Hydrological Processes, 20(17), 3697–3708.

Smeets, C. J. P. ., Duynkerke, P. G., Vugts, H. F. (1998). Turbulence characteristics of the stable boundary layer over a mid-latitude glacier. Part I: A combination of katabatic and large-scale forcing. Boundary-Layer Meteorology, 87, 117–145.

Statistics Canada. (2016). Census of Agriculture, tillage practices used to prepare land for seeding, every 5 years. Retrieved May 12, 2017, from http://www5.statcan.gc.ca/cansim/a03?lang=engandsearchMode=regularSearchandpattern=004-0200..004-0246andtypeValue=-1andsrchLan=-1andp2=31

Steppuhn, H., Dyck, G. E. (1974). Estimating True Basin Snowcover. In Proceedings of Interdisciplinary Symposium on Advanced Concepts and Techniques in the Study of Snow and Ice Resourses. (pp. 314–328).

Steppuhn, H., Erickson, D. (1978). Water conservation for Wheat Production in the Brown and Dark Brown Soil Zones. In Agriculture Canada Research Station (p. 14).

Strudley, M., Green, T., Ascoughii, J. (2008). Tillage effects on soil hydraulic properties in space and time: State of the science. Soil and Tillage Research, 99(1), 4–48.

Wallace, S. (1991). Lagrangian and K-theory approaches in modelling evaporation from sparse canopies, 1325–1340.

Walmsley, J. L., Taylor, P. A., Keith, T. (1986). A simple model of neutrally stratified boundary-layer flow over complex terrain with surface roughness modulations (MS3DJH/3R). Boundary-Layer Meteorology, 36, 157–186.

Weisman, R. N. (1977). Snowmelt: A Two-Dimensional Turbulent Diffusion Model. Water Resources Research, 13(2), 337–342.

Willis, W. O., Haas, H. J., Carlson, C. W. (1969). Snowpack runoff as affected by stubble height. Soil Science, 107, 256–259.

Wilson, J. D. (1989). Turbulent transport within the plant canopy. In T. A. Black, D. L. Spittlehouse, M. D. Novak, and D. T. Price (Eds.), Estimation of areal evapotranspiration IAHS Publication No. 177 (pp. 43–80). Wallingford, UK: IAHS Press.

Zhao, L., Gray, D. M. (1999). Estimating snowmelt infiltration into frozen soils. Hydrological Processes, 13(12–13), 1827–1842. https://doi.org/10.1002/(SICI)1099-1085(199909)13:12/13<1827::AID-HYP896>3.0.CO;2-D

Zhao, L., Gray, D. M., Male, D. H. (1996). Simultaneous Infiltration and Heat Transfer into Frozen Soil. In Fifth International Symposium on Thermal Engineering and Science for Cold Regions.

Zhao, L., Gray, D. M., Male, D. H. (1997). Numerical analysis of simultaneous heat and mass transfer during infiltration into frozen ground. Journal of Hydrology, 200, 345–363.

Zhao, W., Qualls, R. J. (2005). A multiple-layer canopy scattering model to simulate shortwave radiation distribution within a homogeneous plant canopy. Water Resources Research, 41(8). https://doi.org/10.1029/2005WR004016

Chapter 2: Accuracy of snow depth estimation in mountain and prairie environments by an unmanned aerial vehicle

Status: Published November 2, 2016

Citation: Harder, P., Schirmer, M., Pomeroy, J. W. and Helgason, W. D. (2016). Accuracy of snow depth estimation in mountain and prairie environments by an unmanned aerial vehicle. *Cryosphere*, 10, 2559–2571, doi:10.5194/tc-10-2559-2016.

Author Contributions: PH conceptualized the prairie field program, performed all prairie fieldwork, processed prairie data, and wrote all but the mountain portions of the manuscript. MS performed all mountain field work, mountain data processing and wrote the mountain specific portions of the manuscript. JP provided equipment and financial resources for the field campaign. PH, MS, JP, and WH reviewed and revised manuscript.

2.1. Abstract

Quantifying the spatial distribution of snow is crucial to predict and assess its water resource potential and understand land-atmosphere interactions. High-resolution remote sensing of snow depth has been limited to terrestrial and airborne laser scanning and more recently with application of Structure from Motion (SfM) techniques to airborne (manned and unmanned) imagery. In this study, photography from a small unmanned aerial vehicle (UAV) was used to generate digital surface models (DSMs) and orthomosaics for snowcovers at a cultivated agricultural Canadian Prairie and a sparsely-vegetated Rocky Mountain alpine ridgetop site using SfM. The accuracy and repeatability of this method to quantify snow depth, changes in depth and its spatial variability was assessed for different terrain types over time. Root mean square errors in snow depth estimation from differencing snowcovered and non-snowcovered DSMs were 8.8 cm for a short prairie grain stubble surface, 13.7 cm for a tall prairie grain stubble surface and 8.5 cm for an alpine mountain surface. This technique provided useful information on maximum snow accumulation and snowcovered area depletion at all sites, while temporal changes in snow depth could also be quantified at the alpine site due to the deeper snowpack and consequent higher signal-to-noise ratio. The application of SfM to UAV photographs returns meaningful information in areas with mean snow depth > 30 cm, however the direct observation of snow

depth depletion of shallow snowpacks with this method is not feasible. Accuracy varied with surface characteristics, sunlight and wind speed during the flight, with the most consistent performance found for wind speeds < 10 ms^{-1}, clear skies, high sun angles and surfaces with negligible vegetation cover.

2.2. Introduction

Accumulation, redistribution, sublimation and melt of seasonal or perennial snowcovers are defining features of cold region environments. The dynamics of snow have incredibly important impacts on land-atmosphere interactions and can constitute significant proportions of the water resources necessary for socioeconomic and ecological functions (Armstrong and Brun, 2008; Gray and Male, 1981; Jones et al., 2001). Snow is generally quantified in terms of its snow water equivalent (SWE) through measurements of its depth and density. Since density varies less than depth (López-Moreno et al., 2013; Shook and Gray, 1996) much of the spatial variability of SWE can be described by the spatial variability of snow depth. Thus, the ability to measure snow depth and its spatial distribution is crucial to assess and predict how the snow water resource responds to meteorological variability and landscape heterogeneity. Observation and prediction of the spatial distribution of snow depth is even more relevant with the anticipated and observed changes occurring due to a changing climate and land use (Dumanski et al., 2015; Harder et al., 2015; Milly et al., 2008; Mote et al., 2005; Stewart et al., 2004).

The many techniques and sampling strategies employed to quantify snow depth all have strengths and limitations (Pomeroy and Gray, 1995). Traditionally, manual snow surveys have been used to quantify snow depth and density along a transect. The main benefit of manual snow surveying is that the observations are a direct measurement of the SWE; however, it requires significant labour, is a destructive sampling method and can be impractical in complex, remote or hazardous terrain (DeBeer and Pomeroy, 2009; Dingman, 2002). Many sensors exist that can measure detailed snow properties non-destructively, with a comprehensive review found in Kinar and Pomeroy (2015), but non-destructive automated sensors, such as acoustic snow depth rangers (Campbell Scientific SR50) or SWE analyzers (Campbell Scientific CS275 Snow Water Equivalent Sensor), typically only provide point scale information and may require significant additional infrastructure or maintenance to operate properly. Remote sensing of snow from satellite and aerial platforms quantify snow extent at large scales. Satellite platforms can

successfully estimate snowcovered area but problems remain in quantifying snow depth, largely due to the heterogeneity of terrain complexity and vegetation cover. To date, Light Detection And Ranging (LiDAR) techniques have provided the highest resolution estimates of snow depth spatial distribution from both terrestrial (Grünewald et al., 2010) and airborne platforms (Hopkinson et al., 2012). The main limitations encountered are easily observable areas (sensor viewshed) for the terrestrial scanner and the prohibitive expense and long lead time needed for planning repeat flights for the aerial scanner (Deems et al., 2013). Typically, airborne LiDAR provides data with a ground sampling of nearly 1 m and a vertical accuracy of 15 cm (Deems and Painter, 2006; Deems et al., 2013). While detailed, this resolution still does not provide observations of the spatial variability of snow distributions that can address microscale processes such as snow-vegetation interactions or wind redistribution in areas of shallow snowcover, and the frequency of airborne LiDAR observations are typically low, except for NASA's Airborne Snow Observatory applications in California (Mattmann et al., 2014).

An early deployment of a high resolution digital camera on a remote controlled gasoline powered model helicopter in 2004 permitted unmanned digital aerial photography to support studies of shrub emergence and snowcovered area depletion in a Yukon mountain shrub tundra environment (Bewley et al., 2007). Since then, Unmanned Aerial Vehicles (UAVs) have become increasingly popular for small-scale high-resolution remote sensing applications in the earth sciences. The current state of the technology is due to advances in the capabilities and miniaturization of the hardware comprising UAV platforms (avionics/autopilots, Global-Positioning Systems (GPS), Inertial Measurement Units (IMUs) and cameras) and the increases in computational power for processing imagery. The conversion of raw images to orthomosaics and Digital Surface Models (DSMs) takes advantage of Structure from Motion (SfM) algorithms (Westoby et al., 2012). These computationally intensive algorithms simultaneously resolve camera pose and scene geometry through automatic identification and matching of common features in multiple images. With the addition of information on the respective camera location, or if feature locations are known, then georeferenced point clouds, orthomosaics and DSMs can be generated (Westoby et al., 2012). Snow is a challenging surface for SfM techniques due to its relatively uniform surface and high reflectance relative to snow-free areas, which limit identifiable features (Nolan et al., 2015). The resolution of the data products produced by UAVs depends largely on flight elevation and sensor characteristics but can promise accuracies of 2.6

cm in the horizontal and 3.1 cm in the vertical (Roze et al., 2014). The unprecedented spatial resolution of these products may be less important than the fact that these platforms are deployable at a high user-defined frequencies below cloud cover, which can be problematic for airborne or satellite platforms. Manned aerial platforms have the advantage of covering much larger areas (Nolan et al., 2015) with a more mature and clear regulatory framework (Marris, 2013; Rango and Laliberte, 2010) than small UAVs. However, the greater expenses associated with acquisition, maintenance, operation and training required for manned platforms (Marris, 2013), relative to small UAVs, are significant (Westoby et al., 2012). Many snow scientists have expressed great enthusiasm in the opportunities UAVs present and speculate that they may drastically change the quantification of snow accumulation and ablation (Sturm, 2015).

The roots of SfM are found in stereoscopic photogrammetry, which has a long history in topographic mapping (Collier, 2002). Relative to traditional photogrammetry, major advances in the 1990's in computer vision (Boufama et al., 1993; Spetsakis and Aloimonost, 1991; Szeliski and Kang, 1994) has automated and simplified the data requirements to go from a collection of overlapping 2D images to 3D point clouds. Significant work by the geomorphology community has pushed the relevance, application and further development of this technique into the earth sciences (Westoby et al., 2012). Recent application of this technique to snow depth estimation has used imagery captured by manned aerial platforms (Bühler et al., 2015; Nolan et al., 2015) and increasingly with small UAVs (Vander Jagt et al., 2015; Bühler et al., 2016; De Michele et al., 2016). The manned aircraft examples have reported vertical accuracies of 10cm (Nolan et al., 2015) and 30 cm (Bühler et al., 2015) with horizontal resolutions of 5-20 cm (Nolan et al., 2015) and 2 m (Bühler et al., 2015). Unmanned aircraft examples have shown similar accuracies and resolution with vertical errors of reported to be ~10 cm with horizontal resolutions between 50 cm (Vander Jagt et al., 2015) and 10 cm (Bühler et al., 2016). The accuracy assessments of the De Michele et al. (2016), Vander Jagt et al. (2015), and Bühler et al. (2016) studies were limited to a small number of snow depth maps. Bühler et al. (2016) had the most with four maps, but more are needed to get a complete perspective on the performance of this technique and its repeatability under variable conditions.

The overall objective of this paper is to assess the accuracy of snow depth as estimated by imagery collected by small UAVs and processed with SfM techniques. Specifically, this paper

will: 1) assess the accuracy of UAV-derived snow depths with respect to the deployment conditions and heterogeneity of the earth surface, specifically variability in terrain relief, vegetation characteristics and snow depth; and 2) identify and assess opportunities for UAV generated data to advance understanding and prediction of snowcover and snow depth dynamics.

2.2. Sites and Methodology

2.2.1. Sites

The prairie field site (Figure 2.1a) is representative of agricultural regions on the cold, windswept Canadian Prairies, where agriculture management practices control the physical characteristics of the vegetation which, in turn, influence snow accumulation (Pomeroy and Gray, 1995). There is little elevation relief and the landscape is interspersed with wooded bluffs and wetlands. Snowcover is typically shallow (maximum depth < 50 cm) with development of a patchy and dynamic snowcovered area during melt. Data collection occurred at a field site near Rosthern, Saskatchewan, Canada Mountains (52° 42' N, 106° 27' W) in spring 2015 as part of a larger project studying the influence of grain stubble exposure on snowmelt processes. The 0.65 km^2 study site was divided into areas of tall stubble (35 cm, hereafter Tall15) and short stubble (15 cm, hereafter Short15). The wheat stubble (Figure 2.1c), clumped in rows ~30 cm apart, remained erect throughout the snow season, which has implications for blowing snow accumulation, melt energetics and snowcover depletion. Pomeroy et al. (1993, 1998) describes the snow accumulation dynamics and snowmelt energetics of similar environments.

The alpine site, located in Fortress Mountain Snow Laboratory in the Canadian Rocky Mountains (50° 50' N, 115° 13' W), is characterized by a ridge oriented in SW-NE direction (Figure 2.1b, d) at an elevation of approximately 2300 m. The average slope at the alpine site is ~15 degrees with some slopes > 35 degrees. Large areas of the ridge were kept bare by wind erosion during the winter of 2014/2015 and wind redistribution caused the formation of deep snowdrifts on the leeward (SE) side of the ridge, in surface depressions and downwind of krummholz. Vegetation is limited to short grasses on the ridgetop while shrubs and coniferous trees become more prevalent in gullies on the shoulders of the ridge. Mean snow depth of the snowcovered area at the start of the observation period (May 13, 2015) was 2 m (excluding snow-free areas) with maximum depths over 5 m. The 0.32 km^2 study area was divided between

a North and a South area (red polygons in Figure 2.1b) due to UAV battery and hence flight area limitations. DeBeer and Pomeroy (2010, 2009) and MacDonald et al. (2010) describe the snow accumulation dynamics and snowmelt energetics of the area.

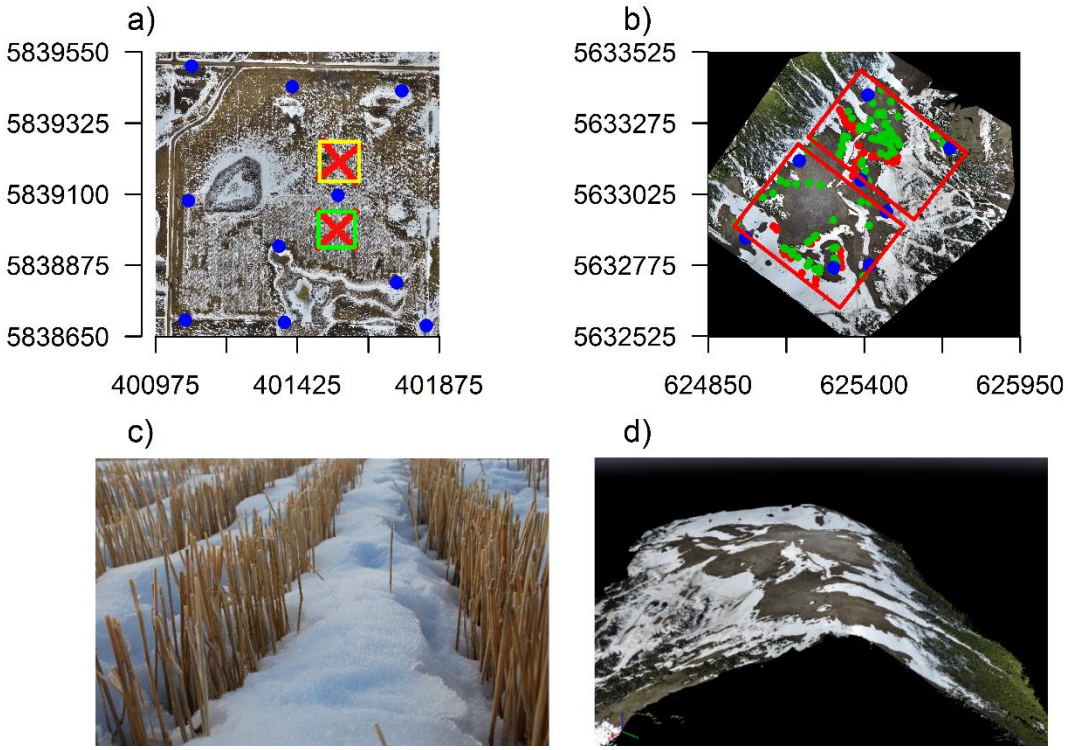

Figure 2.1: Orthomosaics of a) the prairie site located near Rosthern, Saskatchewan and b) the alpine site at Fortress Mountain Snow Laboratory, Kananaskis, Alberta. The prairie site image (March 19, 2015) has polygons depicting areas used for peak snow depth estimation over Short15 (yellow) and Tall15 (green) stubble treatments. The alpine site image (May 22, 2015) was split into two separately processed subareas (red polygons). Red points in a) and b) are locations of manual snow depth measurements while green points at the alpine site b) were used to test the accuracy of the DSM over the bare surface. Ground control point (GCP) locations are identified as blue points. Axes are UTM coordinates for the prairie site (UTM zone 13N) and alpine site (UTM zone 11N). The defining feature of the prairie site was the c) wheat stubble (Tall15) exposed above the snow surface and at the alpine site was the d) complex terrain as depicted by the generated point cloud (view from NE to SW).

2.2.2. Methodology

2.2.2.1. Unmanned Aerial Vehicle - flight planning - operation - data processing

A Sensefly Ebee Real Time Kinematic (RTK) UAV (version 01) was used to collect imagery over both sites (Figure 2.2a). The platform is bundled with flight control and image processing software to provide a complete system capable of survey grade accuracy without the

use of ground control points (GCPs) (Roze et al., 2014). The Ebee RTK is a hand launched, fully autonomous, battery powered, fixed wing UAV with a wingspan of 96 cm and a weight of ~0.73 kg including payload. Maximum flight time is up to 45 minutes with cruising speeds of 40-90 km h^{-1}. A modified consumer grade camera, a Canon PowerShot ELPH 110 HS, captures red, green and blue band imagery as triggered by the autopilot. The camera, fixed in the UAV body, lacks a stabilizing gimbal as often seen on multirotor UAVs, and upon image capture levels the entire platform and shuts off motor, to minimize vibration, resulting in consistent nadir image orientation. The camera has a 16.1 MP 1/2.3-inch CMOS sensor and stores images as JPEGs, resulting in images with 8-bit depth for the three color channels. Exposure settings are automatically adjusted based on a center weighted light metering. Images are geotagged with location and camera orientation information supplied by RTK corrected Global Navigation Satellite System (GNSS) positioning and IMU, respectively. A Leica GS15 base station supplied the RTK corrections to the Ebee to resolve image locations to an accuracy of ±2.5 cm. The Ebee was able to fly in all wind conditions attempted but image quality, location and orientation became inconsistent when wind speed at the flight altitude (as observe by an on-board pitot tube) approached 14 m s^{-1}.

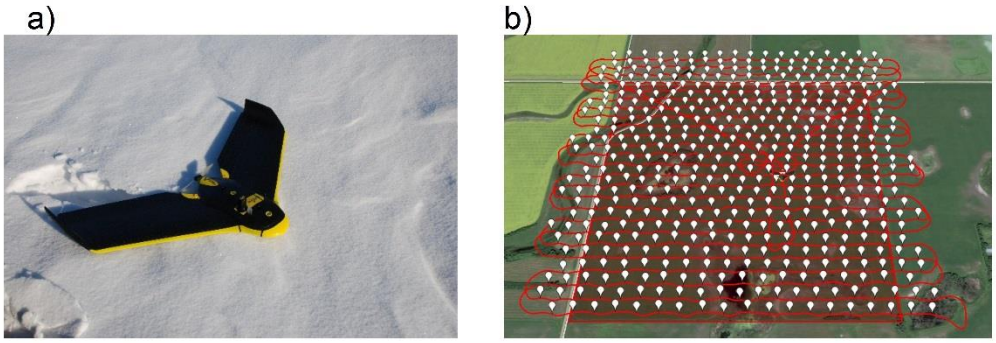

Figure 2.2: a) Sensefly Ebee RTK, b) a typical flight over the prairie site where red lines represent the flight path of UAV and the white placemarks represent photo locations.

At the prairie site, the UAV was flown 22 times over the course of the melt period (March 6 to 30, 2015) with three flights over the snow free surface between April 2 and 9, 2015. A loaner Ebee, from Spatial Technologies, the Ebee distributor, performed the first 11 flights at the prairie site due to technical issues with the Ebee RTK. The geotag errors of the non-RTK loaner Ebee were ±5 m (error of GPS Standard Positioning Service) and therefore required GCPs to generate georeferenced data products. At the alpine site, to reduce variations in the height of

the UAV above the surface in complex terrain, flight plans were adjusted using a 1 m resolution DEM, derived from a LiDAR DEM. The UAV was flown 18 times over melt from 15 May to 24 June 2015 with four flights over bare ground on 24 July 2015. Table 2.1 summarises flight plan attributives of the respective sites. Figure 2.2b shows a typical flight plan generated by the eMotion flight control software for the prairie site.

Postflight Terra 3D 3 (version 3.4.46) processed the imagery to generate DSMs and orthomosaics. Though the manufacturer suggested that they are unnecessary with RTK corrected geotags (error of ±2.5 cm), all processing included GCPs. At the prairie site, 10 GCPs comprised of five tarps and five utility poles were distributed throughout the study area (blue points in Figure 1a). At the alpine site, the north and south areas had five and six GCPs (blue points in Figure 2.1b), respectively comprised of tarps (Figure 2.3a) and easily identifiable rocks (Figure 2.3b) spread over the study area.

Table 2.1: Flight plan specifications

Variable	Prairie Site	Alpine Site
Flight altitude	90 m	90 m
Lateral overlap	70 %	85 %
Longitudinal overlap	70 %	75 %
Ground resolution	3 cm pixel^{-1}	3 cm pixel^{-1}
Number of flights (over snow/over non-snow)	22/3	18/4
Approximate area surveyed per flight	1 km^2	0.32 km^2

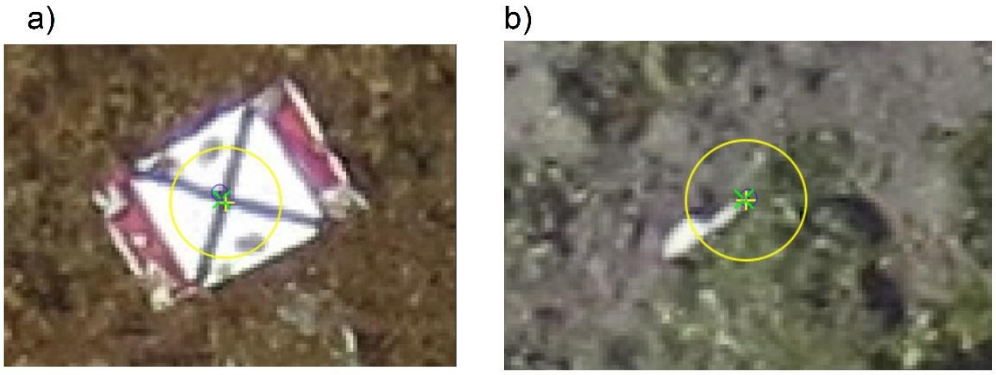

Figure 2.3: Examples of ground control points that included a) tarps (2.2 m x 1.3 m) and b) identifiable rocks at the same magnification as the tarp.

Processing involved three steps. First, initial processing extracted features common to multiple images, optimized external and internal camera parameters for each image, and

generated a sparse point cloud. The second step densified the point cloud and the third step generated a georeferenced orthomosaic and a DSM. Preferred processing options varied between the sites, with the semi-global matching algorithm in the point densification used to minimize erroneous points encountered at the alpine site (see Sect 3.3). Generated orthomosaics and DSMs had a horizontal resolution of 3.5 cm at the prairie site and between 3.5 cm and 4.2 cm at the alpine site.

2.2.2.2. Ground truth and snow depth data collection

To assess the accuracy of the generated DSMs and their ability to measure snow depth, detailed observations of the land surface elevation and snow depth were collected. At the prairie site a GNSS survey, utilizing a Leica GS15 as a base station and another GS15 acting as a RTK corrected rover, measured the location (x, y and z) of 17 snow stakes on each stubble treatment to an accuracy of less than ±2.5 cm. This gives 34 observation points at the prairie site (locations identified as red dots in Figure 2.1a). Over the melt period, the snow depth was measured with a ruler at each point (error of ±1 cm). Adding the manually measured snow depths to the corresponding land surface elevations from the GNSS survey gives snow surface elevations at each observation point directly comparable to the UAV derived DSM. At the alpine site, 100 land surface elevations were measured at points with negligible vegetation (bare soil or rock outcrops) with a GNSS survey to determine the general quality of the DSMs. For eight flights a GNSS survey was also performed on the snowcover (all measurement locations over the course of campaign are highlighted in Figure 2.1b). To account for the substantial terrain roughness and to avoid measurement errors in deep alpine snowpacks, snow surface elevation was measured via GNSS survey and snow depth estimated from the average of five snow depth measurements in a 0.4 m x 0.4 m square at that point. Time constraints and inaccessible steep snow patches limited the number of snow depth measurements to between three and 19 measurements per flight. While the number of accuracy assessment points over snow is limited for each flight the cumulative number of points over the course of the campaigns used to assess accuracy over all flights is not; at the alpine site there were 101 GNSS surface measurements and 83 averaged snow depth measurements available, and at the prairie site 323 measurements on each stubble treatment.

At both the prairie and alpine site, the same GNSS RTK surveying method established GCP locations. Snow surveys (maximum one per day) and DSMs (multiple per day) are only compared if from the same days.

2.2.2.3. Snow depth estimation

Subtracting a DSM of a snow free surface from a DSM of a snowcovered surface estimates snow depth assuming snow ablation is the only process changing the surface elevations between observation times. Vegetation is limited over the areas of interest at the alpine site and any spring up of grasses or shrubs is insignificant, based upon local observations, with respect to the large snow depths observed (up to 5 m). The wheat stubble at the prairie site is unaffected by snow accumulation or ablation. The snow-free DSMs corresponded to imagery collected on for the prairie site and July 24, 2015 for the alpine site.

2.2.2.4. Accuracy assessment

The accuracy of the UAV-derived DSM and snow depth was estimated by calculating the root mean square error (RMSE), mean error (bias) and standard deviation of the error (SD) with respect to the manual measurements. The RMSE quantifies the overall difference between manually measured and UAV derived values, bias quantifies the mean magnitude of the over (positive values) or under (negative values) prediction of the DSM with respect to manual measurements, and SD quantifies the variability of the error.

2.2.2.5. Signal-to-Noise Calculation

The signal-to-noise ratio (SNR) compares the level of the snow depth signal with respect to the measurement error to inform when meaningful information is available. The SNR is calculated as the mean measured snow depth value divided by the standard deviation of the error between the observed and estimated snow depths. The Rose criterion (Rose 1973), commonly used in the image processing literature, is used to define the threshold SNR where the UAV returns meaningful snow depth information. The Rose criterion proposes a $SNR \geq 4$ for the condition at which the signal is sufficiently large to avoid mistaking it for a fluctuation in noise. Ultimately, the acceptable signal to noise ratio depends upon the user's error tolerance (Rose, 1973).

2.3. Results and Discussion

2.3.1 Absolute surface accuracy

The accuracy of the DSMs relative to the measured surface points varies with respect to light conditions at time of photography and differences in snow surface characteristics and extent. This is seen in the RMSE for individual flights varying from 4 cm to 19 cm (Figure 2.4). Only a few problematic flights, which will be discussed in section 3.3.1, showed larger RMSEs, which are marked in blue in Figure 2.4. In general, the accuracy of the DSMs as represented by the mean RMSEs in Table 2.2, were comparable between the prairie Short15 (8.1 cm), alpine-bare (8.7 cm) and alpine-snow (7.5 cm) sites and were greater over the prairie Tall15 site (11.5 cm). Besides the five (out of a total of 43) problematic flights (out of a total of 43 flights), accuracy was relatively consistent over time at all sites. More specifically, the prairie flights simultaneously sampled the Short 15 and Tall15 stubble areas, thus there were only three problematic flights at the prairie site in addition to the two at the alpine site (Figure 2.4). The larger error at Tall 15 treatment is due to snow and vegetation surface interactions. Over the course of melt, the DSM gradually became more representative of the stubble surface rather than the snow surface. More points are matched on the high contrast stubble than the low contrast snow leading to the DSM being biased to reflect the stubble surface. This is apparent in the increasing Tall15 bias as the snow surface drops below the stubble height. By comparing the many alpine-bare points to the limited number of alpine-snow points (3 to 19) the relative difference in errors between the snow and non-snow surfaces was assessed. The benefit of the large amount of alpine-bare points (100) revealed the general errors, offsets and tilts in the DSM. It was concluded that the snow surface errors are not appreciably different from the non-snow surface errors.

Table 2.2: Absolute surface accuracy summary

Area	Variable	Mean[a] (cm)	Maximum[a] (cm)	Minimum[a] (cm)	Total Points[c]
Apine-bare	RMSE	8.7	15	4	1120
Alpine-bare	Bias [b]	5.6	11	1	1120
Alpine-bare	SD	6.2	12	3	1120
Alpine-snow	RMSE	7.5	14	3	101
Alpine-snow	Bias [b]	4.4	13	1	101
Alpine-snow	SD	5.4	13	3	101
Short15	RMSE	8.1	12.5	4.4	357
Short15	Bias [b]	4.4	11.2	0	357
Short15	SD	6.3	9.5	3.2	357
Tall15	RMSE	11.5	18.4	4.9	357
Tall15	Bias [b]	6.6	17.5	0.3	357
Tall15	SD	8.4	14.2	3.1	357

[a] excludes five flights identified to be problematic

[b] mean of absolute bias values

[c] cumulative points used to assess accuracy over all assessed flights

The RTK level accuracy of the camera geotags should produce products with similar accuracy, without the use of GCPs, as those generated with standard GPS positioning and the use of GCPs (Roze et al., 2014). DSMs created with and without GCPs for flights where the Ebee's camera geotags had RTK-corrected positions with an accuracy of ±2.5 cm tested this claim. Nine flights from the prairie site and 22 flights from the alpine site met the requirements for this test. Inclusion of GCPs had little effect on the standard deviation of error with respect to surface observations, but resulted in a reduction of the mean absolute error of the bias from 27 cm to 10 cm and from 14 cm to 6 cm at the prairie and alpine sites, respectively.

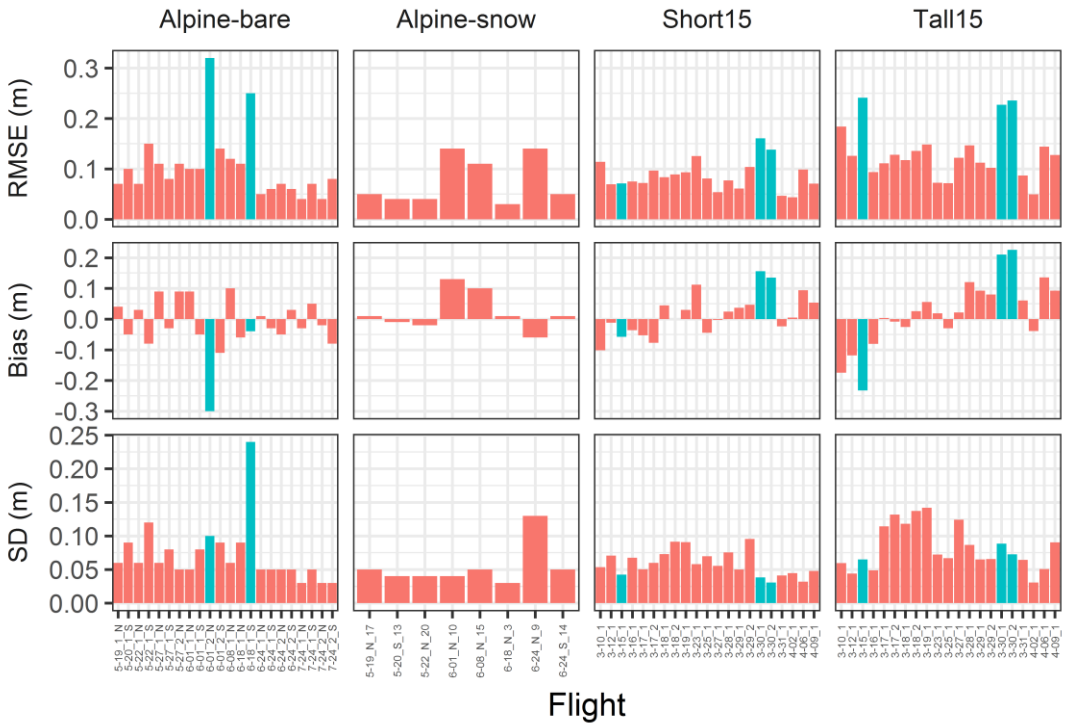

Figure 2.4: Root mean square error (RMSE, top row), Bias (middle row) and standard deviation (SD, bottom row) of DSMs with respect to surface over alpine-bare, alpine-snow, and short15 and tall15 stubble at prairie site, respectively. Blue bars highlight problematic flights and are excluded from summarization in Table 2.2. X-axis labels represent month-date-flight number of the day (to separate flights that occurred on the same day). Alpine-bare accuracies are separated into north or south areas, reflected with a _N or _S suffix. The last number in the alpine-snow x-axis label is the number of observations used to assess accuracy as the number of surface observations varied between 3 and 20.

2.3.2 Snow depth accuracy

The snow depth errors were similar to that of the surface errors with the alpine and Short15 stubble treatment having very similar errors, with mean RMSEs of 8.5 cm and 8.8 cm, but much larger errors over the Tall15 stubble treatment, with a mean RMSE of 13.7 cm (Figure 2.5 and Table 2.3). Snow depth errors were larger than the surface errors as the errors from the snow-free and snowcovered DSMs are additive in the DSM differencing. The usability of snow depth determined from DSM differencing requires comparison of signal-to-noise. Signal-to-noise, in Figure 2.5, clearly demonstrates that the deep alpine snowpacks have a large signal relative to noise and provide useable information on snow depth both at maximum accumulation and during most of the snowmelt period (SNR >7). In contrast, the shallow snowpack at the prairie site, despite a similar absolute error to the alpine site, demonstrates decreased ability to

retrieve meaningful snow depth information over the course of snowmelt; the signal became smaller than the noise. Applying the Rose criterion of a SNR ≥4, it is apparent that only the first flight at the short stubble and the first two flights at the Tall15 treatment provided useful information on the snow depth signal. This is relevant when applying this technique to other areas with shallow, wind redistributed seasonal snowcovers such as those that cover prairie, steppe and tundra in North and South America, Europe and Asia. This is in contrast to other studies which do not limit where this technique can be reasonably applied (Bühler et al., 2016; Nolan et al., 2015).

Table 2.3: Absolute snow depth accuracy summary

Area	Variable	Mean[a] (cm)	Maximum[a] (cm)	Minimum[a] (cm)	Total Points [c]
Alpine	RMSE	8.5	14.0	3	83
Alpine	Bias [b]	4.1	11.0	0	83
Alpine	SD	7.1	12.0	3	83
Short15	RMSE	8.8	15.8	0	323
Short15	Bias [b]	5.4	15.2	0	323
Short15	SD	6.1	10.3	0	323
Tall15	RMSE	13.7	27.2	0	323
Tall15	Bias [b]	9.8	26.4	0	323
Tall15	SD	8.3	13.9	0	323

[a] excludes two flights identified to be problematic
[b] mean of absolute bias values
[c] cumulative points used to assess accuracy over all assessed flights

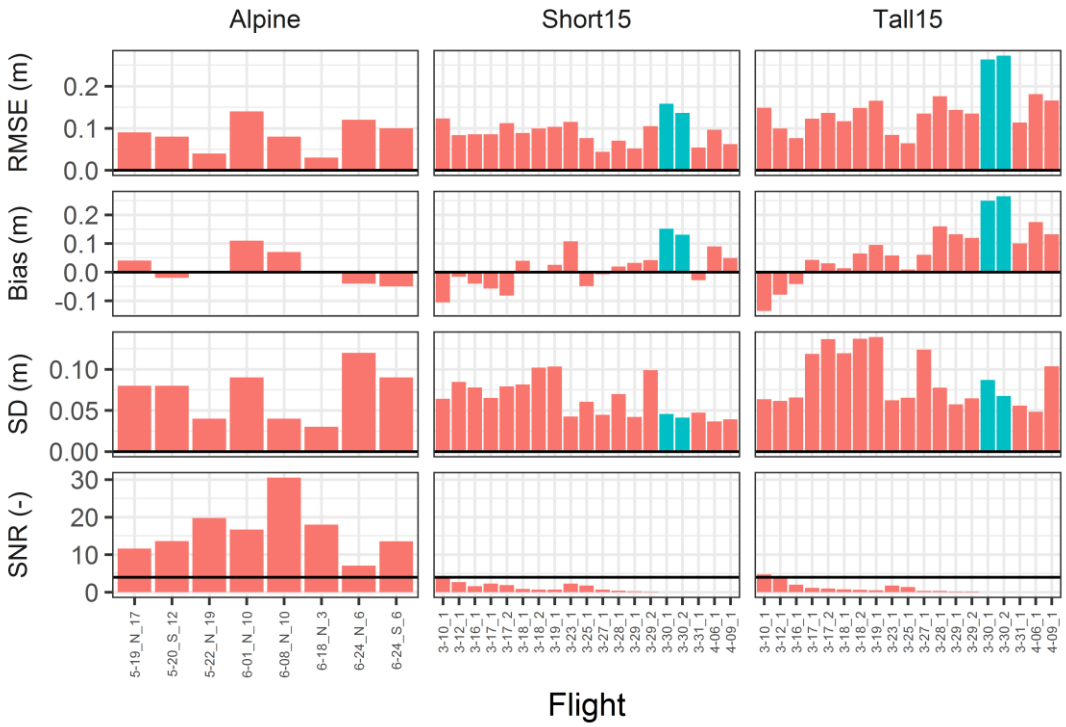

Figure 2.5: Estimated UAV snow depth error with respect to observed snow depth for the alpine site and the Short15 and Tall15 stubble treatments at prairie site. Blue bars highlight problematic flights and are excluded from summarization in Table 2.3. X-axis labels represent month-date. The last number in prairie labels is the flight of the day (to separate flights that occurred on the same day). Alpine labels separate the north or south flight areas suffixed as _N or _S respectively, and the last value is the number of observations used to assess accuracy as they vary between 3 and 19. Horizontal line in the SNR plots is the Rose criterion (SNR ≥4) that is used to identify flights with a meaningful snow depth signal.

2.3.3 Challenges

2.3.3.1 UAV Deployment Challenges

An attractive attribute of UAVs, versus manned aerial or satellite platforms, is that they allow "on-demand" responsive data collection. While deployable under most conditions encountered, the variability in the DSM RMSEs is likely due to the environmental factors at time of flight including wind conditions, sun angle, flight duration, cloud cover and cloud cover variability. In high wind conditions (>14 m s^{-1}) the UAV struggled to maintain its preprogrammed flight path as it was blown off course when cutting power to take photos. This resulted in missed photos and inconsistent density in the generated point clouds. Without a gimballed camera, windy conditions also resulted in images that deviated from the ideal nadir

orientation. The flights for the DSMs with the greatest RMSEs had the highest wind speeds as measured by the UAV. Four of the five problematic flights were due to high winds (>10 m s^{-1}) and were identified by relatively low-density point clouds with significant gaps which rendered DSMs that did not reflect the snow surface characterises.

As the system relies on a single camera traversing the areas of interest, anything that may cause a change in the reflectance properties of the surface will complicate post-processing and influence the overall accuracy. Consistent lightning is important with a preference for clear skies and high solar angles to minimize changes in shadows. Diffuse lighting during cloudy conditions results in little contrast over the snow surface and large gaps in the point cloud over snow, especially when the snowcover was homogeneous. Three flights under these conditions could not be used and were not included in the previously shown statistics. Clear conditions and patchy snowcover led to large numbers of overexposed pixels (see Sect 3.3.2). Low sun angles should be avoided as orthomosaics from these times are difficult to classify due to the large and dynamic surface shadows present and the relatively limited reflectance range.

It is suggested that multirotor UAVs may be more stable and return better data products in windy conditions (Bühler, et al., 2016). There have not been any direct comparison studies that the authors are aware of that validate such assertions. A general statement regarding the use of fixed wing versus multirotor is also impossible with the broad spectrum of UAVs and their respective capabilities on the market. The only clear benefit of using a multirotor platform is that larger, potentially more sophisticated, sensors can be carried and landing accuracy is greater. That being said, the Ebee RTK returns data at resolutions that are more than sufficient for the purposes of this study (3cm $pixel^{-1}$), can cover much larger areas and has a higher wind resistance (>14 m s^{-1}) than many multirotor UAVs. Landing accuracy (±5 m) was also sufficient to locate a landing location in the complex topography of the alpine site. The more important issue relative to any comparison between platform types is that all UAVs will have limited flight times and results are compromised if conditions are windy and light is inconsistent. Until a direct platform comparison study is conducted this experience, and results of other recent studies (Vander Jagt et al., 2015; Bühler et al., 2016; De Michele et al., 2016), suggests that fixed wing platforms, relative to multi-rotor platforms, have similar accuracy and deployment constraints but a clear range advantage.

2.3.3.2 Challenges applying Structure from Motion over snow

Erroneous points over snow were generated in post-processing with the default software settings at the alpine site. These points were up to several metres above the actual snow surface and were mainly located at the edge of snow patches, but also on irregular and steep snow surfaces in the middle of a snow patch. The worst cases occurred during clear sunny days over south-facing snow patches, which were interspersed with these erroneous points. These points are related to the overexposure of snow pixels in the images which had bare ground in the centre and small snow patches on the edges. This is a consequence of the automatically adjusted exposure based on centre-weighted light metering of the Canon ELPH camera. It is recommended that erroneous points could be minimized with the removal of overexposed images; however, this increased the bias and led to gaps in the point cloud, which made this approach inappropriate.

The semi-global matching (SGM) option with optimization for 2.5D point clouds (point clouds with no overlapping points) proved to be the best parameter setting within the post-processing software Postflight Terra 3D. Semi-global matching was employed to improve results on projects with low or uniform texture images, while the optimization for 2.5D removes points from the densified point cloud (SenseFly, 2015). The SGM option removed most of the erroneous points with best results if processing was limited to individual flights. Including images from additional flights resulted in a rougher surface with more erroneous points. This may be caused by changes in the surface lighting conditions between flights. Biases did not change when using SGM though some linear artefacts were visible when compared to default settings. These linear artefacts caused the SD to increase from 1 cm to 3 cm on bare ground. Areas with remaining erroneous points were identified and excluded from the presented analysis. Table 2.4 summarises the extent of the areas removed with respect to the snowcovered area at the alpine site. The fifth problematic flight identified (June 1, 2015 flight over north area of alpine site) had a much larger bias with the inclusion of GCPs and the reason for this cannot be determined. The “black box” nature of this proprietary software and small number of adjustable parameters clearly limits the application of this post-processing tool for scientific purposes.

Table 2.4: Summary of areas excluded due to erroneous points with respect to snowcovered area at Alpine site.

Flight [a]	Snowcovered area (%)	Percentage of snowcovered area excluded (%)
5-19_N	45.9	0.0
5-20_S	32.6	2.0
5-22_N	39.8	0.0
6-01_N	24.0	0.0
6-08_N	12.5	3.2
6-18_N	5.3	19.3
6-24_N	3.1	21.9
6-24_S	3.7	18.9

[a]month-day_portion of study area

2.3.4 Applications of UAVs and Structure from Motion over snow

The distributed snow depth maps generated from UAV imagery are of great utility for understanding snow processes at previously unrealized resolutions, spatial coverages and frequencies. Figure 2.6 provides examples of UAV derived distributed snow depth maps. The identification of snow dune structures, which correspond to in-field observations, is a qualitative validation that UAV derived DSM differencing does indeed provide reasonable information on the spatial variability of snow depth. Actual applications will depend upon the surface, snow depth and other deployment considerations as discussed.

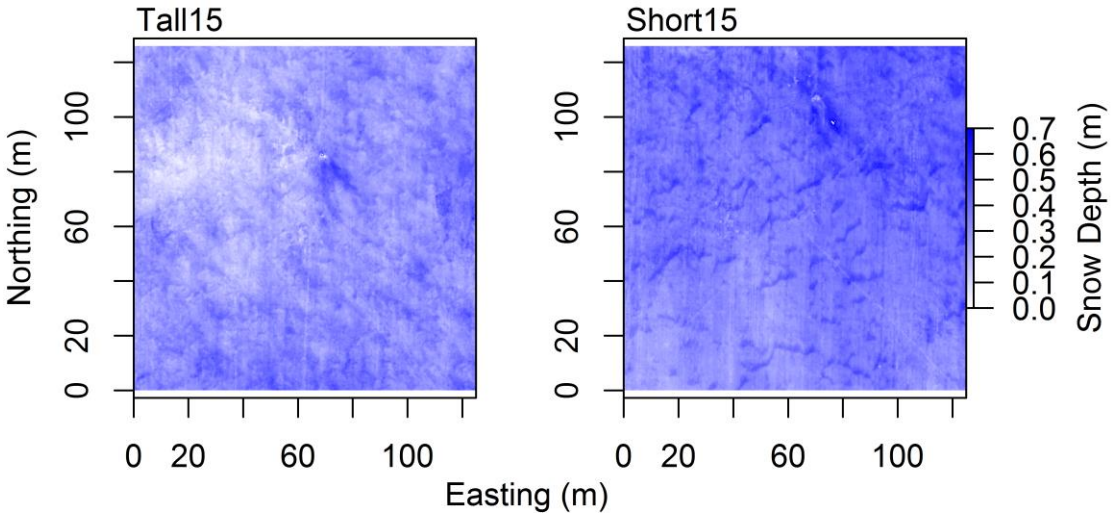

Figure 2.6: Bias corrected distributed snow depth (m) for Short15 and Tall15 stubble treatments at peak snow depth (March 10, 2015) at the prairie site.

Applications at the alpine site also include the ability to estimate the spatial distribution of snow depth change due to ablation (Figure 2.7). To obtain ablation rates, the spatial

distribution of snow density is still needed but it may be estimated with a few point measurements or with parameterizations dependent upon snow depth (Jonas et al., 2009; Pomeroy and Gray, 1995). In Figure 2.7 the mean difference in snow depth between the two flights was 0.9 m; this gives a SNR of ~11 which is more than sufficient to confidently assess the spatial variability of melt.

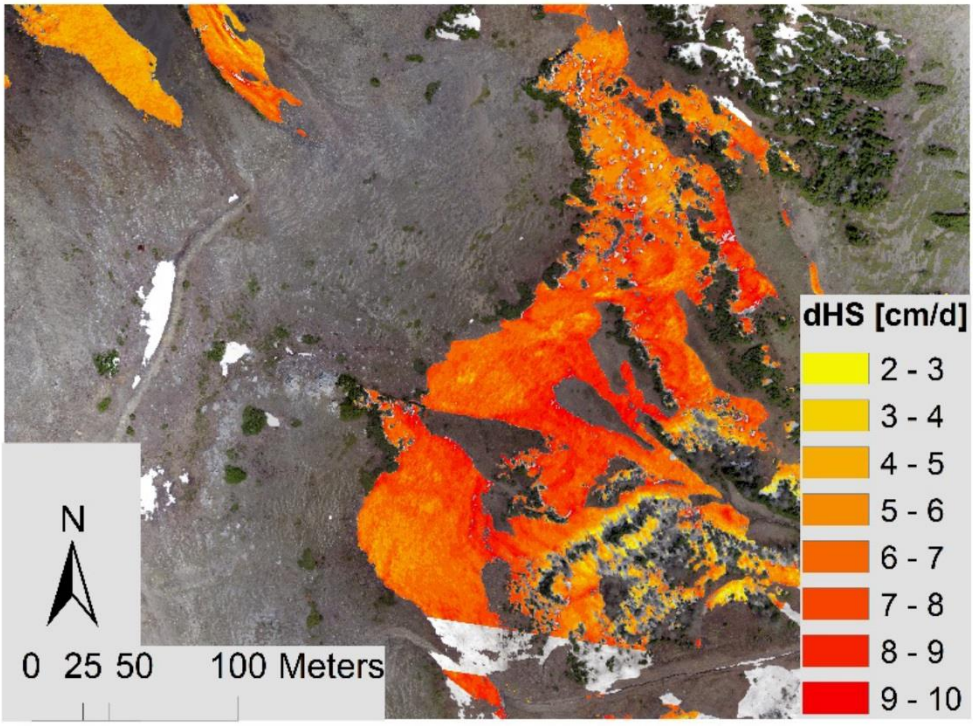

Figure 2.7: Rate of snow depth change (dHS day^{-1}) between May 19 and June 1, 2015 in the northern portion of the alpine site.

Despite the limitations and deployment considerations discussed, the Ebee RTK was capable of providing accurate data at very high spatial and temporal resolutions. A direct comparison between fixed wing and multirotor platforms is necessary to determine how snow depth errors may respond to variations in wind speed and lighting conditions. Until then, based on this experience and results of other recent studies (Vander Jagt et al., 2015; Bühler et al., 2016; De Michele et al., 2016), we do not expect there to be large differences in errors between platform types. Rather, the most important consideration when planning to map snow depth with a UAV should be whether the anticipated SNR will allow for direct estimates of snow depth or snow depth change. The SNR issue limits the use of this technique to areas with snow depths or observable changes sufficiently larger than the SD of the error. We propose a mean snow depth

threshold of 30 cm is necessary to obtain meaningful information on snow depth distribution with current technology. This threshold is equal to four times the mean observed SD (Rose criterion), but will vary with the application, site and user's error tolerance.

The use of SfM in shallow snow environments, such as on the Canadian Prairies, is therefore limited to measuring near-maximum snow depths. Besides providing an estimate of the total snow volume, this information can also inform snowcover depletion curve estimation and description (Pomeroy et al., 1998). Simple snowcover depletion models can be parameterized with estimates of snow depth mean and coefficient of variation (Essery and Pomeroy, 2004), which otherwise need to be obtained from snow surveying. For 2015, coefficients of variation from the peak snow depth maps were 0.255 and 0.173, at the Short15 and Tall15 stubble treatment sites respectively, which are similar to previous observations from corresponding landforms/surfaces (Pomeroy et al., 1998).

In addition to parameterizing snowcover depletion models, UAV data could also be used to test the performance of these same models as Structure from Motion processing of UAV images produces orthomosaics in addition to DSMs. Sequences of orthomosaics are especially useful to quantify the spatio-temporal dynamics of snowcovered area (SCA) depletion processes. Orthomosaics are complementary products to DSMs and their quality is subject to the same deployment conditions as DSMs. Orthomosaics have the same horizontal accuracy and resolution as the DSMs, but without a vertical component; any DSM vertical errors are irrelevant. Interpretation of SCA from orthomosaics is therefore possible regardless of surface characteristics or snow depth. The classification of orthomosaics to quantify surface properties will introduce error, and can be challenging in changing light conditions, which changes the spectral response of snow or non-snowcovered areas across the surface. Typical supervised and unsupervised pixel-based classification procedures can be readily applied. Since UAV imagery is at a much higher resolution than satellite or airborne imagery, classification differences in spectral response due to varying light conditions can be compensated for by using object-oriented classification which also takes into account shape, size, texture, pattern and context (Harayama and Jaquet, 2004).

An example of a snowcovered depletion curve for the prairie site is presented in Figure 2.8. A simple unsupervised classification of the orthomosaic into snow and non-snow classes

quantifies the earlier exposure of the Tall15 stubble treatment relative to the Short15 stubble treatment. The Tall15 stubble surface is an illustrative example of the advantages UAVs offer for SCA quantification. Tall stubble is a challenging surface on which to quantify SCA as snow is prevalent below the exposed stubble surface rendering other remote sensing approaches inappropriate. From an oblique perspective, the exposed stubble obscures the underlying snow and prevents the classification of SCA from georectification of terrestrial photography (Figure 2.9). Due to the surface heterogeneity on small scales (stubble, soil and snow all regularly occurring within 30 cm) satellite, and most aerial, imagery struggles with clearly identifying SCD.To identify features accurately, in this case exposed stubble versus snow, multiple pixels are needed per feature (Horning and DuBroff, 2004). The 3.5 cm resolution of the orthomosaic corresponds to approximately three pixels to span the 10 cm stubble row which is sufficient for accurate SCA mapping over a tall stubble surface. The advantages of high-resolution UAV orthomosaics are obviously not limited to SCA mapping of snow between wheat stubble and can be readily applied to other challenging heterogeneous surfaces where SCA quantification was previously problematic. Snowcover data at this resolution can quantify the role of vegetation on melt processes at a micro-scale, which can in turn inform and validate snowmelt process understanding.

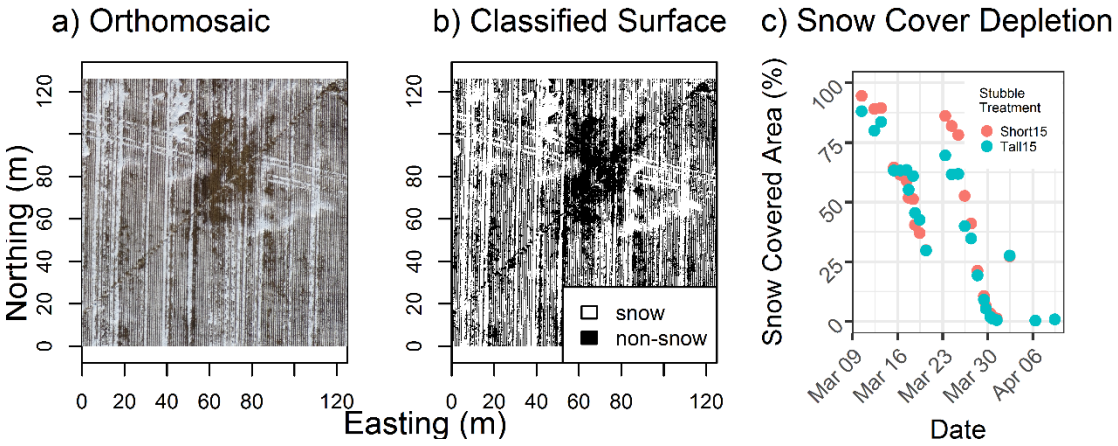

Figure 2.8: Estimation of snowcovered area requires an a) orthomosaic which is then b) classified into snow and non-snowcovered area. This produces a c) snowcover depletion curve when a sequence of orthomosaics are available. The Short15 and Tall15 stubble treatments snowcovered areas at the prairie site are contrasted, with a snowfall event evident on March 23, 2015.

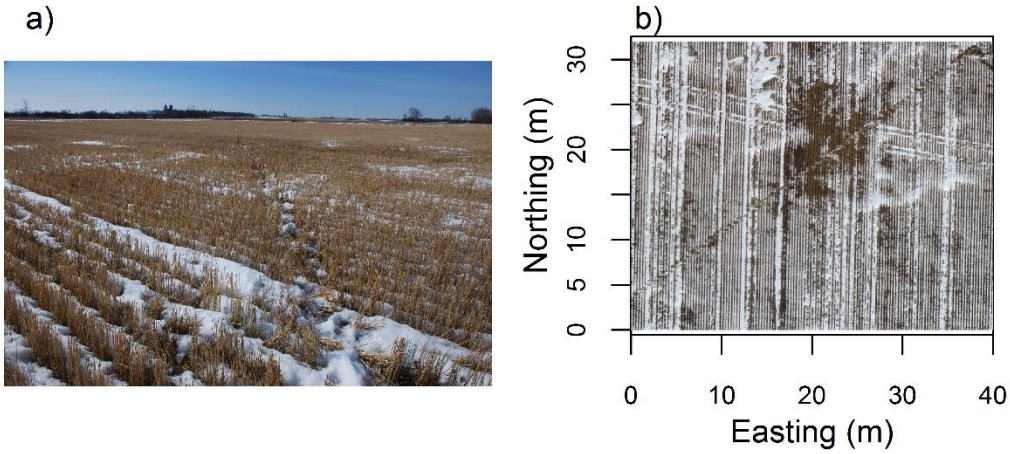

Figure 2.9: a) An oblique photograph demonstrates the issue of tall stubble obscuring underlying snowcover when considered in contrast to b) a UAV orthomosaic of the same area on the same date that clearly shows widespread snowcover.

2.4. Conclusions

The accuracy of DSMs and orthomosaics, generated through application of SfM techniques to imagery captured by a small fixed-wing UAV, was evaluated in two different environments, mountain and prairie, to verify its ability to quantify snow depth and its spatial variability over the ablation period. The introduction of functional UAVs to the scientific community requires a critical assessment of what can reasonably be expected from these devices over seasonal snowcovers. Snow represents one of the more challenging surfaces for UAVs and SfM techniques to resolve due to the lack of contrast and high surface reflectance. Field campaigns assessed the accuracy of the Ebee RTK system over flat prairie and complex terrain alpine sites subject to wind redistribution and spatially variable ablation associated with varying surface vegetation and terrain characteristics. The mean accuracies of the DSMs were 8.1 cm for the Short15 surface, 11.5 cm for the Tall15 surface and 8.7 cm for the alpine site. These DSM errors translate into mean snow depth errors of 8.8 cm, 13.7 cm and 8.5 cm over the Short15, Tall15 and alpine sites respectively. Ground control points were needed to achieve this level of accuracy. The SfM technique provided meaningful information on maximum snow depth at all sites, and snow depth depletion could also be quantified at the alpine site due to the deeper snowpack and consequent higher signal-to-noise ratio. These findings demonstrate that SfM can be applied to accurately estimate snow depth and its spatial variability only in areas with snow depth >30 cm. This restricts SfM applications with shallow, windblown snowcovers. Snow depth estimation accuracy varied with wind speed, surface characteristics and sunlight; the most

consistent performance was found for wind speeds <10 ms^{-1}, surfaces with insignificant vegetation cover, clear skies and high sun angles. The ability to generate good results declined over especially homogenous snow surfaces and southerly slope aspects in mountain terrain. Clear sky conditions were favourable for high snowcovered fractions with limited snow surface brightness contrast. During snowmelt with reduced snowcovered fraction, clear sky conditions caused overexposure of snow pixels and erroneous points in the point clouds.

The challenges of applying SfM to imagery collected by a small UAV over snow complicate the generation of DSMs and orthomosaics relative to other surfaces with greater contrast and identifiable features. Regardless, the unprecedented spatial resolution of the DSMs and orthomosaics, low costs and "on-demand" deployment provide exciting opportunities to quantify previously unobservable small-scale variability in snow depth that will only improve the ability to quantify snow properties and processes.

2.5. Manuscript Integration with Broader Thesis

The ability for UAV imagery and SfM is assessed to determine if it is a better alternative than traditional snow surveying for observing snowmelt dynamics on the Canadian Prairies. These observations, as well as more from a similar field campaign at the same site in 2016, are also critical for informing the hypotheses and models developed in other chapters of this thesis. A key finding of Chapter 2 is that there are significant challenges using this technique to observe SWE depletion in prairie snowpacks. This inability of UAV SFM techniques, due to the identified signal to noise issues, means that snow surveying remains the most reliable method to observed SWE depletion. The snow surveys, used to test the accuracy of the UAV snow depth, can also be used to directly observe SWE depletion across the stubble treatments (0.24 m wheat stubble in 2015 (Short15), 0.35 m wheat stubble in 2015 (Tall 15), 0.24 m wheat stubble in 2016 (Wheat 16), and 0.24 m canola stubble in 2016 (Canola 16)). Unfortunately, the noise due to sampling and observation error, as seen by the overlapping error bounds of SWE in Figure 2.10, is large relative to the shallow snow which limits the confidence of snow surveying to observe small differences in snowmelt over the various stubble treatments. The inability to directly observe the influence of stubble influence upon SWE depletion from UAV observations and snow surveying highlights the uncertainties of these techniques in this challenging domain, but also provides evidence for a compensatory energy balance that regulates SWE depletion despite

obviously different stubble treatments. These observations support the hypotheses, and motivates the development, of the snow-stubble-atmosphere energy balance model in Chapter 4 that explicitly represents snow-stubble-atmosphere surface energy balance compensation. The differences in SCA for the various stubble treatments from UAV observations highlight differences in spatial heterogeneity of the snowcover depletion processes on adjacent crop stubble treatments with similar SWE depletion patterns (Figure 2.10). Previous research has developed a deep understanding of the energy balance in homogenous settings which is clearly inappropriate considering this heterogeneity. The lateral exchange of sensible heat energy with wind over a heterogenous snowcover that enhances snowmelt is rarely considered let alone the latent heat advection that may occur from identification of significant ponded water area upwind of snow patches from the UAV imagery. This provides the evidence for a compensatory mechanism between sensible and latent heat advection that will act to limit SWE depletion even when difference in SCA exist, as seen in Figure 2.10. This supports development and deployment of a novel observation system to directly measure the relative role of sensible and latent heat advection on the snowmelt energy balance in Chapter 3. The sensible and latent heat advection model in Chapter 5 takes advantage of the UAV derived SCA classification, from Chapter 2, to validate the scaling parameters of snowcover geometry which is critical for the modelling of advection. The observational findings of Chapter 2 provide empirical evidence of compensatory energy balance and advection dynamics that are explicitly observed and modelled in Chapters 3, 4, 5, and 6.

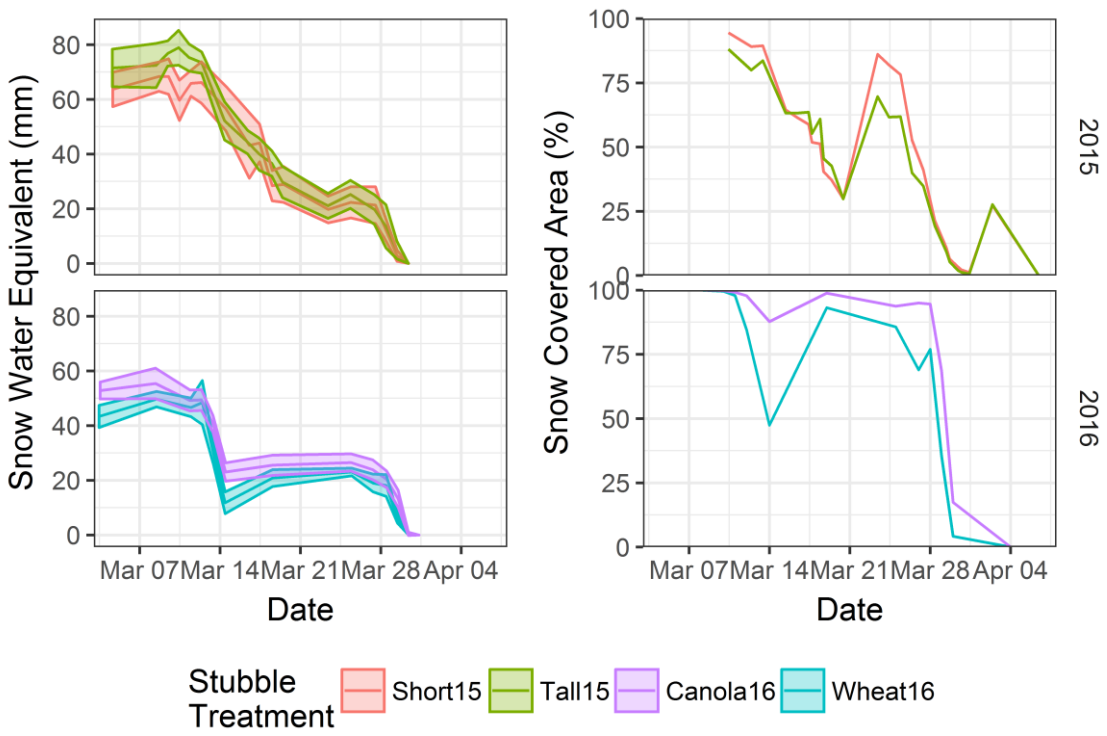

Figure 2.10: Snow water equivalent from snow surveys and snowcovered area from classified UAV orthomosaics for stubble treatments in 2015 and 2016. Bootstrapping of snow depth and snow densities errors are used to estimate the 95% confidence intervals (shaded areas) of the estimated snow water equivalent due to sampling error.

2.6. References

Armstrong, R. L., Brun, E. (2008). Snow and Climate: Physical Processes, Surface Energy Exchange and Modeling. Cambridge, UK: Cambridge University Press.

Bewley, D. S., Pomeroy, J. W., Essery, R. (2007). Solar Radiation Transfer Through a Subarctic Shrub Canopy. Arctic, Antarctic, and Alpine Research, 39(3), 365–374.

Boufama, B., Mohr, R., Veillon, F. (1993). Euclidean Constraints for Uncalibrated Reconstruction. In 4th International Conference on Computer Vision (ICCV ’93) (pp. 466–470). Berlin Germany: IEEE Computer Society.

Bühler, Y., Marty, M., Egli, L., Veitinger, J., Jonas, T., Thee, P., Ginzler, C. (2015). Snow depth mapping in high-alpine catchments using digital photogrammetry. The Cryosphere, 9, 229–243. https://doi.org/10.5194/tc-9-229-2015

Bühler, Y., Adams, M. S., Bösch, R., Sto, A. (2016). Mapping snow depth in alpine terrain with unmanned aerial systems (UAS): potential and limitations. The Cryosphere Discussions. https://doi.org/10.5194/tc-2015-220

Collier, O. (2002). The Impact on Topographic Mapping of Developments in Land and Air Survey: 1900-1939. Cartography and Geographic Information Science, 29, 155–174.

DeBeer, C. M., Pomeroy, J. W. (2009). Modelling snow melt and snowcover depletion in a small alpine cirque, Canadian Rocky Mountains. Hydrological Processes, 23(18), 2584–2599.

DeBeer, C. M., Pomeroy, J. W. (2010). Simulation of the snowmelt runoff contributing area in a small alpine basin. Hydrology and Earth System Sciences, 14(7), 1205–1219.

Deems, J., Painter, T., Finnegan, D. (2013). Lidar measurement of snow depth: a review. Journal of Glaciology, 59(215), 467–479. https://doi.org/10.3189/2013JoG12J154

Deems, J., Painter, T. (2006). LiDAR measurement of snow depth: accuracy and error sources. In Proceedings of the 2006 International Snow Science Workshop (pp. 330–338). Telluride, Colorado.

Dingman, S. L. (2002). Physical Hydrology (2nd ed.). Upper Saddle River, New Jersey: Prentice Hall.

Dumanski, S., Pomeroy, J. W., Westbrook, C. J. (2015). Hydrological regime changes in a Canadian Prairie basin. Hydrological Processes, 29(18), 3893–3904.

Essery, R., Pomeroy, J. W. (2004). Implications of spatial distributions of snow mass and melt rate for snow-cover depletion: theoretical considerations. Annals of Glaciology, 38(1), 261–265. https://doi.org/10.3189/172756404781815275

Gray, D. M., Male, D. H. (1981). Handbook of Snow: Principles, Processes, Management, and Use. Toronto, Canada: Pergamon Press.

Grünewald, T., Schirmer, M., Mott, R., Lehning, M. (2010). Spatial and temporal variability of snow depth and ablation rates in a small mountain catchment. The Cryosphere, 4(2), 215–225. https://doi.org/10.5194/tc-4-215-2010

Harayama, A., Jaquet, J. (2004). Multi-source object-oriented classification of landcover using very high resolution imagery and digital elevation model. UNEP, Switzerland.

Harder, P., Pomeroy, J. W., Westbrook, C. J. (2015). Hydrological resilience of a Canadian Rockies headwaters basin subject to changing climate, extreme weather, and forest management. Hydrological Processes, 29(18), 3905–3924. https://doi.org/10.1002/hyp.10596

Hopkinson, C., Pomeroy, J. W., DeBeer, C. M., Ellis, C. R., Anderson, A. (2012). Relationships between snowpack depth and primary LiDAR point cloud derivatives in a mountainous environment. Remote Sensing and Hydrology, 352, 1–5.

Horning, N., Dubroff, N. (2004). Myths and misconceptions about remote sensing. Version 1.0., 16. Retrieved from http://biodiversityinformatics.amnh.org.

Vander Jagt, B., Lucieer, A., Wallace, L., Turner, M., Durand, D. (2015). Snow Depth Retrieval with UAS Using Photogrammetric Techniques. Geosciences, 5, 264–285. https://doi.org/10.3390/geosciences5030264

Jonas, T., Marty, C., Magnusson, J. (2009). Estimating the snow water equivalent from snow depth measurements in the Swiss Alps. Journal of Hydrology, 378, 161–167. https://doi.org/10.1016/j.jhydrol.2009.09.021

Jones, H. G., Pomeroy, J. W., Walker, D. A., Hoham, R. W. (2001). Snow Ecology: An Interdisciplinary Examination of Snow-Covered Ecosystems. Cambridge, UK: Cambridge University Press.

Kinar, N. J., Pomeroy, J. W. (2015). Measurement of the physical properties of the snowpack. Reviews of Geophysics, 53. https://doi.org/10.1002/2015RG000481

López-Moreno, J. I., Fassnacht, S. R., Heath, J. T., Musselman, K. N., Revuelto, J., Latron, J., … Jonas, T. (2013). Small scale spatial variability of snow density and depth over complex alpine terrain : Implications for estimating snow water equivalent. Advances in Water Resources, 55, 40–52. https://doi.org/10.1016/j.advwatres.2012.08.010

Macdonald, M. K., Pomeroy, J. W., Pietroniro, A. (2010). On the importance of sublimation to an alpine snow mass balance in the Canadian Rocky Mountains. Hydrology and Earth System Sciences, 14(7), 1401–1415.

Marris, E. (2013). Fly, and bring me data. Nature, 498, 156–158.

Mattmann, C. A., Painter, T., Ramirez, P. M., Goodale, C., Hart, A. F., Zimdars, P., … Ave, A. (2014). 24 hour near real time processing and computation for the JPL Airborne Snow Observatory. In Geoscience and Remote Sensing Symposium (IGARSS), 2014 IEEE International (pp. 5222–5225).

De Michele, C., Avanzi, F., Passoni, D., Barzaghi, R., Pinto, L., Dosso, P., Ghezzi, A., Gianatti, R., Della Vedova, G. (2015). Microscale variability of snow depth using U.A.S. technology. The Cryosphere Discussions, 9, 1047–1075. https://doi.org/10.5194/tcd-9-1047-2015

Milly, P. C. D., Betancourt, J., Falkenmark, M., Hirsch, R. M., Kundezewicz, Z. W., Lettenmaier, D. P., Stouffer, R. J. (2008). Stationarity Is Dead: Whither Water Management? Science, 319, 573–574.

Mote, P. W., Hamlet, A. F., Clark, M. P., Lettenmaier, D. P. (2005). Declining mountain snowpack in western North America. Bulletin of the American Meteorological Society, 86(1), 39–49. https://doi.org/10.1175/BAMS-86-1-39

Nolan, M., Larsen, C., Sturm, M. (2015). Mapping snow depth from manned aircraft on landscape scales at centimeter resolution using structure-from-motion photogrammetry. The Cryosphere, 9, 1445–1463. https://doi.org/10.5194/tc-9-1445-2015

Pomeroy, J. W., Gray, D. M. (1995). Snow accumulation, relocation and management. Saskatoon, SK: Science Report No. 7, National Hydrology Research Institute, Environment Canada.

Pomeroy, J. W., Gray, D. M., Shook, K., Toth, B., Essery, R., Pietroniro, A., Hedstrom, N. R. (1998). An evaluation of snow accumulation and ablation processes for land surface modelling. Hydrological Processes, 12, 2339–2367.

Pomeroy, J. W., Gray, D. M., Landine, P. G. (1993). The Prairie Blowing Snow Model: characteristics, validation, operation. Journal of Hydrology, 144(1–4), 165–192.

Rango, A., Laliberte, A. (2010). Impact of flight regulations on effective use of unmanned aircraft systems for natural resources applications. Journal of Applied Remote Sensing, 4. https://doi.org/10.1117/1.3474649

Rose, A. (1973). Vision: Human and Electronic. New York: Plenum Press.

Roze, A., Zufferey, J.-C., Beyeler, A., Mcclellan, A. (2014). eBee RTK Accuracy Assessment. Lausanne, Switzerland.

SenseFly. (2015). Menu Process Options Point Cloud Densification. Retrieved from https://sensefly.zendesk.com/hc/en-us/articles/204542828-Menu-Process-Options-Point-Cloud-Densification

Shook, K., Gray, D. M. (1996). Small-Scale Spatial Structure of Shallow Snowcovers. Hydrological Processes, 10, 1283–1292.

Spetsakis, M., Aloimonost, J. (1991). A Multi-frame Approach to Visual Motion Perception. International Journal of Computer Vision, 6, 245–255.

Stewart, I. T., Cayan, D. R., Dettinger, M. D. (2004). Changes in Snowmelt Runoff Timing in Western North America under a `Business as Usual' Climate Change Scenario. Climatic Change, 62(1–3), 217–232. https://doi.org/10.1023/B:CLIM.0000013702.22656.e8

Sturm, M. (2015). White water: Fifty years of snow research in WRR and the outlook for the future. Water Resources Research, 51, 4948–4965. https://doi.org/10.1002/2015WR017242

Szeliski, R., Kang, S. (1994). Recovering 3D Shape and Motion from Image Streams Using Nonlinear Least Squares. Journal of Visual Communication and Image Representation, 5, 10–28.

Westoby, M., Brasington, J., Glasser, N., Hambrey, M., Reynolds, J. (2012). "Structure-from-Motion" photogrammetry: A low-cost, effective tool for geoscience applications. Geomorphology, 179, 300–314. https://doi.org/10.1016/j.geomorph.2012.08.021

Chapter 3: Local scale advection of sensible and latent heat during snowmelt

Status: Published October 5, 2017

Citation: Harder, P., Pomeroy, J. W., Helgason, W. D. (2017). Local scale advection of sensible and latent heat during snowmelt. Geophysical Research Letters, 44, 9769–9777. https://doi.org/10.1002/2017GL074394

Author Contributions: PH conceptualized the field program, designed and built the instrumentation, performed all fieldwork, performed analysis, and wrote manuscript. JP and WH provided guidance, equipment and financial resources for the field campaign, and reviewed and revised manuscript.

3.1. Abstract

The breakup of snowcover into patches during snowmelt leads to a dynamic, heterogeneous land surface composed of melting snow, and wet and dry soil and plant surfaces. Energy exchange with the atmosphere is therefore complicated by horizontal gradients in surface temperature and humidity as snow surface temperature and humidity are regulated by the phase change of melting snow unlike snow-free areas. Airflow across these surface transitions results in local-scale advection of energy that has been documented as sensible heat during snowmelt, while latent heat advection has received scant attention. Herein, results are presented from an experiment measuring near-surface profiles of air temperature and humidity across snow-free to snowcovered transitions that demonstrates that latent heat advection can be the same order of magnitude as sensible heat advection and is therefore an important source of snowmelt energy. Latent heat advection is conditional on an upwind source of water vapor from a wetted snow-free surface.

3.2. Introduction

Snowcovered area declines and snowcover becomes patchy during the course of snow ablation, significantly influencing snow-atmosphere interactions and snowmelt rates (Granger et al., 2006; Marsh and Pomeroy, 1996; Menard et al., 2014; Pomeroy et al., 1998). The differences

in energetics across snow and non-snow areas leads to a heterogeneous distribution of surface temperatures as snow is limited to a maximum of 0 °C due to phase change. Air flow across patchy snowcover leads to local-scale sensible heat advection (H_A) to snow (Essery et al., 2006; Granger et al., 2002; Liston, 1995; Mott et al., 2013; Weisman, 1977); however, complimentary research on latent heat advection (LE_A) has not occurred.

Measuring advection is challenging and direct observations of its impact on melt rates are recently demonstrated by Mott et al. (2011), who documented consistently greater melt rates on the leading edge of snow patches from repeat terrestrial laser scanning. Field studies to understand the processes describing advection are most frequently based upon observations of near-surface changes in air temperature (T_a) across surface transitions. Abrupt changes in surface temperature and humidity cause internal boundary layers to develop downwind of the transition (Garratt, 1990). Granger et al. (2002; 2006) demonstrated that internal boundary layers of T_a across snow-free to snow transitions, follow an established power law relationship with height, and can be related to H_A through boundary layer integration. In complex terrain, internal boundary layer development may be impeded by atmospheric decoupling of the atmosphere from the snow surface which subsequently suppresses H_A (Mott et al., 2013). Because of challenges with observational approaches, modeling has been used to understand the possible energy and mass flows associated with advection. Early work by Weisman (1977) applied mixing length theory to estimate advection to lakes and snow patches with the model implicitly accounting for both LE_A and H_A. Subsequent approaches have varied in complexity. A simple approach taken by Marsh and Pomeroy (1996) related bare ground sensible heat fluxes to areal average H_A via an advection efficiency term which relates to snowcovered area. The application of internal boundary layer integration (Essery et al., 2006; Granger et al., 2002) to tile models (Essery et al., 2006) whilst accounting for the fractal nature of snowcover (Shook et al., 1993b) has provided another approach to estimate areal average estimates of advection. More complex approaches have employed atmospheric boundary layer models (Liston, 1995) and large eddy simulation (Mott et al., 2015) to quantify the non-linear relationships between snow patch characteristics/geometry and advected energy. Numerical models provide the most detailed description of the processes but are constrained to idealized boundary conditions. The challenge in all observational or modelling approaches surveyed is that none are validated with actual

observations of advection nor explicitly partition advected energy into sensible or latent heat components during snowmelt.

A simple alternative approach to quantify advection in turbulent flow, which does not require representations of internal boundary growth, stability, or surface roughness, is possible by consideration of the two dimensional Reynolds-averaged scalar budget (Paw U et al., 2000)

$$\frac{\partial \bar{c}}{\partial t} + \bar{u}\frac{\partial \bar{c}}{\partial x} + \bar{w}\frac{\partial \bar{c}}{\partial z} + \frac{\partial}{\partial x}(\overline{u'c'}) + \frac{\partial}{\partial z}(\overline{w'c'}) = \bar{S}, \tag{3.1}$$

where c is the scalar of interest, t (s) is time, u (m s^{-1}) is horizontal wind speed, w (m s^{-1}) is vertical wind speed, x (m) is horizontal distance, z (m) is vertical distance and S (scalar unit s^{-1}) is the scalar net source/sink rate. Overbars denote interval averages while primes denote instantaneous deviations from interval averages. The terms, from left, represent storage, horizontal advection, vertical advection, horizontal turbulent flux divergence and vertical turbulent flux divergence. Integrating Equation 3.1 with respect to the profile depth results in a framework to quantify H_A (W m^{-2}) and LE_A (W m^{-2}) for the horizontal advection term from two-dimensional specific humidity (q: kg kg^{-1}) and T_a (°C) profiles to give (Kochendorfer and Paw U, 2011)

$$\int_{z=0}^{z_p} \rho_{air} c_{air} \bar{u} \frac{\partial \bar{T}}{\partial x} dz = H_A, \tag{3.2}$$

and

$$\int_{z=0}^{z_p} \rho_{air} L_s \bar{u} \frac{\partial \bar{q}}{\partial x} dz = LE_A. \tag{3.3}$$

In Equations 3.2 and 3.3, z_p (m) is the profile depth of interest, ρ_{air} (kg m^{-3}) is the density of air, c_{air} (1005 J kg^{-1} K^{-1}) is the specific heat capacity of air and L_s (2.835×106 J kg^{-1}) is the latent heat of sublimation.

A comparable field experiment (Kochendorfer and Paw U, 2011) also examined vertical advection and turbulent fluxes across a smooth (bare soil) to rough (1 m sorghum). These observations demonstrated vertical advection is due to deceleration and upward motion of airflow in the sorghum canopy. For the relatively smaller change in roughness from a short crop stubble (rough) to snow (smooth), vertical advection will have a much smaller impact.

The overall objective of this study is to assess the role of H_A and LE_A from non-snow surfaces to snowcovered surfaces during snowmelt with field observations.

3.3. Methodology

3.3.1. Site

The field site, situated near Rosthern, Saskatchewan, Canada (52.69 °N, 106.45 °W), is representative of the Canadian Prairie agricultural region. Topographic relief is limited and the local landscape is interspersed with woodlands and wetlands. Maximum snow depth is typically less than 0.50 m and the snowcovered area is patchy and dynamic during ablation (Pomeroy and Gray, 1995). Data was collected at the 65 ha study site during March 2015. The surface roughness was defined by the presence of standing wheat stubble which remained erect throughout the snow season. Stubble height was approximately 0.35 m on a tall stubble treatment (Tall 15) and 0.15 m on a short stubble treatment (Short 15).

3.3.2. Instrumentation

Profiles of T_a, q and u are required to estimate advection following the framework conceptualized in Equations 3.1 to 3.3. A mobile system, comprised of sensors mounted on four towers, was developed for rapid deployment to surface transitions of interest (Figure 3.1a). Instrumentation was mounted on an adjustable rail to ensure consistent sensor heights relative to the surface. Wind speed was observed with two Met One 014A three-cup anemometers mounted on the upwind tower at 1.00 m and 2.00 m. Air temperature profiles were measured with 76.2 µm diameter Type-T fine wire thermocouples at 0.04 m, 0.08 m, 0.16 m, 0.32 m, 0.50 m, 1.00 m, 1.50 m and 2.00 m on each tower.

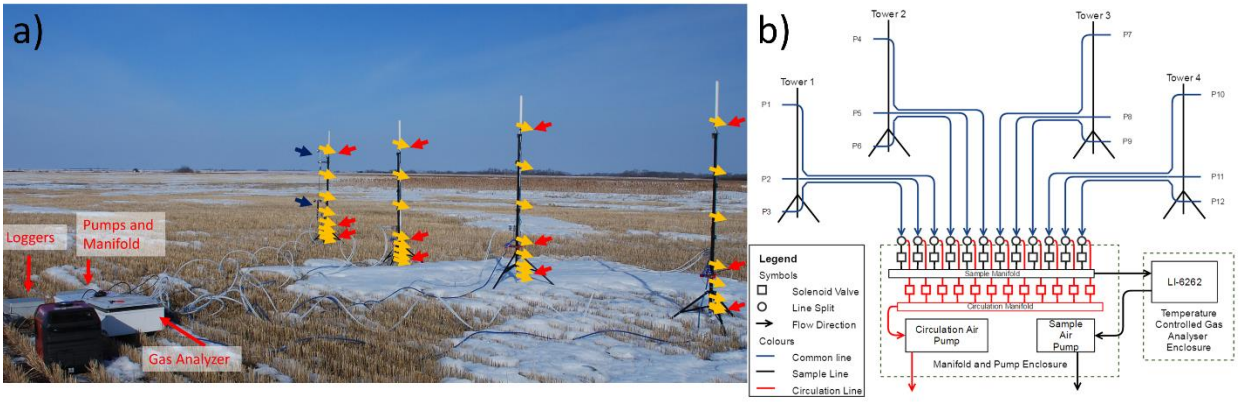

Figure 3.1: a) Deployed atmospheric profile observation system. Sensors are spread over 4 mobile towers and include two 3-cup anemometers (blue arrows), 32 fine wire thermocouples (yellow arrows) and 12 water vapor intakes (red arrows) that b) are routed sequentially to a common gas analyzer.

Measurement of q was challenging due to the high accuracy required to detect small differences over short distances. A q profiling system was developed to route air from 12 intake ports (deployed at 0.08 m, 0.50 m and 2.00 m on the four towers) to a common sensor, a LiCOR-6262 CO_2/H_2O gas analyzer (Li-6262). Figure 3.1b provides a schematic of the system. A dedicated air pump drew air through the manifold system and gas analyzer while another pump circulated air through the remaining 11 lines to prevent in-line condensation and ensure representative air samples at the analyzer. Gas routing was controlled via a datalogger that recorded q and the corresponding intake port at one second intervals. Tube lengths for all ports were 10 m; 1 L min^{-1} flow in a ¼ inch tube gives an estimated 3 s travel time ignoring diffusion in these tubes. Lab testing showed consistent signal stabilization 5 s after port changes. To be conservative during deployments the port was switched every 20 s with only the last 10 s retained for analysis. This gave a four-minute cycle to sample all 12 intakes. The Li-6262 gas analyzer was operated in an insulated, temperature-controlled enclosure and calibrated prior to deployment against a LiCOR-610 dewpoint generator.

The system was deployed over a variety of non-snow to snowcover transitions with Tower 1 upwind of a snow-free to snowcover transition, Tower 2 at the transition and Tower 3 and 4 sequentially downwind of the transition. Analysis was limited to two unique periods of observation; conditions are summarized in Table 3.1 and spatial arrangement of towers and surface visualized in Figure 3.2. These met data quality requirements that include minimum wind speeds, wind direction alignment, sensor performance and consistent sensor displacement with

respect to surface. The 18 March observation period was characterized by an upwind uniform surface of wheat stubble exposed above a continuous snowcover that should correspond to negligible q and large T_a horizontal gradients that will lead to negligible LE_A and large H_A. In contrast, 30 March was characterized by the upwind surface having wheat stubble exposed above patches of ponded water. The 30 March condition should lead to large q and T_a horizontal gradients and therefore both large H_A and LE_A.

Table 3.1: Summary of mean conditions during observation intervals

Attribute	Unit	18 March 2015	30 March 2015
Observation Period		13:00-15:00	11:20-12:00
Number of Analysis Intervals		31	11
Stubble Height	m	0.35	0.2
Tower spacing[a]	m	3.7,3.1,4.4	3,3.6,4.8
Array Bearing	°	161	271
Wind Direction[b]	°	166 (6.4)	274(0.8)
Air Temperature	°C	5.4	7.9
Snow Temperature	°C	0.3	0.3
Relative Humidity	%	60.0	72.1
Wind speed	m s-1	1.6	6.4
Sensible Heat[c]	W m-2	-57.3	-58.4
Latent Heat[c]	W m-2	-22.2	-133.7
Net Radiation	W m-2	326.2	472.6
Stability[d]	-	-0.1	-0.007
Friction Velocity	m s-1	0.20	0.57

[a]Tower spacing is the distance between Tower 1 and 2, Tower 2 and 3 and Tower 3 and 4.
[b]bracketed values are the standard deviation
[c]Areal average turbulent terms from adjacent eddy covariance observations
[s]Stability parameter (z/Obhukov length) observed at 1.8m from adjacent eddy covariance observations

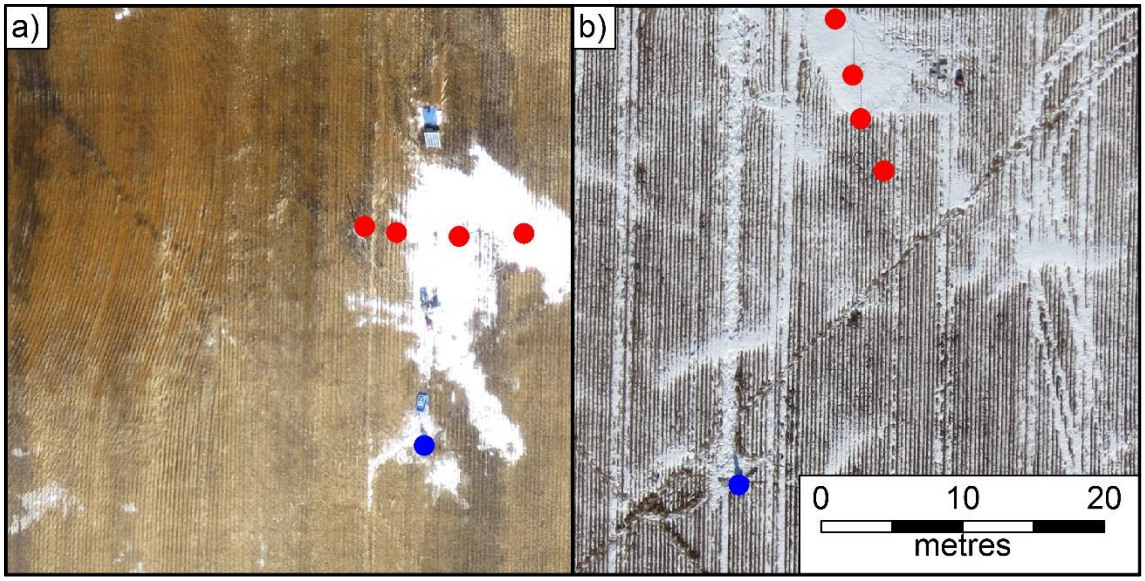

Figure 3.2: Unmanned aerial vehicle imagery of a) 18 March 2015 and b) 30 March 2015 deployments. Red points are locations of towers with tower 1 upwind in non-snow location, tower 2 located at transition and towers 3 and 4 situated sequentially downwind over snow. Towers are in line with the prevailing wind direction over the observation interval. Blue dot is location of eddy covariance system and additional in-field instrumentation.

Incoming radiation was observed with a Kipp and Zonen CNR1 net radiometer at a permanent reference station within 350 m of the deployed array. Outgoing longwave and shortwave terms were observed with a CGR3 pyrgeometer and CMP6 pyranometer respectively at adjacent on-field stations within 50 m of the deployed array. Additional observations at the on-field stations include T_a and relative humidity at 1.65 m height with a shielded HMP45C212, snow surface temperatures with Apogee S-111 Infrared Radiometers, and ground heat flux beneath snowcover with Hukseflux self-calibrating heat flux plates. Eddy covariance instrumentation, Campbell Scientific CSAT3 Sonic anemometer for wind speed and ultrasonic temperatures and LiCOR 7500A open-path infrared gas analyzer for water vapor observations, quantified sensible and latent turbulent heat fluxes, friction velocity, stability, mean wind speed, and mean wind direction at a height of 1.8 m.

3.3.3. Data Analysis

To calculate the advection terms, following Equation 3.2 and 3.3, the point observations of u, T_a, and q were integrated over the profile depth of interest. The $\bar{u}$ for the integrated profile depth was found by fitting observations to the classic logarithmic wind profile

$$\bar{u} = \int_{z=0}^{z_p} \frac{u^*}{\kappa} \log\left(\frac{z + d_0}{z_0}\right) dz, \tag{3.4}$$

where κ is the von Kármán constant (0.4). The displacement height d_0 (m) and surface roughness z_0 (m) are estimated as

$$d_0 = 0.67 h_v \tag{3.5}$$

and

$$z_0 = 0.12 h_v, \tag{3.6}$$

respectively, where h_v (m) is the height of vegetation of the upwind snow-free surface. Mean interval friction velocity (u^*: m s^{-1}) is calculated as

$$u^* = \kappa(\bar{u}_2 - \bar{u}_1) ln\left(\frac{z_2 - d_0}{z_1 - d_0}\right)^{-1}, \tag{3.7}$$

with the mean interval wind speed observations $\bar{u}_2$ and $\bar{u}_1$ (m s^{-1}) observed on tower 1 at heights z_2 (2 m) and z_1 (1 m) respectively. For simplicity it is assumed that the windspeed profile is the same downwind of the snow transition despite differences in surface roughness. The logarithmic wind profile was not corrected for stability. The near surface atmosphere, from EC observations at 1.8 m, was near neutral during observation intervals (Table 1). In addition, the stability corrections are invalid at heights less than 41 $z_0 + d_0$ (Brutsaert and Parlange, 1992) which corresponds 1.1 m for a 0.20 m stubble surface, this is greater than the 0.5 m profile depths of interest.

Other advection studies have interpolated between profiles by fitting predefined curve functions to observations (Essery et al., 2006; Kochendorfer and Paw U, 2011). Due to the diverse profiles encountered, and a limited number of q observation levels, curve fitting with a predefined function is inappropriate. Rather, a layer depth-weighted mean was applied over the integration height

$$\bar{c} = \sum_{i=1}^{i=j-1} \left(\frac{c_{i+1} + c_i}{2}\right)(z_{i+1} - z_i)\, z_p^{-1}, \tag{3.8}$$

where c_i is the i^{th} scalar at measurement heights i from the surface to the top of the profile integration height of interest and j is the number of observation points. Over the

downwind snow surfaces surface T_a was observed from adjacent snow surface temperature measurements and surface q was estimated assuming saturation of the surface air. The upwind towers are more complicated as the surface is not uniform snow. Therefore surface T_a was estimated by linear interpolation of the three lowest observations to the surface. Surface q was estimated by assuming saturation at the interpolated T_a.

3.3.4. Instrumentation Uncertainties

Advection calculations require instrumentation that can observe small gradients in T_a and q in two-dimensions. Unshielded fine-wire thermocouples were selected for measuring T_a due to their fast response time. Despite the small thermocouple diameters these sensors will experience radiative heating that varies with the wind speed profile. The change in thermocouple temperature difference from T_a due to expected wind speed differences at heights from 0.04 to 0.5 m was estimated using Campbell (1969) to be less 0.14 K so the observations are assumed to represent actual gradients. The largest uncertainty of the q observations is due to intermittent port sampling. The occurrence of q or T_a anomalies/plumes from variable upwind footprints could complicate profile interpretations. To minimize the influence of such anomalies, analysis was limited to periods with wind directions aligned with the towers to limit upwind footprint variability and ensure any anomalies impacted all towers. Unlike intermittent q observations, the T_a observations are continuous and examination of these did not identify anomalies that could skew results. The error of the absolute humidity signal of the LI-6262, according to the manufacturer specifications, is 0.01 g m^{-3}. Since gradient calculations require two observations, the differences should be greater than combined error of 0.02 g m^{-3}; 85% of the differences observed were greater than this threshold.

3.4. Results and Discussion

3.4.1. Air Temperature and Water Vapor Profiles

The influence of a surface transition upon q and T_a profiles (Figure 3.3) is evident in upwind and downwind observations showing relatively large differences compared to the small range in observations between towers of the same surface. These differences are clearly associated with rapid change in atmospheric profiles on the leading edge of the snowpack between Towers 2 and 3. The difference in profiles diminishes at heights near 0.50 m which

correspond to the development of an internal boundary layer and the formation of a blending height (Granger et al., 2006, 2002).

Despite the limited sample heights on each profile the observed 0.08 m and assumed surface q values are always greater upwind than downwind of the bare-snow edge; the differences are minimal at 0.50 m. The decrease in q over a snow transition on 30 March validates the concept that q decreases over a snowcovered fetch because of condensation from the moisture-laden warmer air to the colder, relatively dry, snow surface. In contrast the q profiles on 18 March reflect a sublimation condition both upwind and downwind. Advection of LE_A will not occur in this situation but the relatively moist upwind q profile will still act to suppress turbulent exchange of latent heat over snow; this provides a mechanism for why snowmelt latent heat fluxes are routinely observed to be small in this region (Granger and Male, 1978; Pomeroy et al., 1998; Pomeroy and Essery, 1999). The small differences in q between the towers at the 0.50 m and 2.00 m heights (not shown) support the hypothesis of negligible differences in the well-mixed air mass above the internal boundary layer. The q profiles show much smaller differences early in the melt season (18 March) when soils were frozen near the surface and ponded water was absent. Later in the melt period, 30 March, the wet, thawed soil surface and ponded meltwater due to a frost-table just below the surface provided vapor sources that drive the development of larger q gradients.

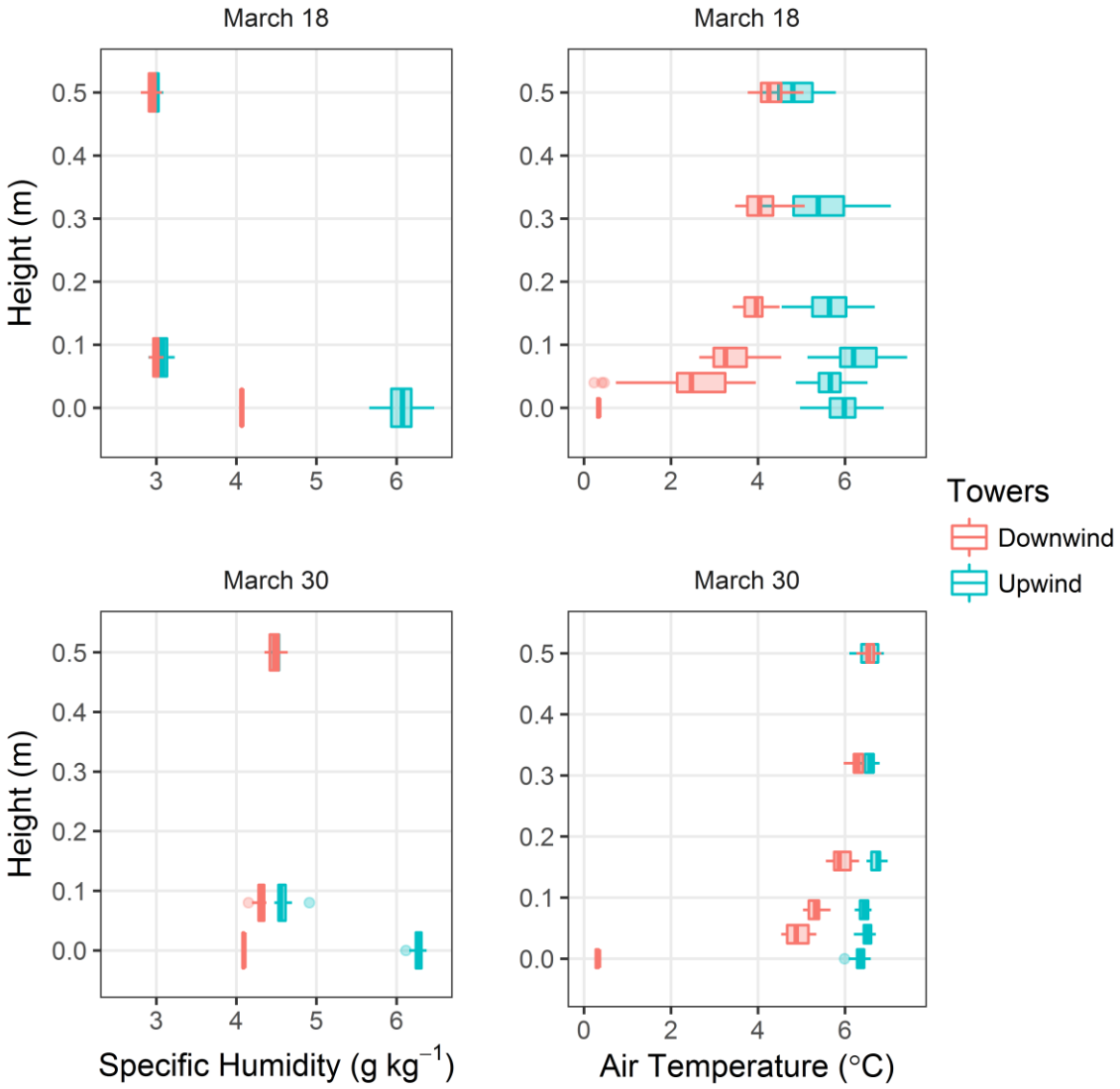

Figure 3.3: Specific humidity and air temperature observations versus height grouped as boxplots upwind and downwind of a snow surface transition for 18 March (top row) and 30 March 2015 (bottom row) observations periods.

3.4.2. Advection Estimation

Advection terms were calculated using gradients between each set of towers so the advection flux could be attributed to a specific tower interval (Figure 3.4). The T_a and q profiles are temporally dynamic which leads to uncertainty in the advection estimates as shown by the ranges of estimates in Figure 3.4. Mean behavior shows negligible H_A and LE_A between Towers 1 and 2 suggesting the air masses are relatively well mixed and in equilibrium with the upwind surface. The Tower 2 to 3 interval, the leading edge of the snow patch, consistently has the

greatest fluxes. The H_A and LE_A for the Tower 3 to 4 interval, further downwind of the edge, is predominantly negligible. During the ideal LE_A period, 30 March, when a strong wind blew from an upwind area of ponded water and wet soil over a snow transition, the mean LE_A was 446 W m^{-2} over the leading edge which is a similar magnitude to the corresponding mean H_A of 404 W m^{-2}. The relatively small LE_A contribution over the leading edge during the 18 March situation is negligible once uncertainty range is considered.

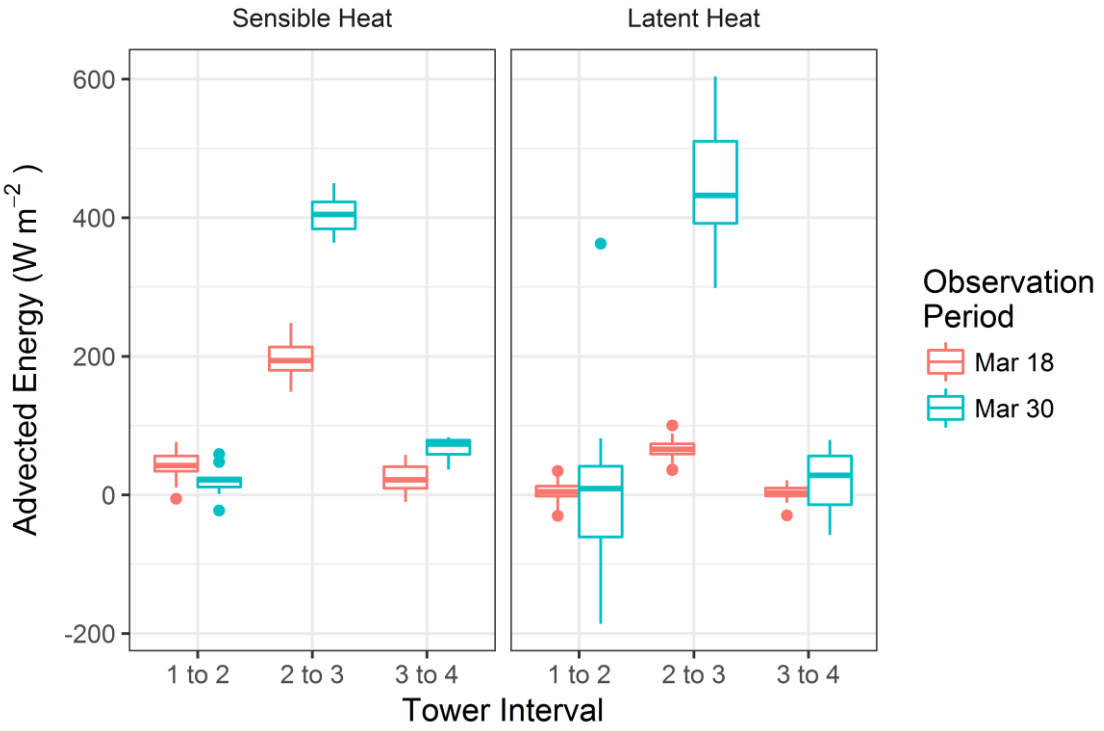

Figure 3.4: Sensible and latent heat advection estimates between each set of towers. The boxplots summarize the 4-minute advection estimates for the respective observations periods.

The measurement of both H_A and LE_A contributions to snowmelt have not previously been reported; the observation that these terms may occur at similar large magnitudes is novel. These estimates reiterate that advection terms are most important on the leading edge of a snow patch as advection energy declines with the downwind development of equilibrium profiles.

3.4.3. Snowmelt Energy Balance implications

To understand the snowmelt implications of LE_A and H_A on the leading edge of a snow patch, consider the melting snow surface energy balance (Gray and Male, 1981)

$$Q_m = R_{net} + H_A + LE_A + G_g, \quad (3.9)$$

where Q_m (W m^{-2}) is the net energy available for snowmelt, R_{net} (W m^{-2}) is the net radiation, and Q_g (W m^{-2}) is the ground heat flux. This energy balance has been simplified by neglecting changes in snowpack internal energy and energy advected by rainfall. The net radiation term is the single largest energy input to the snow, followed closely by H_A and LE_A. Observed Q_g was negligible as available energy was going into melting snow. H_A and LE_A, as a percent of snowmelt energy, were 33% and 11% respectively on 18 March and 31% and 33% respectively on 30 March. The net melt energy on the leading edge of a snowpack results in melt rates of 6.3 mm hr^{-1}and 14.2 mm hr^{-1} for 18 March and 30 March, respectively.

Rather than explicitly observe the H_A and LE_A terms on the leading edge of a snowpack, many observational campaigns rely on EC approaches to constrain the areal average turbulent terms of the energy balance. In this campaign, the areal average sensible and latent heat observations from adjacent EC sensors shows energy fluxes away from the surface. This demonstrates the inappropriateness of EC to estimate the snowmelt energy balance of patchy snow and consideration of H_A and LE_A is required to properly estimate the spatial variability of snowmelt.

Contrasting 18 and 30 March demonstrates that LE_A requires an upwind wetted surface as a source of q. Upwind wetted surfaces that can form sources of q are often found in flat areas with restricted infiltration that permit ponding of meltwater near snow patches. Conditions that favor the ponding of meltwater are frozen well-saturated soils and the presence of depressional storage to hold meltwater runoff in place. These conditions are often met in prairie, grassland or tundra regions which are also characterized by patchy snowcover where H_A has been extensively documented (Granger et al., 2002; Marsh and Pomeroy, 1996; Shook and Gray, 1997). Model results suggest that advected energy can increase sensible heat fluxes in flat environments by about 50% over the first several meters on the leading edge of snowpack (Essery et al., 2006). The Essery et al. (2006) model results for sensible heat are similar to the H_A results of this study and increase confidence in the experimental design and the LE_A results. In contrast, sloping soils found in mountain environments will minimize the formation of ponded melt water on the surface. Sources for LE_A in mountains include concave surfaces that can hold water, but fluxes from these locations might be limited by lower wind speeds and cold stable air pools (Mott et al.,

2015, 2013, 2011). The contribution of LE_A is not expected to be large during rain-on-snow events due to large latent heat sources from the already damp atmosphere (Pomeroy et al., 2016).

3.5. Conclusions

The energy balance of heterogeneous snowcovers has long been recognized to be complicated by the advection of sensible heat from snow-free to snowcovered surfaces. However, the concomitant advection of latent heat from ponded water to snow patches has not been considered as a snowmelt energy source. Examination of T_a profiles over snow-free to snowcovered transitions reconfirms that H_A, driven by surface temperature heterogeneity, is a large source of energy available for snowmelt. The q profiles show that LE_A can also be substantial, but is conditional upon the presence of upwind ponded water and/or wet exposed soils. Under conditions with wet upwind surfaces, the LE_A term was calculated to account for 33% of the net energy available for melt at the leading edge of a snow patch. This was on the same order as the corresponding H_A flux which accounted for another 31% of the net available energy melt. Thus, proper consideration of both sensible and latent heat advection fluxes is required to predict spatial melt rates in environments with patchy snowcover. The dependence of LE_A upon upwind wetted surface q sources means that its overall contribution to snowmelt depends upon the spatial arrangement of surface features, meteorological conditions, soil properties and antecedent conditions.

3.6. Manuscript Integration with Broader Thesis

The identification and quantification of the advection of both sensible and latent heat to the snowpack during melt is novel. A model is needed to determine the overall implications of advection on the melt process beyond the brief observations presented herein. Thus, these observations and hypotheses motivate the development of the sensible and latent heat advection model presented in Chapter 5. The observations are also used to validate the sensible and latent heat advection model in Chapter 5.

3.7. References

Brutsaert, W., Parlange, M. B. (1992). The Unstable Surface Layer Above Forest: Regional Evaporation and Heat Flux. Water Resources Research, 28(12), 3129–3134.

Campbell, G. S. (1969). Measurement of air temperature fluctuations with thermocouples. White Sands Missile Range, New Mexico.

Essery, R., Granger, R. J., Pomeroy, J. W. (2006). Boundary-layer growth and advection of heat over snow and soil patches: modelling and parameterization. Hydrological Processes, 20(4), 953–967.

Garratt, J. R. (1990). The Internal Boundary Layer - A Review. Boundary-Layer Meteorology, 50, 171–203.

Granger, R. J., Male, D. H. (1978). Melting of a prairie snowpack. Journal of Applied Meteorology, 17, 1833–1842.

Granger, R. J., Pomeroy, J. W., Parviainen, J. (2002). Boundary-layer integration approach to advection of sensible heat to a patchy snow cover. Hydrological Processes, 16(18), 3559–3569.

Granger, R. J., Essery, R., Pomeroy, J. W. (2006). Boundary-layer growth over snow and soil patches: Field Observations. Hydrological Processes, 20(4), 943–951.

Gray, D. M., Male, D. H. (1981). Handbook of Snow: Principles, Processes, Management, and Use. Toronto, Canada: Pergamon Press.

Kochendorfer, J., Paw U, K. T. (2011). Field estimates of scalar advection across a canopy edge. Agricultural and Forest Meteorology, 151(5), 585–594. https://doi.org/10.1016/j.agrformet.2011.01.003

Liston, G. E. (1995). Local advection of momentum, heat and moisture during the melt of patchy snow covers. Journal of Applied Meteorology, 34, 1705–1715.

Marsh, P., Pomeroy, J. W. (1996). Meltwater Fluxes At an Arctic Forest-Tundra Site. Hydrological Processes, 10(10), 1383–1400.

Marsh, P., Essery, R., Neumann, N., Pomeroy, J. W. (1999). Model estimates of local advection of sensible heat over a patchy snow cover. In M. Tranter (Ed.), Interactions between the Cryosphere, Climate and Greenhouse Gases (pp. 103–110). IAHS Publ. No. 256.

Ménard, C., Essery, R., Pomeroy, J. W. (2014). Modelled sensitivity of the snow regime to topography, shrub fraction and shrub height. Hydrology and Earth System Sciences, 11(6), 2375–2392. https://doi.org/10.5194/hessd-11-223-2014

Mott, R., Lehning, M., Daniels, M. (2015). Atmospheric Flow Development and Associated Changes in Turbulent Sensible Heat Flux over a Patchy Mountain Snow Cover. Journal of Hydrometeorology, 16, 1315–1340. https://doi.org/10.1175/JHM-D-14-0036.1

Mott, R., Egli, L., Grünewald, T., Dawes, N., Manes, C., Bavay, M., Lehning, M. (2011). Micrometeorological processes driving snow ablation in an Alpine catchment. Cryosphere, 5(4), 1083–1098. https://doi.org/10.5194/tc-5-1083-2011

Mott, R., Gromke, C., Grünewald, T., Lehning, M. (2013). Relative importance of advective heat transport and boundary layer decoupling in the melt dynamics of a patchy snow cover. Advances in Water Resources, 55, 88–97. https://doi.org/10.1016/j.advwatres.2012.03.001

Paw U, K. T., Baldocchi, D. D., Meyers, T. P., Wilson, K. B. (2000). Correction of eddy-covariance measurements incorporating both advective effects and density fluxes. Boundary-Layer Meteorology, 97(3), 487–511. https://doi.org/10.1023/A:1002786702909

Pomeroy, J. W., Essery, R. (1999). Turbulent fluxes during blowing snow: field tests of model sublimation predictions. Hydrological Processes, 13(18), 2963–2975. Retrieved from http://doi.wiley.com/10.1002/(SICI)1099-1085(19991230)13:18%3C2963::AID-HYP11%3E3.0.CO;2-9

Pomeroy, J. W., Gray, D. M. (1995). Snow accumulation, relocation and management. Saskatoon, SK: Science Report No. 7, National Hydrology Research Institute, Environment Canada.

Pomeroy, J. W., Gray, D. M., Shook, K., Toth, B., Essery, R., Pietroniro, A., Hedstrom, N. R. (1998). An evaluation of snow accumulation and ablation processes for land surface modelling. Hydrological Processes, 12, 2339–2367.

Pomeroy, J. W., Fang, X., Marks, D. (2016). The cold rain-on-snow event of June 2013 in the Canadian Rockies - characteristics and diagnosis. Hydrological Processes. https://doi.org/10.1002/hyp.10905

Shook, K., Gray, D. M. (1997). Snowmelt Resulting from Advection. Hydrological Processes, 11, 1725–1736.

Shook, K., Gray, D. M., Pomeroy, J. W. (1993). Geometry of patchy snowcovers. In 50th Annual Eastern Snow Conference (pp. 89–98). Quebec City.

Weisman, R. N. (1977). Snowmelt: A Two-Dimensional Turbulent Diffusion Model. Water Resources Research, 13(2), 337–342.

Chapter 4: Modelling the snowpack energy balance during melt under exposed crop stubble

Status: submitted to Journal of Hydrometeorology on February 22, 2018

Citation: Harder, P., Helgason, W. D., Pomeroy, J. W. (2018). Modelling the snowpack energy balance during melt under exposed crop stubble. Journal of Hydrometeorology. in review.

Author Contributions: PH conceptualized the field program, performed all fieldwork, developed the model, performed analysis, and wrote manuscript. JP and WH provided guidance, equipment and financial resources for the field campaign, and reviewed and revised model formulations and manuscript.

4.1. Abstract

On the Canadian Prairies, agricultural practices result in large areas of standing crop stubble that gradually emerges during snowmelt. However, the dynamics of stubble are not explicitly accounted for in hydrological or energy balance snowmelt models. This paper relates measurable stubble parameters (height, width, areal density, and albedo) to the snowpack energy balance and snowmelt with the new and physically based Stubble-Snow-Atmosphere Model, SSAM. Novel process representations of SSAM quantify the attenuation of shortwave radiation by exposed stubble, the sky and vegetation view factors needed to solve longwave radiation terms, and a resistance scheme for stubble-snow-atmosphere fluxes to solve for surface temperatures and turbulent fluxes. SSAM results were compared to observations of radiometric snow-surface temperature, stubble temperature, snow-surface solar radiation, areal-average turbulent fluxes and snow water equivalent from two intensive field campaigns during snowmelt in 2015 and 2016 over wheat and canola stubble in Saskatchewan, Canada. Uncalibrated SSAM simulations compared well with these observations, providing confidence in the model structure and parameterization. A sensitivity analysis conducted using SSAM revealed compensatory relationships in energy balance terms that result in a subtle increase in net snowpack energy as stubble exposure increases.

4.2. Introduction

Snowmelt is an important source of water for crop germination and early season growth in no-till non-irrigated farming systems commonly found in cold, semi-arid agricultural regions. Stubble, the standing winter residue of cultivated grain and oilseed crops, is characterized by stalks that remain erect throughout snow accumulation and ablation. However, snowmelt models either ignore short vegetation (Gray and Landine, 1987b; Marks et al., 1998), assume protruding vegetation can be represented by modifying surface albedo (Liston and Hiemstra, 2011), or simulate the bending over and burial of grasses and shrubs by snow (Bewley et al., 2007; Liston and Hiemstra, 2011; Ménard et al., 2014). The interactions between stubble stalks and snow occur over large areas with regional implications for hydrology and climate. Cold region no-till crop production systems, characterized by standing stubble, are found throughout the American Midwest, Eurasian Steppes (Derpsch and Friedrich, 2009) and Canadian Prairies. In the Canadian Prairie Provinces (Manitoba, Saskatchewan, and Alberta), the area of no-till crop production increased from 1.7 million hectares in 1990 to 17.3 million hectares in 2016 (Statistics Canada, 2016). Despite the large-scale conversion to no-till systems and the importance of snowmelt water to crop production in cold regions, a detailed quantitative understanding of how the snowpack energy balance changes with the gradual exposure of stubble is lacking.

Forest and short vegetation canopies are analogous to stubble and their influences on the snowmelt energy balance have been the subject of substantial research. Canopies attenuate the transmission of shortwave radiation to (Bewley et al., 2005; Ellis, 2007; Musselman et al., 2015; Pomeroy et al., 2009a; Pomeroy et al., 2008; Reid et al., 2013) and enhance sub-canopy longwave radiation to the snow surface (Essery et al., 2008a; Pomeroy et al., 2009a; Sicart et al., 2006; Webster et al., 2016). Approaches to estimate shortwave attenuation vary between simple Beer's law methods (Mahat and Tarboton, 2012; Pomeroy and Dion, 1996; Sicart et al., 2003) to more complex methods that use either two-stream solutions (Mahat and Tarboton, 2012), consider sky view factors estimated from hemispherical photography (Musselman et al., 2012) or implement computationally-expensive ray tracing (Essery et al., 2008b; Musselman et al., 2015). Longwave radiation contributions are often estimated using sky view factors (Essery et al., 2008b; Pomeroy et al., 2002) in conjunction with observed or modelled canopy temperatures

(Musselman and Pomeroy, 2016; Pomeroy et al., 2009a; Webster et al., 2016). The major difference between stubble and forests interactions on radiation transfer behaviour relate to the relative sizes of the elements. Stubble height, unlike a forest, is on the same order as snow depth, and thus stubble will transition over the melt period from being buried to becoming fully exposed. The shortwave radiation attenuation and longwave emittance from exposed stubble is therefore dynamic. In contrast, forest canopy contributions are generally static as the bulk of the canopy is well above the surface. This makes the stubble influence on the net snow-surface radiation balance dynamic and sensitive to snow depth.

In short and sparse canopies, turbulent transfer is often estimated by local gradient diffusion approaches (K-theory, Wallace, 1991). K-theory predicts that increased stubble exposure over melting snow will increase surface roughness, thereby increasing the ability of the snow and stubble surface to absorb momentum, leading to increasing turbulence and turbulent transfer (Prueger and Kustas, 2005). In contrast, exchange specific to the snow surface below the exposed stubble, the surface of interest in this study, is a function of the stubble exposure and does not reflect the areal average increase in turbulent transfer as predicted by K-theory (Bewley et al., 2010). Alternate resistance parametrizations are required to account for observations of suppressed turbulent transfer due to the decoupling of the surface from the atmosphere by stubble influencing wind velocity profiles (Mahat et al., 2013), displacing the airflow from the surface (Brun et al., 1984; Burt et al., 2005; Cutforth and McConkey, 1997) and ultimately reducing wind speeds at the surface (Aase and Siddoway, 1980).

In the absence of relevant previous research, the extent to which stubble exposure will attenuate shortwave radiation, enhance longwave radiation and modify turbulent fluxes is unclear. It is important to understand how these relative changes will manifest themselves in terms of the net snowpack energy balance over the snowmelt period. The overall objective of this study is to understand how exposed stubble modifies the snowpack energy balance. Specifically, its purpose is to: 1) develop and validate a model to simulate the snowpack energy balance as a function of the exposed stubble characteristics; and 2) use this model to develop a quantitative understanding of the compensatory relationships between stubble characteristics and the snowpack energy balance.

4.3. Stubble-Snow-Atmosphere Snowmelt Model Development

4.3.1. Snowpack Energy Balance

The role of stubble in modifying energy transfer to the underlying snow surface is manifested through the snowpack energy balance, given as (Gray and Male, 1981)

$$SW^*_{snow} + LW^*_{snow} + H_{snow} + LE_{snow} + Q_g + Q_p = Q_m + \frac{dU_{snow}}{dt}, \qquad (4.1)$$

where all terms have units of W m^{-2} and SW^*_{snow} is net shortwave radiation, LW^*_{snow} is net longwave radiation, H_{snow} is sensible heat flux, LE_{snow} is latent heat flux, and Q_p is the flux of energy advected to the snow through precipitation. The ground heat flux (Q_g) is negligible during snowmelt periods on the Canadian Prairies and is hereafter neglected (Granger and Male, 1978; Pomeroy and Goodison, 1997) The sum of the left-hand side of Equation 4.1 is the net energy flux for the snowpack (Q^*_{snow}) that either changes the internal energy of the snowpack ($\frac{dU_{snow}}{dt}$) or melts snow (Q_m). The sign convention is for positive fluxes to be directed towards the snow. The energy balance interactions and mass fluxes for the snow-stubble-atmosphere are visualized in Figure 4.1. Hereafter the model developed will be referred to as *SSAM*.

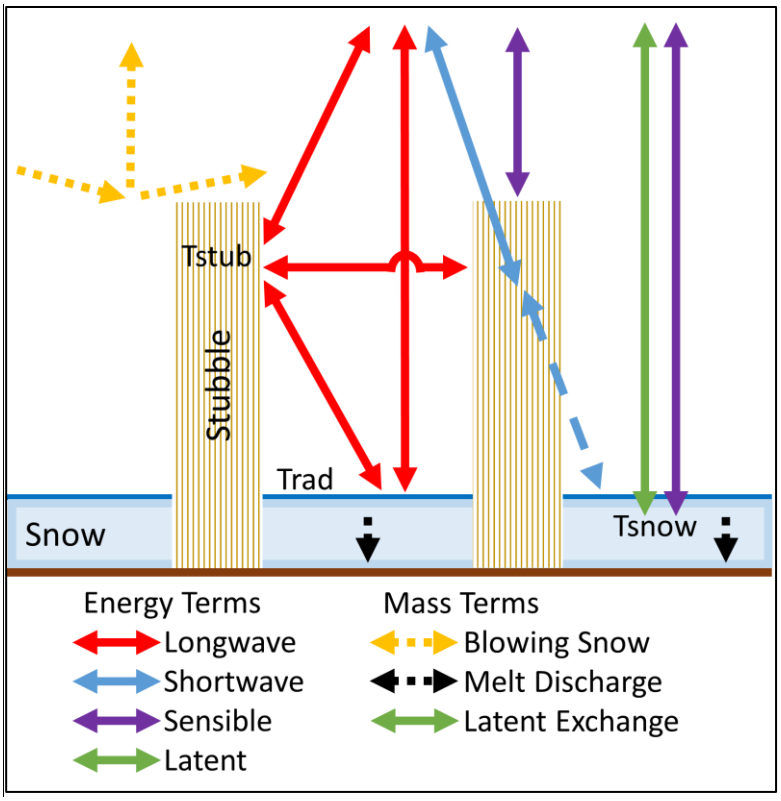

Figure 4.1: Conceptual mass-energy balance interactions of stubble-snow-atmosphere interface. Energy fluxes comprise longwave (red lines) and shortwave (blue lines) radiation, and sensible (purple lines) and latent (green lines) heat fluxes. Temperatures of the snow, snow skin surface (for longwave emittance calculation) and snow are noted as Tstub, Trad, and Tsnow respectively. Mass fluxes are comprised of blowing snow deposition, erosion and sublimation (yellow lines), meltwater discharge (black lines), and latent exchange such as sublimation or deposition (green lines). Fluxes towards the snow are positive.

4.3.1.1. Shortwave Radiation

Beer's law relates light attenuation to the properties of a scattering medium and represents the transmission of shortwave radiation through a stubble canopy. The transmittance (τ) of stubble can be expressed as

$$\tau = e^{-kPAI}, \tag{4.2}$$

where k (-) is the extinction coefficient and PAI (m^2 m^{-2}) is the Plant Area Index. Plant Area Index is conceptualized as the one-sided surface area of vegetation per square meter (Campbell and Norman, 1998; Eagleson, 2002; Shaw and Pereira, 1982). Stubble may be idealized as a collection of uniform vertical cylinders; therefore, PAI is proposed to be estimated as half the vertical surface area of a collection of vertical cylinders, which simplifies to

$$PAI = \pi r h_v \rho_{A-stub}, \tag{4.3}$$

where r (m) is the radius of an individual stubble stalk, h_v (m) is the height of the exposed stubble and ρ_{A-stub} is the areal density of stubble stalks (number of stalks m^{-2}). A minimum h_v is set to 0.001 m to avoid numerical instabilities throughout the model. Shortwave radiation is composed of diffuse (subscript d) and direct beam (subscript b) components. For direct radiation, k_b comprises the ratio of the shadow area to surface area, which for an opaque vertical cylinder simplifies to (Eagleson, 2002)

$$k_b = \frac{1}{\pi} cot(\theta_{elev}), \tag{4.4}$$

where θ_{elev} (rad) is the solar elevation angle. This k_b is modified to account for transmission associated with forward scattering (k_b') through a simple parametrization from Goudriaan (1977):

$$k_b' = k_b \sqrt{1-\omega}, \tag{4.5}$$

where ω (-) is a scattering coefficient that is the sum of a material's reflectance and transmittance (Goudriaan, 1977; Wang, 2003). Stubble stalks are opaque; therefore, it is assumed that $\omega \approx$ stubble albedo (a_{stub}[-]). For diffuse radiation, where the radiation is incident upon a surface from all directions, canopies with a vertical leaf angle distribution have k_d= 0.55 (Eagleson, 2002). In the absence of observations of direct and diffuse shortwave components, the incoming above canopy shortwave ($SW_{atm}^{\downarrow}$ [W m^{-2}]) is partitioned by calculation of the diffuse fraction of incoming shortwave radiation (f_d [-]) with the empirically based model of Reindl et al. (1990). The shortwave radiation incident at the snow surface ($SW_{snow}^{\downarrow}$ [W m^{-2}]) is represented as

$$SW_{snow}^{\downarrow} = (1-f_d) SW_{atm}^{\downarrow} \tau_b + f_d SW_{atm}^{\downarrow} \tau_d, \tag{4.6}$$

where τ from Equation 4.2 is calculated separately for direct (τ_b[-]) and diffuse (τ_d[-]) as

$$\tau_b = e^{-k_b' LAI}, \tag{4.7}$$

and

$$\tau_d = e^{-k_d LAI}. \tag{4.8}$$

The bulk transmittance of the stubble τ_{bulk} (-) is given as

$$\tau_{bulk} = \frac{SW_{snow}^{\downarrow}}{SW_{atm}^{\downarrow}}. \quad (4.9)$$

The net shortwave radiation at the snow surface must account for the albedo of the snow surface (a_{snow}[-]) which gives

$$SW_{snow}^{*} = (1 - a_{snow})SW_{snow}^{\downarrow}. \quad (4.10)$$

The a_{snow} decreases over time as snow ages and undergoes metamorphosis and is estimated prognostically from the application of Verseghy (1991) as

$$a_{snow}(i+1) = (a_{snow}(i) - a_{min})e^{-\upsilon\frac{dt}{3600}} + a_{min}, \quad (4.11)$$

where υ is the albedo decay coefficient (-), a_{min} (0.75) is the minimum snow albedo, dt (s) is the interval duration, and i identifies the time interval. In the event of snowfall a_{snow} is refreshed to 0.90.

4.3.1.2. Longwave Radiation

Net longwave radiation at the snow surface is the sum of incoming ($LW_{snow}^{\downarrow}$ [W m^{-2}]) and outgoing ($LW_{snow}^{\uparrow}$ [W m^{-2}]) longwave radiation. Exposed stubble modifies $LW_{snow}^{\downarrow}$ through changing the stubble surface temperature (T_{stub} [K]) and the sky view factor from the perspective of the snow (vf_{sky}[-]) as (Pomeroy et al., 2009a)

$$LW_{snow}^{\downarrow} = vf_{sky}\, LW_{atm}^{\downarrow} + \left(1 - vf_{sky}\right)\varepsilon_{stub}\sigma T_{stub}^{4}, \quad (4.12)$$

where $LW_{atm}^{\downarrow}$ (W m^{-2}) is the incoming longwave radiation above the canopy, ε_{stub}(-) is the emissivity of the stubble, and σ (5.67×10^{-8} W m K^{-4}) is the Stefan-Boltzmann constant. A novel simulation solution for the vf_{sky} term is expressed in Appendix 4.6.1. The $LW_{snow}^{\uparrow}$ term is expressed via the Stefan-Boltzmann law and depends upon the radiometric snow surface skin temperature (T_{rad} [K]) as

$$LW_{snow}^{\uparrow} = \varepsilon_{snow}\sigma T_{rad}^{4} - (1 - \varepsilon_{snow})LW_{snow}^{\downarrow}, \quad (4.13)$$

where ε_{snow} (-) is the snow emissivity. The first term on the right represents emission from the snow and the right term represents reflectance of the incoming radiation. Emissivity for all sources, snow and stubble, is assumed to be ~1.0 to account for longwave reflections (Mahat and Tarboton, 2012) which removes the reflectance term from Equation 4.13.

4.3.1.2.1. Stubble Temperature

The T_{stub} is estimated by solving the surface energy balance of a stubble stalk; adapted from Musselman and Pomeroy's (2016) bulk approach to simulate the surface temperature of a tree trunk. The surface energy balance of a single stubble stalk is therefore

$$SW^*_{stalk} + LW^*_{stalk} = H_{stalk} + \frac{dU_{stalk}}{dt}, \tag{4.14}$$

where SW^*_{stalk} is net shortwave radiation, LW^*_{stalk} is the net longwave radiation, H_{stalk} is sensible heat flux, and $\frac{dU_{stalk}}{dt}$ is the change in stubble stalk energy storage with respect to time. Fluxes are normalized to the stubble surface area, or volume for $\frac{dU_{stalk}}{dt}$, for a single stalk so all units are in W. Stubble is senescent, so latent heat flux is neglected. Calculation of SW^*_{stalk} uses the transmittance parameterization, Equation 4.9, as

$$SW^*_{stalk} = \frac{(1 - a_{stub})(1 - \tau_{bulk})}{\rho_{A-stub}} \left[SW^{\downarrow}_{atm} + a_{snow}\tau_{bulk}SW^{\downarrow}_{atm}\right], \tag{4.15}$$

where a_{stub} (-) is the albedo of stubble. The first term in braces represents incoming shortwave radiation from the atmosphere and the second term represents a first order reflectance from the snow surface. The residual of τ_{bulk} is the portion of the $SW^{\downarrow}_{atm}$ incident upon the stubble and dividing by ρ_{A-stub} provides the mean incident shortwave radiation for each stalk. This parameterization accounts for the decrease in transmissivity with h_v and conserves energy. The LW^*_{stalk} term is quantified as

$$\begin{aligned} LW^*_{stalk} = A \Bigg[& L^{\downarrow}_{atm}\left(\frac{1 - vf_{stub}}{2}\right) + \sigma\varepsilon_{snow}T^4_{surf}\left(\frac{1 - vf_{stub}}{2}\right) \\ & + vf_{stub}\sigma\varepsilon_{stub}T^4_{stub} - \sigma\varepsilon_{stub}T^4_{stub}\Bigg], \end{aligned} \tag{4.16}$$

where vf_{stub} (-) is the view factor comprised of other stubble from the perspective of a single stalk. The terms consider (from left to right) incoming longwave radiation from the atmosphere, snow and adjacent stubble respectively and emittance from the stalk. An analytical simulation solution to quantify vf_{stub} is shown in Appendix 4.6.2. The residual of vf_{stub} is divided between the underlying snow surface and atmosphere to estimate contributions of each source. The H_{stalk} term is estimated as

$$H_{stalk} = \mathrm{A}\frac{\rho_{air} c_p}{r_s}(T_{stub} - T_a), \tag{4.17}$$

where T_a (K) is the air temperature and r_s (s m^{-1}) is the resistance to sensible heat transfer between the stubble stalk and the atmosphere. The dU_{stalk} term calculates heat storage as a change from the previous interval as (Gouttevin et al., 2015)

$$dU_{stalk}(i) = \beta\big(T_{stub}(i+1) - T_{stub}(i)\big), \tag{4.18}$$

where β (J K^{-1}) is the stubble stalk heat capacity multiplied by the temperature difference in T_{stub} (K) between time steps. The β term is defined as

$$\beta = \mathrm{V}\rho_s c_{stub}, \tag{4.19}$$

where V (m^3) is the stubble stalk volume, ρ_s (kg m^{-3}) is the volumetric mass density of stubble and c_{stub}(J kg^{-1} K^{-1}) is the specific heat capacity of the stubble. For wheat stubble ρ_s is 121 (kg m^{-3}) and c_{stub} is 1630 (J kg^{-1} K^{-1}) (Ahn et al., 2009). A sensitivity analysis, not shown, varied ρ_s and c_{stub} by several orders of magnitude and demonstrated these parameters have a negligible influence on T_{stub}, due to the small volume of the individual stalks, and are hereafter assumed transferable between stubble types. The r_s is a function of forced and free convection coefficients for sensible heat transfer between a stubble stalk and the surrounding air as

$$r_s = \frac{1}{h_{forced} + h_{free}}. \tag{4.20}$$

Following Monteith and Unsworth (2008) ,h_{forced} is calculated as

$$h_{forced} = \frac{D_h \mathrm{N}_{forced}}{2r}, \tag{4.21}$$

where D_h (20.2×10^{-6} m^2 s^{-1} at 10°C; (Denny, 1993)) is the molecular diffusivity for heat in air. The Nusselt number N_{forced} (-) estimates the degree of turbulent transfer due to forced-convection as a function of the Reynolds number (Monteith and Unsworth, 2008):

$$\mathrm{N}_{forced} = \begin{matrix} 0.17Re^{0.62} & Re < 10^4 \\ 0.024Re^{0.81} & 10^4 \leq Re < 10^5 \end{matrix}, \tag{4.22}$$

where Re is the Reynolds number of the stubble stalk cylinder that quantifies the ratio of inertial forces to viscous forces in a fluid,

$$Re = \frac{\rho_{air} r u_h}{\mu}, \tag{4.23}$$

where u_h (m s^{-1}) is wind speed at the top of the stubble canopy, μ (kg m^{-1} s^{-1}) is the viscosity of air and the stubble stalk radius, r, is taken as the length scale. The calculation of $u_h$utilizes the logarithmic wind profile assumption to give

$$u_h = u \frac{ln\left(\frac{h_v - d_0}{z_0}\right)}{ln\left(\frac{z_m - d_0}{z_0}\right)}. \tag{4.24}$$

where u (m s^{-1}) is the wind speed at the measurement height z_m (m), d_0 (m) is the canopy displacement height (Equation 4.35), and z_0 (m) is the aerodynamic roughness length (Equation 4.34). Sutherland (1893) calculates μ as

$$\mu = \frac{d\, T_a^{3/2}}{T_a + s}, \tag{4.25}$$

where d and s are coefficients with values of 1.458×10^{-6} (kg m^{-1} s^{-1} K $^{-1/2}$) and 110.4 (K), respectively. The h_{free} term is calculated as

$$h_{free} = \frac{D_h \mathrm{N}_{free}}{h_v}. \tag{4.26}$$

The free convection Nusselt number (N_{free}) follows Monteith and Unsworth (2008) and is estimated as a function of the Grashof number (Gr):

$$\mathrm{N}_{free} = \begin{matrix} 0.58Gr^{0.25} & Gr < 10^9 \\ 0.11Gr^{0.33} & 10^9 \leq Gr < 10^{12} \end{matrix}, \tag{4.27}$$

where

$$Gr = 1.58 \times 10^8 (h_v)^3 (T_{stub} - T_a). \tag{4.28}$$

4.3.1.2.2. Radiometric Snow-Surface Temperature

The T_{rad} used to simulate $LW_{snow}^{\uparrow}$ is estimated from the energy balance of a infinitesimally small snow surface layer in equilibrium with the atmosphere and thermally decoupled from the underlying snowpack (Pomeroy et al., 2016). This skin surface energy balance is

$$f_a SW_{snow}^{\downarrow} + \varepsilon_{snow}\left(LW_{snow}^{\downarrow} - \sigma T_{rad}^4\right) = -\frac{\rho_{air}}{r_a}\left(c_{air}(T_a - T_{rad}) + L_s\left(q(T_a) - q_{sat}(T_{rad})\right)\right), \quad (4.29)$$

where f_a (0.05, Pomeroy et al. (2016)) is the shortwave absorption factor which represents the amount of shortwave radiation absorbed in the transparent near surface snow layer, ρ_{air} (kg m^{-3}) is the air density, c_{air} (1005 J kg^{-1} K^{-1}) is the specific heat capacity of air, r_a (s m^{-1}) is the aerodynamic resistances for exchange between the surface the atmosphere (Equation 4.32), L_s (2.835×10^6 J kg^{-1}) is the latent heat of sublimation and $q(T_a)$ and $q_{sat}(T_{rad})$ (both kg kg^{-1}) are the specific humidities of the unsaturated air and saturated snow surface, respectively.

4.3.1.3. Turbulent Fluxes

The total sensible and latent turbulent heat exchanges between snow, stubble and the atmosphere are solved in a simple parallel resistance bulk transfer approach. In bulk gradient form

$$H_{snow} = \frac{\rho_{air} c_{air}}{r_a}(T_a - T_{snow}) \quad (4.30)$$

and

$$LE_{snow} = \frac{\rho_{air} L_s}{r_a}[q(T_a) - q_{sat}(T_{snow})], \quad (4.31)$$

where T_{snow} (K) is the snow temperature at the turbulent exchange interface. The parameterization of $r_a$with respect to an emerging stubble, assumes an exponential wind profile within, and a logarithmic wind profile above, the stubble canopy, as (Mahat et al., 2013)

$$r_a = \frac{1}{\kappa^2 u}\ln\left(\frac{z_m - d_0}{z_0}\right)\ln\left(\frac{z_m - d_0}{h_v - d_0}\right) + \frac{h_v}{K_h n}\left[e^{\left[n\left(\frac{h_v - z_0}{h_v}\right)\right]} - 1\right] \quad (4.32)$$

where κ (0.4) is the von karman constant and n (2 [-] for wheat (Brutsaert and Parlange, 1992)) is the exponential wind decay coefficient. The eddy diffusion coefficient (K_h [m^2 s^{-1}]) at h_v, which assumes z_0 is equivalent for momentum, sensible heat, and water vapour exchange (Mahat et al., 2013), is calculated as

$$K_h = \frac{\kappa^2 u(h_v - d_0)}{\ln\left(\frac{z_m - d_0}{z_0}\right)}. \quad (4.33)$$

The Choudhury and Monteith (1988) provide parametrizations for d_0 and z_0 sensitive to vegetation features that were successfully applied to wind profiles observations within stubble canopies (Aiken et al., 2003) as

$$d_0 = 1.1 h_v \log\left(1 + c_{fd} SAI^{\frac{1}{4}}\right), \quad (4.34)$$

and

$$z_0 = 0.3 h_v \left(1 - \frac{d_0}{h_v}\right) + z_{0s}, \quad (4.35)$$

where c_{fd} is the drag coefficient of the stubble element (0.5 [-] from Aiken et al. (2003)) and z_{0s} is the snow-surface roughness (0.005 m (Pomeroy et al., 2016)). The silhouette area index (SAI [m^2 m^{-2}]), the vertical cross section of roughness elements per unit area, is (Aiken et al., 2003)

$$SAI = 2 r h_v \rho_{A-stub}. \quad (4.36)$$

Bulk latent energy exchange is restricted between the snow and atmosphere while sensible heat exchange occurs between the stubble, snow, and atmosphere as,

$$H = H_{snow} + H_{stub}. \quad (4.37)$$

The bulk sensible heat flux contribution from stubble (H_{stub}[W m^{-2}]) is adapted from Ménard et al. (2014) as

$$H_{stub} = A \rho_{A-stub} \frac{\rho_{air} c_{air}}{r_s} (T_a - T_{stub}). \quad (4.38)$$

Turbulent exchange occurs within the snow, not at the infinitesimally thin snow surface represented by T_{rad}, therefore T_{snow} represents a distinct snowpack temperature. The T_{snow} to calculate H_{snow} and LE_{snow} comes from relation to the snowpack internal energy that is detailed in section 4.3.1.5. Atmospheric stability is assumed to be neutral.

4.3.1.4. Energy Advected by Precipitation

The energy advected by precipitation is positive towards the snowpack in the case of rainfall and negative in the case of snowfall. A simple representation is

$$Q_p = \frac{Rainc_{water}(T_i - T_m) + Snowc_{ice}(T_i - T_m)}{dt}, \quad (4.39)$$

where $Rain$ (kg m^{-2}) is rainfall, c_{water} (4184 kJ kg^{-1} K^{-1}) is the specific heat capacity of water, T_i is temperature of the precipitation (K), $Snow$ (kg m^{-2}) is snowfall, c_{ice} (2010 kJ kg^{-1} K^{-1}) is the specific heat capacity of ice, and T_m is the melting temperature of water (273.15 K). The T_i may be assumed from T_a or estimation of the hydrometeor temperature (Harder and Pomeroy, 2013).

4.3.1.5. Internal Energy Change and Melt Energy

During snowmelt Q^*_{snow} often exhibits a diurnal pattern with a negative flux at night, from longwave emittance, and a positive flux during the day, from shortwave and enhanced turbulent terms. Shallow snowpacks have a limited capacity to moderate this variation in energy exchange and to accurately simulate the diurnal pattern of the snowpack warming, ripening, melting, refreezing and cooling the internal energy of a snowpack U_{snow} (J) needs to be explicitly tracked. This is done in an explicit manner as

$$U_{snow}(i+1) = U_{snow}(i) + dU_{snow}. \quad (4.40)$$

Where U_{snow} is initialized at $i = 1$, as function of initial SWE and T_{snow}, as

$$U_{snow}(1) = SWE(1)c_{ice}(T_{snow}(1) - T_m). \quad (4.41)$$

The dependence of U_{snow} on T_{snow} relates dU_{snow} term to the change in T_{snow} over time as

$$dU_{snow} = SWEc_{ice}\big(T_{snow}(i+1) - T_{snow}(i)\big). \quad (4.42)$$

The partitioning of Q^*_{snow} into Q_m and $\frac{dU_{snow}}{dt}$ is a function of whether the snow is isothermal which can be inferred from T_{snow} as

$$Q^*_{snow} = \frac{dU_{snow}}{dt} \quad T_{snow} < T_m$$
$$Q^*_{snow} = Q_m \quad T_{snow} = T_m. \tag{4.43}$$

To avoid runaway cooling of the snowpack, due to numerical instabilities when snow is shallow, a minimum internal energy ($U_{snow-min}$ [J]) is defined as

$$U_{snow-min} = SWE\ c_{ice}\ (T_{min} - T_m), \tag{4.44}$$

where T_{min} (K) is the minimum temperature for the preceding 24 hrs (Gray and Landine, 1988). In any case where U_{snow} is less than $U_{snow-min}$ the associated T_{snow} is reset to that associated with $U_{snow-min}$. The difference in energy may be considered a negative ground heat flux associated with soil cooling/freezing beneath a snowpack in cold conditions. A full description of U_{snow} includes energy associated with ice, water and vapor states. This simple model only tracks the energy of the ice portion as vapor contributions are minimal (Pomeroy and Goodison, 1997) and the liquid water component is a distinct storage term in the mass balance.

4.3.1.6. Energy Balance Solution

SSAM's solution is complicated by the interdependence of T_{stub}, T_{rad}, and T_{snow}. In addition, Equation 4.14 and 4.40 include internal energy storage terms for a stubble stalk and the snowpack, respectively. A prognostic solution is employed within a nonlinear equation solver in R (nleqslv: Hasselman, 2017) that uses a Jacobian optimization scheme with a Broyden update to simultaneously solve the coupled energy balances found in Equations 4.14, 4.29, and 4.1. The solution is initialized with $T_a = T_{stub} = T_{snow}$ during a nighttime interval when temperature differences are minimal. Due to the phase change of water from solid to liquid T_{rad} and T_{snow} must be ≤ 273.15 K. In situations where the solution results in T_{rad} and/or T_{snow}> 273.15 K, T_{rad} and/or T_{snow} are set to 273.15 K, SSAM is rerun and the resulting positive Q_m term is available to ripen or melt snow.

4.3.4. Snowpack Mass Balance

The influence of stubble characteristics upon snow depletion is simulated with coupling of the snowpack energy balance with a simple single layer snowpack mass balance model. The snowpack mass balance allows for simulation of both accumulation and depletion of snow as

$$SWE = Snowfall - M - E + \xi + q_s, \tag{4.45}$$

where M (kg m^{-2}) is melt water discharge, E (kg m^{-2}) is sublimation or deposition, ξ (kg m^{-2}) is snow erosion or deposition from horizontal transport of suspended and saltating snow, and q_s (kg m^{-2}) is the vertical water vapour loss of blowing snow sublimation. In cases of blowing snow, changes in SWE will correspond to changes in U per the ratio $\frac{\mathrm{SWE}+\xi-q_s}{SWE}$ assuming T_{snow} is unaffected. The energy balance is coupled to the snowpack mass balance through conversion of Q_m to melt in terms of equivalent SWE as,

$$M = \frac{Q_m}{L_f} dt, \tag{4.46}$$

where L_f (334 kJ kg^{-1}) is the latent heat of fusion. The LE_{snow} term also represents a mass exchange of either sublimation or deposition and is put into terms of equivalent SWE as,

$$E = \frac{LE_{snow} dt}{L_s}, \tag{4.47}$$

where L_s (2835 kJ kg^{-1}) is the latent heat of sublimation. Only once snow becomes isothermal, $T_{snow} = U_{snow} = 0$, will snow begin to melt. As snow is a porous media the initial melt increases the liquid water content (LWC [kg m^{-2}]) of the snow rather than immediately discharge meltwater from the snowpack. The maximum liquid-water-holding capacity of snow (LWC_{max} [kg m^{-2}]), the amount of water that can be held by snow without draining, defines how much snowmelt is needed to fully ripen a snowpack. This LWC_{max} (kg m^{-2}) is estimated as (Essery, 2015)

$$LWC_{max} = \rho_{water} \phi_{snow} h_s \theta_{lw}, \tag{4.48}$$

where ρ_{water} is the density of water (1000 kg m^{-3}), h_s(m) is the snow depth, θ_{lw}(-) is the liquid water capacity of snow (0.001-0.08, Pomeroy and Brun (2001)) and ϕ_{snow} (-) is snow porosity as,

$$\emptyset_{snow} = 1 - \frac{SWE}{\rho_{ice} h_s}, \tag{4.49}$$

where p_{ice} is the density of ice (917 kg m^{-3}). Once the snowpack is ripe any additional Q_m depletes the SWE and is discharged from the snowpack. Meltwater flow and retention is

complicated by heterogenous snow structure and is shown to have large implications for meltwater discharge from a snowpack (Leroux and Pomeroy, 2017; Marsh and Woo, 1984) but ignored hereafter as snow structure is not represented in the single layer snow model. A negative Q^*_{snow} refreezes the liquid water prior to the cooling of the snowpack. The conditional algorithm used to partition Q^*_{snow} into $\frac{dU_{snow}}{dt}$ or Q_m and track changes in U_{snow}, LWC, SWE is detailed in Figure 4.2.

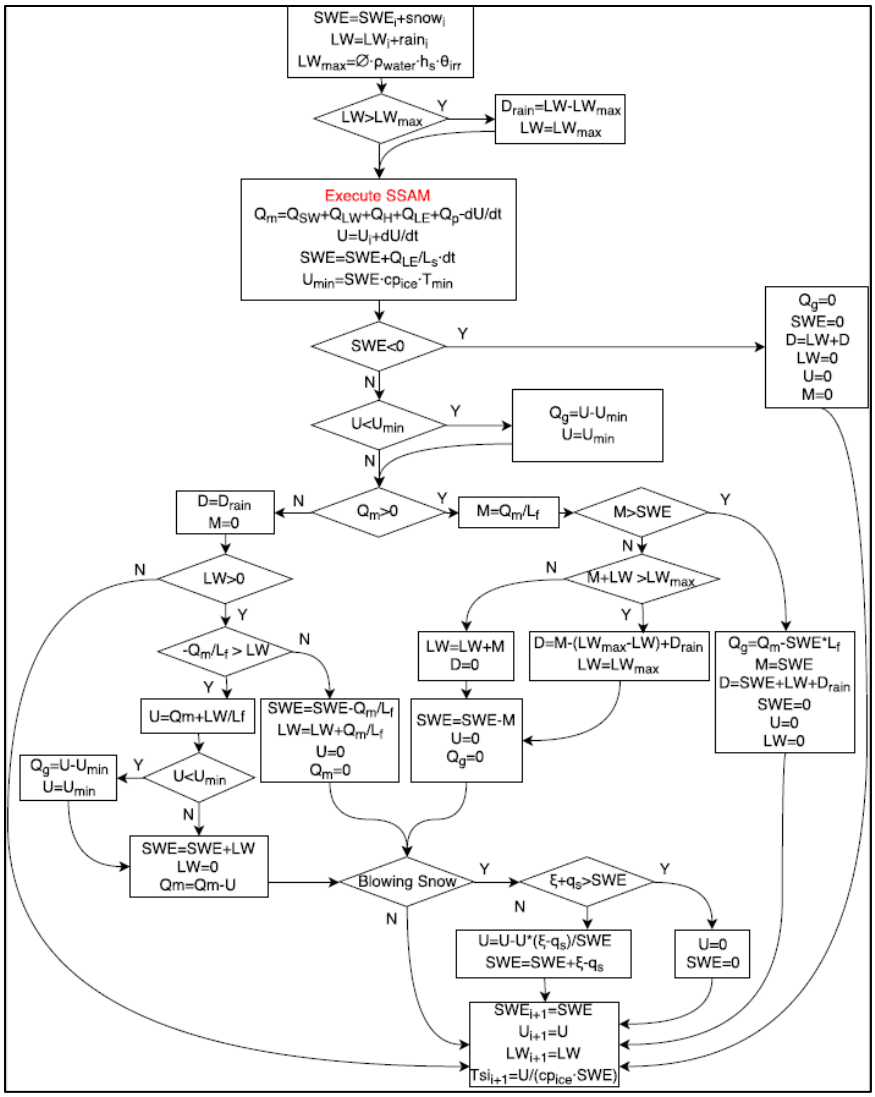

Figure 4.2: Flowchart of model tracking mass (snow water equivalent [SWE], liquid water content [LW], snowfall [snow], rainfall [snow], snowmelt [M], meltwater discharge [D] and blowing snow sublimation [qs] and erosion/deposition [ξ]) and energy (snow internal energy [U], melt energy [Qm], and ground heat flux [Qg]).

4.4. Data and Methods

4.4.1. Site

The field site near Rosthern, Saskatchewan, Canada, is representative of a no-till agricultural region on the northern Canadian Prairies, where agricultural practices control physical characteristics of the vegetation cover. The landscape has little relief and is interspersed with woodlands and wetlands. Snow depth accumulation is typically less than 0.5 m. Pomeroy et al. (1993, 1998) described the snow accumulation and melt energetics of similar environments.

4.4.2. Observations

To assess SSAM, snowmelt field campaigns in 2015 and 2016 collected observations to test SSAM components for a selection of stubble treatments. Site characteristics are summarized in Table 4.1.

Table 4.1: Summary of instrumented sites

Site Name	Surface	Year	Stubble Row Orientation	Stubble Height (m)	Relevant Observed Variables*
Tall15	Wheat	2015	North-South	0.34	$SW_{snow}^{\downarrow}, H, LE, T_{stub}, T_{rad}, h_s$
Short15	Wheat	2015	North-South	0.23	$SW_{snow}^{\downarrow}, H, LE, T_{stub}, T_{rad}, h_s$
Tall15.EW	Wheat	2015	East-West	0.38	$SW_{snow}^{\downarrow}$
Short15.EW	Wheat	2015	East-West	0.18	$SW_{snow}^{\downarrow}$
Wheat16	Wheat	2016	North-South	0.24	$SW_{snow}^{\downarrow}, T_{stub}, T_{rad}, h_s$
Canola16	Canola	2016	East-West	0.24	$SW_{snow}^{\downarrow}, T_{stub}, T_{rad}, h_s$
Reference	Grass	2014+	-	-	$SW_{atm}^{\downarrow}, LW_{atm}^{\downarrow}, T_a, RH, u, Ppt, h_s$

*Ppt = precipitation, h_s=snow depth

4.4.2.1. Shortwave Radiation

Direct observation of $SW_{snow}^{\downarrow}$ employed an array of Apogee SP110 pyranometers. Snow depth is dynamic therefore sensors were mounted on threaded rods to allow vertical adjustment (Figure 4.3). Sensors were cleaned and adjusted to the snow surface after snow accumulation or ablation events. Periods when sensors were buried were removed from the analysis. At each observation site, two pyranometers were placed, one within the stubble row and the other between the stubble rows, to account for variability in $SW_{snow}^{\downarrow}$. Herein, the observations reported from each site are the average of the two sensors.

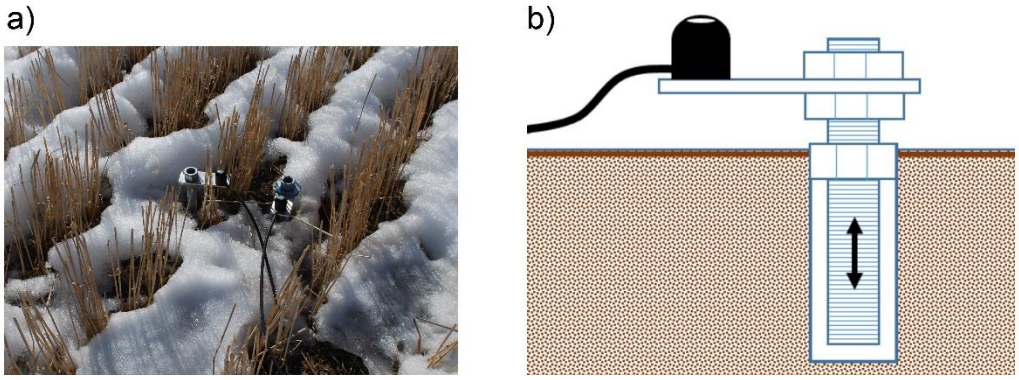

Figure 4.3: a) Typical pyranometer deployment configuration to observe snow surface incoming shortwave radiation. Sensor height controlled by raising and lowering of the threaded rod placed within ABS pipe buried in the ground as detailed in sketch b).

4.4.2.2. Radiometric Snow-Surface Temperature

Snow-surface temperature was observed using Apogee SI-111 infrared radiometers. At each observation site, a SI-111 was fixed to a mobile platform that was shifted as needed to restrict observation to snow surfaces.

4.4.2.3. Stubble Temperature

Stubble temperature is challenging to measure as stubble elements are very small. Two approaches were taken. First, thermocouples (30-gauge Type T) were inserted into the stalks through a small incision. At each site eight thermocouples were inserted over the vertical extent of h_v. A challenge is that thermocouples sample the interior temperature of the stubble, which may differ from the stubble surface. The second approach involved intermittent thermography of the stubble using a FLIR T650 thermal camera. Significant challenges exist with thermography, specifically, the ability to focus on the stubble elements, the smearing of the emitted radiation over the coarse pixels, the variability and uncertainty of surface emissivity and the environmental conditions (Muniz et al., 2014; Shea and Jamieson, 2011). Depending on input uncertainty the standard error of thermography can be up to 3 °C (Muniz et al., 2014). Bias was corrected with the difference between the snow temperature observed by the FLIR and an adjacent SI-111.

4.4.2.4. Eddy covariance

Eddy covariance (EC) instrumentation was deployed during the 2015 observation campaign to Short15 and Tall15 treatments to observe the areal average LE and H. The identical setups used LI-COR 7500A open-path infrared gas analyzers in conjunction with Campbell

Scientific CSAT3 sonic anemometers. Sensor heights were 1.8 m on both sites to ensure the flux footprints remained within the stubble treatment domains while also sampling a representative span of eddy sizes. Data was logged at 20 Hz and post-processed with default settings in Eddy Pro Software (v.6.2.0) to give 30-minute average flux observations. The Mauder and Foken (2006) procedure assessed data quality and only 0 Flag data was used in this study.

4.4.2.5. Meteorological Data

A permanent meteorological reference station adjacent to the instrumented stubble treatments observed $SW_{atm}^{\downarrow}$ and $LW_{atm}^{\downarrow}$ with a Kipp and Zonen CNR1 net radiometer, u and wind direction with a RM Young 05103 Wind Monitor, Ppt with an Alter-shielded Geonor TB-200 weighing gauge and T_a and RH with a Campbell Scientific HMP45C212. Precipitation phase was estimated by applying Harder and Pomeroy's (2013) psychrometric approach and snow undercatch was corrected using the correction of Smith (2009).

4.4.2.6. Stubble Characteristics

Information on stubble characteristics, h_v, r, ρ_{A-stub}, a_{stub} and row spacing (row), is required to parameterize SSAM. These parameters were sampled for the canola and wheat stubble treatments during the observation campaigns. The respective treatments' h_v are given in Table 4.1 with remaining characteristics summarized by crop type in Table 4.2.

Table 4.2: Observed stubble characteristics

Variable	Units	Canola	Wheat
a_{stub}	-	0.36	0.19
row	m	0.3	0.3
r	m	0.012	0.0035
ρ_{A-stub}	stalks m^{-2}	67	435

4.4.2.6.1. Plant Area Index

Independent observations of PAI relative to h_v were obtained with a Decagon AccuPAR LP-80 Ceptometer. The LP-80 is a portable line quantum sensor, 0.84 m probe length with 80 sensors, that measures canopy photosynthetically-active radiation (PAR) transmissivity. Leaf Area Index (LAI), analogous to PAI in this situation, is related to PAR transmissivity with an empirical extinction coefficient (Welles and Cohen, 1996). The LP-80 is appropriate for PAI observations in a short discontinuous stubble canopy and provides an independent validation of

the proposed PAI parametrization (Decagon Devices Inc., 2016). Vertical PAI profiles were obtained by sampling at 0.05 m intervals.

4.4.2.7. Snow Surveys

Snow surveys provided regular observations of h_s, measured by a snow probe, and ρ_{snow}, measured by snow coring with a ESC-30 snow tube. The snow courses for each treatment consisted of 130 h_s and 17 ρ_{snow} observations in 2015 and 90 h_s and 12 ρ_{snow} observations in 2016. Snow surveys were conducted on one to three day intervals during the melt period. Areal average SWE was estimated from multiplication of observed h_s and mean ρ_{snow}. The sampling uncertainty of SWE estimates is quantified with bootstrapping. The means of the h_s and ρ_{snow} observations were resampled, with replacement, 10,000 times to develop robust estimates of the respective 95% confidence interval (CI). The 95% confidence for SWE (CI_{SWE}) is calculated as (Steppuhn and Dyck, 1974),

$$CI_{SWE} = \sqrt{h_s^2 CI_{\rho_{snow}}^2 + \rho_{snow}^2 CI_{h_s}^2}. \tag{4.50}$$

4.4.3. Model Validation

The micro-scale nature of the stubble and snow environment and limitations of available instrumentation prevents direct validation of all SSAM energy balance terms. Assessment of the PAI parameterization compared the estimates, based on observed stubble properties, and the corresponding observed PAI profiles. The $SW_{snow}^{\downarrow}$ assessment spanned from 8 to 29 March for both 2015 (at four sites) and 2016 (at two sites). The PAI for calculation of τ used h_v as the difference between the radiometer height and stubble height and the observed mean ρ_{A-stub} for the respective stubble types. The reference station supplied the $SW_{atm}^{\downarrow}$ observations. SSAM was run with input data from the meteorological reference station from 8 to 29 March for the respective years to test T_{rad}, T_{stub}, areal average LE and H, and SWE performance. Snow properties (SWE, p_{snow} and a_{snow}) were initialized from the snow survey and radiometer observations at the time of maximum observed SWE. The v variable in the a_{snow} term and θ_{lw} were adjusted based on relative field conditions; $v = 0.01$ and $\theta_{lw} = 0.01$ in 2015, as the presence of significant ice layers led to faster a_{snow} decline and lower LWC_{max}, and $v = 0.05$ and $\theta_{lw} = 0.02$ in 2016, as the relatively clean snowpack led to slower a_{snow} decline and greater

LWC_{max}. Model performance was assessed by comparing T_{stub} against the mean temperature of exposed in-situ stubble thermocouples and thermography estimates, T_{rad} against the infrared radiometer observations, H and LE against the EC observations and SWE against snow survey observations.

Model performance was assessed with the root mean square error (RMSE) and model bias (MB). Each test provides a different perspective on model performance: $RMSE$ is a weighted measure of the difference between the observation and model, (Legates and McCabe, 2005) and MB indicates the mean over or underprediction of the model versus observations (Fang and Pomeroy, 2007). All error metrics are rounded to 2 decimal places so any MB values reported as 0 are more accurately less than 0.0049.

4.4.4. Model Sensitivity

The overall influence stubble exposure has on the terms of the snow energy balance was explored with a sensitivity analysis of SSAM. Canola and wheat stubble, defined by Table 4.2 parameters, was simulated with h_v varying from 0 m to 0.5 m at 0.02 m increments. A consistent baseline for the meteorological inputs, corresponding to typical snowmelt conditions in the middle of March in this region, used T_a=3 °C, RH=75%, u= 4 m s^{-1}, $SW_{atm}^{\downarrow}$= 500 W m^{-2}, and $LW_{atm}^{\downarrow}$= 266 W m^{-2}. While keeping these variables constant each meteorological input was varied across a range consistent with daytime snowmelt conditions on the Canadian Prairies (Table 4.3). A sun angle of 37° and an a_{snow} of 0.75 were specified. Steady state conditions, no change in T_{stub} with time, and a ripe snowpack, T_{snow}= 0 °C, are assumed

Table 4.3: Ranges in meteorological data for SSAM sensitivity analysis

Variable	Unit	Minimum	Maximum	Interval
T_a	°C	1	5	1
RH	%	25	100	25
u	m s^{-1}	2	8	2
$SW_{atm}^{\downarrow}$	W m^{-2}	400	700	100
$LW_{atm}^{\downarrow}$	W m^{-2}	200	332	33

4.5. Results and Discussion

4.5.1. Model Performance

4.5.1.1. PAI Parametrization Performance

The PAI parameterization of SSAM controls shortwave radiation interception and turbulent exchange processes. Observations of PAI, as they vary with h_v, are plotted in Figure 4.4a and demonstrate the clear differences between a sparse canola stubble and a dense wheat stubble. The PAI parametrization, Equation 4.3, is plotted against observations in Figure 4.4b and demonstrates that the proposed model accounts for differences in stubble characteristics. The model successfully estimates PAI with low $RMSE$ and MB.

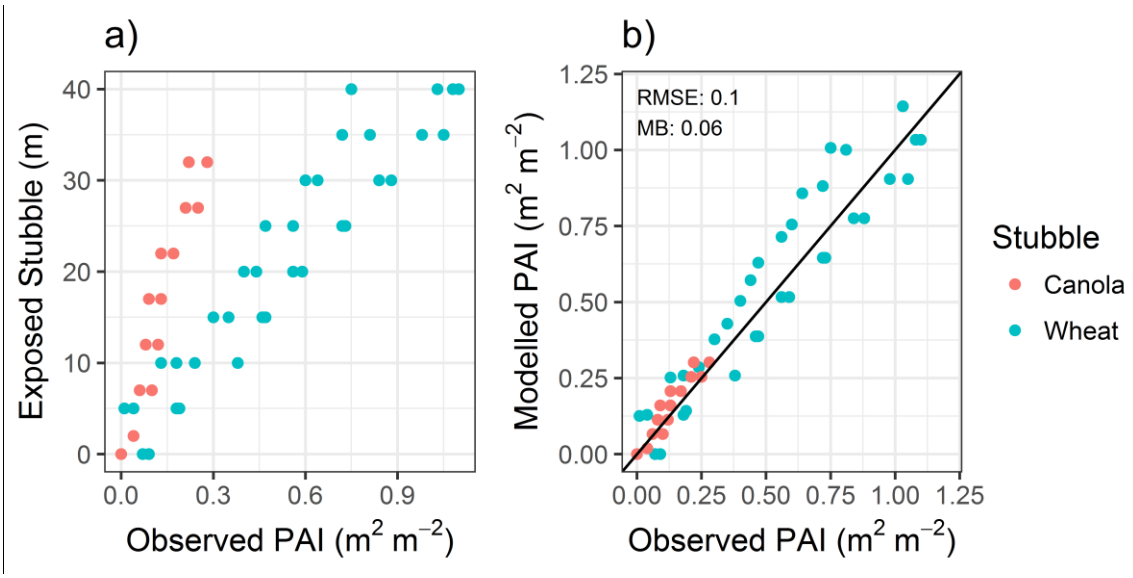

Figure 4.4: a) Profiles of PAI with respect to exposed stubble and b) performance of PAI model relative to observed PAI for both canola and wheat stubble sites. Solid line in b) is the 1:1 line.

4.5.1.2. Shortwave Radiation Performance

The predicted $SW_{snow}^{\downarrow}$ struggles to account for the randomness of the discontinuous stubble that causes the surface to vary between fully exposed and shaded. With only two sensors at each site, the observed $SW_{snow}^{\downarrow}$ is more variable than the areal average behavior on an hourly interval. The effect of stubble gaps and limited sensors is apparent in the relatively large values of $RMSE$ and the scatter of modelled and observed hourly sub-canopy radiation in Figure 4.5. Cumulative radiation is of greater concern for snowmelt modelling than instantaneous values and

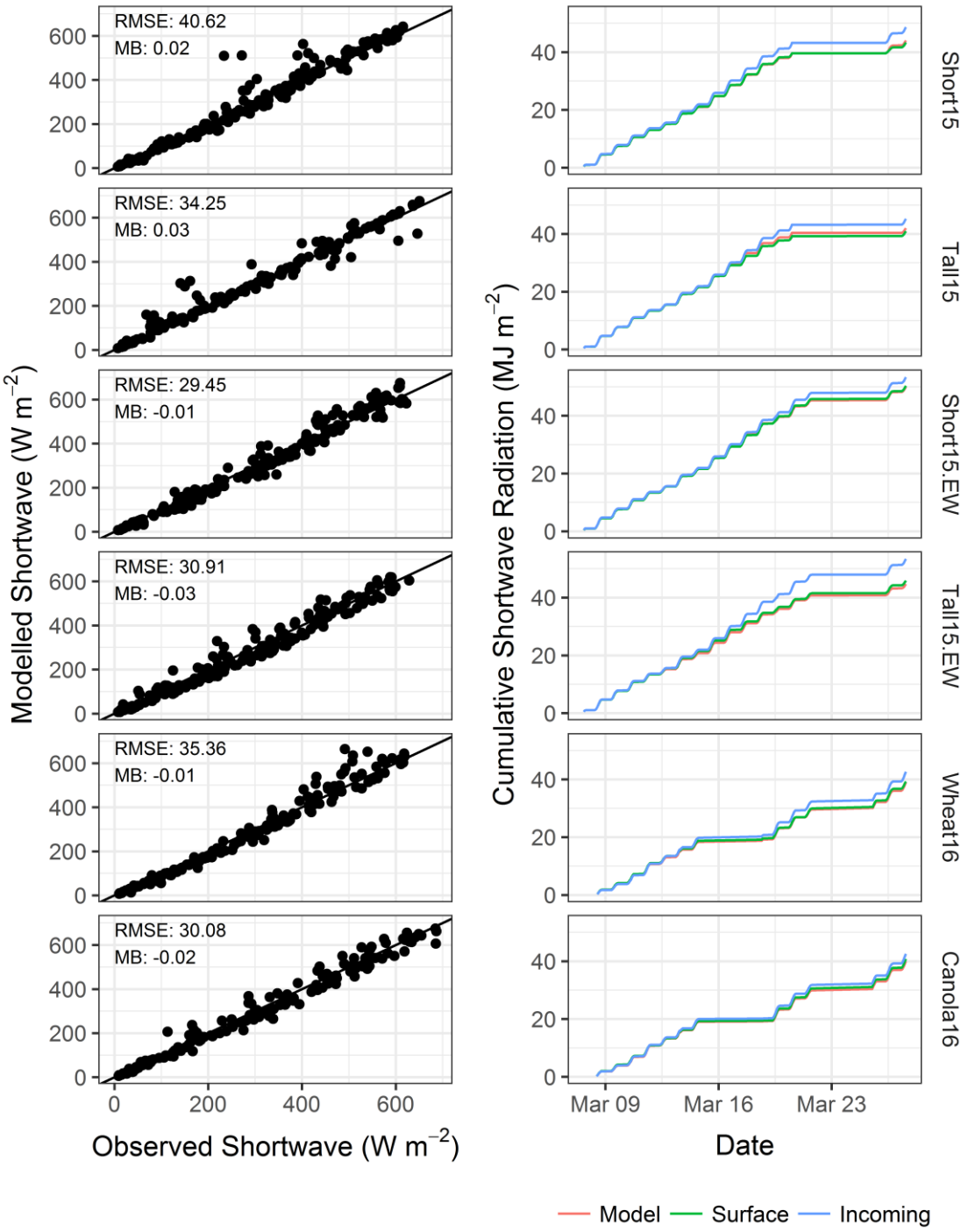

Figure 4.5: Hourly modelled versus observed sub-canopy shortwave radiation (left column) and cumulative hourly shortwave radiation for above canopy observations (blue, Incoming), below canopy observations (green, Surface) and modelled sub-canopy observations (red, Model) for 8 March to 30 March intervals in the respective observation years.

the model and observations are much more appropriate to capture this dynamic. There is little difference in cumulative values as demonstrated with low MB values, +/- 0.03 W m^{-2} and little difference between cumulative observed and modelled sub-canopy radiation (Figure 4.5).

4.5.1.3. Stubble Temperature Performance

The comparison of estimated T_{stub} to observations reveals systematic differences as SSAM consistently overestimates relative to the observations from thermocouples during peak sun angles (Figure 4.6). This is an expected consequence of the core stalk temperature being buffered by the stubble heat capacity and conductivity. The higher FLIR observations, relative to thermocouples, are comparable to SSAM values during the daytime, confirming that surface temperatures exceed the core stalk thermocouple measurements. Considering thermography uncertainty, SSAM is performing well; $RMSE$ of thermography estimates are near the expected FLIR uncertainty of 3 °C (not shown).

4.5.1.4. Radiometric Snow-Surface Temperature Performance

The estimated T_{rad} showed similar accuracies to those reported by Pomeroy et al. (2016) for homogenous snowcover with $RMSE$s between 1.4 and 1.8 °C (Figure 4.7). The temporal relationship between observed and modelled T_{rad} is strong, though SSAM tends to overestimate the nighttime cooling on cold calm nights.

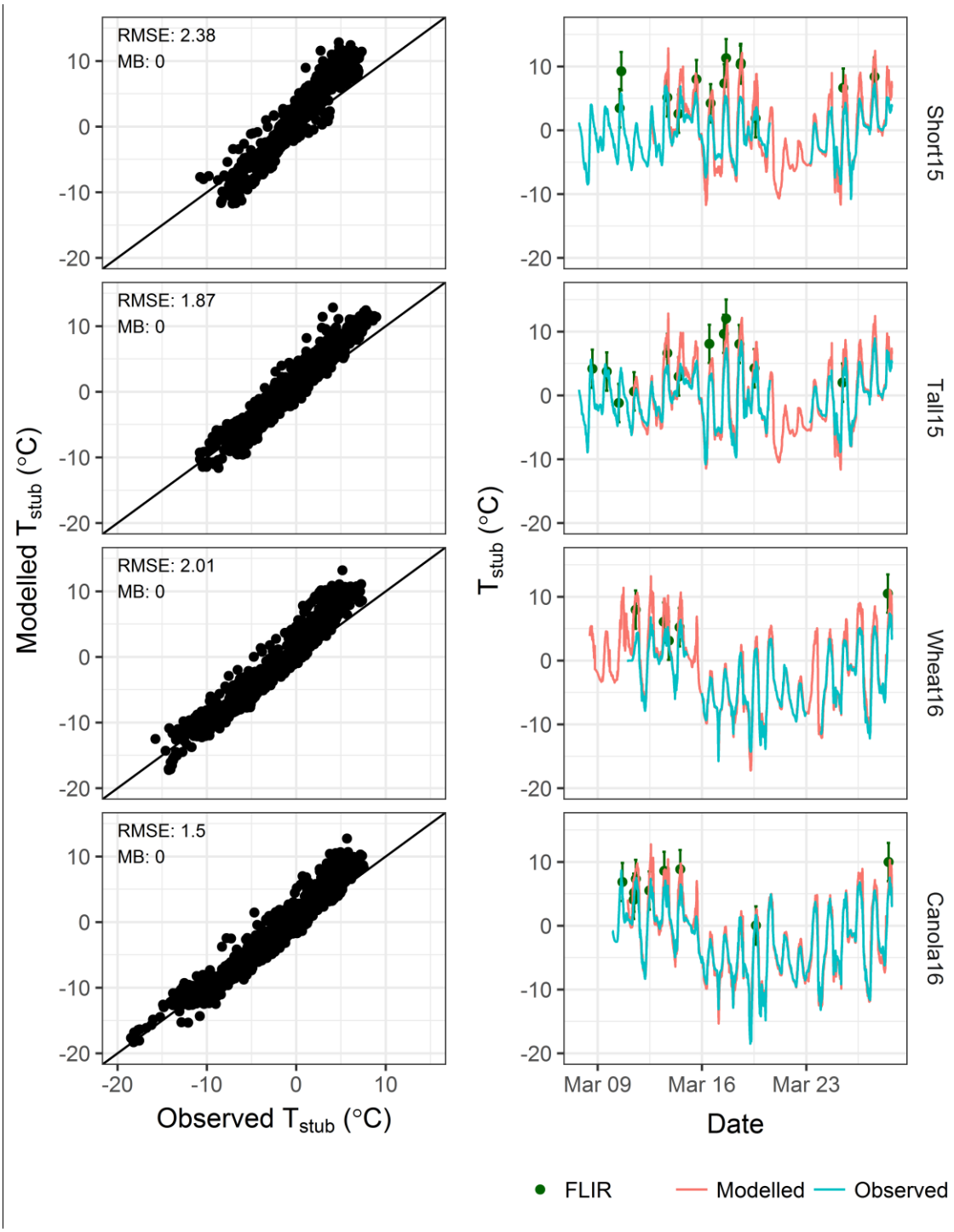

Figure 4.6: Modelled versus observed stubble surface temperatures (T_{stub}) as scatter plots and time series for sites between Mar 8 to March 29 for the respective years. Blue lines are mean stubble temperature measurements of exposed stubble from *in-situ* thermocouple (Observed), green points with error bars (FLIR) are stubble temperature observations from thermography and red lines (Modelled) are simulated stubble surface temperatures.

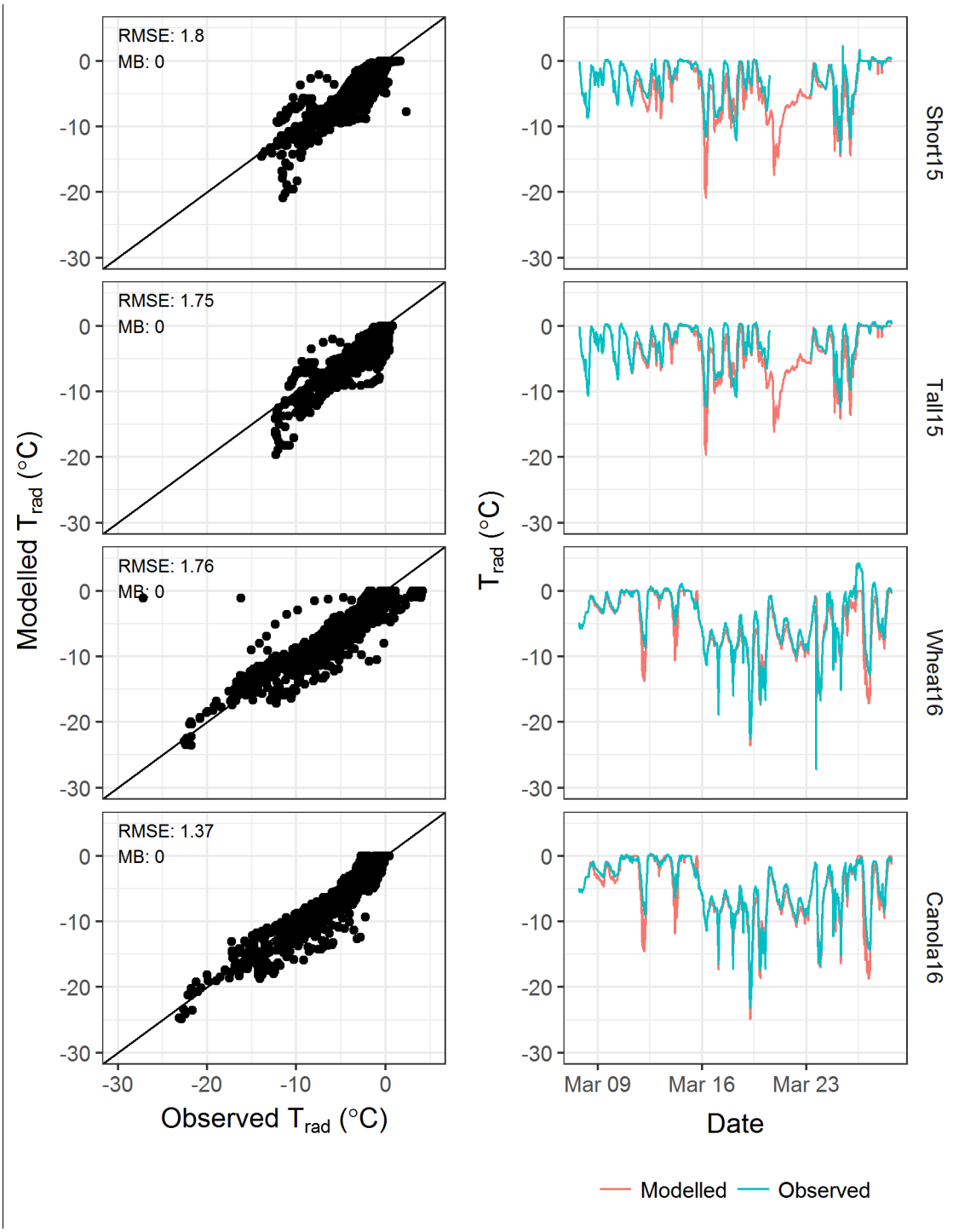

Figure 4.7: Modelled versus observed radiometric snow surface temperatures (T_{rad}) as scatter plots and time series for sites between Mar 8 to March 29 for the respective years. Red lines (Modelled) are modelled snow surface temperature and blue lines (Observed) are observed snow surface temperatures. Observations greater than 0 °C occur when view of SI-111 sensors are contaminated by warm non-snow surfaces prior to relocation.

4.5.1.5. Turbulent Fluxes

Assessment of the turbulent fluxes is limited to Tall15 and Short15 sites. Therefore, transferability of the SSAM resistance scheme to canola is untested. Over wheat treatments, LE showed excellent temporal agreement with limited scatter (Figure 4.8) and low errors while H (Figure 4.9) had weaker performance. The over-prediction of H relates to deficiencies in process representation and differences between what SSAM estimates and EC observations represent. First, the parallel resistance conceptualization does not allow turbulent exchange between snow and stubble that would moderate T_{stub} and T_{snow}; this will lead to overprediction of positive and negative H. In multiple source models H is often calculated with a serial resistance scheme which couples source temperatures through calculation of a canopy air temperature (Best et al., 2011; Ménard et al., 2014; Norman et al., 1995). Unfortunately, the physical process understanding of turbulent exchange between the dynamic exposure of short and sparse stubble elements and snow during melt is insufficient to represent conceptually as a serial resistance scheme. Turbulent exchanges in open environments is intermittent (Helgason and Pomeroy, 2012a, 2012b) and there is no consistent establishment of a distinct within canopy air temperature needed for a serial resistance scheme to be valid. Second, there is a mismatch between the surface characteristics at the point scale of SSAM and the EC flux footprint. The EC observations reflect a flux footprint where the combined spatial variability of the stubble and snow depth will lead to a range of h_v that differs from the model simulated uniform h_v. Snowcover and h_v heterogeneity in the flux footprint are dynamic due to the variability of wind direction in each interval; therefore noise, rather than a systematic bias, is expected and observed in scatterplots of Figures 4.8 and 4.9. Despite differences in assumptions and scales, the representation of areal average H and LE does capture the temporal behavior and magnitude of the observations. The errors are reasonable with respect to the literature as all turbulent transfer parameterizations are challenged by issues of energy balance closure and heterogenous flux footprints (Andreas, 2002; Helgason and Pomeroy, 2012b; Marks et al., 2008).

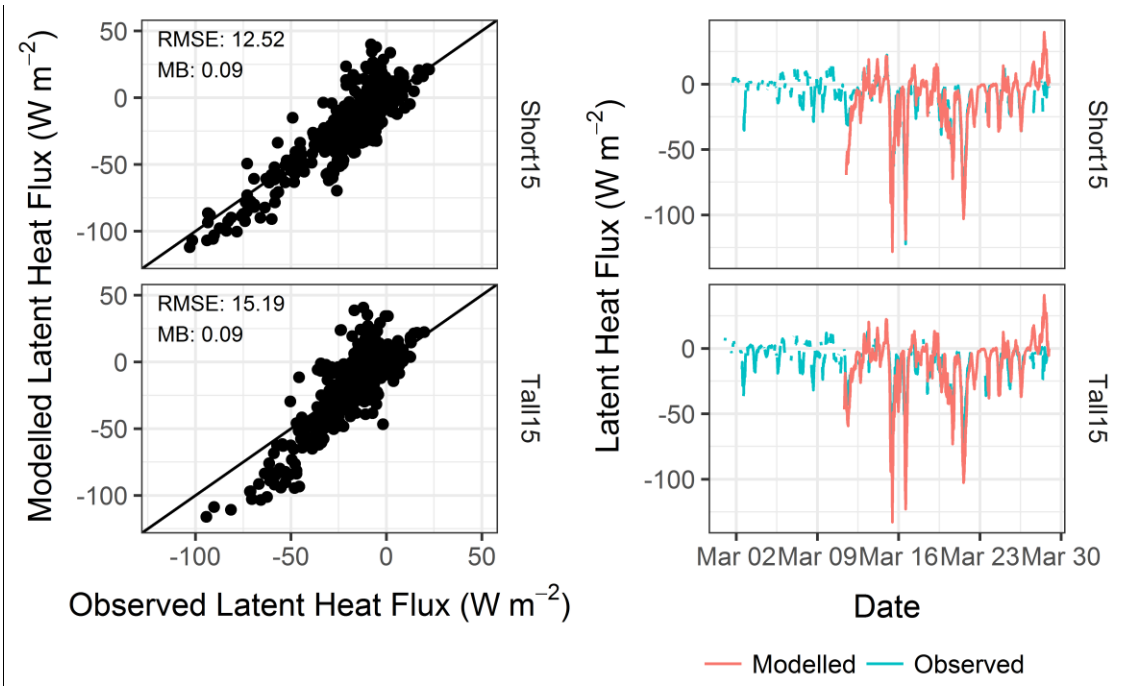

Figure 4.8: Observed and modelled latent heat fluxes over Short15 and Tall15 stubble treatments as scatter plots and time series between March 8 and 29, 2015. Red lines (Modelled) are modelled latent heat fluxes and blue lines (Observed) are observed latent heat fluxes.

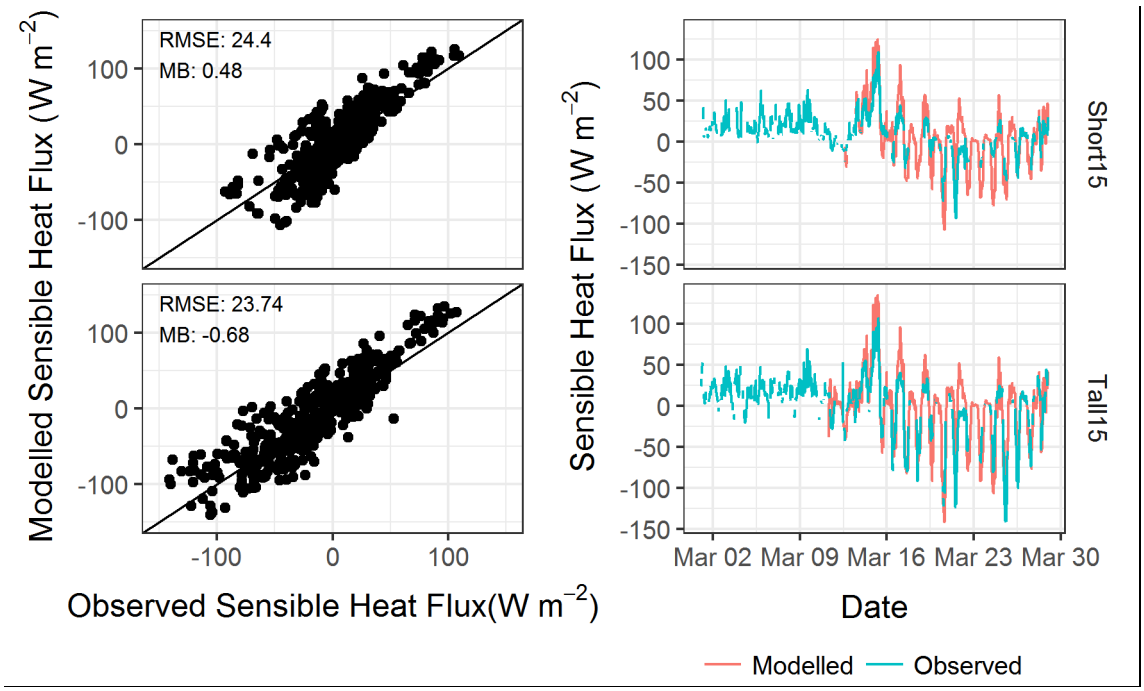

Figure 4.9: Observed and modelled sensible heat fluxes over Short15 and Tall15 stubble treatments as scatter plots and time series between March 8 and 29, 2015. Red lines (Modelled) are modelled sensible heat fluxes and blue lines (Observed) are observed sensible heat fluxes.

4.5.1.6. Snow Water Equivalent

The SWE depletion simulation performed well with respect to the areal average SWE observations from snow surveys (Figure 4.10). Both melt seasons were characterized by an initial rapid melt in early March that was suspended by cooler weather and a moderate snowfall event, with final melt occurring rapidly at the end of March. The main difference was that 2015 had greater pre-melt SWE. The modelled SWE depletion for both seasons captures these dynamics well. The model overestimated the initial melt for Wheat16 treatments and underestimated the initial melt for Tall15. Wheat16 and Canola16 simulations captured the accumulation of the mid-melt snowfall event well while Short15 and Tall15 overestimated SWE after the mid-melt snowfall. The timing and final melt-out sequence was captured for all sites. The SWE RMSEs were greater in 2015 than 2016 but were reasonable at less than 14 mm. These results demonstrate that SSAM's energy balance approach, with respect to independent SWE observations, successfully represented the melting snowpack energy balance and can predict realistic SWE depletion. It is important to reiterate that no calibration was used to optimize model performance, which provides confidence in the model process representations.

4.5.1.7. Validation Summary

A challenge of validating SSAM is that it is extremely difficult to obtain direct observation of the processes represented in the model, due to the small-scale nature of the stubble elements and their dynamic emergence from snow during melt. The successful representation of PAI, $SW_{snow}^{\downarrow}$, T_{stub}, T_{rad}, H, LE, and SWE, observations of state variables or fluxes, provides independent validation of the process representations for each energy balance term. This gives confidence that SSAM can successfully reproduce the complex and dynamic interactions evident between the stubble, snow, and atmosphere. The goal of SSAM is to quantify the energy available to melt snow below an emerging stubble canopy so the demonstrated ability to quantify the role of each energy balance term and how they may compensate for one another is critical.

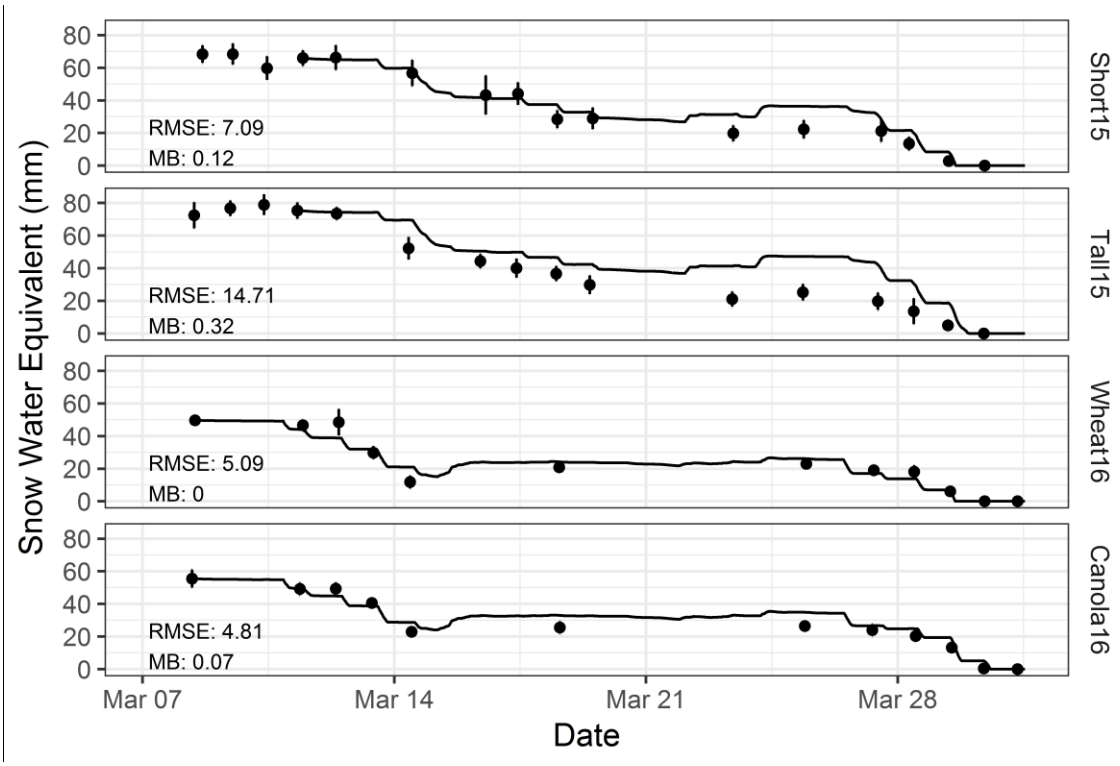

Figure 4.10: Modelled snow water equivalent (lines) and observed snow water equivalent from snow surveys (points) for the respective treatments.

4.5.2. Snow Energy Balance Compensation

The sensitivity analysis of SSAM with respect to variations in stubble properties and meteorological inputs articulates the non-linear interactions that lead to energy balance compensation. Generally, there is a limited change in Q^*_{snow} with respect to increased h_v (Figure 4.11). Increasing h_v increases LW^*_{snow}, as there is more warm stubble in the view factor of the snow surface, while SW^*_{snow} decreases due to the reflection and absorption of $SW^{\downarrow}_{atm}$ in the stubble. Turbulent fluxes, H_{snow} and LE_{snow}, show a complex response to h_v through its relationship with r_a. As h_v increases, the above canopy exchange increases due to z_0 increases, and the within canopy exchange decreases, due to d increases. The surface exchange coefficient, $C_h = \frac{1}{r_a u}$ in Figure 4.12, initially decreases as there is a larger decrease of within canopy exchange than above canopy exchange as stubble emerges from the snow. An inflection point occurs near 0.04 m h_v for both canola and wheat stubble when the rate of change of the within canopy exchange decreases. Greater exchange within the sparse canola canopy leads to an increase in exchange with increased h_v after the inflection point. The denser wheat stubble

exchange has limited change with h_v below the inflection point. The influence of this relationship with exposed stubble is evident in all simulations of Q^*_{snow}.

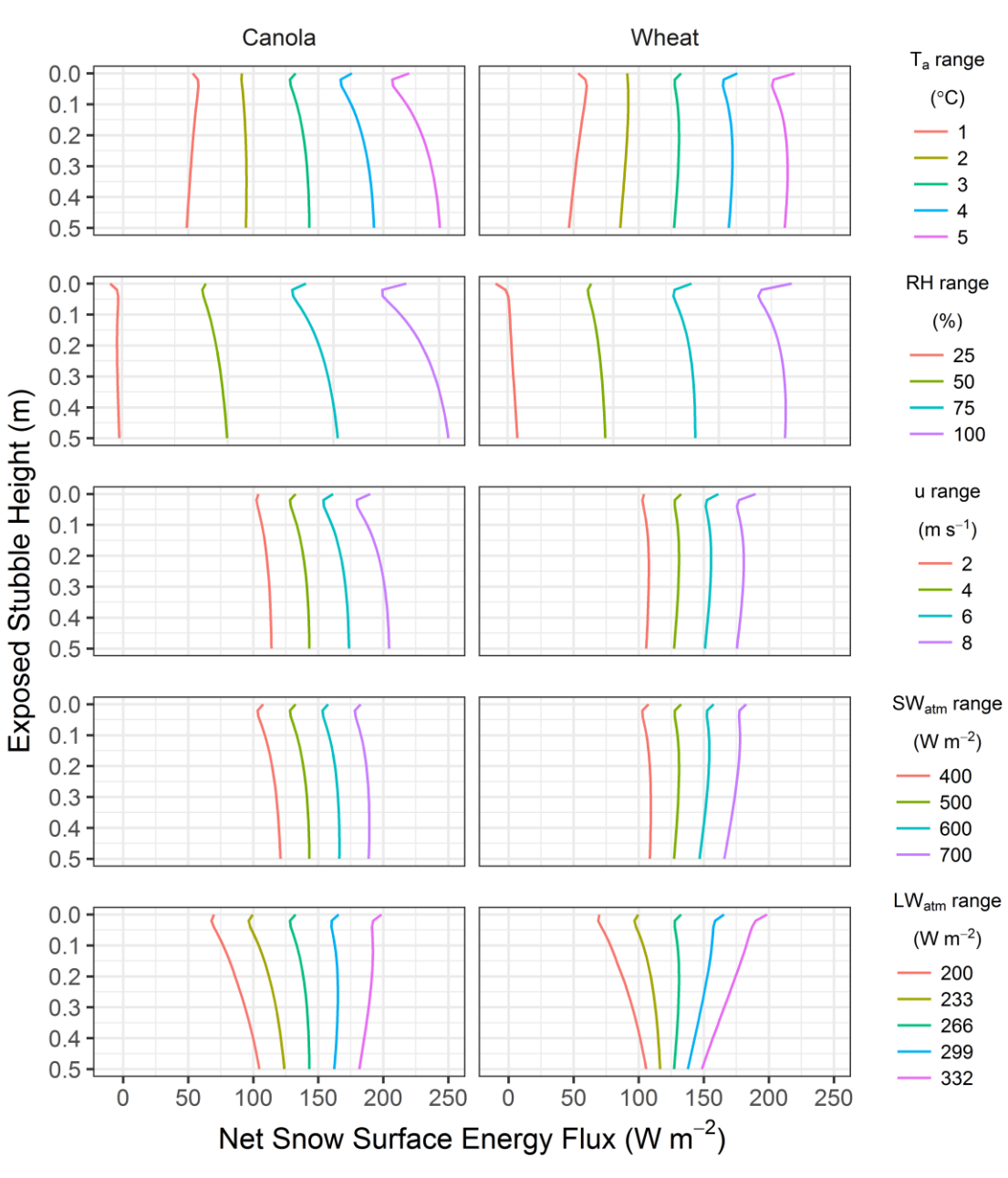

Figure 4.11 Sensitivity of canola and wheat stubble snow surface net energy (Q^*_{snow}) terms with respect to exposed stubble height and variations in air temperature (T_a), relative humidity (RH), wind speed (u), incoming shortwave radiation ($SW^{\downarrow}_{atm}$) and incoming longwave radiation ($LW^{\downarrow}_{atm}$). Meteorological data ranges are specified in the legend while all other inputs are held to a consistent baseline of T_a=3 °C, RH=75%, u= 4 m s^{-1}, $SW^{\downarrow}_{atm}$= 500 W m^{-2}, and $LW^{\downarrow}_{atm}$= 266 W m^{-2}.

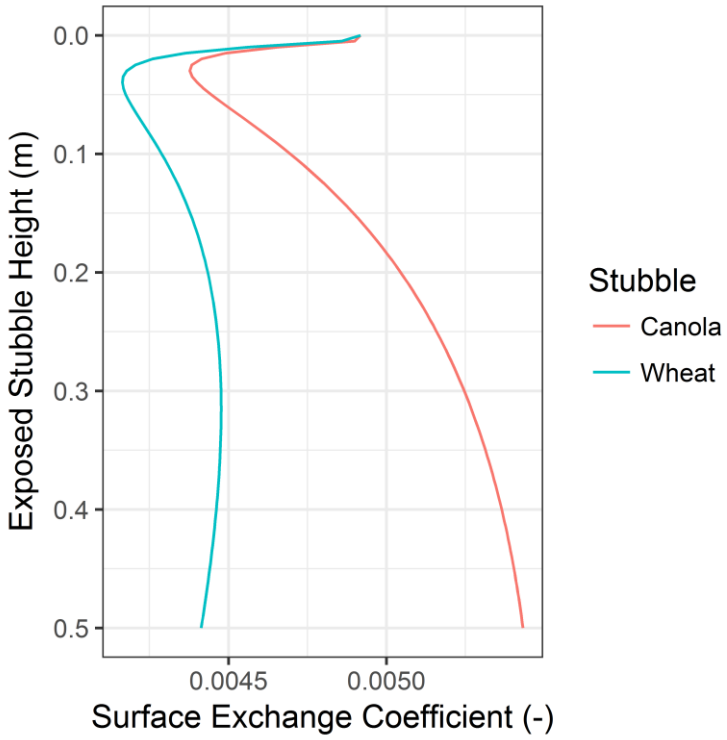

Figure 4.12: Surface exchange coefficient for wheat and canola stubble with respect to variation in exposed stubble height.

The behaviour of the Q^*_{snow} response to stubble exposure with respect to variations in T_a, RH, and u is a consequence of the turbulent snow-atmosphere interactions (Figure 4.13). As is expected for $T_{snow} = 0$ °C, increases in $T_a > 0$ °C will increase H_{snow} and LE_{snow} as temperature and humidity gradients increase. A positive relationship between RH and $Q^*_{snow}$is also demonstrated and, with the conditions simulated, two behaviors are expressed. With $RH = 25\%$ the large negative LE_{snow} forces a negative Q^*_{snow} that will initiate refreezing and possible cooling of the snowpack rather than melt. The LE_{snow} term is quite sensitive to RH and the values for $RH > 25\%$ show large increases that translate into large increases in Q^*_{snow}. There is no response of H_{snow} to RH as RH cannot influence the temperature of a wet isothermal snowpack. Turbulent fluxes are directly related to u and show a clear positive relationship with H_{snow}, LE_{snow}, and Q^*_{snow}. The denser wheat stubble, relative to the more open canola canopy, shows less response in H_{snow}, LE_{snow}, and Q^*_{snow} to variations in h_v, T_a, RH, and u.

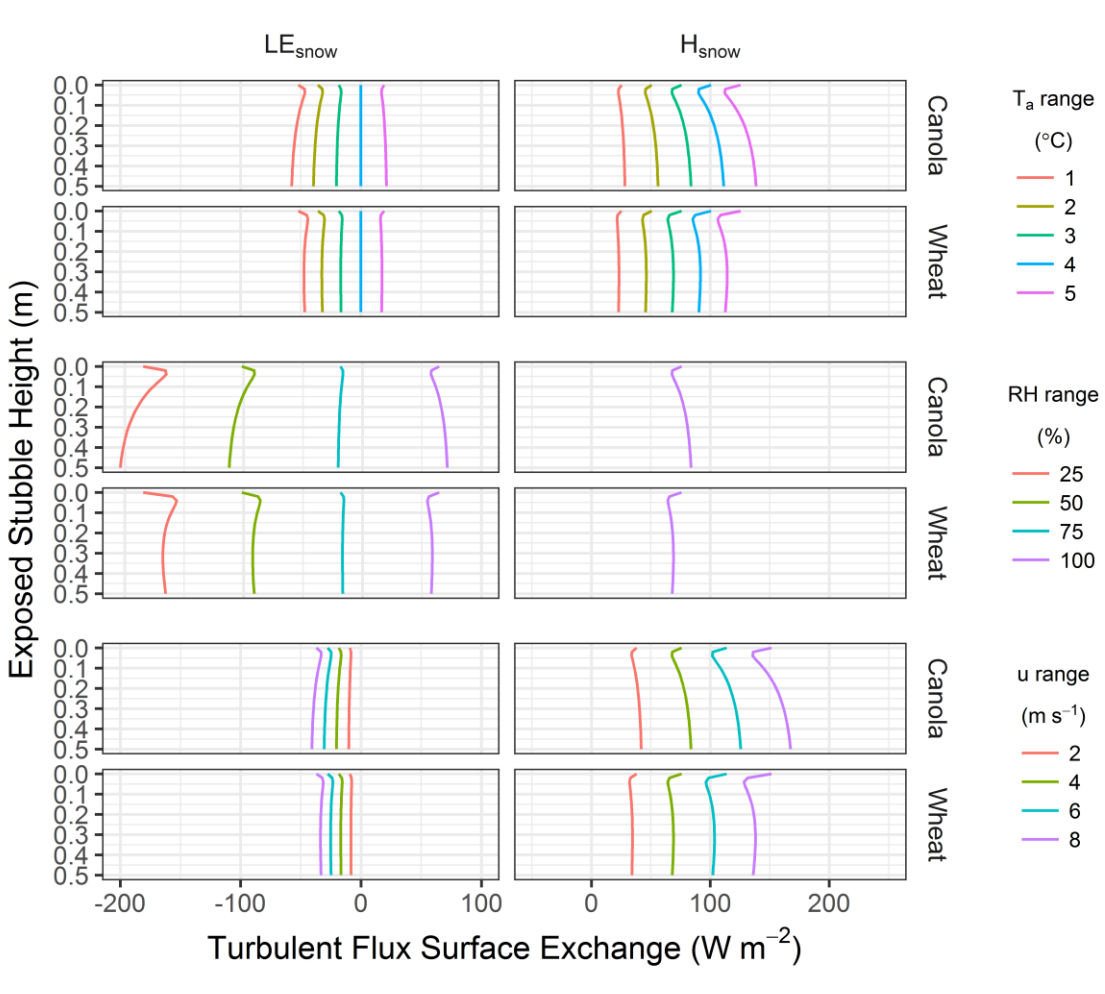

Figure 4.13: Sensitivity of canola and wheat stubble snow surface sensible (H_{snow}) and latent (LE_{snow}) exchange with respect to exposed stubble height and variations in air temperature (T_a), relative humidity (RH), and wind speed (u). Meteorological data is varied by the ranges specified in the legend while all other inputs are held to a consistent baseline of T_a=3 C, RH=75%, u= 4 m s^{-1}, $SW_{atm}^{\downarrow}$= 500 W m^{-2}, and $LW_{atm}^{\downarrow}$= 266 W m^{-2}.

Variations of $SW_{atm}^{\downarrow}$ and $LW_{atm}^{\downarrow}$ have large impacts upon Q_{snow}^{*} that are functions of τ and vf_{sky}, respectively (Figure 4.14). The SW_{snow}^{*} is $SW_{atm}^{\downarrow}$ that is transmitted to and absorbed by the snow; therefore increased $SW_{atm}^{\downarrow}$ will increase SW_{snow}^{*} as a_{snow} and τ are independent terms. There is a small increase in LW_{snow}^{*} with respect to increased $SW_{atm}^{\downarrow}$ as shortwave radiation is absorbed by the stubble and reemitted as longwave radiation. There is minimal response, not shown, in the H_{snow} and LE_{snow} terms to $SW_{atm}^{\downarrow}$ variation. There is an inverse relationship between $LW_{atm}^{\downarrow}$ and Q_{snow}^{*}; as h_v increases vf_{sky} decreases which shifts the source

of incoming longwave at the snow surface from the sky to the stubble. When the longwave flux from the stubble is less than from the sky, in the case of a high $LW_{atm}^{\downarrow}$, LW_{snow}^{*} will decrease with increasing h_v and vice versa. The response of SW_{snow}^{*} and $LW_{snow}^{*}$to $SW_{atm}^{\downarrow}$ and $LW_{atm}^{\downarrow}$ is greater for wheat, relative to canola, as there are greater decreases in τ and vf_{sky} with h_v.

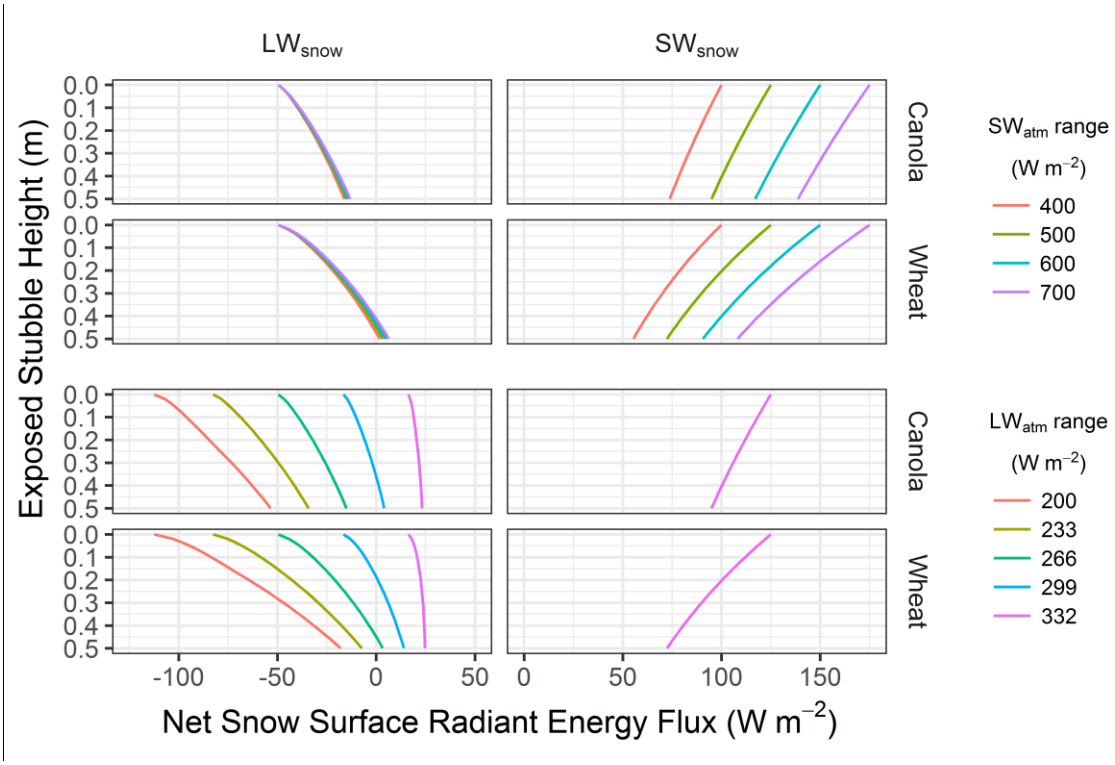

Figure 4.14: Sensitivity of canola and wheat stubble net snow surface shortwave (SW_{snow}^{*}) and longwave (LW_{snow}^{*}) radiation with respect to exposed stubble height and variations incoming shortwave radiation ($SW_{atm}^{\downarrow}$) and incoming longwave radiation ($LW_{atm}^{\downarrow}$). Meteorological data is varied by the ranges specified in the legend while all other inputs are held to a consistent baseline of T_a=3 C, RH=75%, u= 4 m s^{-1}, $SW_{atm}^{\downarrow}$= 500 W m^{-2}, and $LW_{atm}^{\downarrow}$= 266 W m^{-2}.

The cumulative difference in the net energy balance terms over the course of snowmelt will depend upon the dynamic and interacting response of meteorological conditions and stubble exposure. From the sensitivity analysis it is expected that canola or tall stubble will have greater Q_{snow}^{*}, therefore melt rates, than wheat or short stubble. The differences are subtle due to the complex energy balance interactions that act to compensate each other. To fully describe melt patterns in this region differences in snow accumulation due to stubble differences need to be considered.

4.5.3. Implications

The outcome of this work has two main implications. The first is that the lack of representation of stubble emergence in regions of seasonal snowcover and no-till agriculture is a clear deficiency of snowmelt and land-atmosphere models. To improve understanding of land-atmosphere feedbacks, land surface schemes need to include the dynamics of stubble emergence. The dynamic change in C_h with respect to h_v, a decline of 15% and 11% from $h_v = 0$m to $h_v = 0.04$ m followed by a 5 % and 21 % increase from $h_v = 0.04$ m to $h_v = 0.5$ m for wheat and canola stubble respectively, are dynamics currently unsupported in modeling of this region. The strength of the land-atmosphere coupling has consequences for the radiative terms of the energy balance as h_v changes with snowmelt. Land-atmosphere models provide the lower-boundary conditions for numerical weather prediction and climate models and the predictive capacity of weather and climate models, from short to long timescales, will be enhanced with these additional physics. The second is that the clear increase in pre-melt SWE with increasing stubble height (Pomeroy and Gray, 1995) may not necessarily translate into greater frozen soil infiltration. This work demonstrates that the greater melt rates associated with this greater h_v may lead to lower infiltration efficiency and greater runoff efficiency. This potential compensatory relationship requires further research to quantify more fully the hydrological implications of stubble management.

4.5. Conclusions

Quantification of the snow energy balance response to stubble exposure improves the understanding of land-atmosphere interactions and the role of stubble management upon snowmelt processes in semi-arid cold agricultural production regions. The proposed SSAM model represents the snow energy balance underlying exposed stubble and is validated successfully against sub-canopy $SW_{snow}^{\downarrow}$, T_{stub}, T_{rad}, H, LE and SWE observations. A sensitivity analysis of SSAM with respect to stubble exposure and meteorological forcing shows that stubble exposure demonstrates complex energy balance interactions. Generally, stubble will decrease SW_{snow}^{*}, LE_{snow} and H_{snow} and increase LW_{snow}^{*} resulting in a subtle increase in Q_{snow}^{*}. The change in $Q_{snow}^{*}$with h_v may have snowmelt infiltration and runoff implications but requires further study that addresses the stubble influence upon accumulation processes. In contrast, the ability for stubble to change the cumulative values of individual energy balance

terms will have large land-atmosphere modelling implications and provides a compelling argument to include these additional physics into land-atmosphere models. The ability to quantify these stubble-snow-atmosphere energy balance interactions in small and large-scale models is important to understanding the impact of stubble management on snowmelt processes, land-atmosphere interactions, and hydrology in cold agriculture regions.

4.6. Appendices

4.6.1. Snow-Surface Sky View Factor Parameterization

Numerical simulation is employed to calculate the sky view factor (vf_{sky}) from the perspective of a snow surface underlying exposed stubble. The view factor from a surface of a perpendicular cylinder is solved with an analytical solution provided by Sparrow et al. (1962). With vf_{sky} assumed to be the residual of the cylinder view factor, the solution for a single cylinder is

$$vf_{sky}(x) = 1 - \left\{\frac{1}{2\pi}\cos^{-1}(\mathrm{R}) + \frac{1}{\pi}\left[\tan^{-1}\left(\frac{R}{(1-R^2)^{\frac{1}{2}}}\right) - \frac{1+L^2-R^2}{X}\tan^{-1}\left(\frac{X\tan^{-1}\left(0.5\cos^{-1}(\mathrm{R})\right)}{1+J^2+R^2-2R}\right)\right]\right\}, \tag{4.51}$$

where

$$R = \frac{r}{x}, \tag{4.52}$$

$$J = \frac{h_v}{x}, \tag{4.53}$$

and

$$X = ((1+J^2+R^2)^2 - 4R^2)^{\frac{1}{2}}, \tag{4.54}$$

where r (m) is the radius of the cylinder, x (m) is the distance of the surface of interest to the origin of the cylinder and h_v (m) is the height of the cylinder. To simulate an areal average of

vf_{sky}, a collection of stubble stalks is simulated and the contributions of all stalks to a representative surface area are calculated. The simulation procedure is:

- Simulate the stubble locations randomly per ρ_{A-stub}, row, and stubble row width.
- Identify a sample area within the simulation domain that provides a representative estimate of vf_{sky}.
- Identify and remove stalks located behind other stalks relative to the sample area.
- Calculate the distance between the remaining stalks and each selected coordinate of the sample area.
- Calculate individual view factors as per Equation 4.51 and sum to give vf_{sky} at each sample coordinate.
- Calculate mean vf_{sky} from values at each sample coordinate.

The simulation domain used in this analysis is 4 m x 4 m and the sample area is (1 m x 0.5 row spacing) in the middle of the domain. Within this area, the sample coordinates are spaced every 0.02 m in both x and y dimensions.

4.6.2. Stubble-to-Stubble View Factor Parameterization

The stubble-to-stubble view factor (vf_{stub}) is the portion of the view factor from the perspective of a single stubble stalk comprised of other stubble. For two parallel cylinders a solution is given by Juul (1982) as

$$vf_{stub} = A_i C_i, \tag{4.55}$$

where

$$A_i = \frac{1}{2\pi R}\left\{[C^2-(1+R)^2]^{\frac{1}{2}}) - [C^2-(1-R)^2]^{\frac{1}{2}}) + \pi R + (1-R)\cos^{-1}\left(\frac{1-R}{C}\right) - (1+R)\cos^{-1}\left(\frac{1+R}{C}\right)\right. \tag{4.56}$$

$$C_i = 1 - \frac{1}{pi}\left(\cos^{-1}\left(\frac{Y}{Z}\right)\right. \tag{4.57}$$
$$\left. - \frac{1}{2JR}\left\{[(Y + 2X^2)^2 - (2X)^2]^{\frac{1}{2}}\right) \cos^{-1}\left(\frac{RY}{XZ}\right) + Y \sin^{-1}\left(\frac{1}{X}\right) - \frac{\pi}{2}Z\right\}\right),$$

$$R = \frac{r_1}{r_2}, \tag{4.58}$$

$$J = \frac{h_v}{r_2}, \tag{4.59}$$

$$C = \frac{x}{r_2}, \tag{4.60}$$

$$X = \left[\frac{(C^2 - 1)^{\frac{1}{2}} - \frac{\pi}{2}}{\sin^{-1}\left(\frac{1}{C}\right)} + 1\right]^{\frac{1}{2}}, \tag{4.61}$$

$$Y = J^2 - X^2 + R^2, \tag{4.62}$$

and

$$Z = J^2 + X^2 - R^2, \tag{4.63}$$

where r_1 (m) and r_2 (m) are the radii of parallel cylinders 1 and 2, x (m) is the distance between the origins of the cylinders and h_v (m) is the height of the stubble. Simulation for case of mean vf_{stub} in a stubble situation is:

- Simulate the stubble locations randomly per ρ_{A-stub}, stubble row spacing and stubble row width.
- Identify stalk coordinates within the simulation domain that will provide a representative estimate of $vf_{stub.}$
- Identify and remove stalks located behind other stalks relative to the stalks of interest.
- Calculate the distance between each remaining stubble stalk and each selected stalk.
- Calculate individual view factors per Equation 4.55 and sum to give vf_{stub} at each stalk.
- Average all vf_{stub} values at each stalk of interest.

The simulation domain used is 4m x 4m and the stubble stalks of interest are in a 1 m length of row in the middle of the domain.

4.7. Manuscript Integration with Broader Thesis

Chapter 2 provided empirical evidence that stubble characteristics have a limited influence upon SWE depletion despite clear differences in stubble characteristics that will influence the terms of the snow surface energy balance. The observations and model developed here provide the physical understanding to describe the compensatory nature of stubble-snow-atmosphere interactions that describe the SWE observations of Chapter 2. The influence of advection, as observed in Chapter 3 and modeled in Chapter 5, is integrated with this model in Chapter 5 present a more physically complete model of snowmelt on the Canadian Prairies that has been previously been unavailable. The SSAM model developed here in Chapter 4, is a critical component of Chapter 6 that uses SSAM, in addition to the sensible and latent heat advection model of Chapter 5, coupled with blowing snow and frozen soil infiltration processes to provide a physical representation of how stubble characteristics will influence meltwater partitioning.

4.8. References

Aase, J. K., Siddoway, F. H. (1980). Stubble height effects on seasonal microclimate, water balance, and plant development of no-till winter wheat. Agricultural Meteorology, 21, 1–20.

Ahn, H. K., Sauer, T. J., Richard, T. L., Glanville, T. D. (2009). Determination of thermal properties of composting bulking materials. Bioresource Technology, 100(17), 3974–3981. https://doi.org/10.1016/j.biortech.2008.11.056

Aiken, R. M., Nielsen, D. C., Ahuja, L. R. (2003). Scaling effects of standing crop residues on the wind profile. Agronomy Journal, 95, 1041–1046.

Andreas, E. L. (2002). Parameterizing Scalar Transfer over Snow and Ice: A Review. Journal of Hydrometeorology, 3(4), 417–432. https://doi.org/10.1175/1525-7541(2002)003<0417:PSTOSA>2.0.CO;2

Best, M. J., Pryor, M., Clark, D. B., Rooney, G. G., Essery, R., Ménard, C., … Harding, R. J. (2011). The Joint UK Land Environment Simulator (JULES), model description – Part 1: Energy and water fluxes. Geoscientific Model Development, 4(3), 677–699. https://doi.org/10.5194/gmd-4-677-2011

Bewley, D. S., Pomeroy, J. W., Essery, R. (2005). Processes of Solar Radiation Transfer Through a Subarctic Shrub Canopy. In 62nd Eastern Snow Conference (Vol. 39, pp. 109–128). Waterloo, Ontario.

Bewley, D. S., Pomeroy, J. W., Essery, R. (2007). Solar Radiation Transfer Through a Subarctic Shrub Canopy. Arctic, Antarctic, and Alpine Research, 39(3), 365–374.

Bewley, D. S., Essery, R., Pomeroy, J. W., Ménard, C. (2010). Measurements and modelling of snowmelt and turbulent heat fluxes over shrub tundra. Hydrology and Earth System Sciences, 14(7), 1331–1340.

Brun, L. J., Enz, J. W., Larsen, J. K., Fanning, C. (1984). Springtime evaporation from bare and stubble-covered soil. Journal of Soil and Water Conservation, 41, 120–122.

Brutsaert, W., Parlange, M. B. (1992). The Unstable Surface Layer Above Forest: Regional Evaporation and Heat Flux. Water Resources Research, 28(12), 3129–3134.

Burt, C. M., Mutziger, A. J., Allen, R. G., Howell, T. A. (2005). Evaporation Research: Review and Interpretation. Journal of Irrigation and Drainage Engineering, 131, 37–58.

Campbell, G. S., Norman, J. M. (1998). An Introduction to Environmental Biophysics. New York, NY: Springer New York. https://doi.org/10.1007/978-1-4612-1626-1

Choudhury, B. J., Monteith, J. L. (1988). A four-layer model for the heat budget of homogeneous land surfaces. Quarterly Journal of the Royal Meteorological Society, 114, 373–398.

Cutforth, H. W., McConkey, B. G. (1997). Stubble height effects on microclimate , yield and water use efficiency of spring wheat grown in a semiarid climate on the Canadian prairies. Canadian Journal of Plant Science, 77, 359–366.

Decagon Devices Inc. (2016). AccuPAR PAR / LAI Ceptometer Model LP-80 Operators Manual. Pullman WA.

Derpsch, R., Friedrich, T. (2009). Development and Current Status of No-till Adoption in the World. In 18th Triennial Conference of the International Soil Tillage Research Organisation (ISTRO) (p. 13). Izmir, Turkey.

Eagleson, P. S. (2002). Ecohydrology: Darwinian Expression of Vegetation Form and Function. Cambridge, UK: Cambridge University Press.

Ellis, C. R., Pomeroy, J. W. (2007). Estimating sub-canopy shortwave irradiance to melting snow on forested slopes. Hydrological Processes, 21(19), 2581–2593.

Essery, R. (2015). A factorial snowpack model (FSM 1.0). Geoscientific Model Development, 8(12), 3867–3876. https://doi.org/10.5194/gmd-8-3867-2015

Essery, R., Pomeroy, J. W., Ellis, C. R., Link, T. E. (2008a). Modelling longwave radiation to snow beneath forest canopies using hemispherical photography or linear regression. Hydrological Processes, 22(15), 2788–2800.

Essery, R., Bunting, P., Hardy, J., Link, T. E., Marks, D., Melloh, R., … Rutter, N. (2008b). Radiative Transfer Modeling of a Coniferous Canopy Characterized by Airborne Remote

Sensing. Journal of Hydrometeorology, 9(2), 228–241. Retrieved from http://journals.ametsoc.org/doi/abs/10.1175/2007JHM870.1

Fang, X., Pomeroy, J. W. (2007). Snowmelt runoff sensitivity analysis to drought on the Canadian prairies. Hydrological Processes, 21(19), 2594–2609. https://doi.org/10.1002/hyp

Goudriaan, J. (1977). Crop micrometeorology: a simulation study. PhD Thesis. Agricultural University, Wageningen, Netherlands.

Granger, R. J., Male, D. H. (1978). Melting of a prairie snowpack. Journal of Applied Meteorology, 17, 1833–1842.

Gray, D. M., Landine, P. G. (1987). Development and Performance Evaluation of an Energy Budget Snowmelt Model. Division of Hydrology, University of Saskatchewan, Saskatoon, Saskatchewan.

Gray, D. M., Male, D. H. (1981). Handbook of Snow: Principles, Processes, Management, and Use. Toronto, Canada: Pergamon Press.

Harder, P., Pomeroy, J. W. (2013). Estimating precipitation phase using a psychrometric energy balance method. Hydrological Processes. https://doi.org/10.1002/hyp

Hasselman, B. (2017). Solve Systems of Nonlinear Equations: "nleqslv." Retrieved from https://cran.r-project.org/web/packages/nleqslv/nleqslv.pdf

Helgason, W. D., Pomeroy, J. W. (2012a). Characteristics of the Near-Surface Boundary Layer within a Mountain Valley during Winter. Journal of Applied Meteorology and Climatology, 51(3), 583–597. https://doi.org/10.1175/JAMC-D-11-058.1

Helgason, W. D., Pomeroy, J. W. (2012b). Problems Closing the Energy Balance over a Homogeneous Snow Cover during Midwinter. Journal of Hydrometeorology, 13, 557–572.

Juul, N. H. (1982). View factors in radiation between two parallel oriented cylinders of finite length. Journal of Heat Transfer, 104(2), 384–388.

Legates, D. R., McCabe, G. J. (2005). Evaluating the Use of "Goodness of Fit" Measures in Hydrologic and Hydroclimatic Model Validation. Water Resources Research, 35(1), 233–241. https://doi.org/10.1029/1998WR900018

Leroux, N., Pomeroy, J. W. (2017). Modelling capillary hysteresis effects on preferential flow through melting and cold layered snowpacks. Advances in Water Resources, 107, 250–264. https://doi.org/10.1016/j.advwatres.2017.06.024

Liston, G. E., Hiemstra, C. (2011). Representing Grass– and Shrub–Snow–Atmosphere Interactions in Climate System Models. Journal of Climate, 24(8), 2061–2079. https://doi.org/10.1175/2010JCLI4028.1

Mahat, V., Tarboton, D. G., Molotch, N. P. (2013). Testing above- and below-canopy representations of turbulent fluxes in an energy balance snowmelt model. Water Resources Research, 49(2). https://doi.org/10.1002/wrcr.20073

Mahat, V., Tarboton, D. G. (2012). Canopy radiation transmission for an energy balance snowmelt model. Water Resources Research, 48(1), 1–16. https://doi.org/10.1029/2011WR010438

Marks, D., Reba, M., Pomeroy, J. W., Link, T. E., Winstral, A., Flerchinger, G. N., … Elder, K. (2008). Comparing Simulated and Measured Sensible and Latent Heat Fluxes over Snow under a Pine Canopy to Improve an Energy Balance Snowmelt Model. Journal of Hydrometeorology, 9(6), 1506–1522. https://doi.org/10.1175/2008JHM874.1

Marks, D., Kimball, J., Tingey, D., Link, T. E. (1998). The sensitivity of snowmelt processes to climate conditions and forest cover during rain-on-snow : a case study of the 1996 Pacific Northwest Flood. Hydrological Processes, 12, 1569–1587.

Marsh, P., Woo, M. -K. (1984). Wetting front advance and freezing of meltwater within a snow cover: 1. Observations in the Canadian Arctic. Water Resources Research, 20(12), 1853–1864. https://doi.org/10.1029/WR020i012p01853

Mauder, M., Foken, T. (2006). Impact of post-field data processing on eddy covariance flux estimates and energy balance closure. Meteorologische Zeitschrift, 15, 597–609. https://doi.org/10.1127/0941-2948/2006/0167

Ménard, C., Essery, R., Pomeroy, J. W. (2014). Modelled sensitivity of the snow regime to topography, shrub fraction and shrub height. Hydrology and Earth System Sciences, 11(6), 2375–2392. https://doi.org/10.5194/hessd-11-223-2014

Muniz, P. R., de Araújo Kalid, R., Cani, S. P. N., da Silva Magalhães, R. (2014). Handy method to estimate uncertainty of temperature measurement by infrared thermography. Optical Engineering, 53(7), 74101. https://doi.org/10.1117/1.OE.53.7.074101

Musselman, K. N., Molotch, N. P., Margulis, S. Kirchner, P. B., Bales, R. C. (2012). Influence of canopy structure and direct beam solar irradiance on snowmelt rates in a mixed conifer forest. Agricultural and Forest Meteorology, 161, 46–56. https://doi.org/10.1016/j.agrformet.2012.03.011

Musselman, K. N., Pomeroy, J. W., Link, T. E. (2015). Variability in shortwave irradiance caused by forest gaps: Measurements, modelling, and implications for snow energetics. Agricultural and Forest Meteorology, 207, 69–82. https://doi.org/10.1016/j.agrformet.2015.03.014

Musselman, K. N., Pomeroy, J. W. (2016). Estimation of needle-leaf canopy and trunk temperatures and longwave contribution to melting snow. Journal of Hydrometeorology. https://doi.org/10.1175/JHM-D-16-0111.1

Norman, J. M., Kustas, W. P., Humes, K. S. (1995). Source approach for estimating soil and vegetation energy fluxes in observations of directional radiometric surface temperature. Agricultural and Forest Meteorology, 77(95).

Monteith, J.L., Unsworth, M.H. (2008). *Principles of Environmental Physics*. 3rd ed. New York: Elsevier Inc.

Pomeroy, J. W., Brun, E. (2001). Physical Properties of Snow. In H. G. Jones, J. W. Pomeroy, D. A. Walker, and R. W. Hoham (Eds.), Snow Ecology: an Interdisciplinary Examination of Snow-covered Ecosystems (pp. 45–118). Cambridge University Press.

Pomeroy, J. W., Dion, K. (1996). Winter irradiance extinction and reflection in a boreal pine canopy: measurements and modelling. Hydrological Processes, 10(12), 1591–1608.

Pomeroy, J. W., Rowlands, A., Hardy, J., Link, T. E., Marks, D., Essery, R., … Ellis, C. R. (2008). Spatial Variability of Shortwave Irradiance for Snowmelt in Forests. Journal of Hydrometeorology, 9(6), 1482.

Pomeroy, J. W., Goodison, B. E. (1997). Winter and Snow. In W. G. Bailey, .R. Oke, and W. R. Rouse (Eds.), The Surface Climates of Canada (pp. 68–100). Montreal: McGill-Queen's Univ Press.

Pomeroy, J. W., Marks, D., Link, T. E., Ellis, C. R., Hardy, J., Rowlands, A., Granger, R. J. (2009). The impact of coniferous forest temperature on incoming longwave radiation to melting snow. Hydrological Processes, 23(17), 2513–2525.

Pomeroy, J. W., Gray, D. M. (1995). Snow accumulation, relocation and management. Saskatoon, SK: Science Report No. 7, National Hydrology Research Institute, Environment Canada.

Pomeroy, J. W., Essery, R., Helgason, W. D. (2016). Aerodynamic and Radiative Controls on the Snow Surface Temperature. Journal of Hydrometeorology, 2175–2189. https://doi.org/10.1175/JHM-D-15-0226.1

Pomeroy, J. W., Gray, D. M., Hedstrom, N. R., Janowicz, J. R. (2002). Prediction of seasonal snow accumulation in cold climate forests. Hydrological Processes, 16(18), 3543–3558. https://doi.org/10.1002/hyp.1228

Prueger, J. H., Kustas, W. P. (2005). Aerodynamic Methods for Estimating Turbulent Fluxes. Agronomy, 47, 407–436.

Reid, T. D., Essery, R., Rutter, N., King, M. (2013). Data-driven modelling of shortwave radiation transfer to snow through boreal birch and conifer canopies. Hydrological Processes, 15. https://doi.org/10.1002/hyp.9849

Reindl, D. T., Beckman, W. A., Duffle, J. A. (1990). Diffuse Fraction Correlations. Solar Energy, 45(1), 1–7. https://doi.org/10.1016/0038-092X(90)90060-P

Shaw, R. H., Pereira, A. R. (1982). Aerodynamic roughness of a plant canopy: A numerical experiment. Agricultural Meteorology, 26, 51–65.

Shea, C., Jamieson, B. (2011). Some fundamentals of handheld snow surface thermography. Cryosphere, 5(1), 55–66. https://doi.org/10.5194/tc-5-55-2011

Sicart, J. E., Pomeroy, J. W., Essery, R., Bewley, D. S. (2006). Incoming longwave radiation to melting snow: observations, sensitivity and estimation in northern environments. Hydrological Processes, 20(17), 3697–3708.

Sicart, J. E., Pomeroy, J. W., Essery, R., Hardy, J. (2003). Snowmelt in a Canadian Spruce Forest : A Sensitivity Study to the Canopy Cover. In 60th Eastern Snow Conference (pp. 99–110). Sherbrooke, Quebec.

Smith, C. D. (2009). The relationship between snowfall catch efficiency and wind speed for the Geonor T-200B precipitation gauge utilizing various wind shield configurations. In 77th Western Snow Conference (p. 6). Saskatoon, SK.

Sparrow, E., Miller, G., Jonsson, V. (1962). Radiative effectiveness of annular- finned space radiators, including mutual irradiation between radiator elements. Journal of Aerospace Research, 29(11), 1291–1299.

Statistics Canada. (2016). Census of Agriculture, tillage practices used to prepare land for seeding, every 5 years. Retrieved May 12, 2017, from http://www5.statcan.gc.ca/cansim/a03?lang=engandsearchMode=regularSearchandpattern=004-0200..004-0246andtypeValue=-1andsrchLan=-1andp2=31

Sutherland, W. (1893). The viscosity of gases and molecular force. Philosophical Magazine, 5(36), 507–531.

Verseghy, D. L. (1991). Class-A Canadian land surface scheme for GCMS. I, Soil model. International Journal of Climatology, 11, 111–133.

Wallace, S. (1991). Lagrangian and K-theory approaches in modelling evaporation from sparse canopies, 1325–1340.

Wang, Y. P. (2003). A comparison of three different canopy radiation models commonly used in plant modelling. Functional Plant Biology, 30(2), 143–152. https://doi.org/10.1071/FP02117

Webster, C., Rutter, N., Zahner, F., Jonas, T. (2016). Modeling subcanopy incoming longwave radiation to seasonal snow using air and tree trunk temperatures. Journal of Geophysical Research: Atmospheres, 121(3), 1220–1235. https://doi.org/10.1002/2015JD024099

Welles, J. M., Cohen, S. (1996). Canopy structure measurement by gap fraction analysis using commercial instrumentation. Journal of Experimental Botany, 47(302), 1335–1342. https://doi.org/10.1093/jxb/47.9.1335

Chapter 5: A simple model for local scale sensible and latent heat advection contributions to snowmelt

Status: Submitted to Hydrology and Earth System Science Discussions special issue on Understanding and predicting Earth system and hydrological change in cold regions special issue, February 22, 2018

Citation: Harder, P., Helgason, W., Pomeroy, J. W. (2018). A simple model for local scale sensible and latent heat advection contributions to snowmelt. Hydrol. Earth Syst. Sci. Discuss., in review.

Author Contributions: PH conceptualized and coded the model, performed simulations and analysis, and wrote the manuscript. JP and WH provided guidance, and reviewed and revised model formulations and the manuscript.

5.1. Abstract

Local-scale advection of energy from warm snow-free surfaces to cold snowcovered surfaces is an important component of the energy balance during snowcover depletion. Unfortunately, this process is difficult to quantify in one-dimensional snowmelt models. This manuscript proposes a simple sensible and latent heat advection model for snowmelt situations that can be readily coupled to one-dimensional energy balance snowmelt models. An existing advection parameterization was coupled to a conceptual frozen soil infiltration surface water retention model to estimate the areal average sensible and latent heat advection contributions to snowmelt. The proposed model compared well with observations of latent and sensible heat advection providing confidence in the process parameterizations and the assumptions applied. Snowcovered area observations from unmanned aerial vehicle imagery were used to update and evaluate the scaling properties of snow patch area distribution and lengths. Model dynamics and snowmelt implications were explored within an idealized modelling experiment, by coupling to a one-dimensional energy balance snowmelt model. Dry, snow-free surfaces were associated with negative latent heat advection fluxes that compensated for positive sensible heat advection fluxes

and so limited the net influence of advection on snowmelt. Latent and sensible heat advection fluxes both contributed positive fluxes to snow when snow-free surfaces were wet and enhanced net advection contributions to snowmelt. The increased net advection fluxes from wet surfaces typically develop towards the end of snowmelt and offset decreases in the one-dimensional areal average melt energy that declines with snowcovered area. The new model can be readily incorporated into existing one-dimensional snowmelt hydrology and land surface scheme models and will foster improvements in snowmelt understanding and predictions.

5.2. Introduction

Sensible and latent turbulent heat fluxes contributing to snowmelt are complicated during snowcovered area (SCA) depletion by local-scale advection, the lateral redistribution of energy from snow-free surfaces to snow. Unfortunately, many calculations of the snow surface energy balance have largely been limited to one-dimensional model frameworks (Brun et al., 1989; Gray and Landine, 1988; Jordan, 1991; Lehning et al., 1999; Marks et al., 1999) that simulate melt at points without considering variations in SCA. Despite the sophistication of these methods they have not included a comprehensive set of energy budget terms by neglecting local-scale advection of energy.

"The major obstacle to the development of an energy balance model for calculating melt quantities is the lack of reliable methods for evaluating the sensible heat flux. A priority research need is the development of "bulk methodologies" for calculating this term, especially for patchy, snow-cover conditions." (Gray et al., 1986)

In the 32 years since this statement was published there have been a variety of approaches formulated to calculate advection of energy to snowpacks. Earlier work by Weisman (1977) applied mixing length theory to estimate advection to lakes and snow patches with the model implicitly accounting for both latent heat advection (LE_A) and sensible heat advection (H_A). This work was limited to defined snow patches and was proposed when the understanding of the statistical properties of snowcover were insufficient to allow estimation of advection over the course of a melt sequence. Subsequent approaches have varied in complexity. A simple approach taken by Marsh and Pomeroy (1996) related bare ground sensible heat fluxes to areal average H_A via an advection efficiency term related to SCA. The application of internal boundary

layer integration (Essery et al., 2006; Granger et al., 2002) to tile models (Essery et al., 2006) whilst accounting for the fractal nature of snowcover (Shook et al., 1993b) has provided another approach to estimate areal average estimates of advection. More complex approaches have employed atmospheric boundary layer models (Liston, 1995) and large eddy simulation (Mott et al., 2015) to quantify the non-linear relationships between snow patch characteristics/geometry and advected energy. Numerical models provide the most detailed description of the processes but are constrained to idealized boundary conditions. The deficiency of these modelling approaches is that none have been validated with observations of advection nor do they explicitly partition advected energy into H_A or LE_A components during snowmelt. An unrepresented interaction in any model is the LE_A from ponded meltwater which is prevalent in areas of level topography and reduced snowmelt infiltration due to frozen soil (Chapter 3; Harder et al., 2017).

There remains a pressing need for an approach that can estimate areal average H_A and LE_A contributions during snowmelt that can easily integrate with existing one-dimensional snowmelt models. This work seeks to understand the implications of including local-scale H_A and LE_A with one-dimensional snowmelt models. To address this objective, this paper presents a simple and easily implementable H_A and LE_A model. Specific objectives are: to validate the proposed model with observations of advection; to reevaluate the scaling relationships of snowcover geometry with current datasets of snowcover; and to quantify the implications of including advection upon snowmelt.

5.3. Methodology

The methodology to address the research objectives is briefly outlined here. A conceptual and quantitative model framework extended the Granger et al. (2002) advection model, hereafter referred to as the extended GM2002, to also consider LE_A. The performance of the extended GM2002 was evaluated with respect to H_A and LE_A observations as reported in Chapter 3. Snowcover geometry scaling relationships employed in the model framework (Granger et al., 2002; Shook et al., 1993a), originally based on SCA classifications from coarse resolution or oblique imagery, were re-evaluated with high resolution unmanned aerial vehicle (UAV) imagery. The complete model framework, hereafter referred to as the Sensible and Latent Heat Advection Model (SLHAM), was then used to explore the dynamics of the extended GM2002 when coupled with frozen soil infiltration and surface detention storage-fractional water area

parameterizations. Snowmelt simulation performance and implications of including H_A and LE_A were explored with coupling of SLHAM to the Stubble-Snow-Atmosphere snowmelt Model (SSAM) developed in Chapter 4. The model performance of SSAM and SSAM-SLHAM was also compared against the Energy Balance Snowmelt Model (Gray and Landine, 1988); a snowmelt model commonly implemented for snowmelt prediction on the Canadian Prairies. The implications of including advection were evaluated with initial conditions and driving meteorology observed over two snowmelt seasons from a research site located in the Canadian Prairies.

5.3.1. Model framework

Advection is the transfer of heat and mass by the flow of a fluid. In the case of heterogenous snowcover wind will drive the lateral transfer of heat and water vapour from the movement of air from upwind snow-free surfaces to downwind snow surfaces; this is shown conceptually in Figure 5.1a. The upwind snow-free surface is comprised of dry soil and/or ponded water which correspond to warm dry and/or warm moist near surface air properties, respectively, relative to snow which is ≤ 0 °C with saturated near surface air. These horizontal gradients drive a lateral exchange of heat (sensible heat advection) and water vapour (latent heat advection when considering the induced condensation or sublimation) over the leading edge of a snowpack as the scalar profiles transition from the upwind equilibrium profiles to the downwind equilibrium profiles. Examples of air temperature and specific humidity profiles over snow, soil, and water surfaces are shown in Figure 5.1b to articulate the conceptual model of advection and reflect dynamics directly observed in Chapter 3. The integrated differences in profiles between the surface and the mixing height, the point above the surface where no differences due the spatial heterogeneity are evident due to atmospheric mixing, quantify the magnitude and direction of the energy flux. During melt, snow is constrained to be ≤ 0 °C the warm air (above water or soil in Figure 5.1b) will cool as the air moves over snow leading to sensible heat advection to the snowpack. Latent heat advection is dependent upon surface temperature as well as saturation. Thus, air over a dry soil increases in humidity as it moves over snow, this induces greater sublimation and therefore a reduction in snowmelt energy. In contrast the profile above a water surface will decrease in humidity and will induce condensation upon the snow surface, which imparts a release of latent heat or an increase in snowmelt energy. The main challenges in

modelling these dynamics is to constrain the areal extent over which the advection exchange takes place, quantify the gradients in scalar between upwind and downwind surfaces, and relate the scalar gradients to advection fluxes.

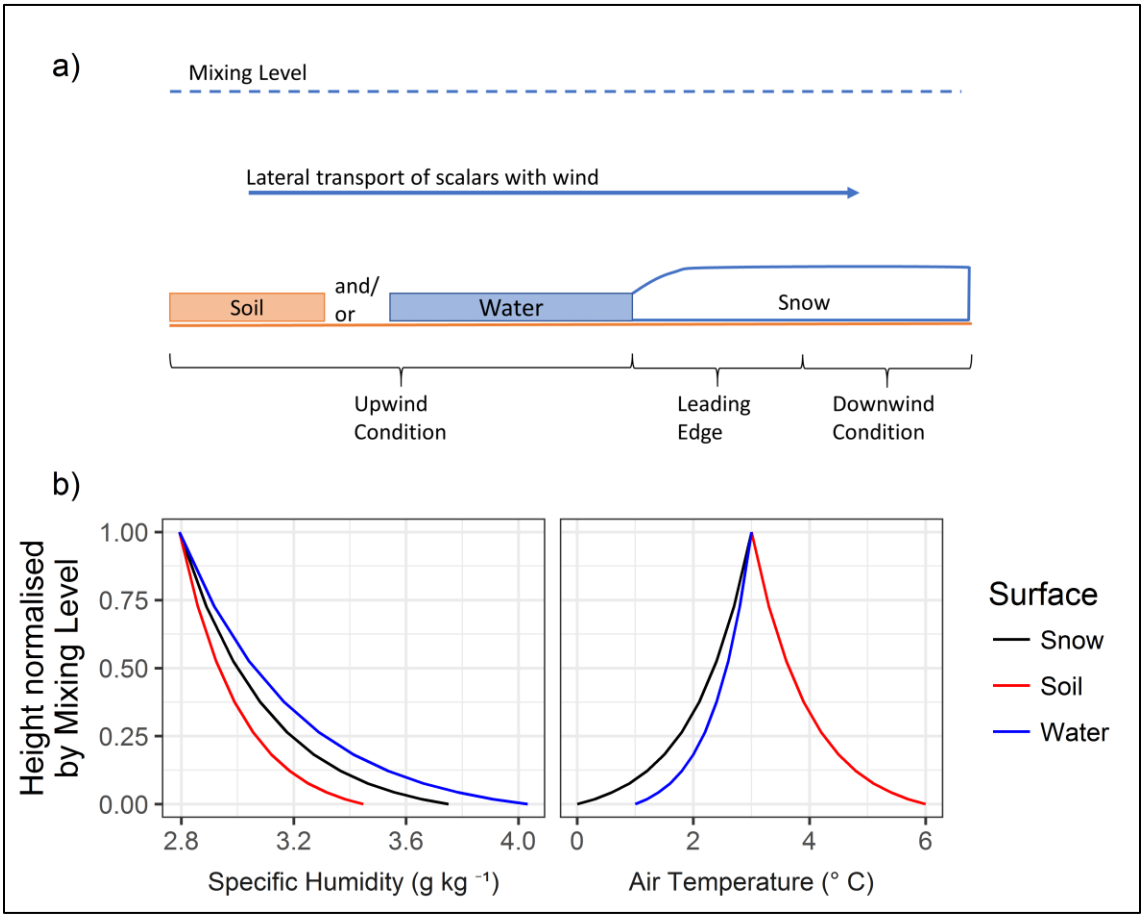

Figure 5.1: a) Conceptual cross section of the advection process during snowmelt and b) conceptual specific humidity and air temperature profiles between snow (0 °C, 100% RH), soil (6 °C, 60% RH) and water (1 °C, 100% RH) surfaces and the mixing height (3 °C, RH of 60%).

Over the course of melt, SCA declines from completely snowcovered to snow-free conditions with the intermediate periods defined by a heterogeneous blend of both. Conceptually the advection of energy to snow therefore is bounded by the areas of snow-free and snowcovered surfaces that constrain energy transfer. Initial melt is dominated by energy advecting from emerging snow-free patches to the surrounding snow (Figure 5.2a). The total amount of energy advected will be limited by the smaller snow-free surface source area available to exchange energy; all energy entrained by air movement across isolated snow-free patches will be completely advected to the surrounding snow surfaces. At the end of snowmelt snow patches

remain in a snow-free domain, and some energy is advected from the warm surrounding snow-free surface to isolated snow patches (Figure 5.2b). The amount of energy advected is limited by the smaller snow surface area available to exchange energy. When the snow surface is the most heterogeneous with a complex mixture of snow and snow-free patches advection occurs between isolated snow-free patches, surrounding snowcover, snow-free surfaces, and isolated snow patches at the same time. Conceptually there will be gradual transitions from isolated snow-free patch to isolated snow patch advection constraints. Marsh and Pomeroy (1996) and Shook et al. (1993b) found that magnitude of the snowmelt advection flux will be greatest when SCA is 40-60% and this range was used to bound the transition of advection constraints. The advection mechanism transitions over the course of the melt and was conceptually related to SCA by a fractional source (f_s) term that assumes a linear weighting between 60% and 40 % SCA as

$$f_s = \begin{cases} 1 & SCA > 0.6 \\ \left(\dfrac{SCA - 0.4}{0.2}\right) & 0.4 \leq SCA \leq 0.6 \\ 0 & SCA < 0.4 \end{cases} \quad (5.1)$$

A f_s of 1 implies the exchange of advection energy is limited by the snow-free patch areas and a f_s of 0 implies the exchange of advection energy is limited by the snow patch areas. Conceptually early advection from snow-free patches will have a more effective energy exchange mechanism than later advection to isolated snow-patches. The unstable temperature profile above a relatively rough warm snow-free surface patch will enhance exchange with the atmosphere, and therefore surrounding snowcover, per unit area of snow-free surface. In contrast, the stable temperature profiles above a cool and smooth isolated snow patch will limit energy exchange per unit area of snow surface.

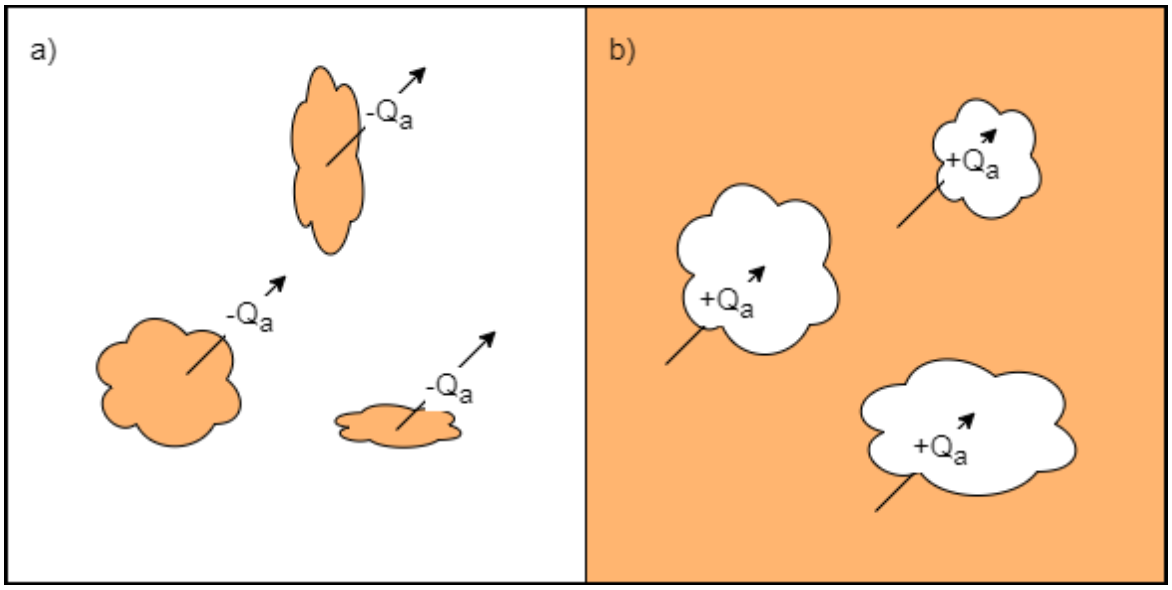

Figure 5.2: Conceptual model of advection dynamics for a) the early melt period where energy is limited to what is transported out of soil (brown) patches to the surrounding snow (white), and for b) the later melt period where snow patches remain and advection energy is limited to that exchanged over the discrete patches.

During snowmelt, meltwater may infiltrate into the frozen soil and any excess will pond prior to and during the runoff phase; these interactions will influence the near surface humidity of the snow-free surface. Thus LE_A may enhance sublimation when the upwind surface is dry or condense and enhance melt when the upwind surface is wet (Chapter 3). Any attempt to model advection must quantify the dynamic spatial properties of the snow and snow-free patch distributions, SCA, fractional water coverage of ponded water, and horizontal gradients of temperature and humidity between snow and snow-free surfaces. With quantification of these processes, existing simple advection parametrizations can be extended to calculate H_A and LE_A contributions to snowmelt in a manner that accounts for the dynamics of the driving variables and processes and still be easily implemented in snowmelt energy balance models. The SLHAM model quantifies the components of the conceptual model outlined in Fig. 5.2.

5.3.1.1. Advection versus distance from surface transition

Granger et al. (2002) developed a simplified approach to estimate the advection over a surface transition from boundary layer integration. Advected energy, Q_A (W m^{-2}), was presented as a power function of patch length, L (m) downwind of a surface transition as

$$Q_A(L) = aL^b. \quad (5.2)$$

The coefficient a (-) scales with wind speed and the horizontal scalar gradient and the coefficient b (-) is a function of the Weisman (1977) stability parameters (W). Parametrizations for these coefficients vary for sensible (H_A) and latent (LE_A) heat advection and whether advection is from a snow-free patch or to a snow patch; parametrizations are summarized in Table 5.1. The GM2002 approach is restricted to considering H_A contributions to snow. To extend this approach to LE_A the a and b parameterizations of GM2002 were assumed to remain valid. The parameterization for coefficient a in the case of LE_A was modified to use the surface vapour pressure gradient (kPa) with division by the psychrometric constant (γ [kPa K^{-1}]). This relates the horizontal water vapour gradient to be in terms of an equivalent temperature gradient; in the units of the original a parametrization. The coefficient b for LE_A uses the humidity stability parameter of Weisman (1977) rather than the temperature stability parameter.

Table 5.1: Parameterizations for extended GM2002

Variable	Sensible Heat Advection (H_A)		Latent Heat Advection (LE_A)	
	From Snow-Free patches	To Snow Patches	From Snow-Free patches	To Snow Patches
a	$-31.7u(T_{sc} - T_{sf})$	$31.7u(T_{sf} - T_{sc})$	$-\frac{31.7}{\gamma}u(e_{sc} - e_{sf})$	$\frac{31.7}{\gamma}u(e_{sf} - e_{sc})$
b	$-0.09 + 31.84W$	$-0.47 - 7.1W$	$-0.09 + 31.84W$	$-0.47 - 7.1W$
W	$-\frac{\kappa g z_{0s}}{u^{*2}}\frac{(T_{sf} - T_{sc})}{T_{sc}}$	$-\frac{\kappa g z_{0s}}{u^{*2}}\frac{(T_{sc} - T_{sf})}{T_{sf}}$	$-0.61\frac{\kappa g z_{0s}}{u^{*2}}(q_{sf} - q_{sc})$	$-0.61\frac{\kappa g z_{0s}}{u^{*2}}(q_{sc} - q_{sf})$

e_{sc} = snow surface vapor pressure (kPa)
e_{sf} = snow-free surface vapor pressure (kPa)
g = acceleration due to gravity (9.81 m s^{-2})
κ = von karman constant (0.4)
q_{sc} = snow surface specific humidity (kg kg^{-1})
q_{sf} = snow-free surface specific humidity (kg kg^{-1})
T_{sc} = snow surface temperature (K)
T_{sf} = snow-free surface temperature (K)
u = wind speed (m s^{-1})
u^* = friction velocity (m s^{-1})
z_{0s} = snow surface roughness (0.005 m)
γ = psychrometric constant (kPa K^{-1})

Surface humidity is rarely observed but is needed to quantify the LE_A term. The e_{sc} was estimated by assuming saturation at the T_{sc}. The e_{sf} is more challenging as it varies with the surface fraction of ponded water (F_{water} [-]) as

$$e_{sf} = F_{water}e_{wat} + (1 - F_{water})e_{soil}. \quad (5.3)$$

The surface water vapor for water surfaces (e_{wat} [kPa]) was estimated by assuming saturation at the surface temperature of the ponded water (T_{wat} [K]). Assuming negligible evaporation from dry soil surfaces during snowmelt, the surface water vapor of soil (e_{soil} [kPa]) can be taken to be the same as actual vapour pressure observed above the surface. The T_{sf} was also weighted by F_{water} as,

$$T_{sf} = F_{water}T_{wat} + (1 - F_{water})T_{soil}, \tag{5.4}$$

where T_{soil} (K) is the dry soil surface temperature. The remaining uncertainties in applying this framework are the representation of the statistical distribution of L, and estimation of F_{water} and SCA.

5.3.1.2. Fractional coverage of ponded water

To estimate F_{water}, the meltwater in excess of frozen soil infiltration capacity was estimated using the parametric frozen soil infiltration equation of Gray et al. (2001). Gray et al. parameterized the maximum infiltration of the limited condition (INF [mm]) as,

$$INF = CS_0^{2.92}(1 - S_I)^{1.64}\left(\frac{273.15 - T_{si}}{273.15}\right)^{-0.45} t_0^{0.44}, \tag{5.5}$$

where C (2.1 [-]) is a coefficient representing prairie soils, S_0 (-) is a surface saturation (generally assumed to be 1), S_i (-) is the antecedent soil saturation, T_{si} (K) is the initial soil temperature, and t_0 (hours) is the infiltration opportunity time. The t_0 term is estimated as the cumulative hours of active snowmelt over the course of the snowmelt period. Excess meltwater (M_{excess} [mm]) is calculated as

$$M_{excess} = \sum_{t=0}^{i} M_t - INF_i \tag{5.6}$$

where M (mm) is the snowmelt since the beginning of melt ($t = 0$) to the present time step i.

To relate $M_{excess}$to a F_{water} , an elevation profile of the microtopography must be known. For simplicity, the furrows that define the microtopography of an agricultural field were

assumed to be represented by a half period, trough to peak, of a sine curve (Figure 5.3). Thus F_{water} is given by the solution of

$$S_{ret} = \frac{1}{\pi} sin(F_{water}\pi) - F_{water} cos(F_{water}\pi) + \ , \tag{5.7}$$

where the ratio of filled detention storage (S_{ret} [-]) is determined from

$$S_{ret} = \frac{M_{excess}}{S_{max}} \tag{5.8}$$

where a user-defined S_{max} (mm) is the maximum detention storage of the surface. Any M_{excess} that is greater than S_{max} is removed as runoff and thereafter unavailable to future infiltration.

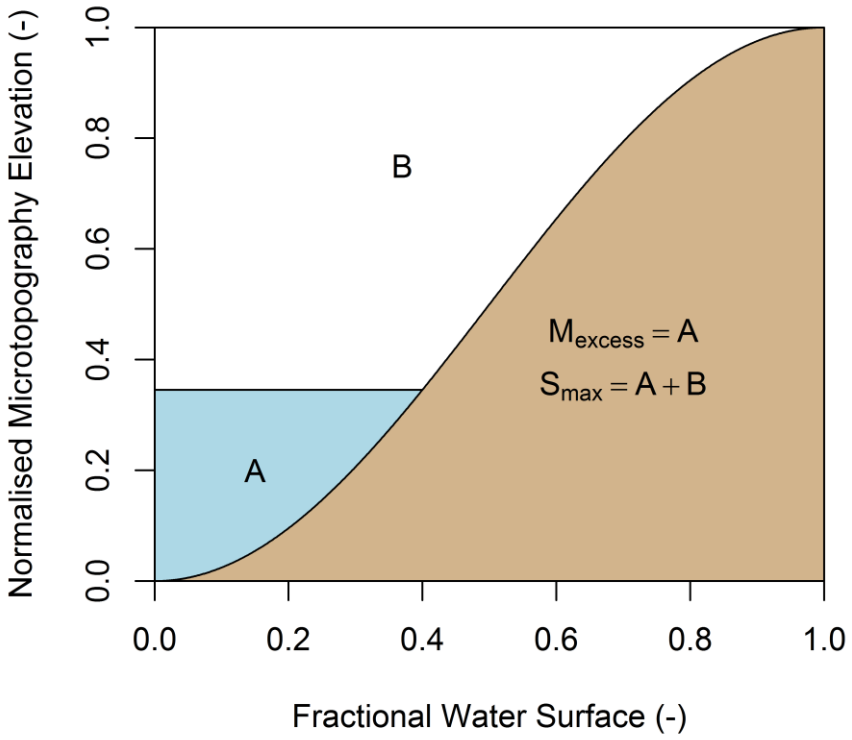

Figure 5.3: Conceptual water-area volume relationship diagram where a cross section of land surface microtopography (brown is soil and blue is water) is assumed to follow a sinusoidal profile.

5.3.1.3. Snowcovered Area

The SCA constrains the overall exchange of energy between the snow surface and the atmosphere. Snow depth and SWE distributions are log-normal and Essery and Pomeroy (2004) took advantage of this to develop a SCA parameterization as,

$$SCA = \tanh\left(1.26\frac{SWE}{\sigma_0}\right), \tag{5.9}$$

where SWE is in mm and σ_0 (mm) is the standard deviation of SWE at the pre-melt maximum accumulation. Other parameterizations of SCA exist and this was selected for its simplicity, relative success in describing observed SCA curves and derivation in similar environments as to what is being modelled.

5.3.1.4. Snow Geometry

Perimeter-area relationships and patch area distributions of snow and snow-free patches show fractal characteristics that can be exploited to simplify the representation of snowcover geometry needed to calculate advection. There are two commonly used scaling relationships. From application of Korcak's law by Shook et al. (1993a) the fraction of snow patches greater than a given area, $F(A_p)$, is given as a power law distribution

$$F(A_p) = \frac{\mathrm{A_p}^{-D_k/2}}{c_1}, \tag{5.10}$$

where c_1 is a threshold value (given as the smallest patch size observed, and hereafter taken as 1 m^2), A_p (m^2) is patch area, and D_k (-) is the scaling dimension. The scaling dimension is the same between snow and snow-free patches, relatively invariant with time, and ranges between 1.2 and 1.6 (Shook et al., 1993a) and is not a fractal dimension (Imre and Novotn, 2016). A relationship between A_p and L was established by Granger et al. (2002) with application of Hacks' law where

$$L = c_2 \cdot A_p^{\frac{D'}{2}} \tag{5.11}$$

where c_2 is a constant taken as 1 and D' was fitted by Granger et al. (2002) to be 1.25.

The relationships of Equations 5.10 and 5.11 were exploited to develop a probability distribution of L. The exceedance fraction (Equation 5.10) was converted to a probability distribution with calculation of probabilities for discrete intervals; this also entailed appropriate selection of intervals. The patch area probability ($p(A_{pi})$) is also equivalent to the probability associated with the probability of patch length ($p(L_i)$), therefore

$$p(L_i) = p(A_{pi}) = F(A_{pi-1}) - F(A_{pi}) \tag{5.12}$$

where i is the index for intervals of A_p that span a range constrained as $c_1 \leq A_p < \infty$. A discrete bin width of ≤ 1 m is advised to capture the large change in $F(A_p)$ at the more frequent small values of A_p. To estimate an areal average advection exchange the normalized areal extent of each patch size was calculated. The limited number of the largest patches will dominate the exchange surface extent. Thus $p(A_{pi})$ is transformed to give a normalized areal fraction of the unit area that is represented by each patch size $f(A_{pi})$ as,

$$f(A_{pi}) = \frac{p(A_{pi})A_{pi}}{\sum p(A_{pi})A_{pi}}. \tag{5.13}$$

The transformation of the probability of occurrence to a fractional area of patch size is visualized in Figure 5.4.

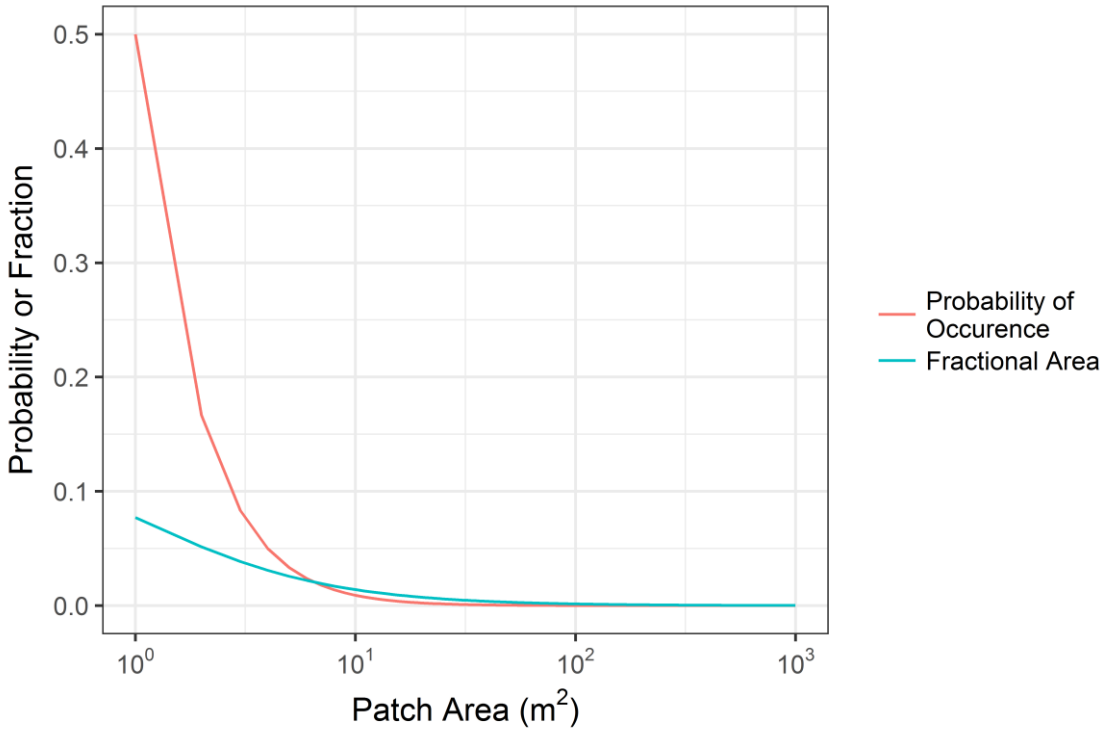

Figure 5.4: Probability of patch size occurrence and its transformation to fractional area patch sizes for a range in patch sizes from 1 m^2 to 1000 m^2.

5.3.1.5. Areal Average Advection

Using the above-described parameterizations of $f(A_{pi})$, L, SCA, F_{water} and INF, and boundary layer integration H_A and LE_A parameterizations, the areal average advection, $\overline{Q_A}$ (W), can be calculated as,

$$\overline{Q_A} = f_s(1-SCA)\sum_{i=1}^{i=A_{max}} f(A_{pi})H_{A,sf} + (1-f_s)SCA\sum_{i=1}^{i=A_{max}} f(A_{pi})H_{A,sc} + f_s(1-SCA)\sum_{i=1}^{i=A_{max}} f(A_{pi})LE_{A,sf} + (1-f_s)SCA\sum_{i=1}^{i=A_{max}} f(A_{pi})LE_{A,sc} \quad (5.14)$$

The terms, from left to right represent the H_A from snow-free patches, H_A to snow patches, LE_A from snow-free patches, and LE_A to snow patches. All summation terms constitute H_A and LE_A for the range of patch areas expected, from 1 m^2 to an environment appropriate

maximum expected patch size (A_{max} [m^2]). Calculation of H_A and LE_A use Equation 5.2 with application of appropriate a and b parameterizations from Table 5.1 and L as calculated with Equation 5.10 from the range of A_p. Advection fluxes for the range of patch sizes encountered are weighted by $f(A_{pi})$, Equation 5.13, to give an areal average maximum flux. The advection process must be constrained to snow-free or snow surfaces over which exchange takes place hence the scaling of the maximum advection by $(1 - SCA)$ and SCA from snow-free patches and to snow patches respectively. The f_s and $(1 - f_s)$ terms quantify the relative contribution from snow-free patches and to snow patches over snowmelt and SCA depletion. The primary controls on the model behaviour are the horizontal gradients of humidity and temperature, and wind speed.

5.3.2. Re-evaluation of Snow-Geometry Scaling relationships

The coefficients for the snowcover geometry relationships are based on oblique terrestrial photography or aerial photography with coarse resolution and limited temporal sampling (Shook et al., 1993a). Recent advances in UAV technologies provide a tool to re-evaluate these relationships with georectified high resolution imagery. During the 2015 and 2016 snowmelt seasons, 0.035 m x 0.035 m spatial resolution red-green-blue (RGB) imagery was collected daily during active melt. This imagery was classified into snow and non-snow areas with pixel-based supervised thresholding of blue band reflectance. Cells that share the same classification and were connected via any of the four mutually adjacent cell boundaries were grouped into snow and non-snow patches. The SDMTools R package (VanDerWal et al., 2014) was used to calculate patch areas. Patch length is a challenging to define and quantify. For this analysis a similar approach to Granger et al. (2002) was used in which the patch length was calculated as the mean of the height and width of the minimum rotated bounding box that contained the entire snow patch. Patches with areas less than 1 m^2 were removed from the analysis as noise and classification artifacts are associated with such small patch sizes. The 1 m^2 area threshold is consistent with the existing literature on advection and snowcover geometry (Granger et al., 2002; Shook et al., 1993a, 1993b). When SCA was less than 50%, snow patch metrics were quantified and when SCA was greater than 50%, snow-free patch metrics were quantified.

5.3.3. Model Dynamics

The influence of the advection model upon snowmelt dynamics was explored with two approaches. The first approach is a scenario analysis where inputs are fixed and a selection of process parameterizations are employed to illustrate the relationship between H_A and LE_A and the snow-free surface humidity dynamics and snowmelt implications. The second approach coupled the SLHAM with an existing one-dimensional snowmelt model to estimate the influence of including or not including the advection process on snowmelt simulations.

5.3.3.1. Scenario Analysis

To explore the dynamics of modelled advection contributions several scenarios were implemented with the model. The first scenario (No Advection) constitutes a baseline for typical one-dimensional model that assumes no advection, the second (Dry Surface) includes advection from a warm dry surface, the third (Wet Surface) includes advection from a warm wet surface, and the fourth (Dry to Wet Surface) includes advection from a warm surface that transitions from dry to wet as a function of the INF-S_{ret}-F_{water} relationships. To understand the implications upon snowmelt for each scenario, input variables were held constant and the model was run until an assumed isothermal snowpack was fully depleted. A constant melt energy, Q_{net} (W m^{-2}), was applied which represents the net snow surface energy balance as estimated via typical one-dimensional model. The initialized SWE was ablated, leading to infiltration excess, detention-storage, runoff, or sublimation. The relative dynamics of the various scenarios are sensitive to the inputs/parameters used, as summarized in Table 5.2, and demonstrate the relationships between H_A and LE_A and the snow-free surface humidity conceptualization and snowmelt implications from a theoretical perspective.

The sensitivity of SLHAM to T_{wat} is also explored to understand the implications upon SWE and SCA depletion, F_{water}, H_A, LE_A and net advection. The Dry to Wet Surface scenario, using the input variables from Table 4.2, was employed to understand the dynamics of T_{wat} variability. A common assumption is that T_{wat} is 0 °C as meltwater immediately after discharge from an isothermal snowpack is 0 °C and underlying frozen soils are ≤ 0 °C. Unlike the snow surface the maximum temperature of ponded water is unconstrained by phase change so values ≥0 °C are expected because of possible low water surface albedos and high shortwave radiation

($SW_{atm}^{\downarrow}$) during the daytime. Analysis of available thermal images from a FLIR T650 thermal camera was used to correct for atmosphere conditions and water surface emissivity. This analysis showed that daytime T_{wat} was generally >0 °C and < 2°C. This range in T_{wat} was used to test the sensitivity of the T_{wat} upon SLHAM dynamics. Intermittency of observations and inherent uncertainties in thermography prevented a more precise estimation of T_{wat}.

Table 5.2: Input variables for scenario analysis of SHLAM dynamics

Variable	Units	Values
T_a	°C	2
T_{soil}	°C	4
T_{sc}	°C	0
T_{wat}	°C	0.5
u	m s^{-1}	4
RH	%	70
Q_{net}	W m^{-2}	15
S_{max}	Mm	10
SI	-	0.5
SWE	Mm	100
σ_0	Mm	25

5.3.3.2. Coupled Advection and Snow-Stubble-Atmosphere snowmelt Model simulations

Conditions controlling advection processes are not constant over snowmelt therefore SLHAM was coupled with a one-dimensional snowmelt model (SSAM) to estimate the role of advection contributions over a snowmelt season. Briefly, SSAM describes the relationships between shortwave, longwave and turbulent exchanges between a snow surface underlying exposed crop stubble and the atmosphere. The surface energy balance was coupled to a single layer snow model to estimate snowmelt. A slight modification of SSAM, or any one-dimensional model that computes areal average snowmelt, is needed to include advection. The energy terms of one-dimensional energy balance models are represented as flux densities (W m^{-2}) over an assumed continuous snowcover and therefore need to be weighted by a SCA parametrization (Equation 5.12) to properly simulate the areal average melt energy available to the fraction of the surface comprised of snow. The SSAM was run with and without SLHAM to explore the impact of advection simulation on SWE. Simulation performance was quantified via root mean square error (RMSE) and model bias (MB) of the simulation SWE versus snow survey SWE

observations. The relative contribution of advection was quantified through estimation of the energy contribution to total snowmelt. A commonly used snowmelt model, the Energy Balance Snowmelt Model (EBSM) of Gray and Landine (1988), was also run to benchmark performance. The EBSM has had wide application in this region and simulation is deployed as an option within the Cold Region Hydrological Modelling (CRHM) platform (Pomeroy et al., 2007). In EBSM the contribution of advection energy is indirectly addressed through simulation of an areal average albedo that varies from a maximum of 0.8 pre-melt, a continuous snow surface, to approach a low of 0.2 at the end of melt, which represents bare soil rather than old snow (Gray and Landine, 1987a). The areal average net radiation, greater than typically received by a continuous snow surface, is assumed to contribute to areal average snowmelt thereby implicitly accounting for advection. While a simple approach to include advection energy for snowmelt, it is unconstrained by SCA dynamics and will overestimate melt for low values of SCA.

The SSAM, SSAM-SLHAM and EBSM simulations were driven by common observed meteorological data, parameters and initial conditions obtained from intensive field campaigns at a research site near Rosthern, Saskatchewan, Canada (52.69 °N, 106.45 °W). The data for the 2015 and 2016 snowmelt seasons reflect relatively flat agricultural fields characterized by standing wheat stubble, 15 cm and 24 cm stubble heights, for the respective years. Observations of T_{soil} required for SLHAM come from infrared radiometers (Apogee SI-111) deployed on mobile tripods to snow-free patches. Unfortunately, no time series of T_{wat} observations are available and values or models to describe T_{wat} for shallow ponded meltwater in a prairie environment have not been discussed in the literature. Like snowpack refreezing, ponded meltwater can also refreeze at night as heat capacity of this shallow water is limited. In this framework, as observations or models of T_{wat} are unavailable, a simple physically guided representation of T_{wat} takes the form of,

$$T_{wat} = \begin{matrix} T_{sc} & T_{sc} < 0\ °C \\ 0.5\ °C & T_{sc} = 0\ °C \end{matrix}. \quad (5.15)$$

For a full description of the field site and data collection methodologies see Chapter 4.

5.4. Results and Discussion

5.4.1. Performance of extended GM2002

The extended GM2002 proposed here was tested using observations reported in Chapter 3 (Harder et al., 2017); the results are summarized in Table 5.3. The model slightly overestimated H_A and LE_A on 30 March 2015, likely due to the limiting assumptions of the GM2002 model. A key missing component of GM2002 is the influence of differences in surface roughness upon the growth of the internal boundary layer. A simple power law relationship with respect to distance from transition is employed in the model. Further work by Granger et al. (2006) demonstrated that boundary layer growth has a positive relationship with upwind surface roughness and that the parametrization employed in GM2002 overestimates the boundary layer, by up to a factor of 2 when upwind surface roughness is negligible. The GM2002 is based upon the integrated difference in temperature through the boundary layer, thus a greater boundary layer depth will increase the estimated advection. This partly explains why the model overestimates values in the situation of a rough upwind surface. Other potential limiting assumptions include homogenous surface temperatures, uniform eddy diffusivities for different scalars, no vertical advection, and neutral atmospheric stability. Despite the model limitations, the acceptable performance in simulating the March 18 and March 30 observations gives confidence that this simple model is reasonable for some applications and provides guidance for future improvements.

Table 5.3: Model parameters, estimates and observations for evaluation of the extended GM2002

Attribute	Unit	18 March 2015	30 March 2015
Observation Transect Length	m	3.1	3.6
T_a	°C	5.4	7.3
T_{sc}	°C	0	0
T_{soil}	°C	6.5	10.5
T_{wat}	°C	0	3[a]
RH	%	60.0	72.1
u	m s^{-1}	1.6	6.4
F_{water}[b]	-	0	0.85
Mean Observed H_A	W m^{-2}	197	404
Mean Modelled H_A	W m^{-2}	175	456
Mean Observed LE_A	W m^{-2}	66	446
Mean Modelled LE_A	W m^{-2}	30	480

[a]Estimated from thermography

[b]Roughly estimated from application of a 1:100 sensor height to flux footprint ratio (Hsieh et al., 2000) as applied to concurrent UAV imagery.

5.4.2. Reevaluation of Snowcover Geometry

Differences exist between the originally reported parameters and those found from the analysis of UAV imagery (mean coefficients summarized in Table 5.4). Early work applying fractal geometry to natural phenomena (Mandelbrot, 1982, 1975) discusses the Korcak exponent as a fractal dimension. More recent work suggests that the Korcak law describing the area-frequency relationship is not a fractal relationship but rather a mathematically similar, but distinct, scaling law (Imre and Novotn, 2016). Therefore, the D_k value is not necessarily >= 1 or <=2 and the identified exponent terms in Table 5.4 near or greater than 2 are plausible. The D' terms are very similar to those previously reported (Granger et al., 2002). From this analysis, it is apparent that application of these parameters between sites must be done with caution as local topography and surface conditions may influence the snow patch size distribution. The lack of a temporal trend of these terms (time series of D_k in Figure 5.5 and D' in Figure 5.6) over the course of snowmelt and equivalence in scaling of snow and snow-free patches implies that locally specific parameters may be applied as constants over the course of the melt and irrespective of snow-free or snow patch type. The resolution of the underlying imagery, differences in classification methodologies and surface characteristics may contribute to some of

the differences in terms observed and those previously reported. An illustrative comparison is that of a tall and short stubble surface. The tall stubble surface snowcover geometry is heavily influenced by the early exposure (and hence classification as non-snow from nadir imagery) of stubble rows which leads to very long and narrow patches even if snow is still present within the stubble. In contrast the oblique imagery of Shook et al. (1993b) and Granger et al. (2002) will not quantify the snow between stubble rows and larger and less complex snow patches would be represented by the previously reported coefficients. Further work is needed to calculate the scaling properties of patches over a more comprehensive variety of topography and vegetation types.

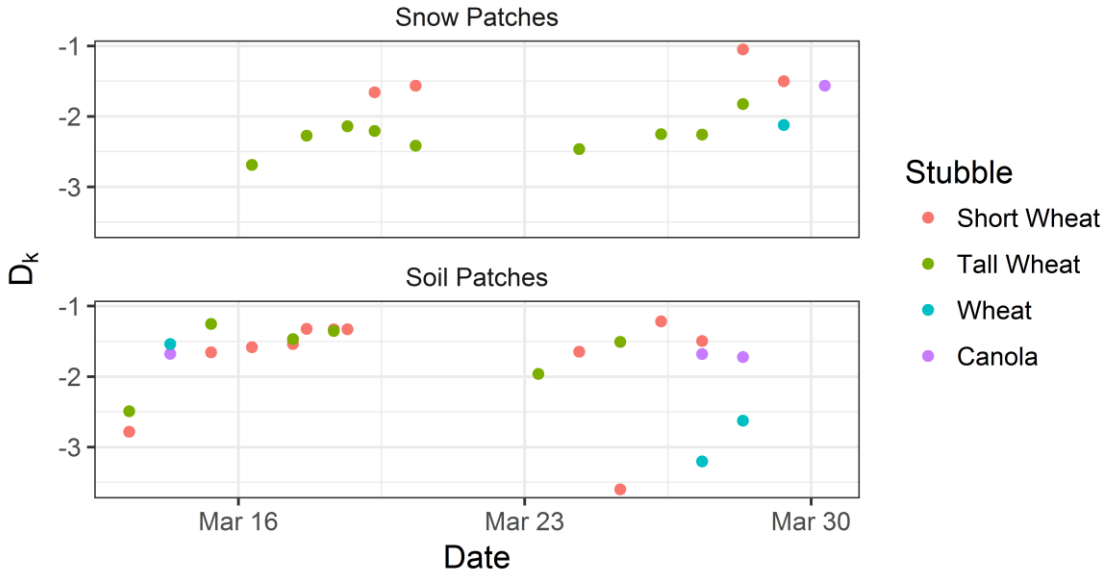

Figure 5.5. Time series of fitted D_k parameter with respect to snow and soil patches for various land covers over the course of snowmelt.

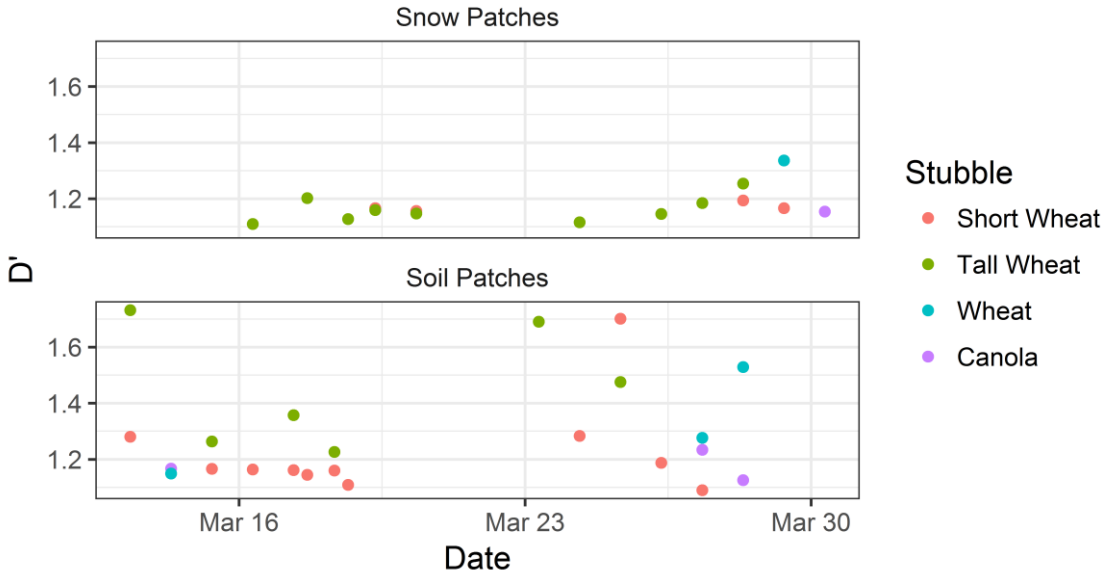

Figure 5.6. Time series of fitted D' parameter with respect to snow and soil patches for various land covers over the course of snowmelt.

Table 5.4: Updated mean snowcover geometry parameters.

Variable	Snow Patches	Soil Patches	Literature Values
D′	1.22	1.35	1.25
D_k	2.00	1.83	1.2-1.6

5.4.3. Implications of including advection in snowmelt models

5.4.3.1. Advection dynamics in scenario simulations

The dynamics of the various scenarios are expressed through visualizations of SWE depletion (Figure 5.7) and magnitudes of the H_A, LE_A and net advection terms (Figure 5.8). A critical consequence of including SCA in snowmelt calculations is that there is a difference in areal average melt rates, assuming the same Q_{net}, between a continuous and heterogeneous snow surface. The Q_{net} in a one-dimensional melt model is in terms of a flux density; an energy flux with a unit area dimension (W m^{-2}). As the areal fraction of snow decreases the corresponding areal average energy to melt snow will also decrease which will decrease the areal average melt rate. This is evident in the melt rate of the No Advection scenario, which decreases with time as the SCA decreases. Including energy from advection, for the Dry Surface, Wet Surface, and Dry to Wet Surface advection scenarios, causes the SWE to deplete faster as there is now an additional energy component that increases as SCA depletes. The additional energy gained from

advection is greater than the reduction of areal average Q_{net} as SCA decreases. LE_A from a constant Wet Surface enhances melt more than any other advection scenario. Despite a reduction in H_A from the cooler surface, the consistently positive LE_A towards the snow leads to a large net advection flux. In contrast, a consistently warm Dry Surface has a much higher H_A flux than the Wet Surface that is partly compensated by a negative LE_A due to sublimation and a decrease in the overall energy for melt from advection. When the surface wetness is parameterized by detention storage and frozen soil infiltration capacity, Dry to Wet Surface, the snow-free surface is dry and warm in the early stages of melt and LE_A is negative and limits melt; as in the Dry Surface scenario. As melt proceeds and F_{water} begins to increase, the upwind T_{sf} cools and the humidity gradient switches resulting in positive LE_A and a decrease in H_A which compound to slow melt relative to the Dry Surface scenario. It is evident that SLHAM can quantify the key advection behaviours.

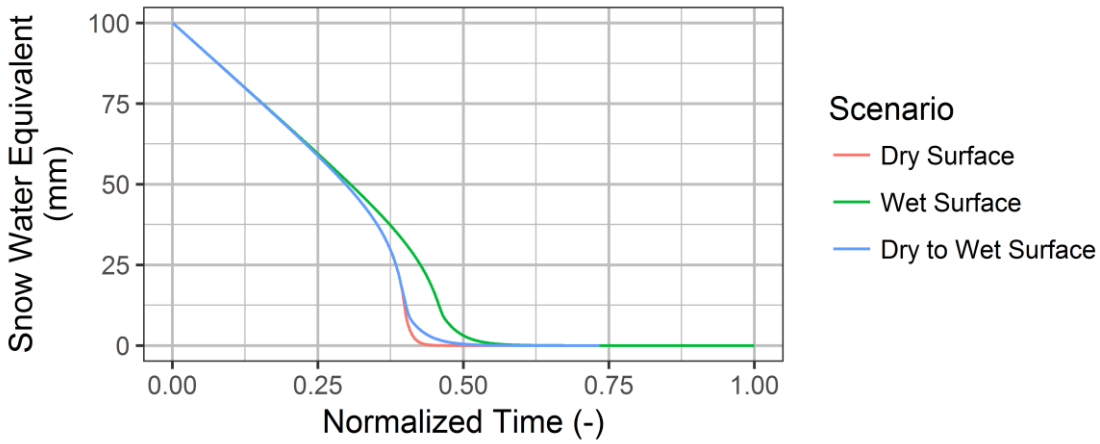

Figure 5.7: Modelled snow water equivalent depletion for various advection scenarios

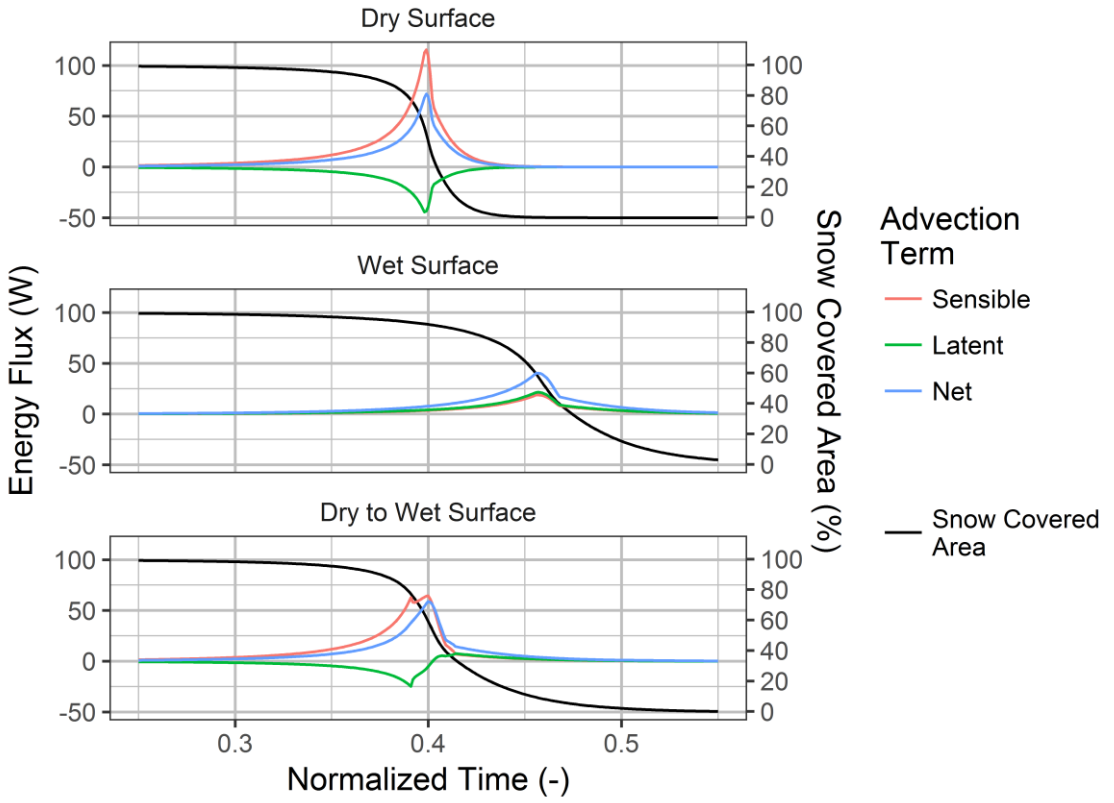

Figure 5.8: Latent heat (green), sensible heat (red) and net (blue) advection components for the SLHAM scenarios plotted with snowcovered area (black).

5.4.3.1.1. Sensitivity to Ponded Water Surface Temperature

The representation of T_{wat} defines the surface temperature and humidity gradients driving advection. Without direct observation or models to describe this variable it is important to explore the sensitivity and behaviour of SLHAM to variations in T_{wat}. A sensitivity analysis of T_{wat} shows that when F_{water}= 0 there is no sensitivity of SLHAM to T_{wat} (Figure 5.9). Once F_{water} is greater than 0, higher values of T_{wat} act to increase rates of SWE and SCA depletion, increase the extent and duration of F_{wat}, decrease the H_A flux, and increase the LE_A and net advection fluxes. A critical feedback of increasing T_{wat} is that the corresponding increase in LE_A is greater than the concomitant decrease in H_A. This dynamic drives the feedbacks that increase the advection contributions, and therefore snowmelt rates, with respect to increasing T_{wat}.

While the advection terms display a relatively large response to T_{wat} the overall influence upon SWE, the dynamic of greatest interest, is limited. Sensitivity to T_{wat} is only expressed towards the end of the snowmelt, when SWE < 15 mm and SCA is depleting rapidly.

Any differences in melt rate from T_{wat} are tempered by the rapid reduction in the SCA exchange surface at the end of snowmelt. The time to melt out, with time normalized relative to the No Advection scenario, was only 8 % faster for the T_{wat}= 2 °C simulation relative to T_{wat}= 0 °C simulation. Whilst clearly important for simulating the dynamics of advection and sources of energy driving snowmelt, T_{wat} has a relatively limited influence upon overall SWE depletion. In the absence of T_{wat}models or observations, the assumptions outlined in Equation 5.15 will have a relatively limited influence upon simulation of SWE with the fully coupled SSAM-SLHAM model.

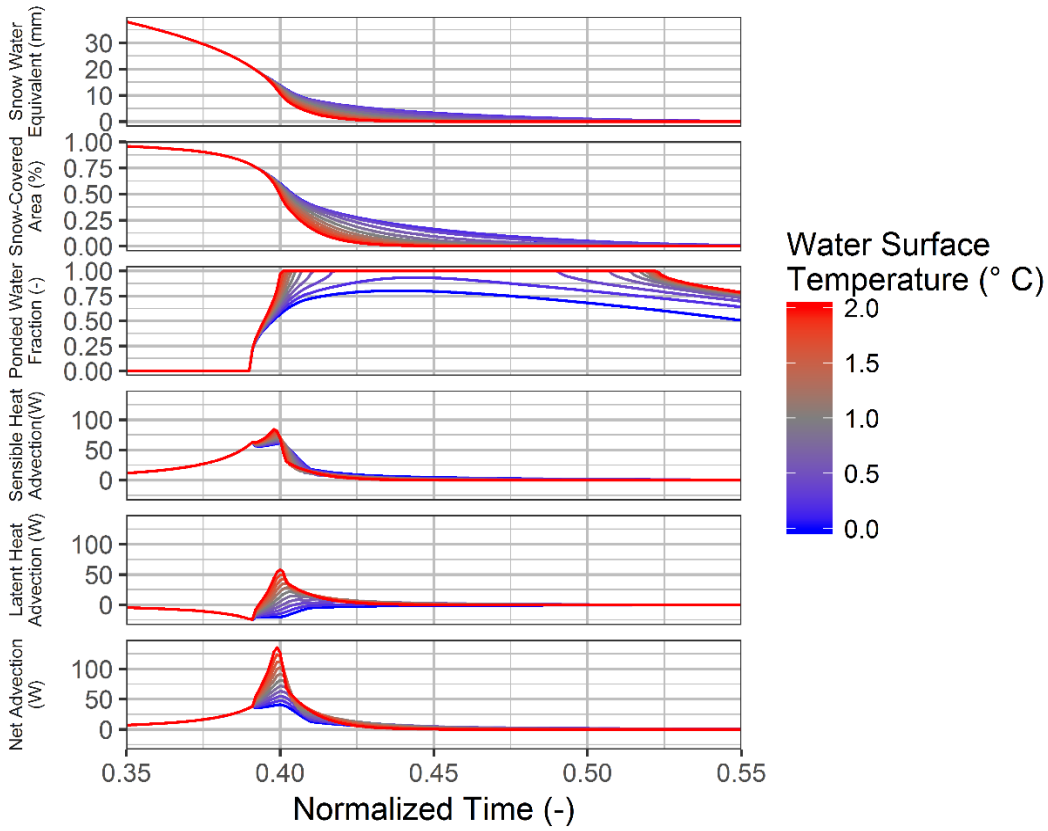

Figure 5.9: Sensitivity of snow water equivalent and snowcovered area depletion, ponded water fraction, sensible heat advection, latent heat advection and net advection with respect to variation in water surface temperature.

5.4.3.2. Advection dynamics in coupled advection and snowmelt models

The scenario analysis demonstrates the melt response to variations in surface wetness but actual snowmelt situations have forcings that vary diurnally and with meteorological conditions. Snowmelt simulations with three models of varying complexity provides insight into the

implications of process representation. SSAM and SSAM-SLHAM show considerable improvement when compared to EBSM (Figure 5.10 and Table 5.5). The SSAM simulation is by itself a significant improvement upon EBSM for SWE prediction during melt. The addition of SLHAM does not change the SWE simulation performance appreciably but does increase the physical realism of the model with its more complete surface energy balance. The SSAM-SLHAM simulations including advection, relative to SSAM simulations without advection, led to lower areal average melt rates in 2015 and higher rates in 2016. The comparison of the simulated melt with snow survey SWE observations showed that the differences are minimal (Figure 5.10 and Table 5.5). While the SSAM-SLHAM simulations do not appreciably change melt rates, the source of energy driving snowmelt does change. Early melt displays no differences as SCA remains relatively homogenous. As SCAdecreases, differences appear due to the corresponding decrease in the vertical snow-atmosphere and radiation fluxes and the increasing advection fluxes. The cumulative net energy from advection for these two seasons contributed energy to melt 4 mm and 5 mm of SWE in 2015 and 2016 respectively (Figure 5.11). The advection energy contribution represents 6.5 % and 10.6 % of total snowmelt in 2015 and 2016, respectively.

Table 5.5: Error metrics of snow water equivalent simulation versus snow survey observations for EBSM, SSAM and SSAM-SLHAM models.

Year	Model	RMSE	MB
2015	EBSM	12.03	0.32
2015	SSAM	6.55	0.13
2015	SSAM-SLHAM	5.89	0.11
2016	EBSM	14.51	0.48
2016	SSAM	4.41	-0.01
2016	SSAM-SLHAM	5.00	-0.05

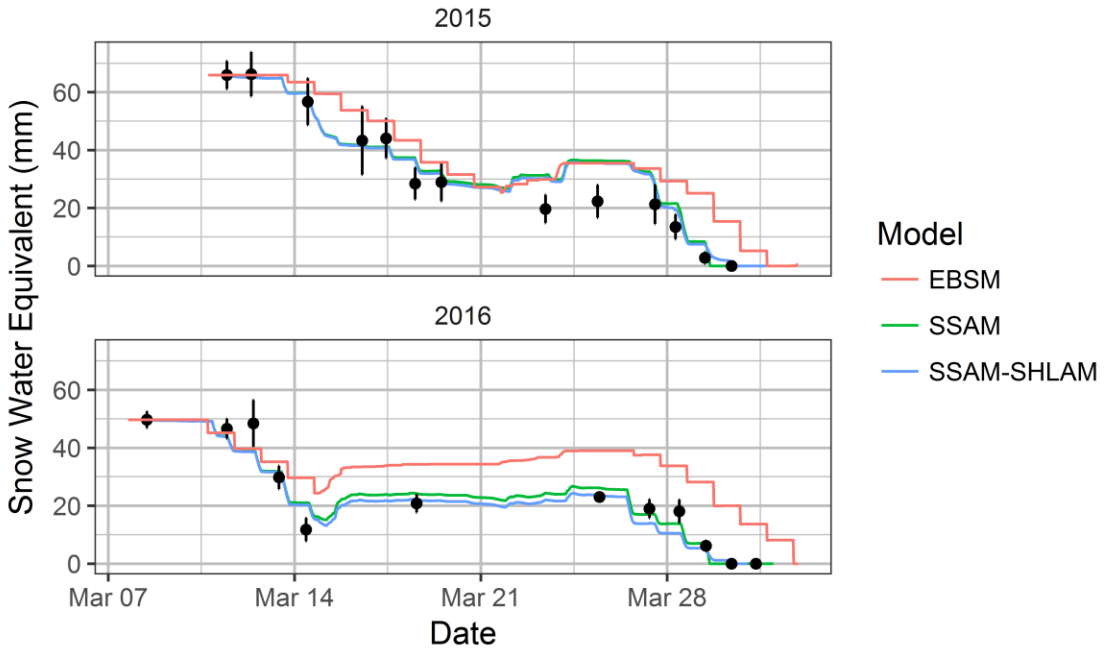

Figure 5.10. Snow water equivalent simulation for EBSM (red line), SSAM (green line) and SSAM-SLHAM (blue line) with respect to snow survey mean (black points) and 95% percentile sampling confidence interval (black lines).

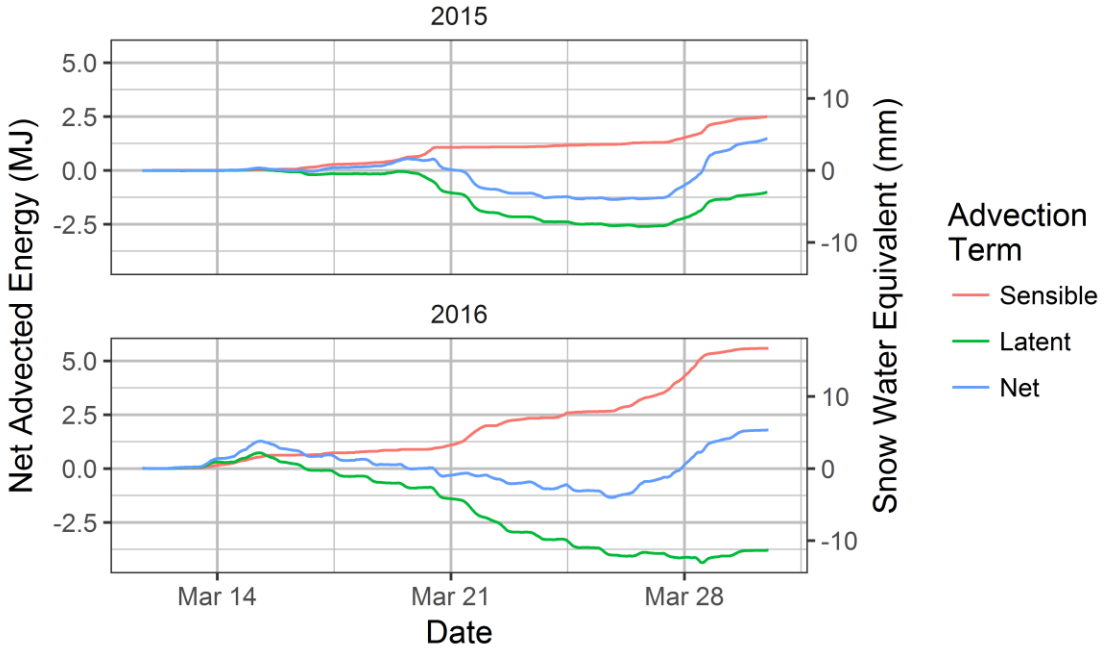

Figure 5.11: Cumulative sensible (red), latent (green) and net (blue) advection terms in terms of energy (MJ: left axis) and equivalent melted snow water equivalent (mm SWE: right axis)

5.4.4. Energy Balance compensation

An unappreciated dynamic of local-scale advection during snowmelt is that LE_A and H_A may be of opposite sign and therefore will compensate for one another leading to a lower net advection contribution. This occurs when the gradients of T and q between a snow-free and snowcovered surface are opposite in sign; a warm but dry snow-free surface upwind of a cool and wet snowcovered surface driving snow surface sublimation. This was evident in the reduction of the advection energy due to a negative LE_A throughout the Dry Surface scenario and early melt of the Dry to Wet Surface scenario (Figure 5.8). In the 2015 and 2016 snowmelt simulations, the accumulated LE_A was negative for much of the melt period which compensated for the consistently positive H_A term (Figure 5.11). LE_A only increased, enhancing the positive H_A contribution, near the end of melt in 2015 when increased surface wetness led to a positive LE_A term.

The advection fluxes may also be of opposite sign to the sensible (H_{snow}) and latent (LE_{snow}) turbulent fluxes between the snow surface and the atmosphere. Inclusion of the advection process therefore influences the overall sensible and latent heat exchange at the snow surface (net exchange). This interaction is further complicated by the varying SCA of the SSAM-SLHAM model versus the complete snowcover assumption of SSAM. Including advection decreased cumulative LE by 1.4 MJ in 2015 and by 3.8 MJ in 2016 (Table 5.6). Cumulative H, when including advection, did not change in 2015 and increased by 5.6 MJ in 2016. The net exchange when including advection shows that the inclusion of LE_A decreases the influence of H_A; the change in net exchange is lower than the change in H exchange (Table 5.6). The role of advection in modifying net exchange is clearly complex and varies by season. Despite differences in magnitude, the opposite signs of LE_A and H_A demonstrate that these energy contributions partially compensate for one another, therefore reducing the net influence of advection on snowmelt. This compensatory relationship has been missed by the sole focus in snowmelt advection research, which has therefore overemphasized the contribution of H_A to snowmelt. This compensatory mechanism also helps to explain why observed latent heat fluxes are often much smaller than model predictions in the meltwater-ponded Canadian Prairies during melt (Granger et al., 1978). The compensation of H_A by LE_A will be a more important interaction

on the Canadian Prairies, or similar level environments, but perhaps less so in mountain regions where complex terrain leads to rapid meltwater runoff

Table 5.6: Cumulative energy from sensible, latent and net exchange for 2015 and 2016 snowmelt simulations with (SSAM-SLHAM) and without (SSAM) advection.

Year	Flux Term	SSAM	SSAM-SLHAM	Difference
		MJ	MJ	MJ
2015	LE	-18.6	-20.0	-1.4
2015	H	30.6	30.6	0
2015	Net	12.0	10.6	-1.4
2016	LE	-27.5	-31.3	-3.8
2016	H	31.0	36.6	5.6
2016	Net	3.5	5.3	1.8

5.4.5. To advect or not to advect?

The simulation of snowmelt with, and without, advection gave minimal differences in the resulting SWE simulation. This demonstrates system insensitivity to processes that on their own appear to be important. This may explain why EBSM, like many other physically based snow melt models (Jordan, 1991; Lehning et al., 1999; Marks et al., 1998), does not accommodate heterogeneous snowcover yet successfully simulates SWE depletion. In EBSM the simulation of an areal average albedo rather than a snow albedo performed relatively well in simulating SWE (Figure 5.10) without considering SCA depletion or advection controls. The modelling challenges of a_{snow} are not limited to EBSM as other a_{snow} parameterizations, especially temperature dependent ones, typically underestimate a_{snow} during melt and therefore indirectly, and perhaps unintentionally, account for advected energy contributions (Pedersen and Winther, 2005; Raleigh et al., 2016). While modelled a_{snow} values that underestimate actual a_{snow} values are effective parameterizations for simulation of SWE, they cannot realistically incorporate the impacts of dust on snow or changes in snow albedo with grain size or wetness. Hence, SCA constraints and advection process conceptualizations are necessary to improve confidence in and applicability of snowmelt models. This is evident when comparing the more accurate and physically complete SSAM-SLHAM simulation of SWE to the EBSM simulation of SWE (Figure 5.10).

Understanding the implications of land-use and climate changes on variables beyond SWE are needed to fully inform coupled modelling of land-atmosphere and radiation feedbacks between land surface and numerical weather or climate models. The framework presented explicitly considers advection and scales it with SCA, u and horizontal gradients which are the primary controls of advection. A simple indication that a more appropriate model conceptualization is being used in this advection framework is that the minimum albedo value simulated is 0.75 is consistent with that for clean, melting snow (Wiscombe and Warren, 1980), whilst the 0.2 in EBSM is not. Whilst the SWE simulation differences are not particularly large, the new model is getting the "right" answer for the "right" reasons and without calibration. By including a more appropriate suite of physical processes, this model can produce realistic melt simulations in areas or years where the variables governing advection deviate from the conditions observed during model development.

5.4.6. Limitations and Future Research Needs

The SLHAM framework replaces the large uncertainty deriving from physically unrealistic albedo parametrizations (Gray and Landine, 1987a; Raleigh et al., 2016) and ignored SCA dynamics (Essery and Pomeroy, 2004) with a more physically realistic framework. The individual process parametrizations still have uncertainties that need to be constrained. The advection versus patch length parametrization of GM2002 lacks inclusion of surface roughness differences and the valid bounds of the parametrizations need clarification. The SCA model of Essery and Pomeroy (2004) is challenged by exposure of vegetation in shallow snow. The conceptual surface water ponding model developed in this work requires field observations or further parameterizations to accurately quantify the relevant variables. The transition of advection mechanism from snow-free sources to snow patch sources uses a conceptualized relationship to SCA. A targeted field campaign is needed to assess the validity of the conceptualized f_s, and its possible relation to the advection efficiency term of Marsh and Pomeroy (1996). An estimate of T_{sf} is needed to implement this framework and will limit application of SLHAM in its current form, as modelling T_{sf} is non-trivial and observations are often unavailable. Ideally a multisource land surface scheme with explicit representation of soils and ponded water is used to represent T_{soil} and T_{wat}. In the interim, the T_{wat} assumptions in Equation 5.15 may be used but need to be tested further. A regression of T_{soil} to incoming

shortwave radiation and T_a is presented in the appendix to provide a simple and physically guided solution to remove this limitation when modelling snowmelt in agricultural regions on the Canadian Prairies. These uncertainties will be addressed in future work and will require additional field observations and model validation, testing, or development.

5.5. Conclusions

To date the development of easily implementable and appropriate models to estimate the advection of H_A and LE_A to snow during melt have proved elusive. The formulation presented here is an initial framework that can be used to augment existing one-dimensional snowmelt models. When tested against observations the extended GM2002 model provides reasonable estimates of both H_A and LE_A and opportunities for improvement of the method are discussed. The scaling parameters necessary to describe the spatial heterogeneity of snow and snow-free patches were re-evaluated with UAV data. Coupling of the simple advection model with snowcover geometry scaling laws, SCA depletion, frozen soil infiltration and a surface detention fractional water area parameterization resulted in a model that meets the objective of a formulation that can account for LE_A and H_A to snow as an areal average contribution. A scenario-based analysis of the model revealed the compensatory influence of LE_A from a warm but dry surface; the LE_A driven sublimation offsets H_A inputs. Coupling SLHAM with SSAM demonstrated that advection constitutes an important portion of melt energy: 11% of the melt observed in the 2016 snowmelt season. The reduced radiation exchange to the snow surface fraction, due to decreasing SCA, is compensated for with an increase in net sensible and latent heat exchange that leads to minimal differences in the SWE depletion. This compensatory dynamic has sometimes allowed one-dimensional energy balance snowmelt models to provide adequate simulation of SWE despite using the "wrong" process conceptualizations. The advection model framework proposed here can be easily coupled to existing one-dimensional energy balance models and is expected improve the prediction of snowmelt in areas dominated by heterogeneous snowcover during melt. Such adoption will permit successful use of more realistic albedo parameterisations. This work provides a guiding framework to address the long identified need to develop "bulk methodologies" for calculating sensible and latent heat terms for patchy snowcover conditions (Gray et al., 1986).

5.6. Appendix

The SLHAM framework requires a T_{soil} value which is a challenging variable to explicitly model during snowmelt. To provide an interim solution a multiple linear regression is developed to estimate T_{soil} from $SW_{atm}^{\downarrow}$ and T_a. This empirical parameterization is appropriate to snowmelt situation on the Canadian Prairies when the surface is comprised of crop residues and should be treated with caution in other domains. The developed regression is physically guided as the main variables controlling T_{soil} is the net radiation, whose variability is dominated by $SW_{atm}^{\downarrow}$, and turbulent fluxes, which are dependent upon the T_a gradients. During nighttime T_{soil} is very similar to T_a while during daytime the additional energy from $SW_{atm}^{\downarrow}$ heats the surface to temperatures above T_a. A multiple regression that contains these parameters provides a simple but effective way to estimate T_{soil} in a manner consistent with energy balance interactions. A full description of the observations used to parameterize this relationship can be found in Chapter 4. Briefly the T_a is observed with a shielded Campbell Scientific HMP45C212 and $SW_{atm}^{\downarrow}$ is observed with a Campbell Scientific CNR1 with both sensors 2 m above the ground surface. The T_{soil} observations from Apogee SI-111 sensors, mounted on mobile tripods to ensure consistent representation snow-free surfaces, sampled surfaces of tall wheat stubble (0.35 m) and short wheat stubble (0.2 m) in 2015 and wheat stubble (0.24 m) and canola stubble (0.24 m) in 2016. Hereafter they are refereed to Tall Stubble, Short Stubble, Wheat and Canola, respectively. All observations were logged at 15-minute intervals. The empirical representation of T_{soil} (°C) in relation to $SW_{atm}^{\downarrow}$(W m^{-2}) and T_a (°C) is,

$$T_{soil} = 0.00339SW_{atm}^{\downarrow} + 0.977T_a - 1.22. \quad (5.16)$$

Model performance was assessed with the root mean square error (RMSE) and model bias (MB). Each test provides a different perspective on model performance: $RMSD$ is a weighted measure of the difference between the observation and model, (Legates and McCabe, 2005) and MB indicates the mean over or underprediction of the model versus observations (Fang and Pomeroy, 2007). The T_{soil} regression provides good estimates of the diurnal variability and magnitudes with respect to observations (Figure 5.12). The highest values during daytime are simulated well which is critical for the appropriate simulation of advection processes. There is low bias for all simulations; MB <1.09 °C. The RMSE's between 1.39 °C and 1.94 °C are negligible as most surface temperature models will simulate errors at a similar

magnitude (Aiken et al., 1997). This parametrization provides a simple but effective workaround if T_{soil} observations are unavailable or unmodeled. This empirical relation should be treated with caution if implemented outside of the conditions found during snowmelt in cropland areas of the Canadian Prairies. In such cases locally derived relationships should be developed or T_{soil} should be explicitly modelled.

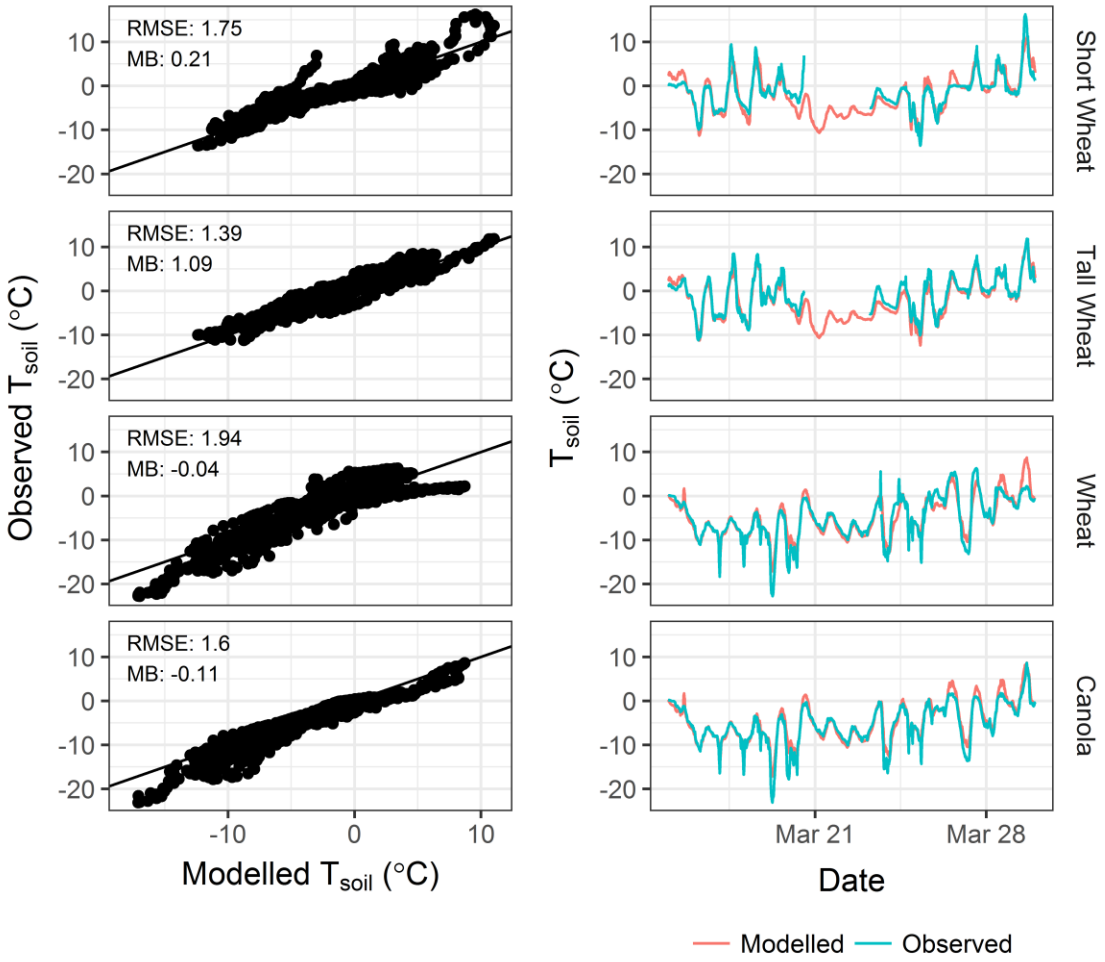

Figure 5.12: Soil surface temperature observed versus modelled as scatter plots (left column) and time series (right column)

5.7. Manuscript Integration with Broader Thesis

Chapter 5 developed the SLHAM model to quantify the areal average sensible and latent heat advection to snow during melt. This contribution required the observations of sensible and latent heat advection from Chapter 3 to conceptualize the model structure and dynamics that needed to be represented as well as to validate the extended GM2002 model. The SCA

classifications of Chapter 2 were used to update and validate the snowcover geometry scaling parameters that underlie the extension of the GM2002 model from a single patch to a heterogenous and dynamic snowcover. The SSAM model of Chapter 4 is also used to discern the implications of including advection upon areal average snowmelt rates. The coupling of SLHAM with SSAM provides the snowmelt portion of the model framework to simulate the influence of stubble on meltwater partitioning in Chapter 6.

5.8. References

Aiken, R. M., Flerchinger, G. N., Farahani, H. J., Johnsen, K. E. (1997). Energy Balance Simulation for Surface Soil and Residue Temperatures with Incomplete Cover. Agronomy Journal, 89, 404–415.

Brun, E., Martin, E., Simon, V., Gendre, C., Coleou, C. (1989). An Energy and Mass Model of Snow Cover Suitable for Operational Avalanche Forecastiong. Journal of Glaciology, 35(121), 333–342.

Essery, R., Pomeroy, J. W. (2004). Implications of spatial distributions of snow mass and melt rate for snow-cover depletion: theoretical considerations. Annals of Glaciology, 38(1), 261–265. https://doi.org/10.3189/172756404781815275

Essery, R., Granger, R. J., Pomeroy, J. W. (2006). Boundary-layer growth and advection of heat over snow and soil patches: modelling and parameterization. Hydrological Processes, 20(4), 953–967.

Fang, X., Pomeroy, J. W. (2007). Snowmelt runoff sensitivity analysis to drought on the Canadian prairies. Hydrological Processes, 21(19), 2594–2609. https://doi.org/10.1002/hyp

Granger, R. J., Male, D. H., Gray, D. M. (1978). Prairie Snowmelt. In Symposium of the Water Studies Institute.

Granger, R. J., Pomeroy, J. W., Parviainen, J. (2002). Boundary-layer integration approach to advection of sensible heat to a patchy snow cover. Hydrological Processes, 16(18), 3559–3569.

Granger, R. J., Essery, R., Pomeroy, J. W. (2006). Boundary-layer growth over snow and soil patches: Field Observations. Hydrological Processes, 20(4), 943–951.

Gray, D. M., Pomeroy, J. W., Granger, R. J. (1986). Prairie Snowmelt Runoff. In Water Research Themes, Conference Commemorating the Official Opening of the National Hydrology Research Centre (pp. 49–68). Saskatoon, Saskatchewan: Canadian Water Resources Association.

Gray, D. M., Toth, B., Zhao, L., Pomeroy, J. W., Granger, R. J. (2001). Estimating areal snowmelt infiltration into frozen soils. Hydrological Processes, 15(16), 3095–3111. https://doi.org/10.1002/hyp.320

Gray, D. M., Landine, P. G. (1987). Albedo Model for Shallow Prairie Snow Covers. Canadian Journal of Earth Sciences, 24(9), 1760–1768. https://doi.org/10.1139/e87-168

Gray, D. M., Landine, P. G. (1988). An Energy-Budget Snowmelt Model for the Canadian Prairies. Canadian Journal of Earth Sciences, 25(8), 1292–1303.

Harder, P., Pomeroy, J. W., Helgason, W. D. (2017). Local scale advection of sensible and latent heat during snowmelt. Geophysical Research Letters. https://doi.org/10.1002/2017GL074394

Hsieh, C. I., Katul, G., Chi, T. W. (2000). An approximate analytical model for footprint estimation of scalar fluxes in thermally stratified atmospheric flows. Advances in Water Resources, 23(7), 765–772. https://doi.org/10.1016/S0309-1708(99)00042-1

Imre, A. R., Novotn, J. (2016). Fractals and the Korcak-law: a history and a correction. The European Physcical Journal H, 69–91. https://doi.org/10.1140/epjh/e2016-60039-8

Jordan, R. (1991). A One-Dimensional Temperature Model for a Snow Cover: Technical Documentation for SNTHERM.89. Hanover, N.H.

Legates, D. R., McCabe, G. J. (2005). Evaluating the Use of "Goodness of Fit" Measures in Hydrologic and Hydroclimatic Model Validation. Water Resources Research, 35(1), 233–241. https://doi.org/10.1029/1998WR900018

Lehning, M., Bartelt, P., Brown, B., Russi, T., Stockli, U., Zimmerli, M. (1999). SNOWPACK model calculations for avalanche warning based upon a new network of weather and snow stations. Cold Regions Science and Technology, 30, 145–157.

Liston, G. E. (1995). Local advection of momentum, heat and moisture during the melt of patchy snow covers. Journal of Applied Meteorology, 34, 1705–1715.

Mandelbrot, B. B. (1975). Stochastic models for the Earth's relief, shape and fractal dimension of coastlines, and number-area rule for islands. Proc. Natl. Acad. Sci. USA., 72, 3825–3838.

Mandelbrot, B. B. (1982). The Fractal Geometry of Nature. New York: Freeman.

Marks, D., Domingo, J., Susong, D., Link, T. E., Garen, D. (1999). A spatially distributed energy balance snowmelt model for application in mountain basins Abstract : Hydrological Processes, 13, 1935–1959.

Marks, D., Kimball, J., Tingey, D., Link, T. E. (1998). The sensitivity of snowmelt processes to climate conditions and forest cover during rain-on-snow : a case study of the 1996 Pacific Northwest Flood. Hydrological Processes, 12, 1569–1587.

Marsh, P., Pomeroy, J. W. (1996). Meltwater Fluxes At an Arctic Forest-Tundra Site. Hydrological Processes, 10(10), 1383–1400.

Marsh, P., Essery, R., Neumann, N., Pomeroy, J. W. (1999). Model estimates of local advection of sensible heat over a patchy snow cover. In M. Tranter (Ed.), Interactions between the Cryosphere, Climate and Greenhouse Gases (pp. 103–110). IAHS Publ. No. 256.

Mott, R., Lehning, M., Daniels, M. (2015). Atmospheric Flow Development and Associated Changes in Turbulent Sensible Heat Flux over a Patchy Mountain Snow Cover. Journal of Hydrometeorology, 16, 1315–1340. https://doi.org/10.1175/JHM-D-14-0036.1

Pedersen, C. A., Winther, J. G. (2005). Intercomparison and validation of snow albedo parameterization schemes in climate models. Climate Dynamics, 25(4), 351–362. https://doi.org/10.1007/s00382-005-0037-0

Pomeroy, J. W., Gray, D. M., Brown, T., Hedstrom, N. R., Quinton, W. L., Granger, R. J., Carey, S. K. (2007). The cold regions hydrological model : a platform for basing process representation and model structure on physical evidence. Hydrological Processes, 21(19), 2650–2667.

Raleigh, M. S., Livneh, B., Lapo, K., Lundquist, J. D. (2016). How Does Availability of Meteorological Forcing Data Impact Physically Based Snowpack Simulations? Journal of Hydrometeorology, 17(1), 99–120. https://doi.org/10.1175/JHM-D-14-0235.1

Shook, K., Gray, D. M., Pomeroy, J. W. (1993a). Geometry of patchy snowcovers. In 50th Annual Eastern Snow Conference (pp. 89–98). Quebec City.

Shook, K., Gray, D. M., Pomeroy, J. W. (1993b). Temporal Variation in Snowcover Area During Melt in Prairie and Alpine Environments. Nordic Hydrology, 24(2–3), 183–198.

VanDerWal, J., Falconi, L., Januchowski, S., Storlie, L. S., Storlie, C. (2014). SDMTools: Species Distribution Modelling Tools: Tools for processing data associated with species distribution modelling exercises. Retrieved from https://cran.r-project.org/package=SDMTools

Weisman, R. N. (1977). Snowmelt: A Two-Dimensional Turbulent Diffusion Model. Water Resources Research, 13(2), 337–342.

Wiscombe, W. J., Warren, S. G. (1980). A Model for the Spectral Albedo of Snow. 1: Pure Snow. Journal of the Atmospheric Sciences, 37, 2712–2733.

Chapter 6: Implications of stubble management on snow hydrology and meltwater partitioning

Author Contributions: PH conceptualized and coded the model, performed simulations and analysis, and wrote the manuscript. JP and WH provided guidance, and reviewed and revised the manuscript.

6.1. Abstract

Spring snowmelt is the most important hydrological event in semi-arid agricultural cold regions, recharging soil moisture and generating the majority of annual runoff. Adoption of zero-tillage agricultural practices means vast areas of the Canadian Prairies, and other analogous regions, are characterized by standing crop stubble. Stubble will influence accumulation through blowing snow processes and snowmelt through the impact of emerging stubble upon the surface energy balance. In addition, spatiotemporal snowcover heterogeneity leads to enhancement of melt by advection of energy from warm-moist snow-free surfaces to cool-dry snow surfaces. Unfortunately, stubble emergence and advection are generally unaccounted for in snow models appropriate to this region and a complete process description has not been available. Here, the stubble influence on accumulation, melt, and meltwater partitioning processes is modelled by coupling a new stubble-snow-atmosphere surface energy balance and local-scale advection models to existing blowing snow and frozen soil infiltration models. Long-term meteorological datasets from sub-humid and semi-arid locations in Saskatchewan, Canada are used to drive the coupled models to quantify the influence of stubble characteristics on accumulation, melt, and meltwater partitioning processes with respect to interannual meteorological variability, antecedent soil moisture, and climatic differences on the Canadian Prairies. The results demonstrate a large range of variability in the response of snow processes to increases in stubble height (h_v). This is due to non-linear process interactions. The mean response associated with increasing h_v is increased total meltwater, melt rate, infiltration, and runoff, and negligible changes in duration of melt. The response of these process to changes in h_v are more pronounced at semi-arid versus sub-humid environments as increases in stubble more effectively suppresses blowing snow sublimation in the windier, drier environment of the southwestern Canadian Prairies. These findings validate and diagnose earlier snow management and meltwater

enhancement field experimental results. Simple recommendations for stubble management to meet specific runoff or infiltration objectives are summarised; stubble management can be an effective tool to influence infiltration volume in dry soils and runoff volume in wet soils. This framework provides an approach to diagnose the influence of stubble management on melt processes to reveal the potential implications on meltwater partitioning in cold semi-arid agricultural production regions.

6.2. Introduction

Springtime snowmelt on the Canadian Prairies is typically the largest annual source for runoff, 80% annually (Gray and Landine, 1988), and can lead to significant infiltration (Granger et al., 1984) which has both hydrological and agricultural implications. Significant work on snow accumulation processes has shown that vegetation, or in the case of cropland - standing stubble, will control the snowcover characteristics and snow water equivalent (SWE) prior to melt (Pomeroy and Li, 2000). In contrast, the sensitivity of the snowmelt energy balance to the presence of exposed crop stubble has not been investigated to understand its role in modifying melt rates during ablation and how that may influence meltwater partitioning. Even subtle stubble influences upon melt rates may be significant as the extent of exposed stubble has regional implications on the Canadian Prairies; over 50% of Canadian Prairie biome (over 25 million hectares) is in crop production and of that 65% was in zero-tillage systems in 2016 (Statistics Canada, 2016). Crop management practices over this large domain are also changing as there has been a large-scale shift from conventional tillage and summer fallowing practices to zero tillage practices beginning in the 1990's (Awada, 2013). The hydrological implications of these shifts, also considering the influence of regional climate variability upon these processes, need to be quantified for agricultural producers to understand the implications of stubble management decisions. Management of stubble to pursue agronomic and hydrologic outcomes is a potential tool to manage hydrology but the sensitivity of meltwater partitioning to stubble characteristics has not been fully quantified.

6.2.1. Snow Accumulation and Stubble

In open environments the dominant process affecting the accumulation and spatial variability of a snowpack is blowing snow (Clark et al., 2011; Pomeroy et al., 1993). The

blowing snow process is a function of snow availability, fetch, wind speed, surface roughness and temperature (Pomeroy et al., 1993) and on the Canadian Prairies can be responsible for the sublimation, transport and redistribution of up to 75% of the annual snowfall (Pomeroy and Gray, 1995). Blowing snow is comprised of three fluxes including saltation, suspension and sublimation and are described by Pomeroy et al. (1993) in the Prairie Blowing Snow Model (PBSM). Stubble controls the surface roughness that, in turn, controls the various blowing snow processes leading to snow erosion or deposition. In areas of little surface roughness, minimal stubble or bare soil, blowing snow is initiated sooner leading to greater sublimation losses and transport (Pomeroy et al., 1991). Areas of greater surface roughness, such as standing stubble, will have greater deposition, although snow erosion can be still initiated when wind velocities produce a shear stress that exceeds the sum of that exerted on the stubble and the threshold shear stress for snow erosion (Pomeroy et al., 1993). Exposure of stubble greatly diminishes the shear stress exerted by the wind on the snow and typically limits snow erosion until the snow depth is near the stubble height (Pomeroy and Brun, 2001); after which filled stubble will behave as a bare surface (Pomeroy and Gray, 1994). The feasibility to manage snow distributions to maximize the pre-melt SWE has been well studied (Pomeroy et al., 1990).

6.2.2. Snowmelt and Stubble

Studies relating stubble and snowmelt have focused on observing the infiltration and runoff responses rather than differences in melt rates or changes to the snowmelt energy balance (Elliot and Efetha, 1999; Granger and Gray, 1984; Nicholaichuk and Gray, 1986; van der Kamp et al., 2003). The primary influence of stubble on the snowmelt process is that it defines the amount of accumulated SWE to be melted, as described in the previous section. Observations by Willis et al. (1969) showed earlier and more rapid snowmelt in stubble plots and it was hypothesized that this was due to stubble conducting more heat into the snowpack, intercepting and absorbing more solar radiation than snow, reflecting energy to the snowpack and providing an effective heat trap against convection. Exposed stubble in snow was also identified as a potential heat sink during the melt period by Nicholaichuk and Gray (1986). Chapter 4 described the development of a stubble-snow-atmosphere model (SSAM) which accounts for stubble characteristics (height, stalk width, row spacing, and stalk density) and quantifies all components of the snow surface energy balance below an exposed stubble. Compensatory processes are

revealed from observation and model results. Specifically, shortwave radiation is attenuated as it passes through stubble, longwave transmission to the snow surface is enhanced from emissions from warm stalks, and turbulent fluxes have a more complex response to stubble exposure. Overall, the longwave, shortwave and turbulent terms largely compensate, resulting in a negligible, but variable, change in energy with stubble exposure (Chapter 4).

A characteristic that challenges melt predictions of shallow snow in arid cold regions, such as the Canadian prairies, is the dynamic heterogeneity of the snowcovered surface. As melt progresses, a completely snowcovered surface will disaggregate into a mosaic of snow-free and snowcovered patches (Shook et al., 1993a). Consequently, the horizontal gradients of surface temperature and humidity in the presence of airflow across surface transitions advects energy to the snow that enhances melt and/or sublimation (Chapter 3). Stubble characteristics influence advection contribution to snowmelt in two ways. First, stubble characteristics will define the surface roughness difference between snow and non-snow surfaces which influences the growth of internal boundary layers which in turn will influence the amount of energy advected; greater roughness will act to increase the advection fluxes (Garratt, 1990; Granger et al., 2006). Unfortunately, simple advection parametrizations lack a dependency on surface roughness differences (Granger et al., 2002) despite observation of differences in boundary layer growth as a function of upwind surface roughness (Granger et al., 2006). Second, when including advection processes in an areal-average modeling framework, the influence of the one-dimensional energy exchanges, as captured by SSAM as areal averages, are limited by the snowcovered area (SCA). Thus, the influence of stubble-snow interactions on snowmelt will decrease over the course of melt as SCA decreases and advection contributions increase. A simple Sensible and Latent Heat Advection Model (SLHAM, Chapter 5) provides a modelling framework to account for advection contributions to melt.

6.2.3. Snowmelt Water Partitioning and Stubble

The partitioning of snowmelt water into infiltration and runoff components is ultimately the process which has the greatest agronomic and hydrologic implications. Crop yields in dryland agriculture are improved with greater soil recharge from meltwater (Staple and Lehane, 1954) while the extent and intensity of springtime overland flooding is a consequence of snowmelt runoff (Dumanski et al., 2015). Direct measurements of snowmelt runoff do not show

clear land cover influences due to the large uncertainty in runoff gauging and delineation of contributing area which is especially problematic on the low relief Canadian Prairies (Hodder et al., 2013). Infiltration into a frozen soil is complicated by the presence of water in the pore spaces in three phases (gas-liquid-solid) which greatly complicates the coupled mass-energy relationships governing the entry and transmission of liquid water from the surface due to phase changes it undergoes or induces within the frozen soil column (Ireson et al., 2013; Zhao et al., 1997). Observational studies from the 1980's on the Canadian prairies were successful in developing empirical understandings of the processes involved. Frozen soil infiltration falls into three classes (Granger and Gray, 1984): Restricted, where the presence of saturated soils, concrete frost, or basal ice layers will inhibit any infiltration leading to all snowmelt water running off, Unlimited, where presence of soil cracks or unsaturated soils with high infiltration rates allow all meltwater to be infiltrated, and Limited, where infiltration is governed by the soil properties and the characteristics of the snowmelt process (Zhao and Gray, 1999).

6.2.4. Stubble and Snow Process Interactions with respect to Canadian Prairie Climate Gradients

Large climatic gradients are evident across the Canadian Prairies. There is a general increase in annual precipitation and decrease in temperature and wind speed moving north and east from southern Alberta (Pomeroy et al., 2005). In winter time this is manifested as greater blowing snow redistribution and sublimation, and frequent mid-winter melts events in the south-west (Pomeroy and Gray, 1995). In contrast, blowing snow processes are limited and mid-winter melts are infrequent in the north and east (Fang and Pomeroy, 2007; Pomeroy and Gray, 1995). A compounding phenomena, isolated to the southwestern prairies, are Chinooks, the North American equivalent of Foehn winds, which are strong, warm, and dry winds that flow down the eastern slopes of the Rocky Mountains and onto the prairies (MacDonald et al., 2018). Chinooks are intermittent but lead to significant sublimation and snowmelt and their influence extend hundreds of kilometers to the east of the Rocky Mountains (MacDonald et al., 2018; Pomeroy and Gray, 1995). From an agricultural perspective, the northern and eastern regions provide more reliable conditions for unirrigated (dryland) crop production and continuous cropping practices while southwestern regions are on the margins of reliable dryland agriculture (Gray and Maule, 1994). The greater wind speeds and more frequent mid-winter melt events of southwestern

regions mean stubble is more effective in retaining snow water equivalent through effective suppression of blowing snow sublimation losses (Pomeroy and Gray, 1995). The aforementioned snow accumulation and redistribution, melt, and infiltration processes, are also expected to respond to climate change which is predicted to increase precipitation and temperature in the Canadian prairies (Erler et al., 2015; IPCC, 2013). Thus, it is critical to understand how the full representation of snow accumulation, melt, and meltwater partitioning will respond to stubble management across this climatic gradient.

6.2.5. Summary and Objectives

Stubble will influence meltwater partitioning through both the snow accumulation and melt processes. There is a positive relationship between h_v and SWE which controls the total amount of water available to form runoff and/or infiltration. In contrast, there is a subtle decrease in the net snow surface energy flux with increasing stubble exposure, which may increase the infiltration opportunity time and promote greater infiltration under taller stubble. The overall response of meltwater partitioning to stubble is clearly non-linear and must consider the antecedent soil moisture (SI) conditions. The stubble controls on meltwater partitioning will also be subject to meteorological variability during snow accumulation and melt periods, complicating the interpretation of a stubble-meltwater partitioning signal (Gray et al. 2001). The relative magnitude of these interactions, and how they may vary across the climatic gradients on the Canadian Prairies, has not been quantified as the stubble-snow surface energy balance relationships found in SSAM (Chapter 4) or advection contributions from SLHAM (Chapter 5) were previously unavailable.

The overall objective of this work is to quantify the influence stubble management has on the snow processes driving meltwater partitioning on the Canadian prairies. Specific objectives are to:

- Develop a physically based process model framework that quantifies snow accumulation, melt, and meltwater partitioning as a function of stubble characteristics.
- Quantify sensitivity and variability of stubble management-meltwater partitioning interactions with respect to initial soil moisture, meteorological variability, and climatic differences in the Canadian Prairies.

6.3. Methodology

The quantification of the role of stubble management on snow processes and meltwater partitioning requires representation of snow accumulation, snowmelt, and frozen soil infiltration to be sensitive to stubble characteristics as well as an approach to account for the inter-annual variability in these non-linear cold region processes. The overall approach will be detailed though describing: 1) the process representations and 2) the overall modelling and analysis approach. The coupled modelling framework described below is a point scale, unit area, representation of processes. Conceptually the model is describing snow accumulation, melt, and infiltration in the middle of a stubble field subject to fully developed blowing snow transport and uniform stubble and soil characteristics.

6.3.1. Process Representations

An appropriate model framework is needed to represent the relevant processes and their interactions driving the stubble meltwater partitioning relationship. The SSAM-SLHAM models developed in Chapters 4 and 5 were designed and validated for the springtime snowmelt period so early and mid-winter snow accumulation processes are simulated with the cold region hydrological modelling (CRHM) platform (Pomeroy et al., 2007). Snow accumulation is simulated by accounting for blowing snow processes as a function of stubble characteristics with the Prairie Blowing Snow Model module (PBSM: Pomeroy et al., 1993). The PBSM assumptions employed in this analysis include an upwind fetch of 1000m, fully developed blowing snow transport, and no net snow transport (snow transport into the field is equal to snow transport out of the field). Snow losses are limited to sublimation from the saltating and suspended snow. Mid-winter melts are simulated with the Energy Balance Snowmelt Model module (EBSM: Gray and Landine, 1988) which is well suited to estimate melt in shallow snowcovers during the winter when turbulent and radiative fluxes are limited by cold temperatures and limited solar radiation. The meltwater from mid-winter melt events are partitioned into infiltration or runoff with the frozen soil infiltration routine of Gray et al., (2001) as implemented in the PrairieInfiltration module of CRHM. The coupled PBSM, EBSM, and PrairieInfiltration CRHM model provides the initial values of snow water equivalent, snow density, cumulative overwinter infiltration and runoff, and infiltration opportunity time for SSAM-SLHAM. In SSAM-SLHAM snow is represented as a single layer and melt is simulated

from the net snowpack energy balance. The SCA is simulated with the parameterization of Essery and Pomeroy (2004) which relies on an estimate of the standard deviation of the maximum SWE. This standard deviation, at a particular interval, is estimated as the maximum of SWE at that interval multiplied by an assumed coefficient of variation (CV) or the previous interval's standard deviation. A CV of 0.33 is assumed which corresponds to the mean reported value for stubble surfaces on the Canadian Prairies (Gray et al., 2001). The meltwater released from the SSAM-SLHAM snowpack is partitioned in the same manner as the PrairieInfiltration module in CRHM with infiltration opportunity time estimated from the duration of active melt as estimated by SSAM-SLHAM. Throughout this model a soil porosity of 0.485 is assumed for a silt loam soil (Clapp and Hornberger, 1978) with a one meter wetting front depth. It is assumed that frozen soil infiltration is initially Limited and will change to Restricted, no infiltration and all subsequent melt becomes runoff, in the case of mid-winter melt and subsequent refreezing forming basal ice lenses (Zhao and Gray, 1999). The transition from a Limited to a Restricted infiltration condition is assumed to occur when daily snowmelt is ≥ 5mm (to identify a mid winter melt event), the subsequent nighttime minimum air temperature is ≤ -10 °C (to identify if the meltwater will subsequently refreeze at the surface), and occurs after January 1st (to avoid the triggering of Restricted conditions from early winter accumulation and melt events)(Pomeroy et al., 2007). This model structure provides the process representations to simulate snow accumulation, springtime snowmelt, and melt-water partitioning as functions of stubble characteristics.

6.3.2. Modelling strategy

Many factors complicate the hydrological response of meltwater production and partitioning to stubble management. Two variables are critical to any response, specifically, 1) antecedent soil saturation (SI) which will influence the infiltration capacity and therefore meltwater partitioning and latent heat advection dynamics and 2) stubble characteristics which will influence the blowing snow accumulation processes and snowmelt energy balance. Meltwater partitioning with respect to SI is simulated by a dry (SI=0.2), moderately saturated (SI=0.6), and saturated soil (SI=1). Stubble management can effectively manipulate two variables in fall; h_v during harvest operations and stubble density if harrowed thereafter. Other stubble characteristics, crop type and row density, are defined during seeding operations. In this

analysis, wheat and canola, the dominant and most different crops from a standing stubble characteristics perspective on the Canadian Prairies, are simulated. Canola and wheat are simulated with h_v varying from 0.001 to 0.5 m.

The non-linearity of snow accumulation and melt processes is exacerbated by inter-annual meteorological differences. Snow accumulation, melt, and infiltration is very sensitive to the dynamic meteorological drivers. This analysis employs observations from 1961 to 2005 of hourly air temperature, relative humidity, wind speed and precipitation from Environment Canada observed at Diefenbaker International Airport in Saskatoon (52.17° N, 106.70° W) and Swift Current (50.28° N, 107.79° W) in Saskatchewan, Canada. Precipitation data for these sites, adjusted for gauge undercatch and homogenized with respect to sensors changes, comes from the Adjusted and Homogenized Canadian Climate Dataset (Mekis and Vincent, 2011). Saskatoon and Swift Current were selected to simulate the sensitivity of meltwater partitioning to stubble management on the opposite ends of the Canadian Prairie climate gradient. Wintertime climate statistics and features are summarized in Table 6.1.

Table 6.1: Winter Climate Characteristics for Saskatoon and Swift Current Saskatchewan

Site	Mean Air* Temperature	Mean* Precipitation	Mean* Windspeed	Winter Features
Saskatoon	-6.9 °C	121 mm	4.5 m s^{-1}	No Chinooks and infrequent mid-winter melt events
Swift Current	-4.2 °C	128 mm	6.1 m s^{-1}	Frequent Chinooks and mid-winter melt events

*Mean climate variables are the October-April averages calculated from the 1961-2004 datasets

SSAM-SLHAM requires meteorological data beyond that found in the long-term meteorological datasets available. The hourly incoming radiation required for the SSAM model is simulated from this dataset with modules in CRHM. Hourly shortwave radiation is simulated from the daily minimum and maximum air temperatures via a modified Annandale et al. (2001) method (Shook and Pomeroy, 2011). Hourly longwave radiation is simulated from air temperature, humidity, and terrain view factors as proposed by Sicart et al. (2006).

6.4. Results and Discussion

The difference in response of the respective variable between that observed for negligible stubble (h_v = 0.001m) and that observed across the simulation range $h_v = 0.001$ m to $h_v = 0.5$ m is presented in Figure 6.1. This analysis shows that there is substantial variability, from interannual meteorological difference, in the response of snow processes to increases in h_v. The mean response of these processes are clearer and show increased total meltwater, melt rate, runoff, and infiltration and negligible change in duration of melt with respect to increases in h_v. The Swift Current site demonstrates a larger mean response and greater range in variability of these terms with h_v relative to Saskatoon. These are non-linear responses because of the complex relationships between blowing snow, the energy balance during melt, meltwater partitioning processes and driving climatology. No discernible differences in hydrological processes are demonstrated between canola and wheat stubble responses and are not discussed hereafter.

6.4.1. Stubble impacts on accumulation

Snow accumulation, as modeled by PBSM, is sensitive to variations in h_v, stubble stalk width, and stubble density. The greater the h_v the greater the amount of snow protected from blowing snow erosion and subsequent sublimation. As a result, increases in h_v will lead to an increase in cumulative meltwater (Figure 6.1). Only once snow accumulation exceeds the capacity of the stubble will blowing snow processes become important, which leads to an inverse relationship between snow accumulation and h_v. Threshold behavior is evident as the mean meltwater rate of change decreases with increased h_v. In many years meltwater shows no response above a specific h_v. For these scenarios the stubble response is limited by snowfall; the accumulated snowfall does not exceed h_v. The greater removal of snow by blowing snow sublimation also predisposes short h_v situations in low snow years to have a greater frequency of complete mid-winter melts. It is evident that the windier Swift Current simulation has a greater, and more variable, increase in meltwater with increasing h_v relative to the Saskatoon simulation. This enhancement of the meltwater h_v relationship is translated into the subsequent snowmelt and meltwater partitioning processes.

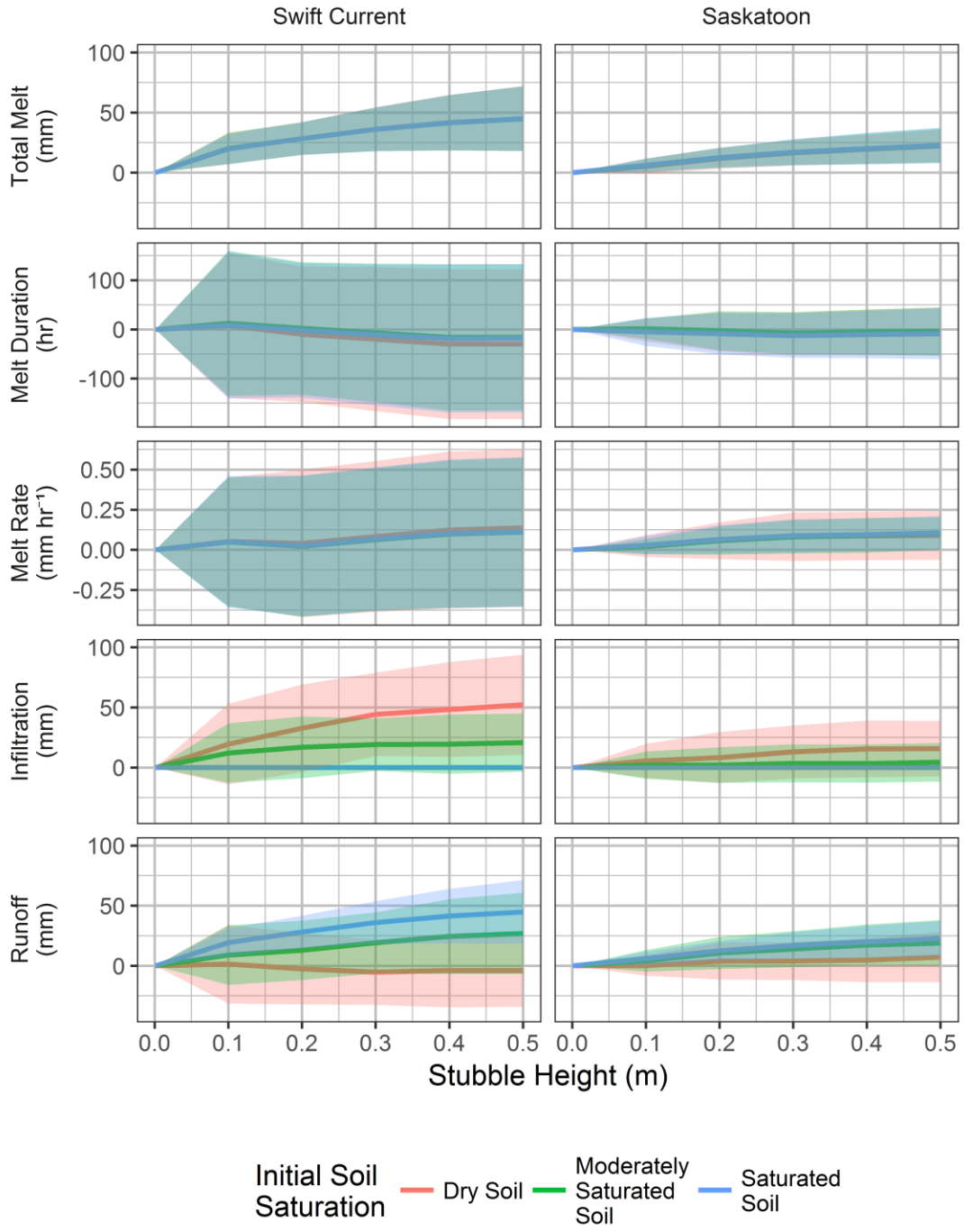

Figure 6.1: Total melt, melt duration, melt rate, cumulative infiltration and cumulative runoff simulations for a range in stubble heights, and presented as the difference from negligible stubble (0.001 m stubble height), for Swift Current and Saskatoon (columns), and initial soil saturation (colours). Lines are the mean and shaded areas reflect the interannual meteorological variability of the 45-year forcing dataset as +/- one standard deviation.

6.4.2. Stubble impacts on melt

The snowmelt process is conditional upon the snow available to melt as well as the energy balance. The interaction of these was simulated with SSAM-SLHAM presented in terms of the duration of snowmelt difference and melt rate change with respect to h_v (Figure 6.1). Despite the greater amount of snow to melt, due to a decrease in sublimation, there is no discernible change in mean melt duration. When melt does occur in this region it is generally rapid and the small differences in available snow do not translate into any consistent or identifiable change in snowmelt duration. Rather there is an increase in mean melt rate with h_v. The different response of mean melt duration and mean rate implies that melt behavior in these simulations is snow limited rather than energy limited. Individual years, and variations in SI, show a large range in response to changes in h_v. Every winter is a unique sequence of events, snowfall, blowing snow, melt, and snowcover depletion, and so the observed response is very non-linear. Little difference in mean melt rate and duration response with h_v are evident between Swift Current and Saskatoon. The greater variability of melt rate and duration in Swift Current are largely due to the more variable total meltwater available to melt and the more frequent mid-winter melt events, which increase the interannual variability of these terms.

6.4.3. Stubble impacts on meltwater partitioning

The influence of stubble upon infiltration and runoff are presented as differences with respect to h_v in Figure 6.1. The infiltration process controls the partitioning of meltwater. It is evident that there is a similar response in mean infiltration and runoff, as grouped by SI, with respect to h_v. While infiltration is assumed to be Limited at the start of the simulation it generally becomes Restricted due to mid-winter melts and refreezing part way through the winter. Therefore, the differences in meltwater with respect to h_v do not automatically translate into increases in infiltration. The increases in available meltwater when mid-winter melts do occur are translated into increases in runoff. The degree of response is related to SI as available moisture capacity, if it can infiltrate prior to frozen soil infiltration class changing to Restricted, is greater for low SI. The greater total meltwater response to h_v at Swift Current drives the larger variability in infiltration and runoff response relative to Saskatoon. The more frequent mid-winter melts driven by the warmer winters and more frequent chinook events exacerbates the non-linearity of the partitioning increasing the variability of the responses.

6.4.5. Implications for stubble management decision making

Stubble management decision making with respect to its influence upon meltwater partitioning seeks to resolve the following question: What h_v should be retained to meet a specific objective? The ability to manage stubble to influence meltwater partitioning has implications for both agricultural water and/or flood management. Meltwater partitioning can be managed for four mutually exclusive objectives that are summarized with respect to desired outcomes, SI, and h_v recommendations in Table 6.2. As frozen soil infiltration capacity often becomes Restricted in the winter, the ability to influence infiltration through stubble management alone is limited. Only in situations where there is low *SI* can infiltration be influenced. In drought years, when infiltration enhancement is typically desired, infiltration can be managed with stubble due to the positive relationship with h_v. To fully take advantage of increasing meltwater with h_v other actions must be taken that directly change the frozen soil characteristics through promotion of cracking with further adoption of zero-tillage (Granger and Gray, 1984) or sub-soil ripping (Gray et al., 1990; Gray et al., 1985). Runoff can be more easily managed with h_v. The dominant control on runoff is the available meltwater, by increasing meltwater through suppression of blowing snow sublimation with increased h_v, runoff increases and vice versa. The stubble management recommendations are specific to meltwater partitioning while agronomic and operational factors will influence actions taken by an agricultural producer.

Table 6.2: Stubble management agronomic and hydrologic objectives and desired outcomes with h_v recommendation

Objective	Desired outcomes	Antecedent Soil Moisture	Stubble height recommendation
Increase infiltration	Agronomic: increase dryland crop yield Hydrologic: increase recharge	Dry	Maximize h_v
		Wet	Negligible h_v influence
Decrease infiltration	Agronomic: minimize saturated areas and increase arable acres Hydrologic: lower water table	Dry	Minimize h_v
		Wet	Negligible h_v influence
Increase runoff	Agronomic: increase reservoir storage for livestock or irrigation Hydrologic: increase wetland and reservoir storage	Dry	Negligible h_v influence
		Wet	Maximize h_v
Decrease runoff	Agronomic: increase arable acres and minimize nutrient transport Hydrologic: decrease flooding	Dry	Negligible h_v influence
		Wet	Minimize h_v

These recommendations are generalized to the Canadian Prairies. Considering the climatic differences, as expressed by differences between sites in Figure 6.1, it is evident that stubble management will be much more effective in managing meltwater partitioning in the southwestern Canadian Prairies. Blowing snow defines accumulation and can be clearly managed with stubble. In contrast, snowmelt process interactions with stubble are compensatory and have a relatively small influence on snow depletion patterns and meltwater partitioning is defined by frozen soil infiltration dynamics, which are independent of stubble. Therefore, any region that is subject to significant blowing snow redistribution, high wind speed open environments, will more effectively use these stubble management recommendations to manage meltwater partitioning for agronomic or hydrological objectives. These recommendations are similar to those presented by Pomeroy et al. (1990). The key distinction is the findings of Pomeroy et al. (1990) relied upon extensive and detailed field campaigns that directly observed these relationships between stubble management and meltwater partitioning. In contrast, this work, using a bottom-up modelling approach, provides a physical process description of these dynamics that was unavailable in the 1980's and 1990's when much of the observational work was done. This physical process framework successfully describes the complex and non-linear relationships to describe how stubble will influence meltwater partitioning.

6.4.6. Limitations/Future Work

The most critical deficiency in this analysis is the quantification of frozen soil infiltration. The frozen soil infiltration parametrization of Gray et al. (2001) is a highly simplified representation of this process. Simulation of ice lenses due to mid-winter melts, to transition between Limited and Restricted infiltration classes, relies on an unverified conceptual threshold-based approach. Variations in tillage practices associated with different stubble types and how that may influence frozen soil infiltration are not understood quantitively and are neglected here. Future work must consider coupling of mass and energy exchanges between the snowpack and soil. Coupling with a physically detailed soil model, such as HAWTS (Zhao and Gray, 1999) or SHAW (Flerchinger, 2000), that can account for energy and mass transfers in a frozen soil will provide a complete physical representation of the stubble-meltwater partitioning relationship. With such a framework it is expected that the snowpack buffering of energy and mass exchange

between the atmosphere and soil, by the h_v dependent snowpack, will have an influence upon soil freezing and thawing and therefore meltwater partitioning.

6.5. Conclusions

The ability to manage and predict snowmelt characteristics through stubble management is valuable to meet agricultural or water management objectives. This work couples process models of blowing snow, stubble-snow-atmosphere energy balance interactions, sensible and latent heat advection, and frozen soil infiltration to explore the process interactions driving snow accumulation, snowmelt, and meltwater partitioning as a function of stubble characteristics. The non-linear and complex interactions lead to significant inter-annual variability in hydrological processes but in general increases in h_v increase available meltwater, melt rates and runoff and decrease sublimation with negligible influence upon melt duration and infiltration. The response and variability of these responses to h_v are much greater for areas subject to more intense blowing snow events such as the southwestern portion of the Canadian Prairies. Quantifying how stubble may influence snowmelt energy and influence melt rates, while important, is still a minor factor relative to the well-established hierarchy of controls governing frozen soil infiltration, antecedent fall soil moisture, the occurrence of mid-winter melts and overall snow accumulation (Pomeroy et al., 1990; Zhao and Gray, 1999). Despite the significant uncertainties of frozen soil infiltration and the complex relationships between snow accumulation and melt processes in stubble this physically based model framework employed herein successfully reproduces previous empirical findings. This framework provides recommendations on stubble management to meet specific meltwater partitioning objectives. Manipulating h_v can influence infiltration in dry/drought years while runoff can be more easily managed in wet conditions. These contributions provide the capacity to predict stubble-snow-meltwater partitioning interactions from a physically-based process perspective. This improves our understanding of hydrology in the context of a changing climate and agricultural practices on the Canadian Prairies that is relevant to other similar cold semi-arid dryland agricultural regions.

6.6. Manuscript Integration with Broader Thesis

Chapter 6 provides a synthesis of the observational, Chapters 2 and 3, and modelling, Chapters 4 and 5, contributions of this thesis with existing representations of blowing snow and

frozen soil infiltration to quantify the overall influence of stubble management upon meltwater partitioning.

6.6. References

Annandale, J. G., Jovanovic, N. Z., Benadé, N., Allen, R. G. (2001). Software for missing data analysis of Penman-Monteith reference evapotranspiration. *Irrig. Sci*, *21*, 57–67.

Awada, L. (2013). Factors Affecting the Adoption of Zero Tillage Innovation on the Canadian Prairies. PhD Thesis. University of Saskatchewan, Saskatoon SK.

Clapp, R. B., Hornberger., G. M. (1978). Empirical Equations for Some Soil Hydraulic Properties. *Water Resources Research*, *14*(4), 601–604.

Clark, M. P., Hendrikx, J., Slater, A. G., Kavetski, D., Anderson, B., Cullen, N. J., … Woods, R. (2011). Representing spatial variability of snow water equivalent in hydrologic and land-surface models: A review. *Water Resources Research*, *47*(7). https://doi.org/10.1029/2011WR010745

Dumanski, S., Pomeroy, J. W., Westbrook, C. J. (2015). Hydrological regime changes in a Canadian Prairie basin. *Hydrological Processes*, *29*(18), 3893–3904.

Elliot, J. E., Efetha, A. A. (1999). Influence of tillage and cropping system on soil organic matter, structure and infiltration in a rolling landscape. *Canadian Journal of Soil Science*, *79*, 457–463.

Erler, A. R., Peltier, W. R., D'Orgeville, M. (2015). Dynamically downscaled high-resolution hydroclimate projections for western Canada. *Journal of Climate*, *28*(2), 423–450. https://doi.org/10.1175/JCLI-D-14-00174.1

Essery, R., Pomeroy, J. W. (2004). Implications of spatial distributions of snow mass and melt rate for snow-cover depletion: theoretical considerations. *Annals of Glaciology*, *38*(1), 261–265. https://doi.org/10.3189/172756404781815275

Fang, X., Pomeroy, J. W. (2007). Snowmelt runoff sensitivity analysis to drought on the Canadian prairies. *Hydrological Processes*, *21*(19), 2594–2609. https://doi.org/10.1002/hyp

Flerchinger, G. N. (2000). *The Simultaneous Heat and Water (SHAW) Model: Technical Documentation*. Boise, Idaho. https://doi.org/Technical Report NWRC 2000-09

Garratt, J. R. (1990). The Internal Boundary Layer - A Review. *Boundary-Layer Meteorology*, *50*, 171–203.

Granger, R. J., Gray, D. M., Dyck, G. E. (1984). Snowmelt Infiltration to frozen Prairie Soils. *Canadian Journal of Earth Sciences*, *21*(6), 669–677. https://doi.org/10.1016/0148-9062(85)92399-X

Granger, R. J., Gray, D. M. (1984). Snowmelt infiltration to frozen prairie soils. *Canadian Journal of Earth Sciences*, *21*(6), 669–677.

Granger, R. J., Pomeroy, J. W., Parviainen, J. (2002). Boundary-layer integration approach to advection of sensible heat to a patchy snow cover. *Hydrological Processes*, *16*(18), 3559–3569.

Granger, R. J., Essery, R., Pomeroy, J. W. (2006). Boundary-layer growth over snow and soil patches: Field Observations. *Hydrological Processes*, *20*(4), 943–951.

Gray, D. M., Toth, B., Zhao, L., Pomeroy, J. W., Granger, R. J. (2001). Estimating areal snowmelt infiltration into frozen soils. *Hydrological Processes*, *15*(16), 3095–3111. https://doi.org/10.1002/hyp.320

Gray, D. M., Landine, P. G. (1988). An Energy-Budget Snowmelt Model for the Canadian Prairies. *Canadian Journal of Earth Sciences*, *25*(8), 1292–1303.

Gray, D. M., Maule, C. P. (1994). Agricultural production and water conservation in semi-arid, cold environments. In *Symposium on Global Environment and Friendly Energy Technology* (p. 17).

Gray, D. M., Granger, R. J., Nicholaichuk, W. (1985). Snowmelt Infiltration To Uncracked, Cracked and Subsoiled Frozen Soils. Division of Hydrology, University of Saskatchewan, Saskatoon, Saskatchewan.

Gray, D. M., Granger, R. J., Nicholaichuk, W. (1990). Snowmelt Infiltration into Completely-Frozen Subsoiled Soils. In *Frozen Soil Symposium* (p. 12). Spokane WS.

Hodder, K., Cade-Menun, B. J., Bell, G., Baker-Ismail, S., Mcmartin, D. W., Perez-Valdivia, C., Wu, K. (2013). Nutrient loss from Saskatchewan cropland and pasture in spring snowmelt runoff. *Canadian Journal of Soil Science*, *93*, 445–458. https://doi.org/10.4141/CJSS2012-042

IPCC. (2013). *Climate Change 2013: The Physical Science Basis. Contribution of Working Group I to the Fifth Assessment Report of the Intergovernmental Panel on Climate Change*. (T. F. Stocker, D. Qin, G.-K. Plattner, M. Tignor, S. K. Allen, J. Boschung, … P. M. Midgley, Eds.). Cambridge, United Kingdom: Cambridge University Press. https://doi.org/10.1017/CBO9781107415324

Ireson, A. M., van der Kamp, G., Ferguson, G., Nachshon, U., Wheater, H. (2013). Hydrogeological processes in seasonally frozen northern latitudes: understanding, gaps and challenges. *Hydrogeology Journal*, *21*(1), 53–66. https://doi.org/10.1007/s10040-012-0916-5

van der Kamp, G., Hayashi, M., Gallen, D. (2003). Comparing the hydrology of grassed and cultivated catchments in the semi-arid Canadian prairies. *Hydrological Processes*, *17*(3), 559–575. https://doi.org/10.1002/hyp.1157

MacDonald, M. K., Pomeroy, J. W., Essery, R. L. H. (2018). Water and energy fluxes over northern prairies as affected by chinook winds and winter precipitation. *Agricultural and Forest Meteorology*, *248*(February 2017), 372–385. https://doi.org/10.1016/j.agrformet.2017.10.025

Mekis, É., Vincent, L. A. (2011). An Overview of the Second Generation Adjusted Daily Precipitation Dataset for Trend Analysis in Canada. *Atmosphere-Ocean*, *49*(2), 163–177. https://doi.org/10.1080/07055900.2011.583910

Nicholaichuk, W., Gray, D. M. (1986). Snow Trapping and Moisture Infiltration Enhancement. In *Fifth Annual Western Provinces Conference*.

Pomeroy, J. W., Brun, E. (2001). Physical Properties of Snow. In H. G. Jones, J. W. Pomeroy, D. A. Walker, and R. W. Hoham (Eds.), *Snow Ecology: an Interdisciplinary Examination of Snow-covered Ecosystems* (pp. 45–118). Cambridge University Press.

Pomeroy, J. W., Gray, D. M., Brown, T., Hedstrom, N. R., Quinton, W. L., Granger, R. J., Carey, S. K. (2007). The cold regions hydrological model : a platform for basing process representation and model structure on physical evidence. *Hydrological Processes*, *21*(19), 2650–2667.

Pomeroy, J. W., Gray, D. M. (1994). Sensitivity of snow relocation and sublimation to climate and surface vegetation. In *Snow and Ice Covers: Interactions with the Atmosphere and Ecosystems* (pp. 213–225). IAHS Publ. No 223.

Pomeroy, J. W., Gray, D. M. (1995). *Snow accumulation, relocation and management*. Saskatoon, SK: Science Report No. 7, National Hydrology Research Institute, Environment Canada.

Pomeroy, J. W., Gray, D. M., Landine, P. G. (1991). Modelling the Transport and Sublimation of Blowing Snow on the Prairies. In *Eastern Snow Conference* (pp. 175–188). Guelph, ON.

Pomeroy, J. W., Gray, D. M., Landine, P. G. (1993). The Prairie Blowing Snow Model: characteristics, validation, operation. *Journal of Hydrology*, *144*(1–4), 165–192.

Pomeroy, J. W., Nicholaichuk, W., Gray, D. M., McConkey, B. G., Granger, R. J., Landine, P. G. (1990). *Snow Management and Meltwater Enhancement: Final Report*. *NHRI Contribution No. CS-90021*. Saskatoon, SK. Retrieved March 6, 2018, from http://www.usask.ca/hydrology/papers/Pomeroy_1990.pdf

Pomeroy, J. W., Li, L. (2000). Prairie and arctic areal snow cover mass balance using a blowing snow model. *Journal of Geophysical Research*, *105*(D21), 26619–26634.

Pomeroy, J. W., de Boer, D., Martz, L. W. (2005). *Hydrology and Water Resources of Saskatchewan*. Centre Report No. 1, Centre for Hydrology, University of Saskatchewan, Saskatoon, SK.

Shook, K., Pomeroy, J. W. (2011). Synthesis of Incoming Shortwave Radiation for Hydrological Simulation. *Hydrology Research*, *42*(6), 433–446.

Shook, K., Gray, D. M., Pomeroy, J. W. (1993). Temporal Variation in Snowcover Area During Melt in Prairie and Alpine Environments. *Nordic Hydrology*, *24*(2–3), 183–198.

Sicart, J. E., Pomeroy, J. W., Essery, R., Bewley, D. S. (2006). Incoming longwave radiation to melting snow: observations, sensitivity and estimation in northern environments. *Hydrological Processes*, *20*(17), 3697–3708.

Staple, W. J., Lehane, J. J. (1954). Wheat yield and use of moisture on substations in southern Saskatchewan. *Canadian Journal of Agricultural Science*, *34*, 460–468.

Statistics Canada. (2016). Census of Agriculture, tillage practices used to prepare land for seeding, every 5 years. Retrieved May 12, 2017, from http://www5.statcan.gc.ca/cansim/a03?lang=engandsearchMode=regularSearchandpattern=004-0200..004-0246andtypeValue=-1andsrchLan=-1andp2=31

Willis, W. O., Haas, H. J., Carlson, C. W. (1969). Snowpack runoff as affected by stubble height. *Soil Science*, *107*, 256–259.

Zhao, L., Gray, D. M. (1999). Estimating snowmelt infiltration into frozen soils. *Hydrological Processes*, *13*(12–13), 1827–1842. https://doi.org/10.1002/(SICI)1099-1085(199909)13:12/13<1827::AID-HYP896>3.0.CO;2-D

Zhao, L., Gray, D. M., Male, D. H. (1997). Numerical analysis of simultaneous heat and mass transfer during infiltration into frozen ground. *Journal of Hydrology*, *200*, 345–363.

Chapter 7: Conclusions, Synthesis, and Future Work

7.1 Conclusions

The research presented here advances our understanding of snowmelt on the Canadian Prairies in key areas that have been previously deficient. The analysis of novel observations from unique data collection systems quantified some of the complexity of snowmelt in agricultural regions of the Canadian Prairies. The improvements in snow observations, identification of new snowmelt energy sources, representation of snow-stubble dynamics and interactions, modelling of sensible and latent heat advection, and the integration into a coupled modelling framework improves understanding and prediction of prairie snowmelt moving forward.

The ability to quantify SCA and its change over time at an unprecedented spatial resolution and accuracy with UAV derived data was clearly demonstrated (Chapter 2). The shallow nature of prairie snowcover meant the error inherent to the estimated snow depth from DSM differencing allows the maximum snow depth, but not the melt progression, to be quantified with confidence. The ability to map maximum snow depth accumulation as a continuous property from a remote sensing platform is a first for the Canadian Prairies. This capability is of great value to observed snow depth dynamics at a high spatial resolution as well as initializing and validating distributed snow models. This work provides the reference to support such work moving forward.

The development of a novel air temperature and water vapour profiling system directly quantified sensible and latent advection (Chapter 3). The identification of latent heat advection as a significant snowmelt energy flux is especially exciting as it has not been previously observed. The relative role of the advection terms with respect to each other, land surface characteristics and the overall energy balance clearly demonstrates the importance and variability of this complex energy redistribution process on snowmelt processes. This work provides the evidence needed to motivate the development of modelling schemes that include sensible and latent heat advection processes in the next generation of snowmelt models.

The influence of crop stubble emergence upon the snow surface energy balance is now quantified from a physical process perspective that was previously unaccounted for in snowmelt models (Chapter 4). The development, and validation, of a stubble-snow-atmosphere energy balance model allows the exploration of the influence of stubble characteristics upon snowmelt from a physical process understanding perspective. These results show that while the net response of stubble energetics may only change snowmelt rates slightly, there are larger implications of stubble exposure for land-atmosphere interactions. The development of SSAM is a scientifically novel advance from both an applied and science perspective. As stubble can be easily represented within the framework from easily measured or estimated parameters, applied research questions that seek to understand the impact of agricultural producer actions on hydrological processes and land-atmosphere process can be addressed. In addition, improving the representation of surface features over the Canadian Prairies and other similar environments will improve the land-atmosphere dynamics that will contribute to improved climate and numerical weather prediction models which rely on such boundary conditions.

The framework proposed for including sensible and latent heat advection into snowmelt models, Chapter 5, provides an initial solution for this dynamic and important energy term. Snowmelt predictions when coupled to SSAM do not change greatly for the two years of testing but allow simulation of snowmelt processes with a more complete and better process description. Inappropriate process assumptions, such as underestimated snow albedo, are no longer needed to simulate realistic snowmelt. Various process representations need to be included in the framework and moving forward incremental improvements will be realized as deficiencies in current conceptualizations are addressed. The ability to couple this advection model to existing one-dimensional energy balance models is an advance that has the potential to quickly and easily improve the physical representations and estimates of existing models.

The cumulative work of the modelling contributions (Chapters 4 and 5), as motivated by the observational findings (Chapters 2 and 3), are synthesized into a couple modelling framework that describes the influence of stubble upon snow accumulation, melt and meltwater partitioning (Chapter 6). The non-linear interactions of this system are complicated and lead to a large range in process variability when modelling the influence of stubble management. The simulation of an increase in total meltwater, runoff, and infiltration, with respect to increases in

stubble height validates earlier empirical research upon snow management and infiltration enhancement. This work provides a bottom-up modeling process understanding that can describe these dynamics from a physical process perspective that has been lacking previously. The analysis employed suggests that stubble management itself has a limited influence upon meltwater partitioning as frozen soil infiltration is still the dominant control. The influence of snow accumulation interactions with stubble are also more important than the compensating stubble-snowmelt interactions which indicate that stubble management effectiveness has a positive relationship to the intensity of blowing snow processes. The southwestern portions of the Canadian Prairies will be able to more effectively manage infiltration or runoff with stubble management relative to northern and eastern regions.

7.2. Synthesis

Two general themes were expressed throughout this thesis. The first is that the novel and detailed observations of snowmelt on the Canadian Prairies were critical in developing new understandings of the processes driving snowmelt. The second is that the models that have developed from these observations reveal extensive compensatory mechanisms that have not had previous description.

Several novel observation systems were employed in the intensive field campaigns to improve the direct quantification of snow and energy balance processes to improve the understanding of prairie snowmelt. The ability to quantify SCA and its change over time at an unprecedented spatial resolution and accuracy with UAV derived data was clearly demonstrated in Chapter 2. The demonstrated inability to observed SWE depletion from UAV's, or differences between stubble treatments with snow surveying, underscores the challenge of understanding, or directly observing, the subtle interactions driving snowmelt on the Canadian Prairies. While this is a criticism of the inability of our tools to measure shallow snowmelt it also implies that there must be energy balance interactions that lead to a moderated response of net energy to stubble emergence. The direct observation of latent heat advection during snowmelt, from development of a novel air temperature and water vapor profiling system in Chapter 3, highlights a gap in understanding of energy exchange processes that has implications for snowmelt. This observation also implies that the current understanding and modelling of the net influence of local-scale advection upon snowmelt may be missing moderating dynamics that overestimate its

importance. Unique observations were also obtained to inform and validate the energy balance process representations of SSAM in Chapter 4. The challenging dynamics of the snow-stubble-atmosphere interface that is subject to local-scale advection required creative and novel implementation of current and new instrumentation to constrain the energy balance interactions to validate models. The detailed novel observations reported here, minimal differences in SWE depletion between stubble treatments, latent heat advection is a relevant process, and observations that informed the snow-stubble-atmosphere interactions of SSAM, emphasize the second theme of the thesis: that the energy balance processes driving prairie snowmelt demonstrate compensatory behavior.

The modelling contributions of this thesis build upon the observations of compensatory processes driving snowmelt on the Canadian Prairies. Model representations of the compensation of the snow surface energy balance below an emerging stubble canopy (Chapter 4) and compensatory sensible and latent heat advection (Chapter 5) articulates a snowmelt system response that is relatively insensitive to processes that on their own seem important. The implications of these compensatory snowmelt interactions upon meltwater partitioning is also evident in the stubble meltwater partitioning dynamics (Chapter 6); the primary controls of meltwater partitioning stubble interactions are blowing snow processes and frozen soil infiltration which are relatively independent of snowmelt rates. The identification of such compensatory relationships are common when increasing the physical complexity of surface energy balance models with some examples reported from terrain shading impacts on snowmelt (Marsh et al., 2012), radiation paradoxes (Ambach, 1974), and forest thinning impacts on snowmelt timing (Ellis et al., 2013). From an operational snowmelt prediction perspective this may be perceived as a motivation to use simpler approaches such as temperature-index, or quasi energy balance temperature-index, snowmelt models (Walter et al., 2005). Rather, this result should motivate the use of more complex and robust models that can account for all process interactions. The non-linearity of the snowmelt system means that there will be unpredictable responses to perturbations, not captured by simple temperature-index snowmelt models, which may lead to pronounced simulation differences. To increase confidence in prediction of snow melt in response to changes in land surface, stubble characteristics, or climate it is recommended to use, and further develop, complex physically-based snowmelt models as described in this thesis.

7.3. Future Work

Intensive study of any topic always leads to identification of additional research opportunities and this work is no exception. The main limitation of the UAV derived snow depth observations is that the signal to noise ratio is too low to confidently observe melt rates in the shallow snows of the Canadian Prairies. Future work to reduce snow depth errors to be sufficient to measure melt may consider software and hardware improvements. From a software perspective this work was conducted with Postflight Terra 3D 3 version 3.4.46, a variant of Pix4D Mapper. Continued improvements in this software, or other commercial packages such as Agisoft Photoscan, may lead to improvements in SfM. A common challenge in using such proprietary black box software packages is that the underlying algorithms are unknown and cannot be easily understood or customized to a specific application. Development of open source alternatives, such as VisualSFM (Changchang, 2011), may be an alternative but overall performance of SfM will always be theoretically limited to vertical errors that are a function of the ground sample distance of the images (Roze et al., 2014). Other avenues of improvement are to utilize alternative point cloud interpolation schemes (Kinar et al., 2017) or use point cloud differencing rather than surface model differencing (James et al., 2017). Hardware improvements are also critical. Cameras with greater resolution, better optics, sampling different bands of the electromagnetic spectrum, and more sensitive sensors may be able to resolve finer and more subtle features in snow that can translate to more accurate surface estimates. The UAV integrated camera available at the time of the field campaign was a Canon PowerShot ELPH 110 HS a 16.1 Megapixel consumer grade camera. Higher grade camera systems, such as a calibrated 100 Megapixel survey grade PhaseOne iXU-RS 1000 camera with a high grade IMU/dGPS, need testing but will undoubtedly provide higher quality data (Mian et al., 2016). High quality Light Detection and Ranging (Lidar) systems with UAV compatible size, weight and power requirements are becoming available and will provide another avenue to measure snow depths, especially snow with limited surface features. This work was limited to small domains of interest but opportunities to apply these techniques on larger extents is promising as platforms and regulations for operating beyond-visual line of sight mature. This high spatio-temporal resolution data of snow depth and snowcover will be a paradigm shift in the understanding of small scale snow processes over large extents.

The observations of sensible and latent heat are novel observations but are hampered by the short intervals of high quality observation data. Future work should use this same methodology to try and observe advection in more situations and environments. More data is needed to understand the dynamics and implications of these fluxes under conditions that may vary with stability, surface roughness, meteorology and turbulence regimes. The lessons learned in this experiment are invaluable in the design of any follow up campaign. A key improvement to implement is the configuration of the apparatus. The main difference in scalar profiles occurred between the tower at the transition and the first tower downwind of the transition. Therefore, any future deployment should focus exclusively upon the leading-edge interval with two towers. This will allow a greater number of intakes per profile which will allow a much finer resolution of the water vapor profiles. A conservative approach was taken to determine the intake port interval/cycle. Analysis of the signal stability after the field campaign concluded that the sampling interval should be halved, from 20 seconds to 10 seconds, which will increase the temporal resolution of the water vapor observations. Finer scaler data will improve the accuracy of the observations and limit the influence of some surface condition assumptions.

Any new model will always benefit from more testing and validation and SSAM is no different. SSAM was validated upon two snowmelt seasons at a specific research site. Future work with SSAM needs to explore its performance subject to different meteorological conditions, stubble types and snow regimes. This will require collection of data that is not commonly recorded, specifically stubble characteristics. Future research opportunities should involve its application in other modelling platforms. SSAM could be configured to operate as a module for the cold-regions hydrological modelling platform, a hydrological response unit based model (Pomeroy et al., 2007). This will facilitate easy and extensive application within a widely applied research model designed for cold regions. Further, it could be implemented in distributed hydrological models such as the Canadian Hydrological Model (Marsh et al., 2017). With application in these modelling platforms that integrate a more complete hydrological cycle, the implications of stubble upon the snow surface energy balance and snowmelt can be explored. Findings can be extended to a regional basis and implications of land management practices or climate change can be examined for hydrological and land-atmosphere impacts. To achieve this the scaling dynamics of SSAM and its parameter sensitivities need to be assessed.

The strength of the proposed sensible and latent heat model is the framework that is presented rather than the model parameterizations themselves. Significant issues exist in the boundary layer parameterization, its extension to latent heat, and the ignoring of differences in surface roughnesses. The challenges of obtaining reliable and fine scale advection fluxes observations are significant and most progress will likely be achieved though development of detailed numerical fluid dynamics models from which simplified representations can be derived. The fractional water area, infiltration and detention storage relationships presented are purely conceptual and detailed observations are needed to test these ideas. A multiscale field campaign would be needed that may utilize high resolution UAV imagery to observed snowcover depletion and surface water area, surveys of microtopography, and in-situ observations of infiltration. A stronger coupling of surface and subsurface processes is needed. This could take the form of a distributed snow model that simulates the heterogenous decomposition of a continuous snowcover that in turn is coupled with a soil model to represent snowmelt water ponding on the surface. Such work will require significant advances in high resolution coupled modelling of spatially disturbed mass and energy balances in soil, snow and atmospheric domains. In the meantime, this framework provides an initial approach to allow for the inclusion of advection processes into existing one-dimensional snowmelt models.

The synthesis of this work with coupled modelling of accumulation, melt and meltwater partitioning with a combination of existing and new models provides a complete process representation of snow-stubble interactions. Like the improvements needed to improve advection modeling, a more detailed understanding of the influence of stubble could be reached with coupling to better frozen soil infiltration processes. The parameterization approach of Gray et al. (2001) is simple to implement but misses some key process interactions. Further work should couple the snow processes to a more detailed soil model such as HAWTS (Zhao et al., 1997) or SHAW (Flerchinger, 2000). More nuanced, and possibly compensatory, interactions may emerge from such implementations. The key issue of soil infiltration restriction due to mid-winter melt events need to be better resolved than the threshold approach implemented here. The ability to account for the non-binary sealing of soil infiltration and its change over the course of a winter due to vapor movement in a soil, soil desiccation if snow free, and other dynamics will likely make the processes interactions even more non-linear.

Current research on the process understanding of shallow prairie snowcover is limited as the higher water yields and scenery of mountainscapes attract much of the focus of cold-regions hydrological research. While often overlooked as being relatively simple, the challenges of improving understanding and predicting melt of thin snowcovers is anything but. Many gaps in understanding still exist and await further study. Hydrology is an inexact science, this is especially so in cold regions when all three phases of water coexist, and it continues to generate a wealth of outstanding research questions.

7.4. References

Ambach, W. (1974). The influence of cloudiness on the net radiation balance of a snow surface with high albedo. Journal of Glaciology, 13(67), 73–84.

Changchang, W. (2011). VisualSFM: A Visual Structure from Motion System. Retrieved from http://ccwu.me/vsfm/

Ellis, C. R., Pomeroy, J. W., Link, T. E. (2013). Modeling increases in snowmelt yield and desynchronization resulting from forest gap-thinning treatments in a northern mountain headwater basin. Water Resources Research, 49, 1–14. https://doi.org/10.1002/wrcr.20089

Flerchinger, G. N. (2000). The Simultaneous Heat and Water (SHAW) Model: Technical Documentation. Boise, Idaho. https://doi.org/Technical Report NWRC 2000-09

Gray, D. M., Toth, B., Zhao, L., Pomeroy, J. W., Granger, R. J. (2001). Estimating areal snowmelt infiltration into frozen soils. Hydrological Processes, 15(16), 3095–3111. https://doi.org/10.1002/hyp.320

James, M. R., Robson, S., Smith, M. W. (2017). 3-D uncertainty-based topographic change detection with structure-from-motion photogrammetry: precision maps for ground control and directly georeferenced surveys. Earth Surface Processes and Landforms, 42(12), 1769–1788. https://doi.org/10.1002/esp.4125

Kinar, N. J., Pomeroy, J. W., Shea, J., Schirmer, M., Harder, P. (2017). 2D Frequency Analysis of Irregularly Sampled Snowpack Properties. In Canadian Geophysical Union. Vancouver, B.C.

Marsh, C., Pomeroy, J. W., Wheater, H., Spiteri, R. (2017). The Canadian Hydrological Model: A multiscale, multiphysics, variable complexity hydrological model. In Canadian Geophysical Union Annual Meeting. Vancouver, B.C.

Marsh, C., Pomeroy, J. W., Spiteri, R. J. (2012). Implications of mountain shading on calculating energy for snowmelt using unstructured triangular meshes. Hydrological Processes, 26(12), 1767–1778. https://doi.org/10.1002/hyp.9329

Mian, O., Hutton, J., Lipa, G., Lutes, J., Gumerov, D., Applanix, S., Chan, W. (2016). Accuracy Assessment of POS AVX 210 integrated with the Phase One iXU150.

Pomeroy, J. W., Gray, D. M., Brown, T., Hedstrom, N. R., Quinton, W. L., Granger, R. J., Carey, S. K. (2007). The cold regions hydrological model : a platform for basing process representation and model structure on physical evidence. Hydrological Processes, 21(19), 2650–2667.

Roze, A., Zufferey, J.-C., Beyeler, A., Mcclellan, A. (2014). eBee RTK Accuracy Assessment. Lausanne, Switzerland.

Walter, M. T., Brooks, E., McCool, D., King, L., Molnau, M., Boll, J. (2005). Process-based snowmelt modeling: does it require more input data than temperature-index modeling? Journal of Hydrology, 300(1–4), 65–75. https://doi.org/10.1016/j.jhydrol.2004.05.002

Zhao, L., Gray, D. M., Male, D. H. (1997). Numerical analysis of simultaneous heat and mass transfer during infiltration into frozen ground. Journal of Hydrology, 345–363.

Appendix A: Data and Code Availability

The following data is available though Phillip Harder (phillip.harder@usask.ca).

Dataset	Description
UAV DSM and Orthomosaics	Digital surface models and orthomosaics of generated from structure from motion from UAV imagery for 2015 and 2016 snowmelt seasons at Rosthern, Saskatchewan field Site
Wind, air temperature and specific humidity profile observations	Observations from advection array apparatus of two-dimensional air temperature, wind speed and humidity over select snow-free to snowcover transitions from snowmelt 2015 at Rosthern, Saskatchewan field site that were basis of advection observations
2015-2016 Meteorological and Energy Balance Observations	Observations of meteorology, radiation, snow temperature, stubble temperature, eddy covariance sensible and latent heat, and snow surveys for 2015 and 2016 snowmelt seasons at Rosthern, Saskatchewan field site that were used to drive and validate SSAM and SLHAM.

Code for the SSAM and SLHAM models developed herein is available under GNU General Public License v3.0 copyright through a GitHub repository found at https://github.com/phillip-harder/.